

**SELECTION OF IONIC LIQUIDS AND DEEP EUTECTIC
SOLVENTS VIA QUANTUM CHEMICAL METHODS AND
LIQUID-LIQUID EQUILIBRIA INVOLVED IN THE EXTRACTIVE
DENITROGENATION OF DIESEL**

HANEE FARZANA BINTI HIZADDIN

**THESIS SUBMITTED IN FULFILMENT OF THE
REQUIREMENTS FOR THE DEGREE OF
DOCTOR OF PHILOSOPHY**

**FACULTY OF ENGINEERING
UNIVERSITY OF MALAYA
KUALA LUMPUR, MALAYSIA**

2016

Name of Candidate: HANEE FARZANA BINTI HIZADDIN

Registration/Matric No.: KHA110108

Name of Degree: Doctor of Philosophy (Ph.D.)

Title of Project Paper/Research Report/Dissertation/Thesis (“this Work”):

SELECTION OF IONIC LIQUIDS AND DEEP EUTECTIC SOLVENTS VIA QUANTUM CHEMICAL METHODS AND LIQUID-LIQUID EQUILIBRIA INVOLVED IN THE EXTRACTIVE DENITROGENATION OF DIESEL

Field of Study: Chemical Engineering

I do solemnly and sincerely declare that:

- (1) I am the sole author/writer of this Work;
- (2) This Work is original;
- (3) Any use of any work in which copyright exists was done by way of fair dealing and for permitted purposes and any excerpt or extract from, or reference to or reproduction of any copyright work has been disclosed expressly and sufficiently and the title of the Work and its authorship have been acknowledged in this Work;
- (4) I do not have any actual knowledge nor ought I reasonably to know that the making of this work constitutes an infringement of any copyright work;
- (5) I hereby assign all and every rights in the copyright to this Work to the University of Malaya (“UM”), who henceforth shall be owner of the copyright in this Work and that any reproduction or use in any form or by any means whatsoever is prohibited without the written consent of UM having been first had and obtained;
- (6) I am fully aware that if in the course of making this Work I have infringed any copyright whether intentionally or otherwise, I may be subject to legal action or any other action as may be determined by UM.

Candidate’s Signature

Date:

Subscribed and solemnly declared before,

Witness’s Signature

Date:

Name:

Designation:

ABSTRACT

The removal of nitrogen compounds from transportation fuel is proven to enhance the efficiency of desulfurization process, which aims to meet the rigorous regulations regarding zero-emissions. Ionic liquids (ILs) and deep eutectic solvents (DESs) were screened for this purpose using quantum chemical methods. Geometry optimization was performed for all involved species at Hartree-Fock level and 6-31G* basis set. Generation of *cosmo* files using Density Functional Theory and Triple zeta valence potential basis set was carried out at single point calculation. The *cosmo* files were used to obtain σ -profiles and σ -potentials for qualitative screening of ILs and DESs. (i) The screening of ILs revealed that cations with an aromatic ring have better capacity as hydrogen bond donors (HBDs) than do non-aromatic cations, whereas the acetate anion appeared to have better affinity towards HBD than did ethylsulfate and methanesulfonate anions. The σ -profile and σ -potential analysis confirmed that there is an interaction between nitrogen compounds and cations via CH- π interaction along with between nitrogen compounds and anions via hydrogen bonding. Moreover, a detailed quantum chemical calculation was performed to investigate the interaction between ILs and nitrogen compounds at molecular level, in which optimized geometry was used to obtain the orbital energies, global scalar properties, interaction energies and partial charges. The calculations indicated that cations with an aromatic ring, that is, imidazolium and pyridinium, combined with either ethylsulfate or methanesulfonate anion have favorable interaction with nitrogen compounds in comparison to cations without an aromatic ring. (ii) The screening of DESs showed that the interaction between nitrogen compounds and DESs is based on hydrogen bonding. Altogether, 94 DESs were examined quantitatively by predicting the values of the activity coefficients at infinite dilution of nitrogen compounds and diesel in the DESs. These were then used to estimate selectivity, capacity and

performance index at infinite dilution as the basis of the screening process taking into account the cation, anion and HBD choices as well as the salt:HBD molar ratio.

Based on the screening results, 22 ternary liquid-liquid equilibria (LLE) experiments were carried out at room temperature and atmospheric pressure to test three ILs – namely 1-ethyl-3-methylimidazolium ethylsulfate, 1-ethyl-3-methylpyridinium ethylsulfate, and 1-ethyl-3-methylimidazolium methanesulfonate, and two DESs – namely tetrabutylammonium bromide/ethylene glycol (1:2) and tetrabutylphosphonium bromide/ethylene glycol (1:2). The aim was to remove non-basic and basic nitrogen compounds from *n*-hexadecane as a model diesel compound. NMR spectroscopy was used for the compositional analysis. Consistency tests were performed to ascertain the reliability of all experimental data. All ternary systems reported distribution ratios and selectivity values greater than unity with minimal cross-contamination between the extract and raffinate phases. The ternary LLE data were correlated with NRTL model and compared with COSMO-RS predictions, both of which were in excellent agreement with the experimental tie-lines. In conclusion, the quantum chemical screening of ILs and DESs explained the interaction between ILs/DESs and nitrogen compounds at molecular level, which facilitates solvent selection for the denitrogenation process. The ternary LLE experiments with the selected ILs and DESs confirmed that these solvents have high potential for industrial extractive denitrogenation.

ABSTRAK

Penyingkiran sebatian nitrogen telah terbukti dapat meningkatkan kecekapan proses penyahsulfuran yang bertujuan untuk mematuhi undang-undang berkenaan produksi bahan api kenderaan yang bebas pelepasan. Pelarut baru, cecair ionik (ionic liquid atau IL) dan pelarut eutektik dalam (deep eutectic solvent atau DES) telah disaring untuk tujuan ini dengan menggunakan kaedah kimia kuantum. Pengoptimaan geometri telah dijalankan untuk semua spesis terlibat pada tahap Hartree-Fock dan “basis set” 6-31G*. Fail-fail *cosmo* dihasilkan menggunakan Density Functional Theory dan “basis set” triple zeta valence potential pada pengiraan titik tunggal. Fail-fail *cosmo* tersebut digunakan untuk mendapatkan σ -profile dan σ -potential untuk saringan IL dan DES secara kualitatif. Hasil kajian mendapati: *i*) Berdasarkan saringan IL, didapati bahawa kation yang mengandungi gelang aromatik mempunyai kapasiti yang lebih baik sebagai penderma ikatan hidrogen (HBD) berbanding kation tanpa gelang aromatik, manakala anion asetat mempunyai daya tarik yang lebih baik terhadap HBD berbanding anion-anion metil sulfat ([EtSO₄]⁻) dan metanasulfonat ([MeSO₃]⁻). Analisis σ -profile dan σ -potential mengesahkan interaksi antara sebatian nitrogen dengan kation menerusi interaksi CH- π manakala antara sebatian nitrogen dengan anion menerusi ikatan hidrogen. Pengiraan terperinci kimia kuantum dijalankan untuk menyelidik interaksi antara IL dengan sebatian nitrogen pada tahap molekular di mana geometri yang dioptimakan digunakan untuk mendapatkan tenaga orbital, ciri-ciri skalar global, tenaga interaksi dan caj-caj separa. Pengiraan yang dibuat menunjukkan bahawa gabungan kation dengan gelang aromatik iaitu imidazolium dan pyridinium, dengan sama ada kation ([EtSO₄]⁻) atau ([MeSO₃]⁻) mempunyai interaksi yang baik dengan sebatian nitrogen berbanding dengan kation tanpa gelang aromatik. *ii*) Saringan DES menunjukkan bahawa interaksi antara sebatian nitrogen dengan DES adalah berasaskan ikatan hidrogen. Sejumlah 94 DES telah diperiksa secara kuantitatif dengan meramal nilai pekali aktiviti pada cairan

tak terhingga bagi sebatian nitrogen dan diesel dalam DES, yang kemudiannya digunakan untuk mentaksir nilai pemilihan, kapasiti, dan indeks prestasi pada cairan tak terhingga sebagai asas untuk proses saringan, dengan mengambil kira faktor kation, anion, HBD dan nisbah molar garam:HBD.

Berdasarkan keputusan saringan, sejumlah 18 set eksperimen keseimbangan cecair-cecair (LLE) telah dijalankan pada suhu bilik dan tekanan atmosfera untuk menguji prestasi tiga IL iaitu 1-ethyl-3-methylimidazolium ethylsulfate, 1-ethyl-3-methylpyridinium ethylsulfate dan 1-ethyl-3-methylimidazolium methanesulfonate, dan dua DES iaitu tetrabutylammonium bromide/ethylene glycol (1:2) and tetrabutylphosphonium bromide/ethylene glycol (1:2) dalam menyingkirkan sebatian nitrogen yang bersifat bukan bes (pyrrole dan indoline) dan bersifat bes (pyridine dan quinoline) daripada *n*-heksadekana sebagai model bahan api diesel. Spektroskopi NMR digunakan untuk analisis komposisi. Ujian konsistensi dijalankan untuk memastikan kesahihan semua data eksperimen. Semua sistem ternari melaporkan nilai pemilihan dan nisbah pengagihan lebih daripada satu dan menunjukkan pencemaran silang yang minimum antara fasa ekstrak dan fasa rafinat dalam semua sistem yang dikaji. Data LLE ternari telah dikorelasikan dengan model NRTL dan dibandingkan dengan ramalan COSMO-RS dan kedua-dua model menunjukkan nilai yang dekat dengan nilai yang didapati melalui eksperimen. Kesimpulannya, saringan IL dan DES secara kimia kuantum memberikan penjelasan tentang interaksi antara unsur-unsur dalam IL dan DES dengan sebatian nitrogen pada tahap molekular, seterusnya memudahkan proses pemilihan pelarut bagi proses penyahnitrogenan. Eksperimen LLE ternari dengan IL dan DES terpilih telah mengesahkan potensi tinggi pelarut-pelarut tersebut untuk kegunaan penyahnitrogenan secara ekstraktif pada peringkat industri.

ACKNOWLEDGEMENT

First and foremost, I thank Allah the Almighty for giving me the opportunity and strength to pursue my studies at doctorate level. Nothing is possible without the help from Allah.

I would like to dedicate this work to everyone who has given me constant support throughout my candidature.

Prof. Mohd. Ali Hashim – Thank you for your trust in me and accepting me to become part of UMCiL (University of Malaya Center for Ionic Liquids) and for your continuous support and guidance since the first day I join the research group.

Dr. Mohamed Omar Hadj-Kali – Thank you for being my advisor since the first day of my studies, for your patience in dealing with me and for being the person I can rely upon throughout my research.

Dr. Inas AlNashef and Dr. Farouq Mjalli – Thank you for your advice and comments on my work in general and for always being there whenever I need advice.

To all staff and colleague of UMCiL and the Department of Chemical Engineering, especially to Ms. Marhaini Mohd Desa, Dr. Muhammad AbdulHakim Alsaadi, Dr. Maan Hayyan, Dr. Adeeb Hayyan and Ms. Muna Ibrahim; thank you for your help, support and guidance.

Muaz Iftikhar, thank you for being such a good boy and being patient while Mommy needs to finish her studies.

Special thanks to my husband, Anas Mohamad Sofian, my parents, my siblings and my in-laws who are always there for me through my ups and downs and who continues to motivate me to finish what I had started. I could not have done it without you.

TABLE OF CONTENTS

ABSTRACT	iii
ABSTRAK	v
ACKNOWLEDGEMENT	vii
TABLE OF CONTENTS	viii
LIST OF FIGURES	xii
LIST OF TABLES	xvi
LIST OF ABBREVIATIONS	xix
NOMENCLATURE	xx
LIST OF APPENDICES	xxii
CHAPTER 1: INTRODUCTION	1
1.1 Background	1
1.2 Problem Statement and Significance of Study	2
1.3 Research Philosophy	3
1.4 Research Objectives	3
1.5 Research Methodology	4
1.6 Outline of the Thesis	5
CHAPTER 2: LITERATURE REVIEW	6
2.1 Challenges in fulfilling the growing demand for zero-emission transportation fuels	6
2.2 Nitrogen content in Diesel Feedstock and its impacts	8
2.3 Methods for Denitrogenation of Fuel	11
2.4 Extractive Denitrogenation as a Promising Separation Method	20

2.5	Ionic Liquids and Deep Eutectic Solvents	23
2.5.1	Introduction to Ionic Liquids	23
2.5.2	Properties of Ionic Liquids	25
2.5.3	Applications of Ionic Liquids in Extractive Denitrogenation	27
2.5.4	Introduction to Deep Eutectic Solvents	37
2.5.5	Properties of Deep Eutectic Solvents	39
2.5.6	Applications of Deep Eutectic Solvents in Liquid-liquid Separation Processes	42
2.6	Computational methods in selecting appropriate ILs and DESs	46
2.6.1	COSMO-RS model	49
2.6.2	COSMO-RS Applications for systems containing ILs and DESs	52
2.6.2	Quantum Chemical Methods for the Selection and Design of ILs and DESs	71
2.7	Summary	76
CHAPTER 3: METHODOLOGY		78
3.1	Step 1: Solvent screening using COSMO-RS	79
3.1.1	COSMO files generation	79
3.1.2	Expressions of Selectivity, Capacity and Performance Index at Infinite Dilution	96
3.2	Step 2: Quantum Chemical Calculation	100
3.2.1	Geometry Optimization	100
3.2.2	Calculation of Orbital Energy Values, Global Scalar Properties and Interaction Energy	100
3.3	Step 3: Liquid-liquid Equilibria Experiment	101
3.3.1	Materials	101

3.3.2	Synthesis of DESs	102
3.3.3	Liquid-liquid Equilibrium Experiment	103
3.3.4	Compositional Analysis	105
3.3.5	Consistency test using Othmer-Tobias and Hand correlations	107
3.3.6	Prediction of Ternary LLE using COSMO-RS model	107
3.3.7	Correlation of LLE data	108
CHAPTER 4: RESULTS AND DISCUSSION		111
4.1	COSMO-RS Screening	111
4.1.1	Qualitative screening of ionic liquids using σ -profiles and σ -potentials	111
4.1.2	Quantitative and Qualitative Screening of DESs	117
4.2	Quantum Chemical Calculation Results	150
4.2.1	Orbital energy values	151
4.2.2	Orbital Energy Gap	158
4.2.3	Global Scalar Properties	162
4.2.4	Interaction Energies	169
4.2.5	Partial Charge Transfer	173
4.2.6	Combination of parameters	177
4.3	Ternary LLE Results	179
4.3.1	Consistency Test	181
4.3.2	Systems with IL [EMIM][EtSO ₄]	182
4.3.3	Systems with IL [EMPY][EtSO ₄]	190
4.3.4	Systems with IL [EMIM][MeSO ₃]	199

4.3.5	Systems with IL [EMIM][EtSO ₄] + [EMPY][EtSO ₄]	208
4.3.6	Systems with TBAB/EG (1:2) DES	214
4.3.7	Systems with TBPB/EG (1:2) DES	223
4.3.8	Distribution Ratio and Selectivity	231
CHAPTER 5: CONCLUSION		242
5.1	Qualitative and Quantitative Screening of ILs and DESs	242
5.2	Quantum Chemical Calculation	245
5.3	Ternary LLE Experimental Work	246
5.4	General conclusion	247
REFERENCES		248
LIST OF PUBLICATIONS AND CONFERENCE PROCEEDINGS		263
APPENDIX		265

LIST OF FIGURES

Figure 2.1	The lone pair of electrons in pyrrole is delocalized and hence not available for donation, making it a non-basic compound.	9
Figure 2.2	The lone pair of electrons in pyridine is localized and hence available for donation, making it a basic compound.	9
Figure 2.3	HDS reaction path for dibenzothiophene as suggested by Gates and Topsoe (Gates and Topsoe, 1997)	12
Figure 2.4	Reaction path for HDN of quinoline as suggested by Eijsbouts et al. (Eijsbouts et al., 1991)	12
Figure 2.5	A schematic figure of 1-ethyl-3-methylimidazolium ethylsulfate as an example of IL.	24
Figure 2.6	Phase diagram for the eutectic mixtures of ChCl with either phenylpropionic acid or phenylacetic acid reproduced from Abbott et al. (Abbott et al., 2004)	41
Figure 4.1	σ -profiles for all (a) cations, (b) anions and (c) heterocyclic nitrogen compounds studied. Dashed straight lines indicate the threshold value for hydrogen bond ($\sigma_{hb} = \pm 0.0085 \text{ e} \text{ \AA}^{-2}$)	112
Figure 4.2	σ -potential for all (a) cations, (b) anions and (c) heterocyclic nitrogen compounds studied. Dashed straight lines indicate the threshold value for hydrogen bond ($\sigma_{hb} = \pm 0.0085 \text{ e} \text{ \AA}^{-2}$)	113
Figure 4.3	σ -profiles for the ionic liquid [EPY][EtSO ₄] and heterocyclic nitrogen compounds. Dashed straight lines indicate the threshold value for hydrogen bond ($\sigma_{hb} = \pm 0.0085 \text{ e} \text{ \AA}^{-2}$)	116
Figure 4.4	σ -potential for the ionic liquid [EPY][EtSO ₄] and heterocyclic nitrogen compounds. Dashed straight lines indicate the threshold value for hydrogen bond ($\sigma_{hb} = \pm 0.0085 \text{ e} \text{ \AA}^{-2}$)	116
Figure 4.5	Depiction of molecular interaction between salt cation, anion, HBD and nitrogen compound. The DES TMAC/EG (1:2) is taken as model DES while pyrrole (a) and pyridine (b) as representative 5-membered and 6-membered nitrogen compounds, respectively. Thick dash represents hydrogen bonding while small dots represent electrostatic interaction.	118
Figure 4.6	σ -profiles of selected DESs and simulated diesel with a) 5-membered compounds and b) 6-membered compounds. Vertical dashed lines represent the threshold value for the hydrogen bond interaction, ($\sigma_{hb} = \pm 0.0085 \text{ e} \text{ \AA}^{-2}$)	120
Figure 4.7	σ -potentials of selected DESs and simulated diesel with a) 5-membered compounds and b) 6-membered compounds. Vertical dashed lines represent the threshold value for the hydrogen bond interaction, ($\sigma_{hb} = \pm 0.0085 \text{ e} \text{ \AA}^{-2}$)	121
Figure 4.8	Selectivity (a) and capacity (b) at infinite dilution for representative DESs towards nitrogen compounds in comparison of the effect of nitrogen heterocyclic structure.	122

Figure 4.9	Selectivity at infinite dilution for nitrogen compounds according to different types of DESs in comparison of the effect of cation choice. a) Choline-based DESs, b) tetramethyl-based DESs, c) tetrabutyl-based DESs, d) phenylammonium and phenylphosphonium-based DESs.	126
Figure 4.10	Capacity at infinite dilution for nitrogen compounds according to different types of DESs in comparison of the effect of cation choice. a) Choline-based DESs, b) tetramethyl-based DESs, c) tetrabutyl-based DESs, d) phenylammonium and phenylphosphonium-based DESs.	130
Figure 4.11	Selectivity at infinite dilution in comparison of anion choice. a) tetramethyl-based DESs. b) tetrabutyl-based DESs.	134
Figure 4.12	Capacity at infinite dilution in comparison of anion choice. a) tetramethyl-based DESs. b) tetrabutyl-based DESs.	136
Figure 4.13	Selectivity at infinite dilution in comparison of HBD choice. a) ChCl-based DES b) TMAC-based DESs.	139
Figure 4.14	Capacity at infinite dilution in comparison of HBD choice. a) ChCl-based DES b) TMAC-based DESs.	140
Figure 4.15	Selectivity at infinite dilution in comparison of salt:HBD molar ratio.	146
Figure 4.16	Capacity at infinite dilution in comparison of salt:HBD molar ratio.	147
Figure 4.17	HOMO and LUMO of [EPY][EtSO ₄]. a) HOMO, b) LUMO.	151
Figure 4.18	HOMO and LUMO location of PYR-[EPY][EtSO ₄] complex. a) HOMO, b) LUMO.	152
Figure 4.19	HOMO and LUMO energy values for individual species (a), ionic liquids (b) and its complexes with PYR (c) and PYRD (d)	153
Figure 4.20	HOMO-LUMO Energy Gap for individual species (a), ionic liquids (b) and its complexes with PYR (c) and PYRD (d)	159
Figure 4.21	Global hardness and global softness for individual species (a), ionic liquids (b) and its complexes with PYR (c) and PYRD (d)	163
Figure 4.22	Electronegativity and electrophilicity index for individual species (a), ionic liquids (b) and its complexes with PYR (c) and PYRD (d)	166
Figure 4.23	Interaction energies for ionic liquid (a) and its complexes with with PYR (b) and PYRD (c)	170
Figure 4.24	Tie-lines for the ternary systems a) [EMIM][EtSO ₄] (1) + pyrrole (2) + <i>n</i> -hexadecane (3), b) [EMIM][EtSO ₄] (1) + pyridine (2) + <i>n</i> -hexadecane (3), c) [EMIM][EtSO ₄] (1) + indoline (2) + <i>n</i> -hexadecane (3) and d) [EMIM][EtSO ₄] (1) + quinoline (2) + <i>n</i> -hexadecane (3) at $T=298.15$ K and P_{atm} . Full circle and solid lines indicate experimental tie-lines, empty circle and dashed lines indicate tie-lines from NRTL calculation and full triangle and dotted lines indicate calculated tie-lines from COSMO-RS model.	187

- Figure 4.25 Tie-lines for the ternary system a) [EMPY][EtSO₄] (1) + pyrrole (2) + *n*-hexadecane (3), b) [EMPY][EtSO₄] (1) + pyridine (2) + *n*-hexadecane, c) [EMPY][EtSO₄] (1) + indoline (2) + *n*-hexadecane and d) [EMPY][EtSO₄] (1) + quinoline (2) + *n*-hexadecane at $T=298.15$ K and P_{atm} . Full circle and solid lines indicate experimental tie-lines, empty circle and dashed lines indicate tie-lines from NRTL calculation and full triangle and dotted lines indicate calculated tie-lines from COSMO-RS model. 196
- Figure 4.26 Tie-lines for the ternary system a) [EMIM][MeSO₃] (1) + pyrrole (2) + *n*-hexadecane (3), b) [EMIM][MeSO₃] (1) + pyridine (2) + *n*-hexadecane (3) c) [EMIM][MeSO₃] (1) + indoline (2) + *n*-hexadecane (3) and d) [EMIM][MeSO₃] (1) + quinoline (2) + *n*-hexadecane (3) at $T=298.15$ K and P_{atm} . Full circle and solid lines indicate experimental tie-lines, empty circle and dashed lines indicate tie-lines from NRTL calculation and full triangle and dotted lines indicate calculated tie-lines from COSMO-RS model. 205
- Figure 4.27 Tie-lines for the ternary system a) ([EMIM][EtSO₄] + [EMPY][EtSO₄]) (1) + indoline (2) + *n*-hexadecane (3) and b) ([EMIM][EtSO₄] + [EMPY][EtSO₄]) (1) + quinoline (2) + *n*-hexadecane (3) at $T=298.15$ K and P_{atm} . Full circle and solid lines indicate experimental tie-lines, empty circle and dashed lines indicate tie-lines from NRTL calculation and full triangle and dotted lines indicate calculated tie-lines from COSMO-RS model. 213
- Figure 4.28 Tie-lines for the ternary system a) TBAB/EG (1:2) (1) + pyrrole (2) + *n*-hexadecane (3), b) TBAB/EG (1:2) (1) + pyridine (2) + *n*-hexadecane (3), c) TBAB/EG (1:2) (1) + indoline (2) + *n*-hexadecane (3) and d) TBAB/EG (1:2) (1) + quinoline (2) + *n*-hexadecane (3) at $T=298.15$ K and P_{atm} . Full circle and solid lines indicate experimental tie-lines, empty circle and dashed lines indicate tie-lines from NRTL calculation and full triangle and dotted lines indicate calculated tie-lines from COSMO-RS model. 220
- Figure 4.29 Tie-lines for the ternary systems a) TBPB/EG (1:2) (1) + pyrrole (2) + *n*-hexadecane (3), b) TBPB/EG (1:2) (1) + pyridine (2) + *n*-hexadecane (3), c) TBPB/EG (1:2) (1) + indoline (2) + *n*-hexadecane (3) and d) TBPB/EG (1:2) (1) + quinoline (2) + *n*-hexadecane (3) at $T=298.15$ K and P_{atm} . Full circle and solid lines indicate experimental tie-lines, empty circle and dashed lines indicate tie-lines from NRTL calculation and full triangle and dotted lines indicate calculated tie-lines from COSMO-RS model. 228
- Figure 4.30 Distribution ratio, D (a) and selectivity, S , (b) of pyrrole as a function of pyrrole concentration in the raffinate phase using various solvents in the ternary LLE experiments. Filled circle indicates [EMIM][EtSO₄], empty circle indicate [EMPY][EtSO₄], filled triangle indicate [EMIM][MeSO₃], empty triangle indicate TBAB/EG (1:2) and filled squares indicate TBPB/EG (1:2). 232

- Figure 4.31 Distribution ratio, D (a) and selectivity, S , (b) of pyridine as a function of pyridine concentration in the raffinate phase using various solvents in the ternary LLE experiments. Filled circle indicates [EMIM][EtSO₄], empty circle indicate [EMPY][EtSO₄], filled triangle indicate [EMIM][MeSO₃], empty triangle indicate TBAB/EG (1:2) and filled squares indicate TBPB/EG (1:2). 234
- Figure 4.32 Distribution ratio, D (a) and selectivity, S , (b) of indoline as a function of indoline concentration in the raffinate phase using various solvents in the ternary LLE experiments. Filled circle indicates [EMIM][EtSO₄], empty circle indicate [EMPY][EtSO₄], filled triangle indicate [EMIM][EtSO₄] + [EMPY][EtSO₄], empty triangle indicate [EMIM][MeSO₃], filled square indicate TBAB/EG (1:2) and empty square indicate TBPB/EG (1:2). 236
- Figure 4.33 Distribution ratio, D (a) and selectivity, S , (b) of quinoline as a function of quinoline concentration in the raffinate phase using various solvents in the ternary LLE experiments. Filled circle indicates [EMIM][EtSO₄], empty circle indicate [EMPY][EtSO₄], filled triangle indicate [EMIM][EtSO₄] + [EMPY][EtSO₄], empty triangle indicate [EMIM][MeSO₃], filled square indicate TBAB/EG (1:2) and empty square indicate TBPB/EG (1:2). 238

LIST OF TABLES

Table 2.1	Average properties of crude oil refined in the US according to year (Poole & Poole, 2010)	6
Table 2.2	Properties of various types of gas oil	7
Table 2.3	The use of organic solvents for extractive denitrogenation of model diesel.	23
Table 2.4	Experimental LLE data on the use of ILs for extractive denitrogenation	31
Table 2.5	Experimental extraction data on the use of ILs to extract nitrogen compounds from model fuel	32
Table 2.6	List of cations and anions abbreviation and full names used in Tables 2.4 and 2.5	37
Table 2.7	Name and structure of typical salt and HBD used in the synthesis of DES	39
Table 2.8	DESs used in liquid-liquid extraction process reported in the literature	45
Table 2.9	Full names and abbreviation of the salts and HBDs mentioned in Table 2.8	46
Table 3.1	Structure, molecular formula and abbreviation for the aromatic nitrogen compound	80
Table 3.2	Structure, molecular formula and abbreviation for cations and anions of the screened ionic liquids	82
Table 3.3	Structure of DES constituent used in this work	87
Table 3.4	Full name and abbreviation of DESs screened using COSMO-RS	93
Table 3.5	Composition of Simulated Diesel	98
Table 3.6	Ionic liquids used in this work	101
Table 3.7	DES constituent used in this work	102
Table 3.8	Aromatic nitrogen compounds used in this work	102
Table 3.9	Model diesel compound used in this work	102
Table 3.10	Solvent for NMR spectroscopy used in this work	102
Table 4.1	Maximum and minimum values for S^∞ , C^∞ and PI reported by DESs for each nitrogen heterocycles.	124
Table 4.2	Summary of the factors affecting the values of S^∞ and C^∞ for denitrogenation using DESs	149
Table 4.3	The most favourable IL for each heterocyclic nitrogen compound according to different parameters	157
Table 4.4	Partial charges (in a.m.u) from NBO analysis for ILs before and after interaction with each nitrogen compounds.	174
Table 4.5	Parameters of Othmer-Tobias and Hand correlation for each ternary LLE system and the values of regression coefficient R^2 .	181
Table 4.6	Ternary tie-lines for the system [EMIM][EtSO ₄] (1) + pyrrole (2) + <i>n</i> -hexadecane (3) at T=25°C and P _{atm}	182
Table 4.7	Ternary tie-lines for the system [EMIM][EtSO ₄] (1) + pyridine (2) + <i>n</i> -hexadecane (3) at T=25°C and P _{atm}	183

Table 4.8	Ternary tie-lines for the system [EMIM][EtSO ₄] (1) + indoline (2) + <i>n</i> -hexadecane (3) at T=25°C and P _{atm}	184
Table 4.9	Ternary tie-lines for the system [EMIM][EtSO ₄] (1) + quinoline (2) + <i>n</i> -hexadecane (3) at T=25°C and P _{atm}	185
Table 4.10	RMSD values for NRTL correlation and COSMO-RS prediction of each ternary LLE system containing [EMIM][EtSO ₄]	189
Table 4.11	The values of NRTL binary interaction parameters for each ternary systems containing the IL [EMIM][EtSO ₄]	189
Table 4.12	Ternary tie-lines for the system [EMPY][EtSO ₄] (1) + pyrrole (2) + <i>n</i> -hexadecane (3) at T=25°C and P _{atm}	191
Table 4.13	Ternary tie-lines for the system [EMPY][EtSO ₄] (1) + pyridine (2) + <i>n</i> -hexadecane (3) at T=25°C and P _{atm}	192
Table 4.14	Ternary tie-lines for the system [EMPY][EtSO ₄] (1) + indoline (2) + <i>n</i> -hexadecane (3) at T=25°C and P _{atm}	193
Table 4.15	Ternary tie-lines for the system [EMPY][EtSO ₄] (1) + quinoline (2) + <i>n</i> -hexadecane (3) at T=25°C and P _{atm}	194
Table 4.16	RMSD values for NRTL correlation and COSMO-RS prediction of each ternary LLE system containing [EMPY][EtSO ₄]	198
Table 4.17	The values of NRTL binary interaction parameters between [EMPY][EtSO ₄] and nitrogen compounds and <i>n</i> -hexadecane	198
Table 4.18	Ternary tie-lines for the system [EMIM][MESO ₃] (1) + pyrrole (2) + <i>n</i> -hexadecane (3) at T=25°C and P _{atm}	200
Table 4.19	Ternary tie-lines for the system [EMIM][MESO ₃] (1) + pyridine (2) + <i>n</i> -hexadecane (3) at T=25°C and P _{atm}	201
Table 4.20	Ternary tie-lines for the system [EMIM][MESO ₃] (1) + indoline (2) + <i>n</i> -hexadecane (3) at T=25°C and P _{atm}	202
Table 4.21	Ternary tie-lines for the system [EMIM][MESO ₃] (1) + quinoline (2) + <i>n</i> -hexadecane (3) at T=25°C and P _{atm}	203
Table 4.22	RMSD values for NRTL correlation and COSMO-RS prediction of ternary LLE systems containing the IL [EMIM][MeSO ₃]	207
Table 4.23	The values of NRTL binary interaction parameters between [EMIM][MeSO ₃] and nitrogen compounds and <i>n</i> -hexadecane	207
Table 4.24	Ternary tie-lines for the system [EMIM][EtSO ₄] + [EMPY][EtSO ₄] (1) + indoline (2) + <i>n</i> -hexadecane (3) at T=25°C and P _{atm}	210
Table 4.25	Ternary tie-lines for the system [EMIM][EtSO ₄] + [EMPY][EtSO ₄] (1) + quinoline (2) + <i>n</i> -hexadecane (3) at T=25°C and P _{atm}	211
Table 4.26	RMSD values for NRTL correlation and COSMO-RS prediction of ternary LLE system containing the mixed ILs [EMIM][EtSO ₄]+[EMPY][EtSO ₄]	214
Table 4.27	The values of NRTL binary interaction parameters between the mixed ILs [EMIM][EtSO ₄]+ [EMPY][EtSO ₄] and nitrogen compounds and <i>n</i> -hexadecane	214

Table 4.28	Ternary tie-lines for the system TBAB/EG (1:2) (1) + pyrrole (2) + <i>n</i> -hexadecane (3) at T=25°C and P _{atm}	216
Table 4.29	Ternary tie-lines for the system TBAB/EG (1:2) (1) + pyridine (2) + <i>n</i> -hexadecane (3) at T=25°C and P _{atm}	217
Table 4.30	Ternary tie-lines for the system TBAB/EG (1:2) (1) + indoline (2) + <i>n</i> -hexadecane (3) at T=25°C and P _{atm}	218
Table 4.31	Ternary tie-lines for the system TBAB/EG (1:2) (1) + quinoline (2) + <i>n</i> -hexadecane (3) at T=25°C and P _{atm}	219
Table 4.32	RMSD values for NRTL correlation and COSMO-RS prediction of ternary LLE systems containing the DES TBAB/EG (1:2)	222
Table 4.33	The values of NRTL binary interaction parameters for each ternary systems containing the DES TBAB/EG (1:2)	222
Table 4.34	Ternary tie-lines for the system TBPB/EG (1:2) (1) + pyrrole (2) + <i>n</i> -hexadecane (3) at T=25°C and P _{atm}	224
Table 4.35	Ternary tie-lines for the system TBPB/EG (1:2) (1) + pyridine (2) + <i>n</i> -hexadecane (3) at T=25°C and P _{atm}	225
Table 4.36	Ternary tie-lines for the system TBPB/EG (1:2) (1) + indoline (2) + <i>n</i> -hexadecane (3) at T=25°C and P _{atm}	226
Table 4.37	Ternary tie-lines for the system TBPB/EG (1:2) (1) + quinoline (2) + <i>n</i> -hexadecane (3) at T=25°C and P _{atm}	227
Table 4.38	RMSD values for NRTL correlation and COSMO-RS prediction of ternary LLE systems containing the DES TBPB/EG (1:2)	230
Table 4.39	The values of NRTL binary interaction parameters between TPBP/EG (1:2) and nitrogen compounds and <i>n</i> -hexadecane	230

LIST OF ABBREVIATIONS

Ionic liquid	IL
Deep eutectic solvent	DES
Hydrogen bond donor	HBD
Nuclear magnetic resonance	NMR
Liquid-liquid equilibrium	LLE
Hydrodesulfurization	HDS
Hydrodenitrogenation	HDN
Conductor-like Screening Model for Real Solvents	COSMO-RS
Non-random two-liquid	NRTL
Universal Quasi-chemical	UNIQUAC
UNIQUAC Functional-group Activity Coefficients	UNIFAC
American Petroleum Institute	API
Straight run gas oil	SRGO
Light cycle oil	LCO
Coker gas oil	CGO
Oil sands gas oil	OSGO
Coal liquid gas oil	CLGO
Fluidized catalytic cracking	FCC
Nuclear magnetic resonance	NMR
Vapor-liquid equilibrium	VLE
Solid-liquid equilibrium	SLE
Group contribution method	GCM
Highest occupied molecular orbital	HOMO
Lowest unoccupied molecular orbital	LUMO
Density functional theory	DFT
Triple zeta valence potential	TZVP

NOMENCLATURE

D	Distribution coefficient
S	Selectivity
x'_1	Mole fraction of solvent in the extract layer
x'_2	Mole fraction of nitrogen compound in the extract layer
x'_3	Mole fraction of <i>n</i> -hexadecane compound in the extract layer
x''_1	Mole fraction of solvent in the raffinate layer
x''_2	Mole fraction of nitrogen compound in the raffinate layer
x''_3	Mole fraction of <i>n</i> -hexadecane compound in the raffinate layer
a	Fitting parameters of Othmer-Tobias correlation
b	Fitting parameters of Othmer-Tobias correlation
c	Fitting parameters of Hand correlation
d	Fitting parameters of Hand correlation
γ^∞	Activity coefficient at infinite dilution
σ, σ'	Polarization charge density
E_{misfit}	Electrostatic misfit energy (kJ/mol/A ²)
E_{hb}	Hydrogen bonding interaction energy (kJ/mol/A ²)
E_{vdW}	van der Waals interaction energy (kJ/mol/A ²)
c_{hb}	Strength coefficient (kJ/mol/A ²)
a_{eff}	Effective contact area (A ²)
τ_{vdW}	Element-specific parameter for dispersion coefficient (kJ/mol/A ²)
α'	General constant (kJ/mol/A ²)
σ_{hb}	Polarization charge density threshold for hydrogen bonding (e/A ²)
A_S	Total surface area for the ensemble S (A ²)
A^{X^i}	Total surface area for the compound X^i (A ²)
$\mu_S(\sigma)$	Chemical potential of a surface segment (kcal/mol/A ²)
$\gamma_S(\sigma)$	Activity coefficient of a surface segment
V^X	Molecular volume of compound X^i (A ³ /mol)
V_S	Average molecular volume of the solvent (A ³ /mol)
V_0	Partial volume of an ethylene unit used for normalisation purposes (A ³ /mol)
R	Universal gas constant
T	Temperature (K)
I	Ionization potential (Hartree)
A	Electron affinity (Hartree)
$-\epsilon_{HOMO}, -\epsilon_{LUMO}$	One electron eigenvalues related to the frontier orbitals (Hartree)
η	Global hardness (Hartree)
S	Global softness (Hartree)
χ	Electronegativity (Hartree)
ω	Electrophilicity index (Hartree)
ΔE	Interaction energy (Hartree)
x_i^{EXP}	Mole fraction of solute i in the experimental definition

$x_i^{\text{COSMO-RS}}$	Mole fraction of solute i in the electroneutral approach
n_i	Number of moles of solute i
n_j	Number of moles of carrier j
n_{DES}	Number of moles of the DES as a whole
n_{cation}	Number of moles of the DES cation
n_{anion}	Number of moles of the DES anion
$n_{HBD/CA}$	Number of moles of HBD or CA in the DES.
H_i	Peak area of a single hydrogen atom in component i
ω	Liquid-liquid splitting ratio
x_i^{L1}	Amount of component i in liquid phase $L1$
x_i^{L2}	Amount of component i in liquid phase $L2$
γ_i^{L1}	Activity coefficients of component i in $L1$
γ_i^{L2}	Activity coefficients of component i in $L2$
τ_{ij}, τ_{ji}	Binary interaction parameters
α_{ij}	Nonrandomness parameter
z	Coordination number

University of Malaya

LIST OF APPENDICES

- APPENDIX A: Selectivity, Capacity and Performance of DESs at Infinite Dilution
- APPENDIX B: Sigma Profiles and Sigma Potentials of Nitrogen Compounds, Cations, Anions and HBDs used for screening of DESs
- APPENDIX C: Quantum Chemical Calculation Results
- APPENDIX D: NMR Spectroscopy for pure compounds used in ternary LLE experiments

University of Malaya

CHAPTER 1: INTRODUCTION

1.1 Background

The increasing usage of transportation fuel has led to the increased emissions of toxic gases. Among the major toxic gases emitted, sulfur and nitrogen oxides have a detrimental effect on air quality and on general public health. These gases cause the formation of acid rain, increase the air pollution index, and are carcinogenic (Turaga et al., 2003). Therefore, regulations have been targeted towards producing a zero-emission transportation fuel, one which would emit a minimal amount of sulfur and nitrogen oxides. Indeed, in developed nations, the limit of sulfur content in transportation fuel was set at 50 ppm in 2001, (*Directive of The European Parliament and of The Council on the quality of petrol and diesel fuels and amending Directive 98/70/EC*, 2001) dropping as low as 15 ppm in 2006 ("US EPA Clean Air Act Tier 2; 1999,"). Further, under new regulations, the upper limit of nitrogen concentration in diesel was reduced in 2011 from less than 70 ppm to less than 0.1 ppm (Anantharaj et al., 2010a; Turaga, et al., 2003).

The conventional method for removing sulfur and nitrogen content is through hydrotreatment: hydrodesulfurization (HDS) and hydrodenitrogenation (HDN). However, although hydrotreatment processes are effective at removing straight-chain sulfur and nitrogen compounds, they are less efficient at removing refractory aromatic sulfur and nitrogen compounds (Song, 2003). Moreover, aromatic nitrogen compounds are known to inhibit the efficiency of the conventional HDS process by competitive adsorption and catalyst poisoning (Zhang et al., 2009). Studies have shown that removing aromatic nitrogen compounds prior to desulfurization increases the efficiency of the HDS process (Almarri et al., 2008). Thus, to produce a zero-emission transportation fuel, knowledge of denitrogenation is of a similar significance to knowledge of the desulfurization of fuel.

Due to the simplicity of its separation mechanism and mild operating conditions, the liquid-liquid extraction process using alternative solvents such as ionic liquids (ILs) and deep eutectic solvents (DESs) is considered to be one of the most viable options for the pre-treatment of gas oil for denitrogenation prior to the desulfurization process. Carefully selected ILs and DESs can be tailored to have favorable properties as extraction solvents including being non-volatile and can be designed according to the desired application requirements.

1.2 Problem Statement and Significance of Study

Recently, oil refineries have started to process crude oil with a higher content of sulfur and nitrogen compounds due to the limited oil reserves remaining in the world. As a result, besides conventional petroleum oil reserves, unconventional fossil-fuel reserves such as tar sands, oil shale, and coal liquids have been considered for inclusion in the diesel pool. Nevertheless, these unconventional fossil-fuel reserves contain higher amounts of sulfur and nitrogen than do conventional ones (Laredo S et al., 2001).

The conventional method for removing sulfur and nitrogen compounds from gas oil is hydrotreatment, which is energy-intensive since it operates at severe conditions (300 atm H₂ and 600 K) (Dong et al., 1997a). In this process, both HDS and HDN take place simultaneously. However, aromatic nitrogen compounds in the gas oil suppress the efficiency of the HDS process via competitive adsorption and catalyst deactivation (Dong, et al., 1997a). Moreover, the HDN process uses up more hydrogen and involves more complex reaction stages than does HDS (Furimsky et al., 2005).

Liquid-liquid extraction using ILs and DESs as green extractive solvents for the removal of nitrogen compounds is seen as an attractive alternative process that can be operated under mild conditions (room temperature and atmospheric pressure). The efficiency of this process greatly depends on solvent performance. However, the selection

of the most appropriate ILs and/or DESs is not trivial due to the many possible choices. Moreover, it is impractical to conduct costly and time-consuming experiments every time there is a need to identify and conclude whether a certain class of ILs or DESs is suitable. Thus, a prediction method is necessary to screen ILs and DESs.

1.3 Research Philosophy

This research aspires to provide recommendations regarding the suitable ILs and DESs for use in extractive denitrogenation in the pursuit of producing a zero-emission transportation fuel. The liquid-liquid extraction process is selected as the most practical option for the pre-treatment of gas oil prior to entering the HDS unit for study, owing to its mild operating conditions and the simplicity of the separation mechanism. Understanding the molecular interactions between solvent and solute is vital for selecting the appropriate solvent for the extraction process. The selection of ILs and DESs as extractive solvents based on predictive methods, such as quantum chemical calculations and COSMO-RS prediction, provides deep insights into the molecular interaction between green solvents and aromatic nitrogen compounds. Ternary liquid-liquid equilibrium (LLE) experiments were performed to investigate the performance of selected ILs and DESs in separating aromatic nitrogen compounds from a model diesel compound and to validate the results of the calculations.

1.4 Research Objectives

This research aims to systematically select and screen potential ILs and DESs for use in extractive denitrogenation of diesel to enhance the efficiency of desulfurization towards the production of zero-emission transportation fuel. To achieve this, specific objectives have been set as follows:

1. To screen potential ILs and DESs for extractive denitrogenation using an *a priori* predictive model, COSMO-RS.
2. To investigate the molecular attributes affecting the selection of ILs for the removal of nitrogen compounds in diesel based on quantum chemical calculations.
3. To validate experimentally the screening process and results of the predictive model by performing a ternary, liquid-liquid equilibria study for systems containing ILs or DESs, nitrogen compounds, and model diesel compounds.
4. To analyze the thermodynamic phase behavior and performance of selected ILs and DESs in separating nitrogen compounds from model diesel compounds.
5. To apply macroscopic thermodynamic models to correlate the experimental data for potential use in design calculations, using process-simulation software.

1.5 Research Methodology

The methodological steps adopted to address the research objectives are as follows:

1. Qualitative and quantitative screening of potential ILs and DESs using COSMO-RS.
2. Evaluation by quantum chemical calculations of molecular interactions in systems containing shortlisted ILs or DESs and aromatic nitrogen compounds.
3. Synthesis of selected DESs.
4. Conducting ternary LLE experiments for systems containing selected ILs or DESs, aromatic nitrogen compounds, and a model diesel compound.
5. Prediction of ternary LLE phase equilibria using COSMO-RS.
6. Compositional analysis of the extraction mixtures using nuclear magnetic resonance (NMR) spectroscopy.
7. Test for consistency of the experimental LLE data using Othmer-Tobias and Hand correlation to establish the validity of the compositional profile.

8. Correlation of the experimental LLE data with the Non-Random Two-Liquid (NRTL) activity coefficient model.

1.6 Outline of the Thesis

This thesis comprises a bibliography and five chapters, as follows:

Chapter 1 provides an overview of the need for the denitrogenation of liquid fuels to meet the stringent environmental regulations requiring the production of a zero-emission transportation fuel.

Chapter 2 discusses a literature review covering the challenges in producing zero-emission transportation fuels, the need for denitrogenation, and a comparison between various existing approaches to removing nitrogen compounds from liquid fuels. In addition, the applications of ILs and DESs in the petroleum refining process are reviewed and summarized.

Chapter 3 explains the research methodology in detail for the screening of ILs and DESs using COSMO-RS, quantum chemical calculations, ternary LLE experiments, compositional analysis using NMR spectroscopy, prediction using COSMO-RS, and correlation with the NRTL model.

Chapter 4 discusses the results and highlights the most important findings of this thesis.

Chapter 5 concludes the thesis and provides recommendations for future work.

CHAPTER 2: LITERATURE REVIEW

2.1 Challenges in fulfilling the growing demand for zero-emission transportation fuels

The decreasing reserve of conventional crude oil remaining in various parts of the world makes a growing dependence on heavy oils and residues which contain inevitably high amount of heteroatoms. Indeed, as shown in Table 2.1, the crude oil available to the refiners nowadays is of low quality where the sulfur content increases in the last 30 years together with the decrease in API gravity while at the same time, the total worldwide consumption of petroleum products continues to increase rapidly. API gravity stands for American Petroleum Institute gravity which indicates whether a petroleum liquid is heavier or lighter than water. Greater number of API gravity indicates that the liquid is lighter than water.

Table 2.1: Average properties of crude oil refined in the US according to year (Song, 2003)

Property	1981	1991	2001
Average Sulfur content of crude oil refined in US (ppm)	8900	11300	14200
API gravity (°API)	33.74	31.64	30.49
Total worldwide petroleum consumption (million barrels/day)	60.90	66.72	77.12

As a consequence, it is inevitable for the energy industry to deal with heavier feedstock which contains higher concentrations of nitrogen and sulfur compounds. One alternative is to blend other refinery hydrocarbon streams into the diesel pool to meet the increasing demand in consumption. Other than the straight run gas oil (SRGO), the refiners may need to blend light cycle oil (LCO), a by-product of fluidized catalytic cracking (FCC) and coker gas oil (CGO), a by-product of delayed coker as input to the diesel production. From Table 2.2, although the CGO has a lower content of sulfur than

SRGO, the concentrations of nitrogen and aromatic compounds are higher in CGO compared to SRGO. Apart from blending LCO and CGO, other unconventional fossil energy resources such as oil sands, coal liquid and shale oil are gaining increasing attention to be part of the diesel pool. However, oil sands gas oil (OSGO) and coal liquid gas oil (CLGO) contains even higher amount of nitrogen compounds up to two orders of magnitude higher than those in the petroleum fractions of diesel range. From Table 2.2, it is observed that while gas oil fractions derived from petroleum contain much higher concentrations of sulfur than nitrogen compounds, CLGO generally have higher nitrogen content than sulfur compounds.

Table 2.2: Properties of various types of gas oil

Properties	SRGO (Al-Barood et al., 2005)	LCO (Laredo et al., 2002)	CGO (Al-Barood, et al., 2005)	AGO (Laredo, et al., 2002)	CLGO (Sumbogo Murti et al., 2002)
Specific Gravity (g/ml)	0.846	1.000	0.876	0.853	NA
API gravity (°API)	NA	19.36	NA	34.5	NA
Sulfur (ppm)	14 000	25 520	7 600	11 550	800
Nitrogen (ppm)	60	22.05	1 020	318	8 000
Aromatics (ppm)	270 000	593 300	375 000	325 600	620 000
Boiling Range (°C)	365	251-375	370	241-360	<300

The conventional method of desulfurization which is hydrodesulfurization (HDS) is able to reduce the sulfur contents to < 50 ppm. However, it is more challenging to use the same method to remove refractory sulfur compounds such as dibenzothiophene and their alkylated derivatives (e.g. 4-methyldibenzothiophene and 4,6-dimethyldibenzothiophene) which remain in the diesel-range transportation fuel even after the HDS process. The limit for sulfur content in diesel set by the US Environmental Protection Agency (EPA) is < 15 ppm by 2010, but it is almost impossible to achieve this standard using HDS process alone. The HDS process is made even more difficult by the

presence of nitrogen compounds which have negative impacts towards the HDS reaction. Sulfur heteroatoms need to be removed from petroleum fractions due to the following reasons:

1. Reduce or eliminate corrosion during refining, handling and/or use of the products
2. Satisfy an acceptable degree of specification
3. Increase the stability and performance of transportation fuels
4. Decrease smoke formation
5. Improve the burning characteristics of the transportation fuel to an environmentally acceptable level

2.2 Nitrogen content in Diesel Feedstock and its impacts

Nitrogen compounds existing in the crude oil derived from petroleum can be categorized into two groups, basic and non-basic compounds.

1. Non-basic (or neutral) compounds have a 5-membered ring structure where the lone pair of electrons is delocalized and contributes to the aromatic π -electron system as illustrated by Figure 2.1. The N atom in these 5-membered ring compounds is connected to a H atom. Non-basic nitrogen compounds can act as weak acids due to the N-H bond and can also act as weak bases due to the basicity of the N atom. Examples of non-basic nitrogen compounds include pyrrole, indole, indoline, carbazole and their alkyl derivatives.

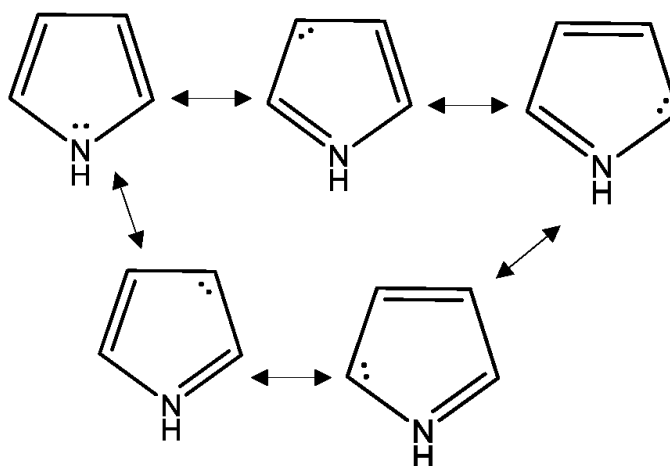


Figure 2.1: The lone pair of electrons in pyrrole is delocalized and hence not available for donation, making it a non-basic compound.

2. Basic compounds have 6-membered ring structure where the lone pair of electrons extends in the plane of the ring and are not part of the aromatic system as illustrated by Figure 2.2. The lone pair of electron on the ring system is responsible for the basicity of the 6-membered ring nitrogen compounds. Examples of basic nitrogen compounds include pyridine, quinoline, benzoquinoline and their alkyl derivatives.

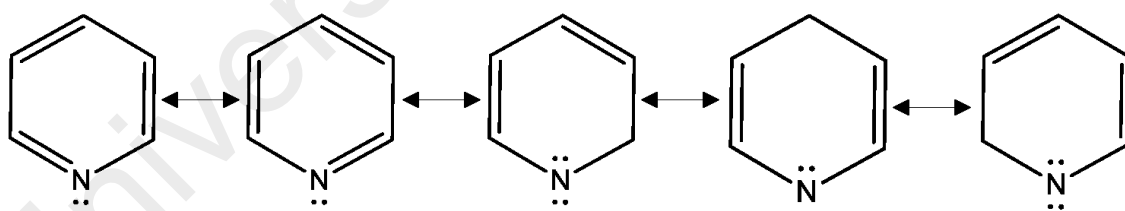


Figure 2.2: The lone pair of electrons in pyridine is localized and hence available for donation, making it a basic compound.

Nitrogen compounds need to be removed at various streams in the oil refinery due to the following reasons:

- a) The catalysts in processes such as isomerization, reforming, catalytic cracking and hydrocracking are very sensitive to nitrogen compounds. Basic nitrogen compounds can

be adsorbed on the acidic sites of the various catalysts used in each of the processes and leads to poisoning of the active sites of the catalysts. For example, basic nitrogen compounds are adsorbed on active acid sites in the catalytic cracker thus reducing the cracking activity of the catalysts used (Furimsky, et al., 2005).

b) The presence of nitrogen compounds in produced fuels affects its stability. The non-basic nitrogen compounds can easily undergo auto-oxidation reaction by an action of molecular oxygen and condensation with the formation of high-molecular color bodies and sediments. Many specialists believed that nitrogen content need to be regulated to below 100 ppm to ensure sufficient stability of the middle distillate fuels. It has been reported that fuel products which contain considerably more nitrogen may also contain unsaturated hydrocarbons, which in turns results in higher bromine numbers. These products show instability in color and a tendency to form sediments (Wandas et al., 2004).

c) It is widely accepted that the removal of refractory sulfur compounds by conventional HDS is extremely challenging and the coexisting nitrogen compounds makes deep desulfurization via HDS even more difficult because presence of nitrogen compounds is known to inhibit the hydrodesulfurization (HDS) process. The inhibiting effects of nitrogen compounds to HDS process can be due to poisoning of two major catalytic sites in the hydrotreatment process which are hydrogenolysis and hydrogenation sites (Kwak et al., 2001). Hydrogenolysis is the process of cleaving the C-X bond, where X is the heteroatom (in the case of hydrotreatment, X could be S or N atom) and hydrogenation is the process of saturating the cleaved heteroatom with hydrogen. According to Kwak *et al.*, the presence of basic nitrogen compounds even at low concentrations markedly suppressed the HDS of 4-methyldibenzothiophene and 4,6-dimethyldibenzothiophene while HDS of dibenzothiophene is almost not affected by nitrogen compounds for nitrogen concentrations of less than 500 ppm (Kwak, et al., 2001). It was also reported that quinoline is a stronger poisoning agent than carbazole where it strongly adsorbs on

hydrogenation and acid sites of the catalysts. HDS of fuel with lower concentrations of sulfur is also more affected by the presence of nitrogen compounds (Turaga, et al., 2003). Other than catalyst poisoning by competitive adsorption with sulfur compounds, the adsorbed nitrogen compounds also act as coking precursors of which the coke then leads to poisoning of the HDS catalysts (Dong et al., 1997b).

d) Conventional hydrotreating process designed for petroleum refinery may not be suitable for upgrading or refining unconventional fossil fuels which may one day be one of the main source of feedstock to fulfil the growing demand. Unconventional fossil fuel such as coal liquids from coal liquefaction and pyrolysis contain much higher concentrations of nitrogen compounds which needs to be removed to meet specified standards and regulations.

2.3 Methods for Denitrogenation of Fuel

The common practice in industry for removal of aromatic compounds including nitrogen and sulfur compounds is hydrotreatment. In hydrotreatment, several processes are simultaneously occurring including hydrodesulfurization (HDS), hydrodenitrogenation (HDN), hydrodeoxygenation (HDO), hydrogenation (HYD), hydrodemetallization (HDM) and hydrodearomatization (HAD) (Furimsky, et al., 2005). Hydrotreatment is energy intensive and costly due to the typical operating conditions at high temperature (300 – 400 °C) and elevated pressure (20-100 atm of H₂) using a specified catalyst such as CoMo/Al₂O₃ or NiMo/Al₂O₃. The removal of nitrogen compounds is more difficult than the removal of sulfur compounds during hydrotreatment because of the low reactivity of nitrogen compounds compared with the sulfur compounds. For example, the HDS reaction path for dibenzothiophene is direct hydrogenolysis of the C-S bond and the formation of H₂S, as shown in Figure 2.3 where the HDS of heterocyclic sulfur compounds can be achieved predominantly by direct C-S cleavage without the need to saturate the benzene ring (Gates et al., 1997).

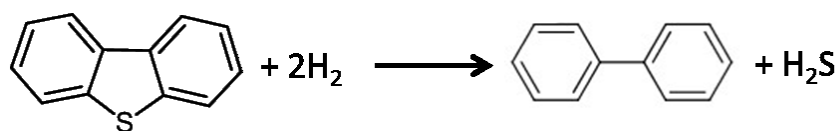


Figure 2.3: HDS reaction path for dibenzothiophene as suggested by Gates and Topsoe (Gates, et al., 1997).

On the other hand, HDN reaction path is more complicated and cannot proceed through direct cleavage of the C-N bond as shown in Figure 2.4 for the HDN of quinoline as suggested by Eijsbouts et al. (Eijsbouts et al., 1991). It was reported that the C-N bond is stronger than the C-S bond and cannot be cleaved directly by hydrogenolysis. Rather, HDN must proceed through the hydrogenation pathway which involves at least the complete hydrogenation of one benzene ring before the C-N cleavage (Furimsky, et al., 2005). From Figure 2.4, the steps for HDN process is first the hydrogenation of the aromatic ring, followed by hydrogenation of the heterocyclic nitrogen ring and finally the hydrogenolysis of the C-N bonds. This is more kinetically difficult than the reaction path for HDS and requires higher consumption of H₂ based on the stoichiometry of the reaction which in turns affect the capital and operational cost for hydrotreatment process.

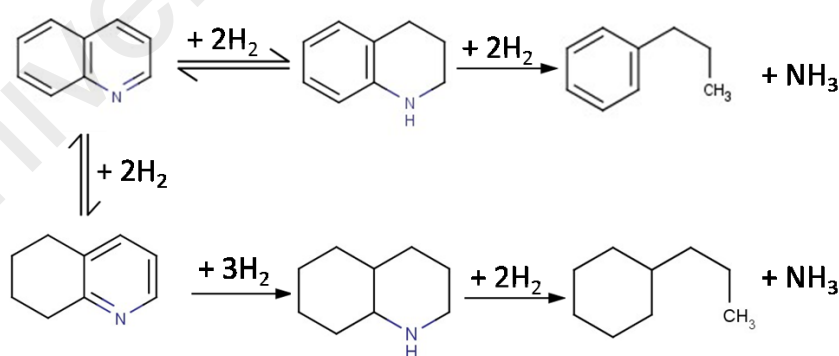


Figure 2.4: Reaction path for HDN of quinoline as suggested by Eijsbouts et al. (Eijsbouts, et al., 1991)

The difficult reaction path for HDN process has driven the research community to explore alternative nitrogen removal methods in the pursuit of finding the most efficient process for denitrogenation of fuels. Among the proposed processes are

- a) Adsorptive denitrogenation,
- b) Chemical oxidative denitrogenation,
- c) Photochemical denitrogenation,
- d) Microbial denitrogenation,
- e) Chemical complexing extraction

Each proposed method will be reviewed in order to compare their separation mechanism and challenges that might be faced if it were to be applied on industrial scale.

a) *Adsorptive denitrogenation using various adsorbent materials*

The most reported method for denitrogenation in the literature after the conventional HDN process is the adsorptive denitrogenation where the aromatic nitrogen compounds are removed using selected adsorbent materials. Laredo et al. provided a comprehensive review on the use of various adsorbent materials for the purpose of adsorptive denitrogenation of middle distillates for enhanced production of ultra-low sulfur fuels (Laredo et al., 2013). The adsorptive denitrogenation process is expected to be performed prior to HDS process in order to reduce or eliminate the presence of aromatic nitrogen compounds in the diesel feed before going into the HDS unit. Adsorptive denitrogenation can be performed in batch or fixed bed procedure. In any procedure, the nitrogen compounds are removed using various adsorbent materials including π -acceptor molecules, methyl viologen-aluminium silicate, activated carbons, activated alumina, zeolites, mesoporous molecular sieves, ion exchange resins (IXR) and metal organic frameworks (MOF).

π -acceptor molecules which are covalently attached on hydrophilic support were used to selectively remove heterocyclic nitrogen compounds from diesel feed by a charge transfer mechanism. Methyl viologen-aluminosilicate was also successfully used to remove nitrogen compounds of low ionization potential from the charge transfer complex very easily. The regeneration of the used adsorbent was achieved by washing with toluene. Another widely used class of adsorbents are various types of activated carbons and activated alumina which have been proven to effectively remove nitrogen compounds. Almarri et al. studied seven representative activated carbon samples and three activated alumina samples and reported that activated carbon showed higher capacity for nitrogen removal compared to activated alumina samples (Almarri, et al., 2008). The oxygen functionality of the activated carbons is reported to be the potential determining factor towards the adsorption capacity of nitrogen compounds whereas the nature of active sites affects selectivity for various nitrogen and sulfur compounds. Zhang et al. reported that a mesoporous molecular sieve named Ti-HMS was highly efficient in removing nitrogen compounds from liquid fuels with a spontaneous physical process (Zhang, et al., 2009). Lithium-modified mesoporous silica adsorbents was prepared by Koriakin et al. to remove nitrogen compounds selectively from residue diesel from HDS process and it was found that these adsorbents exhibited a stronger adsorption affinity for nitrogen compounds than for sulfur compounds and were also easily regenerated using an organic solvent (Koriakin et al., 2010).

Other adsorbent materials used in adsorptive denitrogenation are ion exchange resins (IXR) and metal organic framework (MOF). Ion exchange resins were used by Xie et al. to remove carbazole and dibenzothiophene in a mixture of dodecane and toluene as the model fuel (Xie et al., 2010). It was found that the ion exchange resins have high affinity for the neutral nitrogen compounds via hydrogen bonding between the chloride anion with non-bonding electrons and the neutral nitrogen compounds.

To ensure the adsorption of neutral nitrogen compounds, the presence of N-alkylated pyridinium cation is essential. Regeneration of the IXR was readily performed with polar organic solvents like methanol. Metal organic frameworks are highly porous materials which are formed of inorganic subunits and organic linkers that exhibit multiple complexing functions. This enables a unique variety of potential interactions inside the pores. In adsorptive denitrogenation, the MOF of type MIL-101 showed remarkable adsorption capacity and selectivity towards nitrogen compounds from straight run gas oil (SRGO), light cycle oil (LCO) and other model mixtures (Nuzhdin et al., 2010). This was reported to be due to coordination of nitrogen atoms to the CrIII centres of the MOF which facilitates the stacking interactions between the MOF adsorbent and the aromatic compounds. It was also reported that at equilibrium, the adsorption capacity of the MOF-type adsorbents was almost twice that of activated carbons. However, the cost of MOF is notably higher than the activated carbons.

To summarize, adsorptive denitrogenation prior to hydrotreatment was proven to improve the efficiency of both HDN and HDS processes to produce ultra-low-sulfur diesel (ULSD). The efficiency of adsorptive denitrogenation strongly depends on the choice of adsorbent materials, which should be chosen considering their adsorption capacity, selectivity towards nitrogen compounds, regenerability, lifetime and price of the materials.

b) Oxidative Denitrogenation / Chemical Oxidation

Oxidative desulfurization (ODS) or denitrogenation (ODN) can be operated under moderate conditions and without the requirement of H₂ and catalyst. In ODS and ODN, the aromatic heterocyclic compounds are oxidized into other products which can then be easily removed by conventional separation processes such as distillation, solvent

extraction or adsorption because the properties of the resulting oxidation products differ significantly from the hydrocarbons that constitute the fuel oil.

Shiraishi et al. carried out a detailed investigation on desulfurization and denitrogenation reactivity for light oils using hydrogen peroxide (H_2O_2) and a mixture of H_2O_2 with acetic acid (AcOH) as the oxidizing agent (Shiraishi et al., 2002). Three model nitrogen compounds (aniline, indole and carbazole) were individually dissolved in xylene and were treated with H_2O_2 and AcOH. The reaction product of aniline was azoxybenzene and it was carbazole-1,4-diole for carbazole. For indole, the product contained different types of N-H, C=O and OH groups in its polymeric structure. It was found that the denitrogenation rate for aniline and indole is almost 100% effective while the rate for carbazole is significantly lower. The order of reactivity for the nitrogen compounds was as follows: aniline > indole > carbazole. After the oxidation reaction, extraction process was employed using an azeotropic mixture of acetonitrile/water for the removal of the oxidation reaction products in light oils.

Another report of oxidative denitrogenation was provided by Ishihara et al. who investigated the oxidative denitrogenation of aniline, indole, quinoline, acridine and carbazole using various oxidative agents (H_2O_2 , tert-butylhydroperoxide, ozone) and catalysts (titanosilicate and vanadosilicate) (Ishihara et al., 2005). The denitrogenation activity for the nitrogen compounds follows the order: aniline > indole > quinoline > acridine > carbazole. Carbazole was reported to be particularly refractory to oxidation process. It was found that the use of different oxidative agent and catalyst lead to different reaction product and that the selectivity of the oxidation reaction depends on the selection of oxidative agent, catalyst, pH and operating conditions. Also, oxidation of nitrogen-containing compounds gives a rich chemistry depending on the experimental conditions which makes the identification of the oxidation products challenging and difficult to achieve.

Although oxidative denitrogenation can be used to achieve up to 100% conversion of the heterocyclic nitrogen compounds in liquid fuels, the demerits of the process include the difficulty to identify the oxidation products and the need to use other conventional separation process to remove the oxidized products from the fuel.

c) Photochemical denitrogenation

Shiraishi et al. reported the use of photochemical denitrogenation which is a combination of UV irradiation by high pressure mercury lamp followed by liquid-liquid extraction using oil/acetonitrile two-phase systems (Shiraishi et al., 2000). In photochemical denitrogenation, nitrogen-containing compounds which are known to have relatively large polarities are distributed into the polar acetonitrile phase where they are photodecomposed to form highly polarized compounds which do not distribute into the non-polar light oil phase. This way, the removal of nitrogen compounds from light oils to acetonitrile can be carried out under moderate operating conditions. Based on the work of Shiraishi et al. on the photochemical desulfurization and denitrogenation of vacuum gas oil (VGO), the nitrogen concentration in the VGO solution initially decreases as a result of contact with acetonitrile. Then, it decreases dramatically with photoirradiation time. The nitrogen compounds distributed in the acetonitrile phase are photodecomposed efficiently into highly polarized compounds such as NO_3^- anion. The denitrogenation rate was found to depend upon the ratio of VGO/decane and the ratio of VGO solution/acetonitrile. In their work, the nitrogen content of VGO was successfully decreased to up to < 11 wt% of the feed concentration. However, the process becomes more difficult for highly substituted carbazoles. The extent of efficiency for this particular process depends upon the VGO solution ratio, VGO/acetonitrile ratio and photoirradiation time.

d) Microbial denitrogenation

Benedik et al. provided a comprehensive review on the use of microbial denitrogenation for fossil fuels (Benedik et al., 1998). In microbial denitrogenation, biological degradation or microbial transformation of nitrogen heteroaromatics using microorganisms capable of degrading nitrogen species were utilized to remove the nitrogen compounds from liquid fuels by means of anaerobic and aerobic degradation. The microorganisms can be obtained from the waste-water sludge, hydrocarbon-contaminated soil and water, industrial effluents and coal- and shale- liquefaction sites. For example, carbazole can be completely metabolized to CO₂ and biomass or converted to anthranilic acid or other intermediates. These converted compounds are believed to cause less catalyst inhibition than their parent compounds and many polar intermediates could readily be extracted from petroleum streams. Besides, carbazole enrichment cultures are capable of degrading a wide range of alkylcarbazoles present in crude oil generally yielding water-soluble non-toxic metabolites. However, such biochemical engineering processes have not yet been widely applied to hydrocarbon processing because several engineering issues need to be addressed. These issues include the type of catalyst to be used in the reaction, cell immobilization or retention in a second (aqueous) liquid phase, catalytic activity and stability of the reaction, nutrient requirements for cell maintenance, mass transfer, mixing and demixing, biological containment and disposal of any by-product or biomass.

e) Chemical complexation / complexing extraction

Complexing extraction utilizes the interaction between an electron pair donor and an electron pair acceptor or between a Lewis base and a Lewis acid which forms a complexing force. Complexing extraction can have a higher capacity and selectivity than conventional extraction due to the complexing force being stronger than van der Waals

force in conventional extraction. Qi et al. carried out reversible chemical complexation with a volatile carboxylic acid to extract nitrogen compounds from catalytically cracked diesel oil (Qi et al., 1998). They utilized the basicity of the basic nitrogen compounds found in catalytically cracked diesel oil which can strongly react with Lewis acid such as carboxylic acid. In the process, aqueous acetic acid as the solvent is mixed with feed oil and left to stand for a period of time. The mixture will separate into two phases, which are acetic acid/water phase and oil phase. The acetic acid/water phase will undergo distillation process to separate the nitrogen compounds and recover the aqueous acetic acid solvent and the oil phase will also be distilled to obtain the treated oil and recover the solvent for further use. The separation principle of nitrogen compounds based on reversible chemical complexation using acetic acid solution is shown in Equation 2.1:



$\bar{\text{N}}$ is the nitrogen compound in the oil species and $\dot{\text{N}}$ is in the acetic acid/water species. The results indicate that the extraction recovery of nitrogen compounds increased with increasing concentration of acetic acid and that basic nitrogen compounds are more easily extracted than non-basic nitrogen compounds due to the higher Lewis basicity that the basic compounds have. Although extraction recovery of nitrogen compounds increases with the volume ratio of solvent to feed, the recovery of catalytically cracked diesel oil does not follow the same trend. The factors determining the extent of denitrogenation include complexing agent volume ratio, wt% of the metallic ion used, solvent to oil ratio, reaction time and reaction temperature.

Zhang et al. reported the use of complexing extraction process for denitrogenation in straight-run diesel (Zhang et al., 2013). In their work, the complexing extraction agent was formed by dissolving a certain amount of complexing agent in methanol. Thereafter, a certain amount of diesel is taken according to the appropriate ratio of solvent to oil and

a certain amount of complexing extraction agent was added. The mixture is agitated violently for a certain time and at a specified temperature before the mixture is finally deposited and delaminated for a period of time. The complexing agent used was a mixture of methanol/acetic acid/water at various volume ratios. Then, different types of metallic ions are chosen to refine the straight-run diesel at different wt % (between 0 and 0.5 wt%).

2.4 Extractive Denitrogenation as a Promising Separation Method

Extractive denitrogenation or liquid-liquid extraction process to remove nitrogen compound is seen as a potentially promising candidate to replace HDS and HDN. This is mainly due to its simple separation mechanism and ability to be operated under mild conditions. In liquid-liquid extraction (LLE), the feed contains the material to be removed, *i*. The solvent used is miscible with component *i* but immiscible with the feed phase. LLE utilizes the interaction between the feed and solvent phases which will cause some of the component *i* to be transferred from the feed phase to the solvent phase. After extraction, the mixture of feed and solvent phases will separate into two phases, namely the extract phase (solvent-rich phase with the extracted component *i*) and raffinate phase (feed phase with the remaining amount of component *i*). Important factors affecting the efficiency of LLE process are the solvent selection, extraction time, surface area for interaction and operating temperature. Operating pressure has a very mild effect towards the efficiency of LLE process.

In extractive denitrogenation, nitrogen compounds are transferred from the oil phase into the solvent phase during the mixing process in the extraction column. From the mixing tank, the oil and solvent phases go into a separator where the phases will separate into extract and raffinate phases. The raffinate phase contains treated fuel oil with small amount of nitrogen compounds and the extract phase contains solvent and extracted nitrogen compounds. The treated oil removed of nitrogen compounds can then be fed to HDS unit and the solvent used can be recovered by means of distillation to

separate the extracted nitrogen compounds. Attractive features of extractive denitrogenation include the moderate operating conditions as it is applicable at low temperature and pressure. The process also does not change the chemical structure of the oil components because no reaction occurred, only physical interaction between the components involved. Extraction is also a conventional separation process without the need of special equipment and thus can be readily integrated into the existing refinery plant.

Solvent selection is crucial in order to achieve high nitrogen removal from liquid fuels. The solvent should have high selectivity, high capacity and high distribution ratio towards the solute to be extracted to ensure efficient separation. The selected solvent should also be insoluble in the feed phase and easily regenerated. During the extraction process, minimal solvent loss is desired, thus, low vapour pressure and low volatility of the solvent are crucial. Favourable transport properties for easy handling of solvent should also be considered including the density, viscosity, surface tension and corrosivity. In addition, for its industrial application, the solvent must comply with safety and environmental regulations such as low toxicity and poses no adverse effects on the environment. Last but not least, the solvent must be affordable and abundant for use on large scale.

Numerous research has been done in pursuit of finding the best solvent for denitrogenation using extractive denitrogenation process. Table 2.3 shows various organic solvents which have been reported for use in extractive denitrogenation at 298.15 K and atmospheric pressure, which are methanol, ethanol, N-methylformamide (NMF) and N,N-dimethylformamide (DMF) along with the values of distribution coefficient and selectivity. Won et al. reported high values of distribution coefficient and selectivity for the use of methanol to remove both 5-membered and 6-membered nitrogen compounds from *n*-hexadecane as the model diesel compound (Won et al., 2002). Higher values of

distribution coefficient and selectivity were reported for 5-membered compounds (pyrrole and indole) and aniline, which is a phenyl group attached to an amino group. Lower values were reported for 6-membered nitrogen compounds (pyridine, quinoline, acridine), however the values are still above unity which means that all of the nitrogen compounds have a good solubility with methanol. Ethanol was also used to extract the same nitrogen compounds from *n*-hexadecane by Hwang et al. but the solvent reported much lower values of distribution coefficient and selectivity for all of the nitrogen compounds compared to methanol (Hwang et al., 2007). The same group later used the solvents N-methylformamide (NMF) and N,N-dimethylformamide (DMF) for removal of pyrrole, indole, pyridine, quinoline and aniline from *n*-hexadecane (Kim et al., 2009).

These organic solvents were reported to have good values of distribution coefficient and selectivity. However, their use for separation processes on industrial scale have many drawbacks. For example, methanol and ethanol are both flammable and have toxic effects on humans and animals whereas NMF and DMF are proven to have toxic effects. Besides, some of the conventionally used organic solvents in industry other than these four solvents poses challenges such as producing azeotropic mixture and have low boiling point which limits the operable temperature range. A need for alternative “green solvents” to replace organic solvent is thus inevitable.

In recent times, a growing number of publications reporting the use of a new class of solvents namely ionic liquids and deep eutectic solvents for use in separation processes including liquid-liquid extraction for extractive denitrogenation. The definition and properties of these new class of solvents will be discussed in the next sub-section.

Table 2.3: Organic solvents used for extractive denitrogenation of model diesel.

Organic Solvent	Hydrocarbon (model fuel)	Nitrogen compound	Distribution Coefficient Range	Selectivity Range	Reference
Methanol	<i>n</i> -hexadecane	pyrrole	22.56-29.81	27.25-157.12	(Won, et al., 2002)
		indole	18.60-24.18	23.64-119.65	
		pyridine	3.30-12.44	4.10-68.34	
		quinoline	3.95-8.18	4.81-40.20	
		acridine	3.71-8.83	13.53-76.46	
		aniline	22.32-33.82	26.32-198.20	
Ethanol	<i>n</i> -hexadecane	pyrrole	2.59-6.04	5.50-19.12	(Hwang, et al., 2007)
		indole	1.92-6.10	5.73-14.82	
		pyridine	1.13-1.48	1.45-8.84	
		quinoline	1.02-1.26	1.03-8.98	
		acridine	1.27-1.50	2.40-7.08	
		aniline	2.16-8.90	8.90-23.72	
N-methylformamide (NMF)	<i>n</i> -hexadecane	pyrrole	5.69-14.77	5.69-88.65	(Hwang et al., 2008)
		indole	13.58-26.42	18.82-80.67	
		pyridine	1.26-2.10	1.32-40.843	
		quinoline	1.43-2.42	1.46-32.52	
		aniline	7.72-11.58	7.72-70.39	
N,N-dimethyl formamide (DMF)	<i>n</i> -hexadecane	pyrrole	5.91-45.70	0.14-4.42	(Kim, et al., 2009)
		indole	11.58-30.28	0.67-2.11	
		pyridine	1.65-4.16	0.26-0.46	
		quinoline	1.39-4.46	0.32-1.07	
		aniline	8.86-222.29	0.17-12.99	

2.5 Ionic Liquids and Deep Eutectic Solvents

2.5.1 Introduction to Ionic Liquids

The discovery of the first ionic liquid (ethyl-ammonium nitrate [EtNH₃][NO₃]) was in 1914 by Walden but there was not much attention given to ionic liquids (ILs) at that time (Koel, 2008; Letcher, 2004). Development of ILs continues to blossom in 1934 with the report of a patent on pyridinium-based molten salts which were able to dissolve certain amount of cellulose. However, ILs start to attract attention in the 1960s where the

first generation of ILs were chemically characterized. This first generation was sensitive to air and moisture and was mainly composed of cations like dialkylimidazolium and alkylpyridium derivatives and anions like chloroaluminate and other metal halides. In the 1970s and 1980s, ILs were studied mainly for electrochemical applications.

The second generation of ILs surfaced in the 1990s where the ILs are formed with weakly coordinating anions like tetrafluoroborate (BF_4) and hexafluorophosphate (PF_6) that were more stable towards air and moisture. By the mid-1990s, few research groups in the scientific community were well-versed in the basic understanding of the concept of ILs and the new class of ILs as we know today becomes increasingly popular by the end of 1990s and continue to gain growing attention until now.

A simple definition of ILs would be liquids that are comprised entirely by ions or salts occurring naturally in liquid form. Ideally, ILs should have relatively low melting points than those of conventional salts and are liquids at ambient temperature. However, the term ionic liquid also includes those solvents with melting temperature less than 100°C . ILs are composed of large, asymmetric and loosely coordinating organic cations and small inorganic or organic anions. The loose coordination of the cations and anions prevents it from packing and therefore inhibits crystallization of the salt. Figure 2.5 shows a schematic figure of 1-ethyl-3-methylimidazolium ethylsulfate as an example of IL.

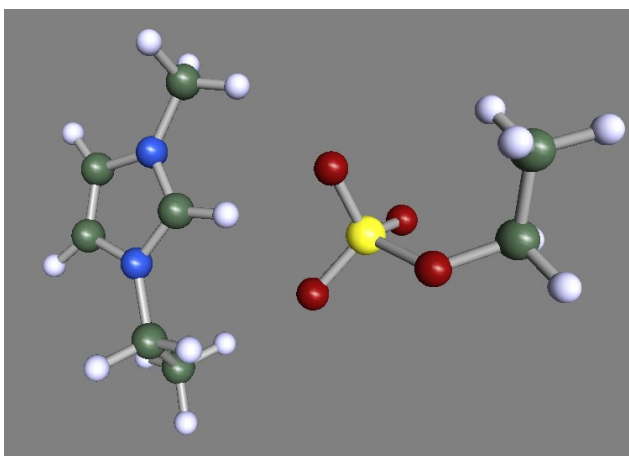


Figure 2.5: A schematic figure of 1-ethyl-3-methylimidazolium ethylsulfate as an example of IL.

There is literally no limit in the number of possible existing ILs which can result from various combinations of cations and anions (Holbrey et al., 1999). It is widely believed that some properties of the ILs such as thermal stability and miscibility depend on the anion while other physical properties such as viscosity, surface tension and density depend on the structure of the cation. Thus, the ILs can be designed for a particular application or for a particular set of properties by interchanging the combination of cation and anion and their structure. This attribute is the reason behind the term “designer solvent” is given to ILs (Freemantle, 1998). Due to the huge number of possibly existing ILs, it is impossible to screen all possible ILs for any particular application.

2.5.2 Properties of Ionic Liquids

The most popular property of ILs which makes them so attractive for use in the field of green chemistry is their very low measurable vapour pressure. Paulechka et al. reported the value of measurable vapour pressure of 1-butyl-3-methylimidazolium bis(trifluoromethanesulfonyl)imide as low as 1.22×10^2 Pa at $T=458$ K (Paulechka et al., 2005). The negligible vapour pressure of ILs facilitates their handling and leads to reduced emission and workers' exposure hazards when used in industry (Earle et al., 2000). Although ILs have generally high thermal stability, it should be noted that the upper limit for ILs is usually thermal decomposition rather than vaporization. At high temperatures, it is expected that the vapour pressure of ILs becomes detectable. Even so, the thermal stability is more of a concern than the vapour pressure in the high-temperature regime (Earle et al., 2006). Earle et al. also reported the separation of two ILs by distillation, proving that certain IL structures which are known for their very high thermal stability can still be evaporated and re-condensed under relatively mild conditions. Other researchers also reiterated that the non-volatility of ILs is not a property that can be assumed for all thermally stable ILs. Rather, vapour pressure just like any other property

depends upon the combination between cation and anion and needs to be determined experimentally for each new ionic liquid (Paulechka, et al., 2005) (Zaitsau et al., 2006).

On the other hand, ILs have a significantly wider liquid range than common organic solvents which allows their remarkable kinetic control. The wide liquid range in ILs may be attributed to the asymmetrical coordination between the cation and anion. Besides, it may also be due to the dominant Coulombic charge-charge interactions which are balanced against the rotational and vibrational freedom of the ions. Absence of strong hydrogen bonding is also a major factor to the low melting points of ILs (Brennecke et al., 2001) (Blanchard et al., 2000).

However, ILs become increasingly popular as new class of solvents due to their ability to solvate a wide range of organic, inorganic and polymeric materials including organometallic compounds (Wilkes et al., 1982). They are also attractive choices for multiphase systems because they can be immiscible with a number of organic solvents and water due to their ability to provide a highly polar and at the same time non-coordinated medium (Huddleston et al., 1998). Other favourable properties of ILs include high electrochemical stability and high ionic conductivity (Marsh et al., 2004).

In recent years, green engineering looks forward to a more holistic approach such as life cycle analysis in a particular chemical process to be called “green” or sustainable process. Indeed, life cycle analysis of a chemical process using ILs includes not only the positive environmental impact which can be obtained due to the ILs negligible vapor pressure, but also takes into account the production of ILs before the separation process begins and disposal of ILs and/or their derivatives at the end of the process.

The synthesis processes of ILs often involve several steps, use of some reagents and include a final purification process for the IL to be usable. These processes involve quaternization of ions, mixing, heating and purification of the final product. The

complexity of the process, its energy consumption and the expensive raw materials leads to a high cost of production of ILs which makes them not practical for a large scale application. Although studies on the decomposition of ILs at the end of the chemical process are still in development and even if there is not much data available on the toxicology of ILs, there is an inevitable potential toxicological issue associated with ILs as they may form hazardous hydrolysis products and are poorly biodegradable (Domínguez de María et al., 2011).

2.5.3 Applications of Ionic Liquids in Extractive Denitrogenation

Owing to the favourable properties of ILs as a promising alternative to conventional organic solvents, the use of ILs has been reported in numerous liquid-liquid separation processes in the petrochemical processing field.

In recent years, several researchers have reported the use of ILs as solvents to remove heterocyclic nitrogen compounds from gasoline and diesel. The reported data can be categorized into two groups: i) ternary liquid-liquid equilibrium (LLE) data and ii) experimental liquid extraction process. In the first category, the data will be discussed in terms of the IL solvent performance i.e. distribution ratio and selectivity whereas in the second category, the data will be compared according to their experimental variable such as the extraction efficiency, extraction time, IL to oil ratio and operating temperature.

Ternary LLE data are important to identify the phase behaviour for the mixture of liquids in a given system. Through the phase diagram, the miscibility of the solvent towards the solute to be separated can be evaluated. Besides, the phase behaviour type can also be identified if they demonstrate either Type I, Type II or Type III ternary LLE phase diagram. Ternary LLE data are also of primary importance for conceptual process design and development of separation processes especially when using process simulation software where excess Gibbs energy activity coefficient model is required for thermodynamic modeling of the separation process. From the ternary LLE data, the

binary interaction parameters of the activity coefficient models such as non-random two-liquid model (NRTL) and Universal Quasi-chemical model (UNIQUAC) can be obtained by regression of these experimental data. The separation efficiency and solvent selection parameter based on ternary LLE data is evaluated based on the value of selectivity and distribution coefficient of the solvent towards the solute.

In liquid extraction experiments, the data are used to evaluate the operating parameters regarding the extraction efficiency of the solvent towards the solute.

The operating parameters evaluated include the extraction and settling time, solvent to feed ratio and operating temperature. The effectiveness of the separation process is measured using extraction efficiency, which is described in Equation 2.2:

$$\text{Extraction efficiency} = \frac{(\text{Initial concentration} - \text{Final concentration})}{\text{Initial concentration}} \times 100\% \quad \text{Eq. 2.2}$$

Nevertheless, data collected from the liquid extraction experiment cannot be used for design and development of a liquid extraction process using process simulation software.

Table 2.4 shows a summary of ternary LLE data reported in the literature at 298.15 K and atmospheric pressure. Pyridine is the only representative nitrogen compound reported for ternary LLE data where ILs were used as extraction solvents. The model fuel compounds representative of gasoline were *n*-hexane, *n*-heptane, *n*-pentane, iso-octane and toluene. Most of the ILs used were imidazolium-based ILs with only one report using pyridinium based IL in ternary LLE data by Francisco et al. (Francisco et al., 2010). However, the imidazolium-based ILs reported were of a variety of combination with various anions. The reported values of distribution ratio (*D*) and selectivity (*S*) ranges are also shown in Table 2.4. At low pyridine concentration in the feed mixtures, high values of *D* and *S* were reported compared to increased pyridine concentration in the feed mixtures.

Table 2.5 shows a summary of extraction experiment data collected from the literature where the performance of various ILs in extractive denitrogenation were compared based on the nitrogen compounds used, operating temperature, IL to oil ratio, extraction time and the resulting extraction efficiency. The full names and abbreviations of ILs listed in Table 2.4 and Table 2.6 can be referred to in Table 2.6. In the collection of extraction experimental data, a wider variety of nitrogen compounds were reported in the extraction experiment using ILs, which includes both basic nitrogen compounds (pyridine, piperidine, quinoline, acridine) and neutral nitrogen compounds (pyrrole, indole, carbazole). Most model fuel compounds were representative of gasoline, with a few reports using model diesel compounds. Imidazolium-based ILs are still a widely reported extraction solvent with variation in the cation constituent and anion combinations.

Extraction of pyridine and piperidine from *n*-dodecane as model diesel compound using [BMIM][BF₄] were reported by Zhang et al. and the reported extraction efficiencies are 45% and 9%, respectively (Zhang et al., 2003). Chloride-based ILs were used to remove 150 ppm of carbazole from straight run diesel fuel at 60°C with extraction efficiencies between 48% and 58% (Xie et al., 2008). Huh et al. compared the use of ionic liquids with and without addition of ZnCl₂ to remove quinoline, indole and acridine, respectively, from a mixture of *n*-heptane and *n*-octane as the model oil (gasoline) (Huh et al., 2009). In their work, imidazolium-based IL with different alkyl chain length and anion combinations ([EtSO₄]⁻, [MeSO₄]⁻, [EtPHO₃]⁻, [Et₂PO₄]⁻ and [Bu₂PO₄]⁻) were compared with and without the addition of ZnCl₂. It was reported that imidazolium-based ILs were proven to be effective extractants for the denitrogenation of basic nitrogen compounds and that the performance of dialkylimidazolium alkyl sulphate ILs for extractive denitrogenation dramatically improved to up to more than twice with the addition of ZnCl₂. The extraction of indole as representative neutral nitrogen compound

does not have a significant improvement using imidazolium-based ILs with or without ZnCl_2 addition because even without the addition of ZnCl_2 the efficiency is already >90%. Dicyanamide-based ILs with imidazolium- and sulfonium-based cations were used by Asumana et al. to extract carbazole and pyridine from a mixture of *n*-hexane and toluene at room temperature and 1:1 IL to oil ratio (Asumana et al., 2011). The extraction efficiency is as high as 100% for carbazole using imidazolium-based dicyanamide ILs and more than 80% extraction efficiency was achieved using sulfonium-based dicyanamide ILs. Whereas, the extraction efficiency for pyridine only ranges from 58% to 72% using the same types of ILs with imidazolium-based dicyanamide ILs reporting higher values of extraction efficiency than those with sulfonium-based cations. The use of cyano-based ILs was also reported by Hansmeier et al. for extractive denitrogenation of a model fuel mixture containing all three nitrogen compounds of pyrrole, indole and carbazole in a mixture of *n*-heptane, toluene and tetralin at room temperature and 1:1 IL to oil ratio (Hansmeier et al., 2011). Consistent with the results obtained by Asumana et al., the removal of neutral nitrogen compounds via extraction process with IL extractant achieved >99% extraction efficiency as was reported by Hansmeier et al. More recently, Wang et al. reported the use of water-soluble $[\text{H}_2\text{PO}_4]$ -based ILs to extract quinoline from *n*-heptane at 60°C and 1:10 IL to oil ratio (Wang et al., 2014). Out of the three $[\text{H}_2\text{PO}_4]$ -based ILs used, only $[\text{HMIM}][\text{H}_2\text{PO}_4]$ showed very poor extraction efficiency, i.e. 0% whereas the other $[\text{H}_2\text{PO}_4]$ -based ILs used reported >99% extraction efficiency of quinoline. Adding water to the ILs at 2:1 IL to water ratio was proven to enhance the rate of denitrogenation especially for $[\text{HMIM}][\text{H}_2\text{PO}_4]$ of which extraction efficiency improved from 0% to 12.5% when water was added. It was also reported that the acidity of ILs have a great influence on the denitrogenation efficiency of basic compounds such as quinoline which was used in this work.

Table 2.4: Experimental LLE data on the use of ILs for extractive denitrogenation

Ionic Liquid	Nitrogen compound	Model fuel compound	<i>D</i> range	<i>S</i> range	Reference
[HMMPY][NTf ₂]	pyridine	<i>n</i> -hexane	2.08-19	6.34-100.15	(Francisco, et al., 2010)
[OMIM][BF ₄]	pyridine	<i>n</i> -hexane	1.35-6.46	3.3-53.65	(Alonso et al., 2010)
[OMIM][NTf ₂]	pyridine	<i>n</i> -hexane	1.51-9.14	2.97-36.77	
[EMIM][EtSO ₄]	pyridine	<i>n</i> -hexane	1.02-3.02	5.17-316.25	
[BMIM][Otf]	pyridine	<i>n</i> -heptane	1.52-7.38	4-61	(Kędra-Królik et al., 2011)
[EMIM][SCN]	pyridine	<i>n</i> -heptane	1.12-4.82	6.8- 1208.9	(Kędra-Królik et al., 2011)
[DMIM][MP]	pyridine	<i>n</i> -heptane	0.61-1.19	6.3-49.6	
[EMIM][MeSO ₃]	pyridine	<i>n</i> -pentane	0.2-0.78	2.9-10.7	(Ravilla et al., 2012)
[EMIM][EtSO ₄]	pyridine	<i>n</i> -pentane	0.21-0.9	1.4-66.5	
[EMIM][EtSO ₄]	pyridine	iso-octane	0.48-0.95	5.9-40.8	
[EMIM][Ac]	pyridine	<i>n</i> -pentane	0.76-1.64	2.6-6.4	
[EMIM][Ac]	pyridine	iso-octane	0.14-0.92	0.7-5.2	
[EMIM][NTf ₂]	pyridine	<i>n</i> -hexane	1.81-6.2	7.39-157	(Rodríguez-Cabo, Soto, et al., 2013)
[EMIM][Ac]	pyridine	<i>n</i> -hexane	0.89-2.12	5.16-670	(Rodríguez-Cabo, Arce, et al., 2013)
[EMIM][DEP]	pyridine	<i>n</i> -hexane	1.27-5.13	6.66-103	
[PMIM][NTf ₂]	pyridine	<i>n</i> -hexane	1.59-2.38	5.77-57.86	(Rogošić et al., 2014)
[PMIM][NTf ₂]	pyridine	<i>n</i> -heptane	1.44-2.37	5.49- 65.79	
[PMIM][NTf ₂]	pyridine	iso-octane	1.70-2.90	7.98-63.89	
[PMIM][NTf ₂]	pyridine	toluene	1.66-3.32	3.48-5.81	

Table 2.5: Experimental extraction data on the use of ILs to extract nitrogen compounds from model fuel. RT indicates room temperature.

No.	IL used	Nitrogen compound	Model oil	Amount (unit)	Temperature (°C)	IL:oil ratio	Extraction time (mins)	Extraction efficiency (%)	Reference
1	[BMIM][BF ₄]	pyridine	<i>n</i> -dodecane	779 ppm	RT	1:5	30	45	(Zhang, et al., 2003)
2	[BMIM][BF ₄]	piperidine	<i>n</i> -dodecane	661 ppm	RT	1:5	30	9	
3	[BMIM][Cl]	carbazole	straight-run diesel fuel	150 ppm	60°C	1:10	60	48	(Xie, et al., 2008)
4	[OPY][Cl]	carbazole	straight-run diesel fuel	150 ppm	60°C	1:10	60	58	
5	[DMIM][MeSO ₄]	quinoline	<i>n</i> -heptane, <i>n</i> -octane	500 ppm	RT	1:5	30	36.2	
6	[EMIM][MeSO ₄]	quinoline	<i>n</i> -heptane, <i>n</i> -octane	500 ppm	RT	1:5	30	47.9	
7	[BMIM][MeSO ₄]	quinoline	<i>n</i> -heptane, <i>n</i> -octane	500 ppm	RT	1:5	30	52.7	
8	[OMIM][MeSO ₄]	quinoline	<i>n</i> -heptane, <i>n</i> -octane	500 ppm	RT	1:5	30	57.3	(Huh, et al., 2009)
9	[HEIM][EtSO ₄]	quinoline	<i>n</i> -heptane, <i>n</i> -octane	500 ppm	RT	1:5	30	40.8	
10	[EMIM][EtSO ₄]	quinoline	<i>n</i> -heptane, <i>n</i> -octane	500 ppm	RT	1:5	30	40.6	
11	[BEIM][EtSO ₄]	quinoline	<i>n</i> -heptane, <i>n</i> -octane	500 ppm	RT	1:5	30	55.3	

12	[EMIM][EtPHO ₃]	quinoline	<i>n</i> -heptane, <i>n</i> -octane	500 ppm	RT	1:5	30	40.7
13	[BMIM][EtPHO ₃]	quinoline	<i>n</i> -heptane, <i>n</i> -octane	500 ppm	RT	1:5	30	45.7
14	[EMIM][Et ₂ PO ₄]	quinoline	<i>n</i> -heptane, <i>n</i> -octane	500 ppm	RT	1:5	30	54
15	[BMIM][Bu ₂ PO ₄]	quinoline	<i>n</i> -heptane, <i>n</i> -octane	500 ppm	RT	1:5	30	52.7
16	[EMIM][Cl]	quinoline	<i>n</i> -heptane, <i>n</i> -octane	500 ppm	RT	1:5	30	29
17	[EMIM] ₂ [ZnCl ₂ Br ₂]	quinoline	<i>n</i> -heptane, <i>n</i> -octane	500 ppm	RT	1:5	30	49.3
18	[HEIM][EtSO ₄]-ZnCl ₂	quinoline	<i>n</i> -heptane, <i>n</i> -octane	5000 ppm	RT	1:5	30	86.5
19	[EMIM][EtSO ₄]-ZnCl ₂	quinoline	<i>n</i> -heptane, <i>n</i> -octane	5000 ppm	RT	1:5	30	89.2
20	[BEIM][EtSO ₄]-ZnCl ₂	quinoline	<i>n</i> -heptane, <i>n</i> -octane	5000 ppm	RT	1:5	30	91.2
21	[EMIM][MeSO ₄]- ZnCl ₂	quinoline	<i>n</i> -heptane, <i>n</i> -octane	5000 ppm	RT	1:5	30	88.4
22	[BMIM][MeSO ₄]- ZnCl ₂	quinoline	<i>n</i> -heptane, <i>n</i> -octane	5000 ppm	RT	1:5	30	89.8
23	[OMIM][MeSO ₄]- ZnCl ₂	quinoline	<i>n</i> -heptane, <i>n</i> -octane	5000 ppm	RT	1:5	30	93.9
24	[EMIM][Et ₂ PO ₄]- ZnCl ₂	quinoline	<i>n</i> -heptane, <i>n</i> -octane	5000 ppm	RT	1:5	30	47.5

25	[BMIM][Bu ₂ PO ₄]- ZnCl ₂	quinoline	<i>n</i> -heptane, <i>n</i> -octane	5000 ppm	RT	1:5	30	43.1
26	[EMIM][EtPHO ₃]- ZnCl ₂	quinoline	<i>n</i> -heptane, <i>n</i> -octane	5000 ppm	RT	1:5	30	38.3
27	[EMIM][Cl]- ZnCl ₂	quinoline	<i>n</i> -heptane, <i>n</i> -octane	5000 ppm	RT	1:5	30	64.3
28	[EMIM][Cl]-ZnCl ₂ (2:1 ratio)	quinoline	<i>n</i> -heptane, <i>n</i> -octane	5000 ppm	RT	1:5	30	68.9
29	[EMIM][EtSO ₄]	indole	<i>n</i> -heptane, <i>n</i> -octane	5000 ppm	RT	1:5	30	98.7
30	[EMIM][EtSO ₄]	indole	<i>n</i> -heptane, <i>n</i> -octane	5000 ppm	RT	1:20	30	94.5
31	[EMIM][EtSO ₄]-ZnCl ₂	indole	<i>n</i> -heptane, <i>n</i> -octane	5000 ppm	RT	1:5	30	100
32	[EMIM][EtSO ₄]- ZnCl ₂	indole	<i>n</i> -heptane, <i>n</i> -octane	5000 ppm	RT	1:20	30	92.7
33	[BEIM][EtSO ₄]	indole	<i>n</i> -heptane, <i>n</i> -octane	5000 ppm	RT	1:5	30	100
34	[BEIM][EtSO ₄]- ZnCl ₂	indole	<i>n</i> -heptane, <i>n</i> -octane	5000 ppm	RT	1:5	30	100
35	[DMIM][MeSO ₄]	indole	<i>n</i> -heptane, <i>n</i> -octane	5000 ppm	RT	1:5	30	97.8
36	[DMIM][MeSO ₄]- ZnCl ₂	indole	<i>n</i> -heptane, <i>n</i> -octane	5000 ppm	RT	1:5	30	98.7
37	[EMIM][EtSO ₄]	acridine	<i>n</i> -heptane, <i>n</i> -octane	5000 ppm	RT	1:5	30	38.7

38	[EMIM][EtSO ₄]-ZnCl ₂	acridine	<i>n</i> -heptane, <i>n</i> -octane	5000 ppm	RT	1:5	30	84.7	
39	[BEIM][EtSO ₄]	acridine	<i>n</i> -heptane, <i>n</i> -octane	5000 ppm	RT	1:5	30	40.2	
40	[BEIM][EtSO ₄]-ZnCl ₂	acridine	<i>n</i> -heptane, <i>n</i> -octane	5000 ppm	RT	1:5	30	86.5	
41	[DMIM][MeSO ₄]	acridine	<i>n</i> -heptane, <i>n</i> -octane	5000 ppm	RT	1:5	30	33.5	
42	[DMIM][MeSO ₄]- ZnCl ₂	acridine	<i>n</i> -heptane, <i>n</i> -octane	5000 ppm	RT	1:5	30	83.8	
43	[BMIM][N(CN) ₂]	carbazole	<i>n</i> -hexane, toluene	259 ppm	25°C	1:1	20	100	
44	[EMIM][N(CN) ₂]	carbazole	<i>n</i> -hexane, toluene	259 ppm	25°C	1:1	20	100	
45	[S ₂][N(CN) ₂]	carbazole	<i>n</i> -hexane, toluene	259 ppm	25°C	1:1	20	96.04	
46	[EtMe ₂ S][N(CN) ₂]	carbazole	<i>n</i> -hexane, toluene	259 ppm	25°C	1:1	20	83.40	
47	[BMIM][N(CN) ₂]	pyridine	<i>n</i> -hexane, toluene	500 ppm	25°C	1:1	20	72.20	(Asumana, et al., 2011)
48	[EMIM][N(CN) ₂]	pyridine	<i>n</i> -hexane, toluene	500 ppm	25°C	1:1	20	69.13	
49	[S ₂][N(CN) ₂]	pyridine	<i>n</i> -hexane, toluene	500 ppm	25°C	1:1	20	63.30	
50	[EtMe ₂ S][N(CN) ₂]	pyridine	<i>n</i> -hexane, toluene	500 ppm	25°C	1:1	20	58.87	

51	[3-mebupy][N(CN) ₂]	pyrrole, indole, carbazole	toluene, tetralin, <i>n</i> - heptane	0.5 wt% 0.5 wt% 250 ppm	RT	1:1	15	>99	
52	[4-mebupy][N(CN) ₂]	pyrrole, indole, carbazole	toluene, tetralin, <i>n</i> - heptane	0.5 wt% 0.5 wt% 250 ppm	RT	1:1	15	>99	
53	[4-mebupy][SCN]	pyrrole, indole, carbazole	toluene, tetralin, <i>n</i> - heptane	0.5 wt% 0.5 wt% 250 ppm	RT	1:1	15	>99	
54	[bmim][C(CN) ₃]	pyrrole, indole, carbazole	toluene, tetralin, <i>n</i> - heptane	0.5 wt% 0.5 wt% 250 ppm	RT	1:1	15	>99	(Hansmeier, et al., 2011)
55	[bmim][N(CN) ₂]	pyrrole, indole, carbazole	toluene, tetralin, <i>n</i> - heptane	0.5 wt% 0.5 wt% 250 ppm	RT	1:1	15	>99	
56	[bmim][SCN]	pyrrole, indole, carbazole	toluene, tetralin, <i>n</i> - heptane	0.5 wt% 0.5 wt% 250 ppm	RT	1:1	15	>99	
57	[HMIM][H ₂ PO ₄]	quinoline	<i>n</i> -heptane	150 mg/L	60°C	1:10	90	0	
58	[BMIM][H ₂ PO ₄]	quinoline	<i>n</i> -heptane	150 mg/L	60°C	1:10	90	99.64	
59	[MIMPS][H ₂ PO ₄]	quinoline	<i>n</i> -heptane	150 mg/L	60°C	1:10	90	99.9	
60	[HMIM][H ₂ PO ₄]+H ₂ O (2:1 mass ratio)	quinoline	<i>n</i> -heptane	150 mg/L	60°C	1:10	90	12.5	(Wang, et al., 2014)
61	[BMIM][H ₂ PO ₄]+H ₂ O (2:1 mass ratio)	quinoline	<i>n</i> -heptane	150 mg/L	60°C	1:10	90	99.59	

Table 2.6: List of cations and anions abbreviation and full names used in Tables 2.4 and 2.5

Cation		Anion	
[HMMPY]	1-hexyl-3,5-dimethylpyridinium	[NTf2]	bis(trifluoromethylsulfonyl)imide
[OMIM]	1-octyl-3-methylimidazolium	[BF ₄]	tetrafluoroborate
[EMIM]	1-ethyl-3-methylimidazolium	[EtSO ₄]	ethyl sulfate
[BMIM]	1-butyl-3-methylimidazolium	[Otf]	trifluoromethanesulfonate
[DMIM]	1,3-dimethylimidazolium	[SCN]	thiocyanate
[PMIM]	1-pentyl-3-methylimidazolium	[MP]	methylphosphonate
[3-mebupy]	3-methyl-N-butylpyridinium	[MeSO ₃]	methanesulfonate
[4-mebupy]	4-methyl-N-butylpyridinium	[Ac]	acetate
[S ₂]	ethylated tetrahydrothiophenium	[DEP]	diethylphosphate
[EtMe ₂ S]	ethyldimethylsulfonium	[N(CN) ₂]	dicyanamide
[OPY]	1-octylpyridium	[C(CN) ₃]	tricyanomethanide
[HEIM]	1-hexyl-3-ethylimidazolium	[Cl]	chloride
[BEIM]	1-butyl-3-ethylimidazolium	[MeSO ₄]	methyl sulfate
[MIMPS]	1-methyl-3-(3-sulfopro-pyl)-imidazolium	[EtPHO ₃]	ethylphosphite
		[Et ₂ PO ₄]	diethylphosphate
		[Bu ₂ PO ₄]	dibutylphosphate
		[H ₂ PO ₄]	dihydrogen phosphate

2.5.4 Introduction to Deep Eutectic Solvents

A new generation of solvents namely Deep Eutectic Solvents (DESs) has gained increasing attention as a low-cost alternative to ILs. By definition, a DES is a salt combined with a hydrogen bond donor (HBD) or a complexing agent (CA). The salt normally used to create a DES consists of a large quarternary ammonium or phosphonium cation, combined with a halide anion. When the salt is combined with a HBD or a CA at a certain ratio, the HBD or CA will form a complex with the halide anion, thus lowering the freezing point of the produced eutectic mixture far from its individual constituent (Zhang et al., 2012). DESs are characterized by a large depression of freezing point and are liquid at temperatures below 150°C with most of them being liquid at room temperature up to 70°C.

DES was first described by Abbot et al. for a mixture of choline chloride (ChCl) and urea with a molar ratio of 1:2 (Abbott et al., 2004). The melting point of ChCl is 302°C and for urea is 133°C, but when mixed at 1:2 ChCl:urea the melting point of the mixture depresses to 12°C. In a molecular dynamic study performed by Sun et al. on the DES (ChCl/urea), the interaction energies of cation and anion in the ChCl salt is compared before and after mixing with the complexing agent (urea) (Sun et al., 2013). It was found that the addition of complexing agent reduces the interaction energy between the cation and anion of the salt and increases the interaction energy between the anion and the complexing agent which causes lowering the melting point of the eutectic mixture.

DESs are seen as potential candidates to replace ILs because they have physico-chemical properties comparable to ILs especially the negligible vapour pressure which is characteristic of its non-volatility. Additionally, DESs have several advantages compared to ILs which include: (1) simplicity of synthesis process because the materials can be easily mixed and ready to be used without requiring further purification provided that the individual components are of high purity, (2) very cheap because of the low cost of raw materials and ease in synthesis process and (3) DESs are expected to have good bio-compatibility due to their constituents being organic compounds such as choline chloride and urea (Dai et al., 2013; Jhong et al., 2009). However, although DESs are considered as potential alternatives to ILs in many applications, DESs cannot be considered as ILs because they are not composed entirely by ionic species like ILs and because they can also be obtained from non-ionic species.

Till date, various types of DESs were being reported in the literature with the most widely reported DESs are based on quaternary ammonium and quaternary phosphonium salts combined with HBDs of various types such as alcohol, polyol, carboxylic acids and amides. The use of DESs for large scale use is also feasible because the synthesis of DESs is highly atom economic, easy to handle and no further purification is required.

Table 2.7 shows the typical structures of salts and HBDs used for DES synthesis commonly reported in the literature.

Table 2.7: Name and structure of typical salts and HBDs used in the synthesis of DESs

Salt	HBD
choline chloride	Urea
chlorocholine chloride	Glycerol
tetramethylammonium chloride	ethylene glycol
tetrabutylammonium bromide	diethylene glycol
methyltriphenylphosphonium bromide	malonic acid

2.5.5 Properties of Deep Eutectic Solvents

The physico-chemical properties of DESs are very similar to those of common ILs including their density, viscosity, surface tension, conductivity and chemical inertness (Zhang, et al., 2012). Like ILs, DESs are chemically tailorable solvents because they can be designed by appropriate combination of various quaternary salts with different HBDs and at different ratios. Any change in the salt or HBD constituent and salt:HBD ratio will result in a different set of physical and chemical properties. Here, the properties of DESs relevant to liquid-liquid separation processes i.e. freezing point, density, viscosity and surface tension are described.

Freezing Point

The significant depression of freezing point when a DES is formed is believed to be due to the interaction between the halide anion of the salt and the HBD component. In general, eutectic mixtures with freezing point below 150°C are still considered a DES but ideally those with a eutectic freezing point below 50°C are more attractive to be used as solvents (Zhang, et al., 2012). The depression of freezing point depends on the strength of hydrogen bond formed between the salt anion and the HBD component. Zhang et al. reported that stronger hydrogen bonding between the salt anion and the HBD leads to lower depression of freezing point. Higher molar ratio of HBD also leads to further depression of the freezing point. Figure 2.6 shows an example of a phase diagram for eutectic mixtures of ChCl with either phenylpropionic acid or phenylacetic acid as the HBD. From Figure 2.6, the lowest freezing point depression occurs when the mol % of the acids are at 67%, which corresponds to ChCl/acid molar ratio of 1:2. In other words, two acid molecules are required to form complex with each Cl anion in ChCl in order to form a eutectic mixture. Abbott et al. reported that the freezing point of a salt and HBD eutectic mixtures depend on the lattice energy of the DESs, the interaction between the anion and HBD and the entropy change from the formation of a liquid phase (Abbott, et al., 2004).

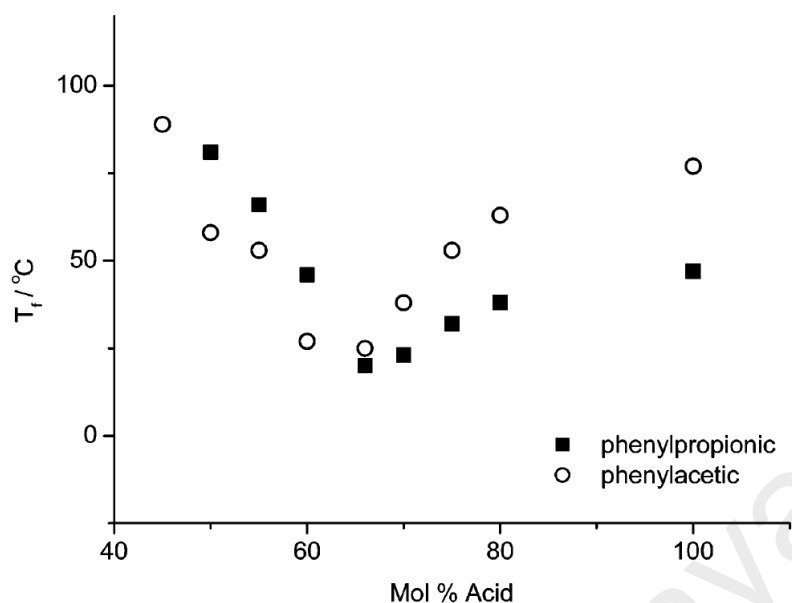


Figure 2.6: Phase diagram for the eutectic mixtures of ChCl with either phenylpropionic acid or phenylacetic acid reproduced from Abbott et al. (Abbott, et al., 2004)

Density

One of the most important physical properties of a solvent is the density. Most of DESs exhibit densities higher than that of water. The reported values of density for DESs range between 1.04 and 1.63 kg m⁻³ (Zhang, et al., 2012) (Ru et al., 2012). It is believed that the molecular organization or packing of the DESs contributes to the different values in density among the DESs. Besides, densities of the DESs are also affected by the salt:HBD molar ratio. For example, for the DES ChCl/glycerol, the density decreases with increase in mole fraction of ChCl (Zhang, et al., 2012).

Viscosity

In general, DESs exhibit relatively high viscosities (> 100cP) at room temperature. Factors contributing to the high values of viscosity of DESs are mainly the extensive hydrogen bond network present between each DES component, resulting in a lower mobility of free species within the DES (Zhang, et al., 2012). The large size of ion

and very small void volume available in most DESs also contribute to the high viscosity, apart from other forces than hydrogen bonding such as electrostatic forces and van der Waals interaction. The chemical nature of DES components also affects the viscosity of DESs such as the type of salt, type of HBD, salt:HBD molar ratio, temperature and water content. In general, viscosity of DESs decreases with increasing temperature.

Surface Tension

Till date, the data about DESs surface tension are very scarce. However, the reported values were larger than the surface tension of most molecular solvents and are comparable to those of imidazolium-based ILs. Garcia et al. reported a collection of experimental surface tension values from the literature of which the values range between 40 and 66 mN m⁻¹ (García et al., 2015). It is expected that the surface tension of DESs follows the same trend to viscosity, i.e. the values depend highly on the strength of intermolecular interaction that governs the formation of DESs (Zhang, et al., 2012).

2.5.6 Applications of Deep Eutectic Solvents in Liquid-liquid Separation Processes

The applications of DESs are widely known in the field of electrochemistry since they gained increasing interest in the 1990s. However, applications of DESs also vary including drug solubilisation, production and purification of biodiesel, gas adsorption such as CO₂ solubility, metal processing such as metal electrodeposition, metal extraction and metal electropolishing and finally separation of liquid-liquid mixtures (Smith et al., 2014).

Unlike ILs, applications of DESs for liquid-liquid separation have not been widely reported in the literature. Up to now, the applications of DESs for this purpose can be summarized into separation of aromatic/aliphatic mixtures, separation of azeotropic mixtures and desulfurization of fuels as shown in Table 2.8. In this table, the DESs were annotated to indicate the salt/HBD with salt:HBD molar ratio in parentheses. Table 2.9

shows the full name and abbreviations of each salt and HBD used in Table 2.8. Kareem et al. were the first group to report the use of DES for liquid-liquid separations particularly in the petrochemical processing field, where they used the DES methyltriphenylphosphonium bromide (MTPPBr) with ethylene glycol (EG) at salt:HBD molar ratios of 1:4, 1:6 and 1:8 to separate benzene from *n*-hexane (Kareem, Mjalli, Hashim, & AlNashef, 2012). The DESs used provided superior results compared to sulfolane and *N*-formylmorpholine which are the most widely used conventional solvents for aromatic/aliphatic separation. They also found that the DESs used have lower viscosity than sulfolane. Furthermore, there is no presence of the DES constituent in the raffinate layer. The same group later reported the use of DESs consisting of tetrabutylphosphonium bromide (TBPB) with either EG or sulfolane at various salt:HBD/CA molar ratios to extract toluene from *n*-heptane (Kareem, Mjalli, Hashim, Hadj-Kali, et al., 2012). It should be noted here that sulfolane is not a HBD thus the term complexing agent (CA) is used instead of HBD. The separation of toluene from *n*-heptane was also performed by the same group using different DESs based on ethyltriphenylphosphonium iodide (ETPPI) combined again with either EG or sulfolane at various molar ratios (Kareem et al., 2013). In both reports, the DESs were able to trap both EG and sulfolane in the extract layer. This represents a significant achievement because when EG and sulfolane are used individually, they are present in the raffinate layer which leads to extra cost and energy consumption for solvent recovery. With the use of DESs, the solvent recovery is simplified to only the extract layer. More recently, the DES tetrabutylammonium bromide (TBAB) with sulfolane at molar ratio 1:4 was used to separate BTEX aromatic compounds (benzene, toluene, ethylbenzene and *m*-xylene) from *n*-octane (Mulyono et al., 2014). The DES used reported moderate values of selectivity and distribution ratio compared to conventional organic solvents and ILs used for separation of similar feed mixtures. However, the advantage of using DES over

conventional solvents despite of the lower values of selectivity and distribution ratio lies in the fact that there is no presence of DES constituent reported in the raffinate phase thus less cost and energy for solvent recovery whereas the advantage of using DES over IL lies in the simple fact that the DESs are easier to synthesis and thus lower in cost.

DESs were also used for the separation of azeotropic mixture of ethanol and *n*-heptane as reported by Oliveira et al. where the DESs were made of ChCl mixed with either glycerol, levulinic acid, or EG at salt:HBD molar ratio of 1:2 (Oliveira et al., 2013). Oliveira et al. reported very high values of distribution ratios and selectivities for all of the DES towards ethanol due to the formation of strong hydrogen bonding between the HBD and ethanol. Among the DESs, ChCl/Gly (1:2) and ChCl/EG (1:2) have lower distribution ratio but high selectivity, compared with ChCl/LA having high distribution ratio and low selectivity. The difference in distribution ratio and selectivity values was attributed to the different structural features of HBDs present in each DES.

Li et al. experimentally screened sixteen different DESs to extract benzothiophene from *n*-octane for use in desulfurization of liquid fuels (Li et al., 2013). Among the screened DESs, they reported that the DES ChCl/Pr (1:2), TBAC/Pr (1:2) and TBAC/PEG (1:2) reported the highest extraction efficiency. From the extraction experiments, it was found that extraction of benzothiophene from *n*-octane can be conducted up to five times without significantly compromising the extraction efficiency. The DESs became saturated after six times of repeated use and lost its extraction capacity. The used DESs can be recycled by simply washing with organic solvent such as diethyl ether and when reused for extraction, the efficiency is comparable to fresh DESs. Up to now, there is no report on the use of DESs for extractive denitrogenation of liquid fuels yet. However, since DESs have been used for separation of aromatic compounds from aliphatic compounds including desulfurization, it is believed that DESs have the potential to be used as extraction solvents for denitrogenation as well.

Table 2.8: DESs used in liquid-liquid extraction process reported in the literature

Application	Feed mixture	DES	Reference
Aromatic/aliphatic separation	benzene + <i>n</i> -hexane	MTPPBr/EG (1:4)	(Kareem, Mjalli, Hashim, & AlNashef, 2012)
		MTPPBr/EG (1:6)	
		MTPPBr/EG (1:8)	
	toluene + <i>n</i> -heptane	TBPB/EG (1:2)	(Kareem, Mjalli, Hashim, Hadj-Kali, et al., 2012)
		TBPB/EG (1:4)	
		TBPB/EG (1:6)	
		TBPB/EG (1:8)	
		TBPB/Sul (1:2)	
		TBPB/Sul (1:4)	
		TBPB/Sul (1:6)	
	toluene + <i>n</i> -heptane	ETPPI/EG (1:6)	(Kareem, et al., 2013)
		ETPPI/EG (1:8)	
		ETPPI/EG (1:10)	
		ETPPI/Sul (1:4)	
		ETPPI/Sul (1:6)	
benzene + <i>n</i> -octane toluene + <i>n</i> -octane ethylbenzene + <i>n</i> -octane <i>m</i> -xylene + <i>n</i> -octane	TBAB/Sul (1:4)	(Mulyono, et al., 2014)	
	TBAB/Sul (1:4)		
	TBAB/Sul (1:4)		
	TBAB/Sul (1:4)		
Azeotropic mixture	ethanol + <i>n</i> -heptane	ChCl/Gly (1:2)	(Oliveira, et al., 2013)
		ChCl/LA (1:2)	
		ChCl/EG (1:2)	
Desulfurization	benzothiophene + <i>n</i> -octane	ChCl/Pr (1:2)	(Li, et al., 2013)
		TBAC/Pr (1:2)	
		TBAC/PEG (1:2)	
		ChCl/MA (1:2)	
		ChCl/Gly (1:2)	
		ChCl/EG (1:2)	
		TMAC/EG (1:2)	
		TMAC/PA(1:2)	
		TBAC/MA (1:2)	
		TBAC/Gly (1:2)	
TBAC/EG (1:2)			
TBAC/PA (1:2)			
TBAC/CA (1:2)			
TBAC/AA (1:2)			

Table 2.9: Full names and abbreviation of the salts and HBDs mentioned in Table 2.8

Salt		HBD / CA	
MTPPBr	methyltriphenylphosphonium bromide	EG	ethylene glycol
TBPB	tetrabutylphosphonium bromide	Sul	sulfolane
ETPPI	ethyltriphenylphosphonium iodide	Gly	glycerol
TBAB	tetrabutylammonium bromide	LA	levulinic acid
ChCl	choline chloride	Pr	propionate
TBAC	tetrabutylammonium chloride	PEG	polyethylene glycol
TMAC	tetramethylammonium chloride	MA	malonic acid
		PA	phenylacetic acid
		CA	caproic acid
		AA	acetic acid

2.6 Computational methods in selecting appropriate ILs and DESs

As discussed in previous section, due to the huge number of possibly existing ILs, it is practically impossible to screen all existing ILs for a particular separation process. Similarly with DESs, the variation of possibly existing DESs is also huge if not more than those of ILs. Besides the huge number of ILs and DESs to choose from, the lack of database on the physico-chemical and thermodynamic properties of ILs and DESs also poses a challenge in the screening and selection process. The physico-chemical and thermodynamic properties of conventional solvents are well established and predictable whereas that is not the case for ILs and DESs. Due to limitation in time and cost, experimental method alone cannot be relied upon in designing and selecting appropriate ILs and DESs for any processes, in this work, extractive denitrogenation particularly. Therefore, computational methods to model and predict the behavior of systems containing ILs or DESs become inevitable.

The parameters to be considered when designing a DESs include i) salt type: salt cation substructure, phosphonium, ammonium or sulfonium-based cation, alkyl chain length, choice of anion, ii) HBD type: HBD can be of various chemical families such as carboxylic acids, amides, alcohols and polyols and iii) salt:HBD molar ratio: as discussed

previously, the salt:HBD molar ratio affects the physico-chemical properties of DESs and different ratios lead to the formation of a new DES. Therefore, for the purpose of designing an IL or a DES for a certain process, it is necessary to acquire knowledge on the relationship between the fundamental properties of the system such as electronic and molecular structure and macromolecular physical and chemical properties. Quantum chemical methods can be considered as among the most practical approaches to screen and select ILs and DESs for extractive denitrogenation. Finding a relationship between gas-phase electronic structure and experimentally observed behavior of the system through *ab initio* computational procedure is useful for predicting the features of ILs and further can be used for choosing appropriate pairing of ILs (Zhan et al., 2003). Consequently, similar approaches can also be used to choose pairing of DESs constituent.

A thermodynamic model based on quantum chemical calculations was developed by Andreas Klamt in 1999 (Klamt, 1995). The model, namely COSMO-RS which stands for **C**Onductor-like **S**creening **M**Odels for **R**eal **S**olvents serves as a bridge between quantum chemistry and chemical engineering thermodynamics. COSMO-RS translates the quantum chemical calculation results into something more familiar to the chemical engineering practitioners. The main advantages of COSMO-RS are i) the solid theoretical background of the model based on statistical thermodynamics principles, ii) the lack of need for experimental data, thus saving cost, time and energy required to conduct experiments and iii) a fast and reliable method for solvent screening based on prediction of thermodynamic properties and behaviour. Further details on the background theory of COSMO-RS and quantum chemical calculation methods used in this work is described in the next subsections.

Other than COSMO-RS, other attempts to create a COSMO-based model to connect quantum chemistry and chemical engineering thermodynamics have been taken up by Lin and Sandler (Lin et al., 2002) and by Grensemann and Gmehling (Grensemann

et al., 2005). Lind and Sandler developed a COSMO-RS reimplementation named COSMO-SAC which stands for Conductor-like Screening Model – Segment Activity Coefficient model. In COSMO-SAC, instead of using chemical potential of segments to generate σ -potential and later used to calculate thermodynamic properties of compounds and mixture, activity coefficient of segments are used. COSMO-SAC model developers claim that this model is thermodynamically consistent unlike the original COSMO-RS model but this has been refuted by Klamt et al. who proved otherwise (Klamt, 2002). An important advantage of COSMO-SAC is the implementation of the model into a widely used process simulation software, ASPEN Plus.

In the original COSMO-RS model, hydrogen bonds are formed regardless of the involved atoms when donor and acceptor segments are available in the solution. However, Grensemann and Gmehling opined that hydrogen bondings in real solutions only occur between polarized hydrogen atoms connected to strongly electronegative atoms such as oxygen, nitrogen or other strong electronegative atoms. This has been taken into account in COSMO-RS (OI) by introducing a second σ profile only for surface segments of atoms where hydrogen bondings are physically meaningful. Since the chemical potential of one surface segment is influenced by the chemical potential of all the other surface segments in the ensemble S , the two σ profiles had to be combined. This was achieved by replacing the screening charge density σ with the following new descriptor, η which is a simple combination of the screening charge density σ and the type δ of the bonding. A large amount of data from the Dortmund Data Bank (DDB) was used to verify the validity of COSMO-RS(OI) prediction during the development of this model. However, since the conception of COSMO-RS(OI) model until now, there is no reported development of any improvement towards its parameterization of prediction quality. This model was also not widely used in prediction of physical properties and thermodynamic behavior due to its poor prediction performance reported in the literature.

2.6.1 COSMO-RS model

There are two parts of COSMO-RS; i) the COSMO part is an extension of the quantum mechanics' Continuum Solvation Model (CSM) which was developed by Klamt and Schuurman in 1993 (Klamt et al., 1993) and ii) the extension to Real Solvents (RS) part where the statistical thermodynamics approach is described based on COSMO calculation. Thus, COSMO-RS is a two-steps approach: i) COSMO calculation of molecules using density functional theory and ii) statistical thermodynamics of the molecular interactions. In COSMO-RS, molecules are placed in a conductor as the reference state. The basic idea of COSMO-RS is to quantify the interaction energy of interacting species in terms of its polarization charge densities, σ and σ' . The molecular interactions represented in COSMO-RS are the electrostatic misfit energy (E_{misfit}), hydrogen bond interaction (E_{hb}) and van der Waals interaction (E_{vdW}).

Electrostatic misfit energy and hydrogen bond interaction energy are represented in terms of σ and σ' by the following expressions:

$$E_{misfit}(\sigma, \sigma') = a_{eff} \frac{\alpha'}{2} (\sigma + \sigma')^2 \quad (\text{Eq. 2.3})$$

$$E_{hb} = a_{eff} c_{hb} \min(0, \sigma\sigma' + \sigma_{hb}^2) \quad (\text{Eq. 2.4})$$

The less specific van der Waals interaction energy is taken into account in a slightly more approximate way by the following expression:

$$E_{vdW} = a_{eff} (\tau_{vdW} + \tau'_{vdW}) \quad (\text{Eq. 2.5})$$

From these expressions, there are five universal adjustable parameters, which are:

a_{eff} is the effective contact area,

α' is a general constant

c_{hb} is strength coefficient

σ_{hb} is the polarization charge density threshold for hydrogen bond

τ_{vdW} is the element-specific parameter for dispersion coefficient

The determination of the values for these parameters is based on large database of experimental data depending on which basis set is used for parameterization. Nevertheless, these parameters are universal and need not to be adjusted to specific systems unlike the conventional approaches like the majority of activity coefficient models.

Representation of Statistical Thermodynamic in the COSMO-RS Model

It is important to bear in mind that the polarization charge density σ is the only descriptor determining the interaction energies in the COSMO-RS model. σ -profile is a distribution function or histogram which gives the relative amount of surface with polarity σ in the molecule while σ -potential is the chemical potential of a segment which describes the affinity of the solvent for a molecular surface of polarity σ .

In general, consider a mixture (an ensemble S) consisting of several compounds X^i with molar concentrations x_i . Thus, the σ -profile of the system is the weighted sum of the σ -profiles of the components, i.e.

$$p_S(\sigma) = \sum_{i \in S} x_i p^{X^i}(\sigma) \quad (\text{Eq. 2.6})$$

For an efficient statistical thermodynamics, it is useful to consider a normalized ensemble. Thus, the ensemble S of interacting molecules is reduced to an ensemble of interacting pairs of surface segments. Therefore, the σ -profile for the normalized ensemble is:

$$p'_S(\sigma) = \frac{p_S(\sigma)}{A_S} = \frac{\sum_i x_i p^{X^i}(\sigma)}{\sum_i x_i A^{X^i}} \quad (\text{Eq. 2.7})$$

Where A_S is the total surface area of the ensemble S and A^{X^i} is the total surface area of compound X^i . In this condition, the assumption made is that there is no free surface in the bulk of the liquid, thus each piece of the surface segment has a contact pair. This assumption is valid for a state far from the critical region. Under this boundary condition, the chemical potential of a surface segment in the normalized ensemble can be represented using the following equation:

$$\mu_S(\sigma) = -RT \ln \left\{ \int d\sigma' p_S(\sigma') \exp \left(\frac{\mu_S(\sigma) - E_{int}(\sigma, \sigma')}{RT} \right) \right\} \quad (\text{Eq. 2.8})$$

The activity factor of a surface segment, $\gamma_S(\sigma)$ can be defined by

$$\ln \gamma_S(\sigma) = \frac{\mu_S(\sigma)}{RT} \quad (\text{Eq. 2.9})$$

From this expression, the chemical potential of a surface segment can be rewritten as

$$\ln \gamma_S(\sigma) = -\ln \left\{ \int d\sigma' p'_S(\sigma') \gamma_S(\sigma') \exp \left(-\frac{E_{int}(\sigma, \sigma')}{RT} \right) \right\} \quad (\text{Eq. 2.10})$$

Based on the equations above, we can determine the chemical potential of a solute X in the ensemble S , μ_S^X .

$$\mu_S^X = \mu_{\text{residual},S}^X + \mu_{\text{combinatorial},S}^X \quad (\text{Eq. 2.11})$$

The residual part of the chemical potential is the part resulting from the interactions of the surfaces in the liquid. This can be obtained by integrating the function of $\mu_S(\sigma)$ over the solute surface, i.e.

$$\mu_{\text{residual},S}^X = \int p^X(\sigma) \mu_S(\sigma) d\sigma \quad (\text{Eq. 2.12})$$

The combinatorial part of the chemical potential which results from the different shapes and sizes of the solute and solvent molecules can be represented by a Staverman-Guggenheim expression:

$$\mu_{\text{combinatorial},S}^X = -RT \left\{ \lambda \ln A_S + L_1^{SG} + \frac{z}{2} \frac{V^X}{V_0} L_2^{SG} \right\} \quad (\text{Eq. 2.13})$$

With

$$L_1^{SG} = 1 - \frac{A^X}{A_S} + \ln \frac{A^X}{A_S} \quad \text{and} \quad L_2^{SG} = 1 - \frac{V^X A_S}{V_S A^X} + \ln \frac{V^X A_S}{V_S A^X} \quad (\text{Eq. 2.14})$$

Where

V^X = the molecular volume of compound X

V_S = the average molecular volume of the solvent

V_0 = the partial volume of an ethylene unit used for normalisation purposes

For consistency, the COSMO areas and volumes are used in these expressions instead of the tabulated van der Waals areas and volumes of the UNIFAC group contribution method.

Finally, the activity coefficient of a solute in a liquid S is defined by

$$\gamma_S^X = \exp \left(\frac{\mu_S^X - \mu_X^X}{RT} \right) \quad (\text{Eq. 2.15})$$

2.6.2 COSMO-RS Applications for systems containing ILs and DESs

Applications of COSMO-RS model for systems containing ILs are tremendous. A comprehensive review on the uses of COSMO-RS for solvent screening in general has been done by Eckert and Klamt where they presented the COSMO-RS applications to thermodynamic problems including vapour-liquid equilibria (VLE), liquid-liquid equilibria (LLE), solid-liquid equilibria (SLE), partition coefficient and vapour pressure of mixtures of organic solute and solvents (Eckert et al., 2002). By using COSMO-RS, there is virtually no restriction on the structure of molecules to be predicted, unlike using group contribution methods (GCMs) where the application is limited to the groups and sub-groups available. However, the quality of predictions by COSMO-RS is usually

slightly lower than that of GCMs because of the general parameterization used in the calculations. Under the prediction of VLE, one can also predict the excess enthalpies, excess Gibbs energy, vapour-liquid phase diagrams and activity coefficient values. However, predictions of VLE using COSMO-RS rely upon the solving of fugacity equalities where the vapor pressure law appears in the fugacity term. Although COSMO-RS has a kind of QSPR for predicting vapour pressure laws, it is well known that prediction results for VLE are very poor. Hence COSMO-RS software documentation suggests to provide at least one experimental vapour pressure value. This reduces the purported universality of COSMO-RS and this might be a serious problem for VLE with ILs and DESs where vapor law is not well known or difficult to measure.

For the prediction of LLE, the experimental tie-lines are well met by COSMO-RS predictions and the temperature dependency of the LLE is reproduced correctly where the root mean square for the prediction of partition coefficient is generally within the accuracy range expected for an *a priori* method. For the prediction of SLE, some modifications have to be made because COSMO-RS is a theory of liquids i.e. ensemble of disordered molecules. Prediction of supercooled melt is required for compounds below their melting point. In the prediction of SLEs, there are three examples which can be applied using COSMO-RS, which are i) estimation of the Gibbs energy of fusion using melting point and entropy of fusion data, ii) prediction of solubility mole fraction and iii) prediction of Hansen solubility parameter. COSMO-RS was also used to predict vapour pressure of liquids at arbitrary temperature.

A more specific review on the use of COSMO-RS for property prediction of mixtures containing ILs was done by Diedenhofen and Klamt (Diedenhofen et al., 2010). In this review, the different approaches to describe ILs in COSMO-RS i.e. (i) electroneutral approach, (ii) meta-file approach and (iii) ion-pair approach were compared. In electroneutral approach, the two ions are described as separate molecules

with equal mole fractions. This approach pictures ILs as two distinct ions and thus is closer to reality where the ions are moving freely in the liquid phase. However, extra care should be taken when using this approach regarding the definitions and reference state of the computed thermodynamic property. Definitions in electroneutral approach refer to the mole fraction representation in experimentally determined properties or the properties determined by prediction using COSMO-RS i.e. whether using the laboratory binary or the ternary approach where the ions are treated as separate species in the system. Whereas the reference state refers to interpretation of the result i.e. if the result is obtained using binary or ternary description of the mole fraction and if the property predicted or measured is dependent upon the mole fraction.

The meta-file approach combines the two ions in a single file and thus, the surface charge σ , the area and the volume of the two ions are combined while taking into account the interactions with the two distinct ions. In this case, errors in the chemical potential might arise if the IL is present at a finite concentration in the mixture because the entropic term of the whole IL is used. The third approach i.e. ion pair approach, uses a *.cosmo* file of an ion pair and so does not describe the reality of a molten salt very well because it pictures a fixed orientation of the cation and anion as the system consists of ion pairs with the same structure only. In some cases, one approach is superior to the others based on accuracy of the results. For example, Palomar et al. found a better correlation when using the ion-pair approach for the prediction of molar volumes instead of the meta-file approach, which may be due to weaker hydrogen bond capacity caused by counter ion interaction in the ion pair approach compared to the meta-file approach (Palomar et al., 2007; Palomar et al., 2008). However, in the case of prediction of enthalpies of vaporization of the ILs 1-ethyl-3-methylimidazolium ethylsulfate, 1-butyl-3-methylimidazolium dicyanamide and 1-alkyl-3-methylimidazolium bis(trifluoromethanesulfonate), both ion-pair and electroneutral approaches exhibit good

agreement with experimental results (Diedenhofen et al., 2007). Banerjee et al. used the ion-pair and meta-file approaches to predict the VLE and LLE data for systems containing ILs and reported that the meta-file approach was superior to ion-pair approach (Banerjee et al., 2008). Other than the difference in mole fraction definition, meta-file and electroneutral approach are different in the combinatorial contribution to the chemical potential and the conformer treatment where the combinatorial term depends on the mole fraction definition, molecular areas and volumes of the species. In COSMOtherm software package, electroneutral approach is the default approach to describe ILs because it is considered the most flexible description of an IL in the liquid phase.

In their review, Diedenhofen and Klamt also discussed the applications of COSMO-RS to predict activity coefficient at infinite dilution (γ^∞), gas solubilities and Henry's constant, binary and ternary LLE, VLE and IL screening and tailoring. The use of COSMO-RS to predict activity coefficient at infinite dilution was first done in 2003, where the γ^∞ values of 38 solutes comprising of hydrocarbons, alcohols and polar organics in the ILs 1-ethyl-3-methylimidazolium bis(trifluoromethylsulfonyl)imide, 1-butyl-3-methylpyridinium tetrafluoroborate and 1-ethyl-2,3-dimethylimidazolium bis(trifluoromethylsulfonyl)imide, were performed using the electroneutral approach (Diedenhofen et al., 2003). The results obtained have similar accuracy to that observed for normal organic solvents. Banerjee and Khanna used a special version of COSMO-RS implementation which is the variation originally used for the prediction of LLE of neutral compounds to predict γ^∞ values of solutes in phosphonium-based ILs and obtained an average absolute deviation of about 11.5% (Banerjee et al., 2006). The prediction of gas solubility and Henry's Law's constants using COSMO-RS is also reported greatly due to increasing attention for CO₂ capture using ILs with an interest to address global warming problem. Prediction of γ^∞ values can also be used for IL screening and tailoring for separation processes. Jork et al. screened ILs for use as entrainers in the distillation of

tetrahydrofuran/water and methylcyclohexane/toluene mixtures using predicted γ^∞ values of the compounds in ILs (Jork et al., 2005). The same approach of predicting γ^∞ values to screen ILs was also applied by Lei et al. for separation of hexene/hexane and extraction of drugs from urine and by Kumar et al. for thiophene extraction from diesel for desulfurization process (Kumar et al., 2009; Lei et al., 2006).

COSMO-RS is also used for the prediction of binary and ternary LLE for systems containing ILs. The prediction of binary LLE for systems containing ILs was first done by Marsh et al. for mixtures of alcohol and 1-butyl-3-methylimidazolium hexafluorophosphate in 2002 using both meta-file and electroneutral approaches (Marsh et al., 2002). Marsh et al reported that better results are obtained when using the electroneutral approach. In 2006, Domanska et al. published two studies on binary LLE prediction using COSMO-RS for the mixtures of 1-alkyl-3-methylimidazolium methylsulfate (alkyl=methyl and butyl) and several esters, ketones and hydrocarbons using the equimolar ion mixture approach (Domańska et al., 2006). Based on their results, the predicted curve lines are similar to the experiments while the quantitative values show significant disagreement with the experimental values. Freire et al. reported two studies on the prediction of binary LLE using COSMO-RS: one for systems of IL-alcohol and another for IL-water using the electroneutral approach (Freire et al., 2007; Freire et al., 2008). It was reported that the IL-water systems are described much better than the IL-alcohol systems, albeit COSMO-RS provided reasonable qualitative agreement with experimental results for IL-alcohol systems. It was also reported that COSMO-RS is able to predict some factors affecting the mutual solubilities including the cation alkyl chain length in the systems of IL-alcohols and IL-water.

For the prediction of ternary LLE, Banerjee et al. used a variant of COSMO-RS which was refitted for LLE prediction of mixtures of neutral compounds to predict 36 ternary LLE data containing ILs and alcohols, ethers, alkanes and aromatic compounds

(Banerjee et al., 2007; Banerjee, et al., 2008). Both meta-file and ion-pair approaches were used to describe ILs based on imidazolium and pyridinium cations with sulfates, bis(trifluoromethylsulfonyl)imide, hexafluorophosphate and chloride anions. It was reported that prediction with ion-pair approach gave results with reduced accuracy.

In this work, COSMO-RS is applied to predict liquid-liquid equilibrium behaviour and liquid extraction performances for systems containing ILs and DESs. More attention is given to the separation of aromatic and aliphatic mixtures, desulfurization and denitrogenation. In the next subsections, the discussion will revolve around the applications of COSMO-RS for screening of ILs for the aforementioned purposes using three approaches:

- i) qualitative screening of ILs using σ -profile and σ -potential
- ii) screening of ILs using prediction of activity coefficient at infinite dilution
- iii) prediction of ternary LLE phase diagrams

Qualitative screening of ILs using σ -profile and σ -potential

σ -profiles and σ -potentials are COSMO-RS representations of molecular interactions of compounds and their mixtures. Both σ -profile and σ -potential contain a wealth of information on how the compounds behave and interact with themselves or with other molecules. σ -profile is a probability distribution function which describes the amount of surface in the ensemble having a screening charge density between σ and $d\sigma$. Negative partial charges of atoms cause positive screening charge density and vice versa. The peaks at certain values of σ show presence and/or absence of hydrogen bond donor and hydrogen bond acceptor capability and also the polarity or non-polarity of a compound. The threshold value for hydrogen bonding is $\sigma_{hb} = \pm 0.0084 \text{ e } \text{\AA}^{-2}$. Compounds with peaks at $\sigma < -\sigma_{hb}$ indicate presence of hydrogen bond donor whereas compounds with peaks at $\sigma > +\sigma_{hb}$ indicate presence of hydrogen bond acceptor. σ -potential describes the

affinity of a species towards the surface with screening charge density σ . For example, a compound exhibiting a curve with negative slope at $\sigma < -\sigma_{hb}$ indicates affinity towards hydrogen bond donor and if it exhibit a curve with negative slope at $\sigma > +\sigma_{hb}$, this indicates its affinity towards hydrogen bond acceptor. The σ -profiles and σ -potentials can be used for preliminary qualitative solvent screening as reported by Eckert and Klamt (Eckert, et al., 2002).

Garcia-Chavez et al. reported the use of σ -profile to screen ILs as solvent for the extraction of monoethylene glycol from aqueous streams. The screening using σ -profile was done because the predicted values of activity coefficient at infinite dilution by COSMO-RS calculations showed huge deviation when compared to experimental data. ILs selected based on the qualitative screening using σ -profiles were then experimentally evaluated and good agreement was reported (Garcia-Chavez et al., 2012). In another report by Zhou et al., three ILs namely 1-butyl-3-methylimidazolium tetrafluoroborate, 1-butylpyridinium thiocyanate and 1-butylpyridinium tetrafluoroborate were used to extract benzene from cyclohexane (Zhou et al., 2012). The σ -profiles were used *a posteriori* to explain the experimental ternary LLE obtained rather than for a priori ILs' screening.

Although σ -profile and σ -potential are useful to elucidate the molecular interactions, it remains a qualitative approach which depends on one's skill and ability to interpret the σ -profile and σ -potential graph. As a consequence, this approach may only be used for preliminary screening of new solvents and must be combined with more detailed screening quantitative methods.

Prediction of Activity Coefficient at Infinite Dilution

A reliable quantitative method based on COSMO-RS for solvent screening consists of predicting the value of activity coefficient at infinite dilution (γ^∞) for the

solutes in the potential solvents. γ^∞ is important for screening of ILs in separation processes such as liquid extraction and extractive distillation where the separation efficiency highly depends on the selected solvent. γ^∞ is an essential parameter because it indicates the extent of molecular interactions between the solute and solvent at miniscule concentration of the solute. In fact, when removing aromatic nitrogen compounds from diesel, the most difficult part is to eliminate of the last residual traces.

Kumar and Banerjee used COSMO_LL, a variation of COSMO-RS which has been reparameterized for the prediction of LLE for neutral system to screen a total of 264 ILs from a combination of 11 cations and 24 anions using the prediction of γ^∞ values of thiophene and simulated diesel fuel in the ILs (Kumar, et al., 2009). The predicted γ^∞ values were then used to estimate the selectivity, capacity and performance index at infinite dilution. The cations of the ILs were from imidazolium, pyridinium, pyrrolidinium and quinolinium families. It was reported that for imidazolium-based ILs, the selectivity depends on the alkyl chain length of the anion where selectivity decreases with increasing number of alkyl side group within the ring of the anion. In general, ILs with small cations reported higher values of selectivity but lower values of capacity. Increase in capacity is reported with the increase in alkyl chain length of the 1-alkyl side chain of the cations. As the size of cation increases, more diesel components can be accommodated on the IL along with thiophene, thus decreasing the selectivity but increasing the capacity. ILs with anions which have sterical shielding around the charge center are the most favourable for desulfurization such as tetrafluoroborate, hexafluorophosphate, tetracyanoborate and trifluoromethanesulfonate anions. Amongst the cations, ILs with imidazolium cation gave greater values of selectivity with thiophene compared to six-membered cation because of its similar structure with thiophene.

Anantharaj and Banerjee screened a total of 156 ILs from a combination of 6 cations and 26 anions for the removal of aromatic nitrogen compounds from simulated

diesel fuel by prediction of γ^∞ using COSMO-RS method (Anantharaj, et al., 2010a). The six cations comprised of a mixture of aromatic cations (1-ethyl-3-methylimidazolium, 1-ethylpyridinium, 1,2,4-trimethylpyrazolium) and non-aromatic cations (4-ethyl-4-methylmorpholinium, 1-ethyl-1-methylpiperidinium, 1-ethyl-1-methylpyrrolidinium). The predicted γ^∞ values were then used to calculate the selectivity, capacity and performance index at infinite dilution. Various effects were studied towards the predicted values of γ^∞ , S^∞ , C^∞ and P.I. including the effect of nitrogen compound heterocyclic structure, anion structure and cation structure. It was found that non-aromatic cations combined with smaller size anions such as acetate and thiocyanate showed high selectivity, capacity and performance index for both 5-membered and 6-membered nitrogen compounds because aromatic cations possessed high steric hindrance compared to non-aromatic cations. The performance of anions was found to depend upon several factors including the number and type of electronegative atoms (N, S, O, F) and charge on the electronegative atoms. 5-membered nitrogen compounds report higher values of S^∞ , C^∞ and P.I. because of the higher electronegativity of the heteroatom compared to the 6-membered compounds. Following the success of screening ILs for denitrogenation process, Anantharaj and Banerjee later applied similar approach to screen a total of 168 ILs from a combination of 6 cations and 28 anions for the removal of aromatic sulfur from model diesel oil (Anantharaj et al., 2011a). Additional explanation on the values of γ^∞ obtained was provided using the σ -profiles of cations and sulfur compounds. It was concluded that ILs with smaller cation structure without aromatic ring combined with a heavier sterical shielding effect on an anion charge centre is important for the separation of sulfur compounds.

Gutierrez et al. stated that conventional methodologies for solvent screening based on the strength of interactions between solutes and solvents at infinite dilutions do not represent accurately the conditions in industrial operations, especially when strong

interactions between the solute and solvent occur (Gutiérrez et al., 2012). As a consequence, they proposed a solvent selection methodology for separating aromatic and nonaromatic hydrocarbons (toluene/methylcyclohexane), olefin and paraffin hydrocarbon (1-hexene/hexane) and ethanol and water mixtures by extractive distillation process. In their method, the activity coefficient and selectivity at infinite dilution were predicted and the influence of the alkyl chain length and degree of branching of every cation was analysed. The selectivity, solubility and relative volatility at finite dilution of the solute in some ILs are obtained experimentally and compared with predicted values. It was found that COSMO-RS underestimates the value of γ^∞ in conventional solvents and overestimates the value of γ^∞ in ILs, although the predictions for ILs seem to be more accurate. COSMO-RS was able to predict qualitatively the strength of the interactions between solutes and solvents and it was also able to predict the temperature influence towards the interactions.

Reddy et al. measured the values of γ^∞ of polar and nonpolar organic solutes in the IL polyethylene glycol (PEG-5) coconium methylsulfate using gas-liquid chromatography at four different temperatures (313, 323, 333 and 343 K) (Reddy et al., 2013). The solutes comprised of alkanes, cycloalkanes, alk-1-enes, alk-1-ynes, aromatics, alcohols and ketones. The measured results for the selected solutes hexane, hex-1-ene, cyclohexane, benzene and ethanol were compared against predicted values of γ^∞ using COSMO-RS where the IL was described using the electroneutral approach with equal molar ratio of cation and anion. They reported good overall agreement between experimental values and COSMO-RS predicted values of γ^∞ . COSMO-RS marginally over predicts the values of γ^∞ for benzene and hex-1-ene and under predicts for cyclohexane and ethanol, but performed fairly well for predictions of hexane. Selectivities at infinite dilution (S_{12}^∞) have been calculated for separation model mixtures of hexane (1)/benzene (2), hexane (1)/hex-1-ene (2), cyclohexane (1)/benzene (2) and

hexane (1)/ethanol (2). In general, good agreement was obtained between experimental and predicted values of (S_{12}^{∞}) derived from the experimental and predicted values of γ^{∞} . More recently, Lyu et al. reported the screening of ILs for the separation of benzene and cyclohexane using COSMO-RS prediction of γ^{∞} values in 264 ILs comprised of 12 cations and 22 anions (Lyu et al., 2014). Similar to previous reported works, the values of γ^{∞} were used to estimate the selectivity, distribution ratio and performance index at infinite dilution. COSMO-RS prediction of γ^{∞} values were validated by comparing with experimental values of selectivity at infinite dilution for benzene and cyclohexane in selected ILs, namely 1-ethyl-3-methylimidazolium tetrafluoroborate, 1-butyl-3-methylimidazolium tetrafluoroborate, 1-hexyl-3-methylimidazolium tetrafluoroborate and 1-octyl-3-methylimidazolium tetrafluoroborate at different temperatures. Experimental findings reported that selectivity increases with increasing temperature and increase in cation alkyl chain and the predicted selectivity values follow the same trend. Based on the screening results, for most cations the distribution ratio for benzene is higher in ILs with anions containing Cl atom, such as chloride, tetrachloroaluminate and tosylate. This is attributed to the more delocalized electrons that the anions have compared to anions containing F atom because anions with more delocalized electrons show weaker interactions with cations, which in turn promotes the interaction of IL with benzene.

Based on the reported works on using COSMO-RS predicted values of γ^{∞} for screening of ILs for liquid separation processes, it can be deduced that this is a fairly reliable method based on COSMO-RS for solvent selection because it gives quantitative values and the calculation results can be compared against experimental data. Shortlisted solvents from the screening process have also been proven to be effective solvents based on experimental validation. However, care should be taken when using COSMO-RS predicted γ^{∞} for solvent screening because it has also been reported that the predicted values gave considerable deviation from experimentally derived values for certain

systems. Thus, in order to overcome this drawback, it is recommended to start by a benchmarking of the predicted values of γ^∞ with experimental data for the separation systems of interest, for example, aromatic/non-aromatic mixtures, olefin/paraffin mixtures or alcohol/water mixtures before proceeding to screen a large number of ILs with various solutes and carriers using COSMO-RS. It should also be mentioned that the prediction of γ^∞ using COSMO-RS should only be done for preliminary screening purposes and a more detailed calculation and simulation of the separation process is necessary for design calculation.

Prediction of liquid-liquid equilibrium for systems containing ILs

One of the most useful applications of COSMO-RS is the ability to predict thermodynamic phase diagram without the need of any experimental data. COSMO-RS has been successfully applied to predict ternary LLE phase diagrams for the separation of aromatic from aliphatic hydrocarbons using ILs as the extracting solvents. The importance of ternary LLE phase diagram for design calculation has been discussed earlier in Section 2.5.3. Ferrerira et al. have conducted a comprehensive review on the use of COSMO-RS for prediction of ternary LLE phase diagrams for the separation of aromatic and aliphatic hydrocarbons using ILs (Ferreira et al., 2012). They have collected a total of 188 experimental tie-lines of ternary LLE systems comprised of aromatic + aliphatic + ILs at various temperatures from the literature. The experimental data were used to evaluate COSMO-RS ability in describing the phase behaviour of the systems and whether COSMO-RS is able to predict several factors influencing the phase behaviour such as the structural characteristics of the hydrocarbon molecules and ILs. The ternary systems collected were related to applications in petrochemical and refinery processes and is in close interest with the work done in this thesis. Evaluation of COSMO-RS prediction also includes the prediction of selectivities and distribution ratios among the coexisting phases. Structural factors such as aromaticity, chain length, cyclization and

positional isomerism of the hydrocarbons, cation core and anion nature and length of the side alkyl chain length of the ILs were also analysed and discussed regarding the impact that they have on the LLE phase behaviour. RMSD was used to evaluate the goodness of COSMO-RS prediction of the phase diagrams.

COSMO-RS is able to reproduce the effect of cyclization of the aliphatic hydrocarbons on the shape and size of the miscibility gap and of the bimodal curves and tie lines for the systems composed of various aliphatic hydrocarbons + benzene + [EMIM][EtSO₄]. Moreover, it gave a particularly good description of the very low solubilities of ILs in the hydrocarbon-rich phase. The effect of alkane chain length of aliphatic hydrocarbons in the ternary systems is also well described by COSMO-RS with good accuracy on the mutual solubility. However, the quality of COSMO-RS prediction of selectivity and distribution ratio decreases with increasing alkane size, which may be due to the sensitivity of the selectivity and distribution ratio values at very low concentrations of alkane in the IL-rich phase.

The effect of aromatic structural characteristics on the phase behaviour is also well captured by COSMO-RS model with small discrepancy observed between the experimental data and predicted bimodal curves, where the mixture miscibility decreases with increasing alkyl side chain length of the aromatic structure whereas the absolute slope of the tie lines increases with increasing aromatic content and increase in the alkyl side chain length. The trend of selectivity and distribution ratio is also predicted adequately by COSMO-RS. Ferreira et al. included ternary systems from ILs of different cation family including imidazolium, pyridinium, ammonium and phosphonium-based. COSMO-RS is capable of describing the bimodal curve for the studied systems with different cation family although with less accuracy at the region with higher aromatic content. For systems containing ILs with pyridinium-based cations, COSMO-RS can also describe correctly the phase behavior with changing pyridinium isomers in the cation i.e.

para, meta or ortho substitutions. The predicted selectivities and distribution ratios were described satisfactorily if we take into account the uncertainty on the hydrocarbon-rich concentrations. The IL cation alkyl chain length influences the phase behavior in that the immiscibility region decreases with increasing cation side alkyl chain length and the phase diagrams change from Type 2 to Type 1. COSMO-RS describes adequately the trends observed for the change in mutual solubility, binodal curves, tie lines slope and the values of selectivity and distribution ratio. However, the quality of the binodal curve prediction by COSMO-RS decreases for systems with longer alkyl chains, whereas the predicted selectivities and distribution ratios are satisfactory. ILs anion does not have a significant impact on the mutual solubilities among the ternary systems, except for [NTf₂]-based ILs. In general, COSMO-RS manage to capture qualitatively the impact on the binodal curves, tie lines slopes and the selectivities and distribution ratios with the changing anions except for the systems containing ILs with the anions methylsulfate, ethylsulfate, hexafluorophosphate and tetrafluoroborate. For these systems, the predicted binodal curves deviates considerably from the experimental data, which indicates that COSMO-RS is less reliable to describe the effect of anions on the phase behavior of mixtures, especially anions that present strong interactions with the cations. The effect of temperature on the phase behaviour was investigated using the system *n*-hexane + benzene + [1,3-C₂mpy][EtSO₄] at temperatures ranging from 283 to 328 K. It was observed that there is small variation of the experimental LLE binodal curve where increase in temperature leads to increased miscibility with a contraction of the immiscibility region, whereas the tie lines slope become more negative with increasing temperature. The selectivities and distribution ratios are slightly influenced by the temperature, although there is decrease in value with increasing temperature. COSMO-RS is able to reproduce the temperature effect on the ternary LLE phase diagram with small differences between the experimental and predicted binodal curves at the IL-rich

phase. COSMO-RS satisfactorily describes the change in selectivities and distribution ratio albeit some discrepancy between the predicted and experimental values. The results suggested that the quality of COSMO-RS prediction degrades with increasing temperature, however, more experimental data are required to ascertain this.

In summary, COSMO-RS prediction is able to qualitatively describe the phase equilibria of the ternary systems composed of aromatic + aliphatic + IL, although the most reliable predictions are provided particularly for the most immiscible systems. This is because in COSMO-RS, the calculations consider that the interactions are completely performed at the interface of the virtual conductor environment surrounding the molecules and thus perform better for poorly miscible systems. Due to the large number of samples taken to conduct the analysis and the comprehensive discussion on factors affecting the phase behaviour, the review by Ferreira et al. is sufficient to be based upon for evaluating the quality of COSMO-RS prediction of ternary LLE phase diagram, selectivity and distribution ratio for ternary systems of aromatic+aliphatic+ILs. However, the ability of COSMO-RS to predict phase behaviour for ternary systems containing ILs with heteroaromatic compounds, mixed ILs, or quaternary systems also need to be evaluated. This will be discussed in the next paragraphs.

Kumar and Banerjee collected a total of 15 ternary LLE systems containing thiophene + aliphatic hydrocarbon + imidazolium-based IL conducted at room temperature from the literature and used COSMO-RS model to predict the ternary LLE phase diagram for each system with the electroneutral approach to describe the ILs (Kumar, et al., 2009). The average RMSD obtained for the 15 ternary LLE systems is 8.43%, which is satisfactory considering COSMO-RS a totally predictive method.

Later, Varma et al. performed ternary LLE experiments to extract benzothiophene from n-hexane using the ILs 1-ethyl-3-methylimidazolium ethylsulfate

([EMIM][EtSO₄]) and 1-ethyl-3-methylimidazolium acetate ([EMIM][Ac]) at room temperature. COSMO-RS calculation was performed to predict the ternary LLE phase diagram and compared with the experimental tie line and the RMSD values were equal to 4.36% and 7.87% for systems containing respectively [EMIM][EtSO₄] and [EMIM][Ac]. Although the RMSDs for both systems indicates that COSMO-RS gave a fairly accurate predictions, the COSMO-RS predicted tie lines plotted on the same phase diagram with experimental tie lines showed considerable deviation between the predicted and experimental values, especially at higher concentration of benzothiophene in the feed mixture. However, COSMO-RS was able to predict the negative slopes of the experimental tie lines. Additionally, it was reported that higher selectivity and lower distribution ratio were obtained using [EMIM][EtSO₄] whereas lower selectivity and higher distribution ratio were obtained using [EMIM][Ac] and COSMO-RS was able to predict the same trends.

Anantharaj and Banerjee reported the use of COSMO-RS to predict LLE phase behavior for quaternary system for the simultaneous separation of thiophene and pyridine from iso-octane at 298 K using three ILs: [EMIM][EtSO₄], [EMIM][Ac] and 1-ethyl-3-methylimidazolium methanesulfonate ([EMIM][MeSO₃]). COSMO-RS calculations were carried out using electroneutral approach to describe the IL. It was reported that the COSMO-RS plots of predicted tie lines provide a clear visualisation of the change in the slope of the tie line (from positive to negative) as a result of change in the anion structure. The negative slope is quite visible at low concentration of thiophene and pyridine in the feed mixture. However, COSMO-RS fails to reproduce the correct extract phase composition for all three systems where it underestimates the concentrations of iso-octane in the IL-rich phase. The RMSDs for each system are 4.49%, 8.26% and 7.4% for systems containing [EMIM][EtSO₄], [EMIM][MeSO₃] and [EMIM][Ac],

respectively. In general, the COSMO-RS prediction for quaternary system containing IL is fairly good considering no additional modification necessary on the model.

Similar approach on modeling quaternary LLE system phase behaviour using COSMO-RS was reported by Manohar et al. where the same three ILs ([EMIM][EtSO₄], [EMIM][MeSO₃] and [EMIM][Ac]) were used to extract thiophene and pyridine from *n*-pentane. It was reported that the predicted tie lines agree quantitatively and qualitatively with experimental tie lines for the system containing [EMIM][Ac] in both extract and raffinate phases. However, high deviation between predicted and experimental tie lines was observed for the systems containing [EMIM][EtSO₄] and [EMIM]MeSO₃] where the length and shape of the immiscible region differ greatly particularly in the extract phase. The deviations are quite high particularly in the upper phase of the phase diagram where the predicted and experimental tie line slopes are in opposite direction because COSMO-RS was not able to predict the change in sign of the tie lines in these two systems. The deviations may be due to the absence of representation of cross hydrogen bonding in COSMO-RS modeling for multi-component mixtures which may be caused the presence of several possible interactions between the ILs and thiophene and pyridine molecules where hydrogen bond interaction plays a major role.

The three ILs were again investigated for use in simultaneous separation of thiophene and pyridine, this time from toluene as the model fuel compound by Anantharaj and Banerjee (Anantharaj et al., 2013). In their report, the COSMO-RS predicted tie-lines agree qualitatively with the experimental tie lines, whereas the length and shape of the immiscible region deviate slightly particularly in the IL-rich phase. COSMO-RS was unable to predict the change in sign of the tie line in the three quaternary systems at low solute concentrations. In this case, the deviation between COSMO-RS prediction and experimental tie lines was attributed to ILs being depicted as hydrogen bonded polymeric molecules and the polymeric nature of ILs is still present when they are mixed with

aromatic components. Besides, mixtures of ILs and aromatic compounds are known to form liquid clathrates. During COSMO calculation which uses unimolecular method, the screening charges are computed by placing a single molecule in the midst of an infinite conductor. Thus, an estimation of hydrogen bond energy which originates from a network is not represented in the calculation. Despite this, the prediction of COSMO-RS is considered good taking into account the method to be unimolecular.

COSMO-RS can also be used to predict quaternary LLE phase behaviour with mixed IL instead of mixed solutes (e.g. thiophene + pyridine). It has been reported that mixing certain ILs may improve the separation efficiency. Potdar et al. reported separation of benzene from hexane using mixture of [EMIM][EtSO₄] and [EMIM][MeSO₃] and predicted the quaternary phase behaviour using COSMO-RS (Potdar et al., 2012). COSMO-RS was also used to predict the optimal ratio of [EMIM][EtSO₄] to [EMIM][MeSO₃] by predicting the selectivity and distribution ratio as a function of mole fraction of [EMIM][EtSO₄]. The point of intersection between the selectivity and distribution ratio curve indicates the optimal ratio for the IL mixture. The COSMO-RS predicted tie lines for the quaternary system agree well qualitatively and quantitatively with experimental data with reported RMSD of 5.25%. Thus, it can be safely concluded that COSMO-RS is able to predict phase behaviour for ternary and quaternary systems containing ILs and heteroaromatic without any modification to the model.

On the other hand, the application of COSMO-RS model for systems containing DES for any separation process is scarce. Till date, there are only two reports of using COSMO-RS for the prediction of ternary LLE phase diagrams and the values of selectivity and distribution coefficient for systems containing DES. Mulyono et al. reported the separation of benzene, toluene, ethylbenzene and m-xylene from *n*-octane using the DES tetrabutylammonium bromide/sulfolane at 1:4 molar ratio (Mulyono, et

al., 2014). COSMO-RS calculations were performed using the COSMOtherm software package where the DES is represented using the electroneutral approach where the DES constituent are treated as three distinct species in the liquid form, i.e. cation, anion and complexing agent. The predicted tie lines are not in good agreement with experimental tie lines but good qualitative agreement was obtained in terms of correct slopes of the tie lines. The reported RMSDs are all less than 10% except for system containing benzene which reports RMSD of 12.7%. It was also observed that COSMO-RS gave better prediction at low aromatic concentrations. COSMO-RS was also used to predict the selectivity and distribution ratio and although it overestimated the distribution ratio, the trend is in accordance with experimental results. The same group later used COSMO-RS to predict ternary LLE phase diagram for DES based on a combination of more than one HBD and CA, tetrabutylammonium bromide combined with ethylene glycol and pyridine at various molar ratios to separate ethylbenzene from *n*-octane (Hizaddin et al., 2015). The predicted tie lines were compared with experimentally obtained tie lines and the average RMSD obtained was 3.67%. Although the COSMO-RS predictions were not as close to the experimental data, the predicted tie lines are in favourable agreement with experimental tie lines. COSMO-RS is able to predict the LLE for varying combination ratios of the DES constituent. COSMO-RS was also used to predict selectivity and distribution ratio. COSMO-RS underestimated the distribution ratios of the DESs, although it qualitatively reproduced the same trend as the experimental values. Prediction of selectivity by COSMO-RS was not as accurate as the prediction of distribution ratio trend, but still showing the correct trend for the selectivity as the experimental values.

2.6.2 Quantum Chemical Methods for the Selection and Design of ILs and DESs

The local forces acting on individual molecules within an IL can be understood through the electronic structure of the components and ion-pairing interactions. Through quantum chemical calculation, the interaction energy, partial charges, highest occupied molecular orbital (HOMO) and lowest unoccupied molecular orbital (LUMO) energy values and energy gap can be used to extract a wealth of information regarding interacting species, based on its ionization potential, electron affinity and global scalar properties such as hardness, softness, electronegativity and electrophilicity index. This approach was undertaken by Anantharaj et al. for simultaneous desulfurization and denitrogenation of diesel oil where they compared potential ILs based on the HOMO/LUMO energy values, gap and scalar properties (Anantharaj et al., 2010b). In the study, the IL 1-benzyl-3-methylimidazolium tetrafluoroborate ([BeMIM][BF₄]) was concluded to be the most suitable IL for simultaneous removal of thiophene and pyridine. More recently, Wagle et al. published a report on the interaction between ILs and polycyclic aromatic hydrocarbons (PAH) through quantum chemical calculation, where they investigated the binding energies, orbital energies and partial charge transfer between ILs and PAH in order to deduce which IL have the most favorable interaction with the PAHs (Wagle et al., 2013). Zhou et al. investigated the interactions between thiophene and the ILs 1-butyl-3-methylimidazolium tetrafluoroborate ([BMIM][BF₄]) and 1-butyl-3-methylimidazolium hexafluorophosphate ([BMIM][PF₆]) by performing geometry optimization on five clusters of thiophene-cation, thiophene-anions and thiophene-ILs (Zhou et al., 2008). It was discovered that the interaction of thiophene with ILs are mainly via Coulombian attraction. From an earlier experimental result which reported the ratio of interaction between thiophene:[BMIM][BF₄] and thiophene:[BMIM][PF₆] as 2.4:1 and 3.5:1 respectively, Zhou and co-workers concluded based on the calculations that the reason why the molar ratio of thiophene: IL is higher for [BMIM][PF₆] is due to strong

electron donation of phosphorus atom to the fluorine atoms, apart from the difference in compactness of the two IIs.

HOMO/LUMO energy values

In principle, all heterolytic reactions can be simplified as examples of interactions between filled atomic or molecular orbitals and empty atomic or molecular orbitals. When two molecular orbitals interact, two new orbitals will be produced. One of the new orbitals is higher in energy than the original one (i.e. the antibonding orbital) and one is lower in energy (i.e. the bonding orbital). When dealing with interacting molecular orbitals, the two orbitals that interact are generally the HOMO of one molecule and the LUMO of another molecule. An electron removed from an atom or molecule is taken from the HOMO while the electron added to another atom or molecule is added to the LUMO. HOMO and LUMO are also known as frontier orbitals and they are essential in determining the amount of energy required to add or remove electrons in a molecule. HOMO is associated with the tendency of a species to donate electron and is characteristic for nucleophile components while LUMO is associated with the tendency to receive electron and is characteristic for electrophilic components.

Ionization Potential and Electron Affinity

Ionization potential (I) is defined as the ability of a ligand to donate precisely an electron to an acceptor and is represented by the energy required to remove one or more electron from an atom or ion. Electron affinity (A) is defined as the ability of a ligand to accept precisely an electron from a donor and is related to the amount of energy released when an electron is added to an atom. HOMO energy is related to the ionization potential as approximated based on Koopmann's theorem while LUMO energy is used to estimate the electron affinity in a similar way:

$$I = -\epsilon_{HOMO} \quad (\text{Eq. 2.16})$$

$$A = -\epsilon_{LUMO} \quad (\text{Eq. 2.17})$$

where $-\epsilon_{HOMO}$ and $-\epsilon_{LUMO}$ are the one electron eigenvalues related to the frontier orbitals as defined in Kohn-Sham Density Functional Theory, which is a version of Koopmann's theory at DFT level. It should be noted that these equations are only exact for hydrogenic atoms and serve only as an approximation for other atoms since the electron movement after ionization occurred are not taken into account (Zhan, et al., 2003). Species with low HOMO energy indicate high ionization potential (better electron donors) while those with high LUMO energy indicate high electron affinity (better electron acceptors).

Global Scalar Properties

The HOMO-LUMO energy gap can be determined from the HOMO and LUMO energy values and further, important properties in quantum chemical calculation such as the hardness (η), softness (S), chemical potential (μ), electronegativity (χ) and electrophilicity index (ω) can be determined. The energy gap between the HOMO and LUMO is related to the hardness of a molecule by the following expression:

$$\eta = \frac{\epsilon_{LUMO} - \epsilon_{HOMO}}{2} = \frac{I - A}{2} \quad (\text{Eq. 2.18})$$

Molecules with a large HOMO-LUMO gap are hard molecules which means highly stable and not keen to charge transfer because they resist changes in their electron number and distribution. Soft molecules have a small HOMO-LUMO gap which means they only require small energy amount to get them to the excited states and thus are more polarizable. In terms of reactivity, soft molecules are more reactive than hard molecules especially when electron transfer is necessary for the reaction. Softness (S) is defined as the opposite of molecule hardness and is expressed as:

$$S = \frac{1}{\eta} = \frac{2}{\epsilon_{LUMO} - \epsilon_{HOMO}} = \frac{2}{I - A} \quad (\text{Eq. 2.19})$$

Electronegativity (χ) is another property which is useful to make predictions about chemical behaviour because it describes the ability of a molecule to attract electrons and can be determined by the average value of the HOMO and LUMO energy values as defined by Mulliken (Pearson, 1986):

$$\chi = \frac{-(\epsilon_{HOMO} - \epsilon_{LUMO})}{2} = \frac{I+A}{2} \quad (\text{Eq. 2.20})$$

Chemical potential (μ) describes the tendency of an electron to escape and is defined as the first derivative of the total energy with respect to the number of electrons in a molecule. In terms of molecular orbital theory, μ is simply the negative of electronegativity value:

$$\mu = \frac{dE}{dN} = \frac{\epsilon_{HOMO} - \epsilon_{LUMO}}{2} = -\frac{I+A}{2} \quad (\text{Eq. 2.21})$$

Electrophilicity index (ω) describes the electrophilic power of a ligand i.e. the ability of a ligand to accept as many electrons as possible. Parr et al. elaborated on the definition of electrophilicity index and compared it with the definition of electron affinity by explaining that while electron affinity describes the capability of a ligand to accept only one electron from the environment, electrophilicity index measures the energy lowering of a ligand due to maximal electron flow between donor and acceptor (Parr et al., 1999). Electrophilicity index and electron affinity are related, but they are not equal. As suggested by Parr and co-workers, the mathematical expression for electrophilicity index is described as follows:

$$\omega = \frac{\mu^2}{2\eta} = \frac{\left(\frac{\epsilon_{HOMO} - \epsilon_{LUMO}}{2}\right)^2}{\epsilon_{LUMO} - \epsilon_{HOMO}} \quad (\text{Eq. 2.22})$$

Interaction Energy

Interaction energy corresponds to the decrease in energy when two molecules interact. This can be calculated by the difference between the energy of the system or complex and the sum of energy of its constituent molecules (Yang, 2003). Thus, the interaction energy of the ion pair in the IL can be determined by the difference in total energy of IL and sum of the total energy of each cation and anion:

$$\Delta E = E_{IL} - (E_{CAT} + E_{AN}) \quad (\text{Eq. 2.23})$$

Where E_{IL} is the total energy of an IL, E_{CAT} and E_{AN} are the total energy of cation and anion, respectively. Meanwhile, the interaction energy between the IL and the heterocyclic nitrogen compound can be written as follows:

$$\Delta E = E_{IL-N} - (E_{IL} + E_N) \quad (\text{Eq. 2.24})$$

Where E_{IL} and E_N are the total energy of IL and the nitrogen compound, respectively. Negative values of interaction energy indicate favorable interaction between the molecules in the system as this means that minimum energy is required to break the molecule or complexes.

Charge distribution

Charge distribution in a system which relates to the molecular and atomic orbitals and atomic centres can be determined by doing a population analysis. Different population analysis methods are available depending on how the electron density is partitioned. From population analysis, we can assign charges to atoms and this is useful to give a rough idea on the charge distribution in a molecule based on information on where the electron density in a system resides. In population analysis methods, each atom is assigned a “partial charge”. The charge distribution is qualitatively different depending on the method used. Most common population analysis methods are Mulliken population

analysis, Natural Bond Orbital (NBO) analysis and Bader's Atoms in Molecules (AIM) analysis. Mulliken population analysis is the oldest and simplest method but it is very dependent on the basis set used. AIM analysis is believed to be the most theoretically sound method because it does not depend on basis sets or integration grid, rather it solely relies on the properties of the electron density. However, AIM analysis could be time consuming for large molecules or complexes. NBO analysis is also a popular method where the natural atomic orbitals in the actual molecular environment are determined for the population analysis. It is also proven that NBO analysis has been successfully used to investigate the partial charge transfer within the parent compound (Lü, Qu, et al., 2013; Zhou, et al., 2008). From the partial charges, the chemical reactivity can be explained and the differences in hydrogen bonding, electrostatic interaction and CH- π interaction is considered (Anantharaj et al., 2011c).

2.7 Summary

The remaining oil reserves contain higher amount of sulfur and nitrogen compounds whilst the regulations are becoming more stringent in setting the limits for sulfur and nitrogen contents in the diesel fuel. Among the methods for denitrogenation reviewed, liquid-liquid extraction is an attractive approach because it can be operated under mild conditions. ILs and DESs have been used as the extracting solvent in the liquid-liquid extraction process and have been shown effective to remove aromatic compounds from aliphatic hydrocarbons. Nevertheless, the reported use of ILs for denitrogenation of diesel is limited whereas reports on the use of DESs for denitrogenation is absent. The huge number of existing ILs and DESs necessitates a systematic approach to screen and select them for use in desired separation processes. COSMO-RS and quantum chemical calculation have both been proven to be fast and reliable methods for ILs screening with the advantage of requiring minimal input from the experimental data. Till date, there is no report on the use of COSMO-RS to screen

DESs for denitrogenation of diesel. The current work utilises COSMO-RS and quantum chemical calculations to screen ILs and DESs for denitrogenation of model diesel compound and to elucidate the molecular interactions between ILs and DESs and the nitrogen compounds based on the calculation results.

University of Malaya

CHAPTER 3: METHODOLOGY

In order to fulfil the objectives of this research, the following methodology was adopted:

- Step 1: Screening of ILs and DESs using COSMO-RS model. This was done by predicting the activity coefficient at infinite dilution (γ^∞) and then by using the predicted values of γ^∞ to estimate the maximum selectivity, capacity and performance index of each solvent towards the studied aromatic nitrogen compounds.
- Step 2: Based on the results of COSMO-RS screening, quantum chemical calculation was performed to elucidate the molecular interaction between the shortlisted ILs and DESs and the aromatic nitrogen compounds. The quantum chemical calculation results were used to calculate the interaction energy, global scalar properties and partial charge transfer for the binary systems of ILs/DESs with aromatic nitrogen compounds.
- Step 3: Ternary liquid-liquid equilibrium experiments for the separation of aromatic nitrogen compounds from model diesel compound using the screened ILs/DESs were performed at room temperature and atmospheric pressure. These experiments were conducted in order to satisfy three objectives:
 - i) Validate the COSMO-RS screening results,
 - ii) Evaluate the performance of ILs and DESs in separating the nitrogen compound,
 - iii) Regress the NRTL model parameters of the ternary LLE systems to be used in process simulation software to assess industrial feasibility.

In this chapter, each step of the methodology is described in detail.

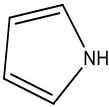
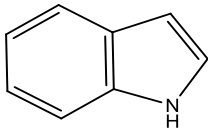
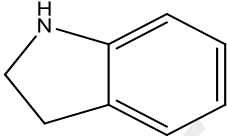
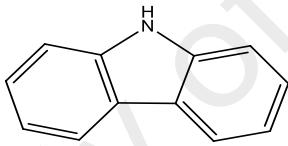
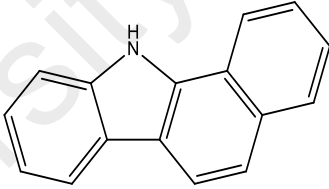
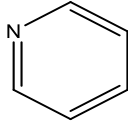
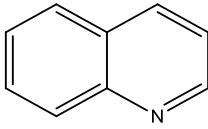
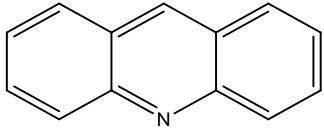
3.1 Step 1: Solvent screening using COSMO-RS

3.1.1 COSMO files generation

In order to use COSMO-RS as a screening tool or for any other calculation, it is a prerequisite is to generate the *.cosmo* files of all components involved. The *.cosmo* file of a molecule contains information on the screening charge density (σ) of the segmented molecule in a virtual conductor environment. To create a *.cosmo* file, the molecule's geometry is optimized and a single point calculation is performed. The optimized geometry can be done at the same level or differently than the single point calculation.

The aromatic nitrogen compounds present in the diesel fuel can be categorized into neutral and basic compounds. In neutral compounds such as pyrrole, indole, indoline, carbazole and benzocarbazole, the lone pair electrons on the nitrogen atom are delocalized around their aromatic ring. The opposite is true for basic compounds such as pyridine, quinoline and benzoquinoline where the lone-pair electrons on the nitrogen atom are not tied up in the π -electron cloud of the heterocyclic ring (Won, et al., 2002). Basic compounds are believed to have stronger inhibition effects towards the HDS process compared to the neutral compounds. However, neutral compounds have higher concentration in liquid fuels where 70% of the nitrogen compounds in liquid fuels are non-basic while the rest are basic compounds (Turaga, et al., 2003). The aromatic neutral nitrogen compounds studied in this section are pyrrole, indole, indoline, carbazole and benzocarbazole whereas pyridine, quinoline and benzoquinoline are studied as representative of basic nitrogen compounds. The structure, molecular formula and abbreviation of these nitrogen compounds are reported in Table 3.1.

Table 3.1: Structure, molecular formula and abbreviation for the aromatic nitrogen compound

Name	Structure	Molecular Formula	Abbreviation
Pyrrole		C_4H_5N	PYR
Indole		C_8H_7N	INDO
Indoline		C_8H_9N	INDL
Carbazole		$C_{12}H_9N$	CAR
Benzocarbazole		$C_{16}H_{11}N$	BCAR
Pyridine		C_5H_5N	PY
Quinoline		C_9H_7N	QU
Benzoquinoline		$C_{13}H_9N$	BQU

Screening of Ionic Liquids for Denitrogenation

For the screening of ILs, 6 cations and 3 anions are chosen to form a combination of 18 ILs. The 6 cations comprising the ILs are 1-ethyl-3-methylimidazolium ([EMIM]), 4-ethyl-4-methylmorpholinium ([EMMOR]), 1-ethyl-1-methylpiperidinium ([EMPIPE]), 1-ethyl-1-methylpyrrolidinium ([EMPYRO]), 1-ethylpyridinium ([EPY]) and 1,2,4-trimethylpyrazolium ([TMPYRA]). The chosen cations are a mixture of aromatic cations i.e. [EMIM], [EPY] and [TMPYRA] and non-aromatic cations i.e. [EMMOR], [EMPIPE] and [EMPYRO] while the alkyl chain are kept short i.e. ethyl and methyl as it has been reported that ILs with short alkyl chain of cations are able to extract aromatic compounds better than those with longer alkyl chain of cations (Ferreira, et al., 2012). The three anions included for screening are acetate ([Ac]), ethylsulphate ([EtSO₄]) and methanesulfonate ([MeSO₃]). ILs with these anions are commonly found in the literature for use of extracting aromatic compounds from aromatic/aliphatic mixture. The structure, chemical formula and abbreviation of each cation and anion are represented in Table 3.2.

Geometry optimization job was performed for each individual species of cation, anion and nitrogen compounds. Initial structures for each component were drawn and the job was executed to perform geometry optimization at Hartree-Fock level and 6-31G* basis set. The optimization job was performed using the Turbomole 6.4 software package.

Thereafter, the *.cosmo* file generation via single point calculations were performed using the optimized geometry. The single point calculation was performed at DFT level with Becke-Perdew functional and triple zeta valence potential (BP-TZVP) basis set to create the *.cosmo* files using Turbomole 6.4 Software Package (TURBOMOLE, 2012). This is to enable the use of TZVP parameterization in the COSMOthermX software where

the software package requires that the *.cosmo* file must be at the same level and basis set with the chosen parameterization. TZVP parameterization was chosen because it gives more meaningful values in terms of hydrogen bonding interaction which is a vital interaction between the aromatic nitrogen compounds and ionic liquids.

Table 3.2: Structure, molecular formula and abbreviation for cations and anions of the screened ionic liquids

Name	Structure	Molecular Formula	Abbreviation
1-ethyl-3-methylimidazolium		C ₆ H ₁₁ N ₂	[EMIM]
4-ethyl-4-methylmorpholinium		C ₇ H ₁₆ O	[EMMOR]
1-ethyl-1-methylpiperidinium		C ₈ H ₁₈ N	[EMPIPE]
1-ethyl-1-methylpyrrolidinium		C ₇ H ₁₆ N	[EMPYRO]
1-ethylpyridinium		C ₇ H ₁₀ N	[EPY]
1,2,4-trimethylpyrazolium		C ₆ H ₁₁ N ₂	[TMPYRA]
Acetate		CH ₃ COO	[Ac]
Ethyl sulphate		C ₂ H ₅ SO ₄	[EtSO ₄]
Methylsulphonate		CH ₃ SO ₃	[MeSO ₃]

These *.cosmo* files were then exported to the COSMOthermX Version C30_1401 software for further calculations using COSMO-RS model such as σ -profile and σ -potential interpretation, calculation of γ^∞ and the prediction of ternary liquid-liquid equilibria. All COSMO-RS calculations in COSMOthermX were done using TZVP parameterization, with parameterization file BP_TZVP_C30_1401.ctd.

The screening of ILs was done qualitatively by analysing the σ -profile and σ -potential of the cations, anions and aromatic nitrogen compounds.

Screening of Deep Eutectic Solvents for Denitrogenation

Similarly for systems of aromatic nitrogen compound and DESs, geometry optimization was performed for each of DESs constituent i.e. cation, anion and hydrogen bond donor (HBD) at Hartree-Fock level and 6-31G* basis set before a single point calculation was conducted at DFT level with BP-TZVP basis set. The halide anions need not to be optimized because they are single atom anions. Similar to the screening of ILs, the single point calculations were all done at BP-TZVP basis set so that they can all be used in COSMOthermX software using the TZVP parameterization.

The objective is to screen potential DESs for the removal of aromatic nitrogen compounds from diesel fuel by studying the effect of i) the choice of salt cation, ii) the choice of salt anion, iii) the choice of HBD and iv) the ratio between salt and HBD in the DES mixture. Activity coefficient at infinite dilution of each nitrogen compound in every DES was predicted. Thereafter, the performance of DES for the separation of aromatic nitrogen compound is evaluated using selectivity, capacity and performance index at infinite dilution based on the values of γ^∞ predicted. The structure of the DES constituents investigated in this work are provided in Table 3.3 whereas the list of DESs screened in this work is shown in Table 3.4. The DESs are divided into six categories which are, a) choline-based DESs where the salt cations are different forms of choline cation, b)

tetramethyl-based DES where the salt cations are tetramethylammonium and tetramethylphosphonium cations with chloride anions, c) tetramethyl-based DES where the salt cations are tetramethylammonium and tetramethylphosphonium cations with bromide anions d) tetrabutyl-based DES where the salt cations are tetrabutylammonium and tetrabutylphosphonium cations with chloride anion, e) tetrabutyl-based DES where the salt cations are tetrabutylammonium and tetrabutylphosphonium cations with bromide anion and f) DESs based on salts with phenylammonium and phenylphosphonium cations both with chloride or bromide anion.

The DESs are represented by adapting the representation of ILs in COSMOthermX due to their similar nature. As stated in the previous chapter, there are three approaches to represent ILs in COSMO-RS: i) the electro-neutral approach, ii) the ion pair approach and iii) the meta-file approach. Approach i) is considered to be closer to the real nature of ILs because it describes the two ions as separate species in a liquid mixture (KG, December 12th 2012). Hence, this approach was implemented in this work to describe the DES in COSMO-RS. Indeed, it is reported that in liquid form the HBD forms a complex with the halide anion of the salt and thereby lowering the interaction energy between the salt cation and the salt anion (Zhang, et al., 2012). Therefore, in liquid form it can safely be assumed that there are three distinct species constituting the DES which are the cation, anion and HBD. For example, consider a DES with a salt:HBD molar ratio of 1: n . In laboratory situation, this means that the DES consists of 1 mole of cation, 1 mole of anion and n mole of HBD. Comparing the representation of IL in COSMOthermX as 1:1 for its cation:anion ratio, the DES is represented as 1:1: n for its cation:anion:HBD ratio.

However, similar to using approach i) for representing ILs in COSMOthermX, the mole fractions obtained by COSMO-RS calculation by COSMOthermX need to be converted to reflect actual experimental definition of the mole fraction. This can be done as follows:

The experimental definition of mole fraction of solute in a mixture of solute, carrier and DES is given by:

$$x_i^{\text{EXP}} = \frac{n_i}{n_i + n_j + n_{\text{DES}}} \quad (\text{Eq. 3.1})$$

Meanwhile in COSMOthermX, the definition of mole fraction in COSMO-RS by using the approach i) is given by:

$$x_i^{\text{COSMO-RS}} = \frac{n_i}{n_i + n_j + n_{\text{Cation}} + n_{\text{Anion}} + n_{\text{HBD}}} \quad (\text{Eq. 3.2})$$

where x_i^{EXP} is the mole fraction of solute i in the experimental definition, $x_i^{\text{COSMO-RS}}$, the mole fraction of solute i in the electroneutral approach, n_i , the number of moles of solute i , n_j , the number of moles of carrier j , n_{DES} , the number of moles of the DES as a whole, n_{cation} , the number of moles of the DES cation, n_{anion} , the number of moles of the DES anion, and n_{HBD} , the number of moles of HBD in the DES. From equations 3.1 and 3.2, the conversion from calculated mole fraction in COSMOthermX ($x_i^{\text{COSMO-RS}}$) to the experimental framework (x_i^{EXP}) can be obtained as follows:

$$x_i^{\text{EXP}} = \frac{x_i^{\text{COSMO-RS}}/v_i}{\sum_k x_k^{\text{COSMO-RS}}/v_k} \quad (\text{Eq. 3.3})$$

where v_i stands for the stoichiometric coefficient of each species in the mixture (i.e. solute, carrier, cation, anion, HBD).

The conversion of activity coefficient in COSMOthermX uses the same approach:

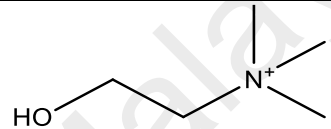
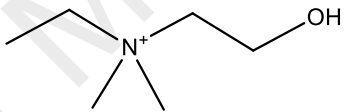
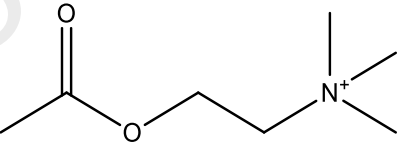
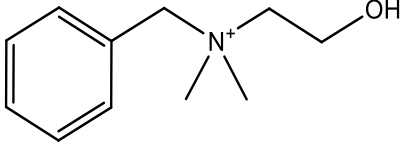
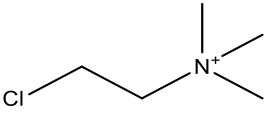
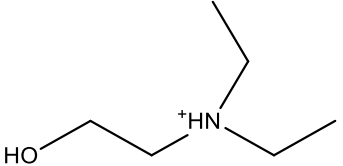
$$\gamma_i^{\text{LAB}} = \gamma_i^{\text{COSMO-RS}} \times \sum_k \left(\frac{x_k^{\text{COSMO-RS}}}{v_k} \right) \quad (\text{Eq. 3.4})$$



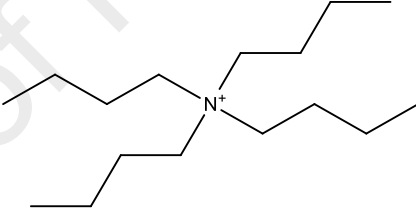
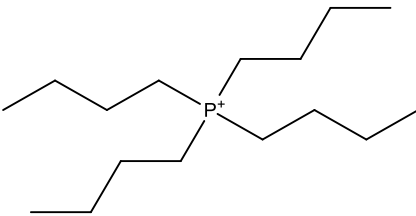
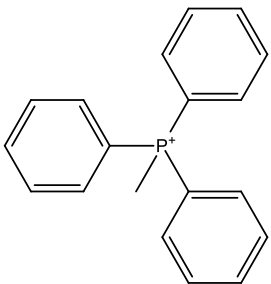
At infinite dilution, $\sum_k \left(\frac{x_k^{\text{COSMO-RS}}}{v_k} \right) = \sum_k \frac{1}{v_k^{\text{DES}}}$

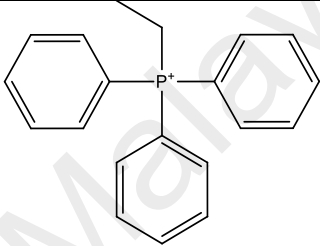
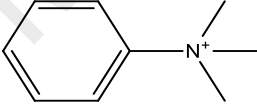
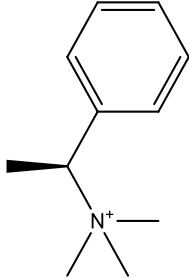
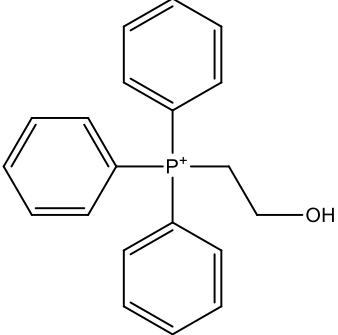
$$\therefore \gamma_i^{\infty, \text{LAB}} = \sum_k \frac{1}{v_k^{\text{DES}}} \gamma_i^{\infty, \text{COSMO-RS}} \quad (\text{Eq. 3.5})$$

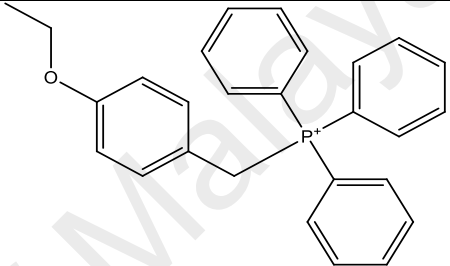
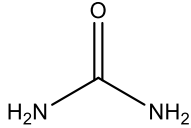
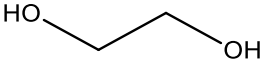
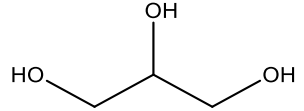
University of Malaya

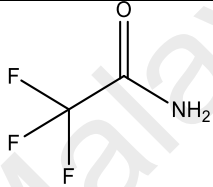
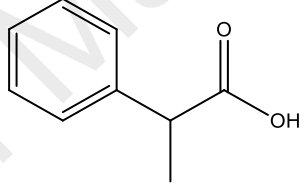
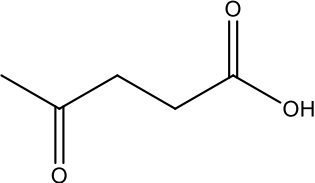
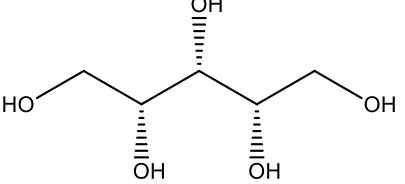
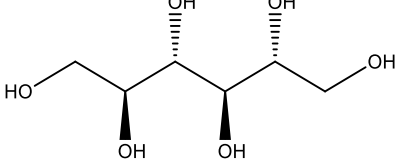
Table 3.3: Structure of DES constituents used in this work

Type	Name	Structure	Molecular Formula
	2-hydroxy-N,N,N-trimethylethanaminium (choline)		$C_5H_{14}NO^+$
	ethyl-(2-hydroxyethyl)-dimethylammonium (ethylcholine)		$C_6H_{16}O^+$
Cation	2-acetoxy-N,N,N-trimethylethanaminium (acetylcholine)		$C_7H_{16}NO_2^+$
	N-benzyl-2-hydroxy-N,N-dimethylethanaminium		$C_{11}H_{18}NO^+$
	2-Chloro-N,N,N-trimethylethanaminium (chlorocholine)		$C_5H_{13}ClN^+$
	N,N diethylenethanol ammonium		$C_6H_{16}NO^+$

Type	Name	Structure	Molecular Formula
Cation	tetramethylammonium		$C_4H_{12}N^+$
	tetramethylphosphonium		$C_4H_{12}P^+$
	tetrabutylammonium		$C_{16}H_{36}N^+$
	tetrabutylphosphonium		$C_{16}H_{36}P^+$
	Methyltriphenylphosphonium		$C_{19}H_{18}P^+$

Type	Name	Structure	Molecular Formula
Cation	ethyltriphenylphosphonium		$C_{20}H_{20}P^+$
	Phenyltrimethylammonium		$C_9H_{14}N^+$
	N,N,N-Trimethyl-1-phenylethanaminium		$C_{11}H_{18}N^+$
	(2-Hydroxyethyl)triphenylphosphonium		$C_{20}H_{20}OP^+$

Type	Name	Structure	Molecular Formula
	4-Ethoxybenzyltriphenylphosphonium		$C_{27}H_{26}OP^+$
Anion	chloride	Cl^-	Cl^-
	bromide	Br^-	Br^-
	fluoride	F^-	F^-
HBD	Urea		CH_4N_2O
	Ethylene glycol		$C_2H_6O_2$
	Glycerol		$C_3H_8O_3$

Type	Name	Structure	Molecular Formula
	2,2,2-Trifluoroacetamide		$C_2H_2F_3NO$
	Phenylpropionic acid		$C_9H_{10}O_2$
	Levulinic acid		$C_5H_8O_3$
HBD	Xylitol		$C_5H_{12}O_5$
	D-Sorbitol		$C_6H_{14}O_6$

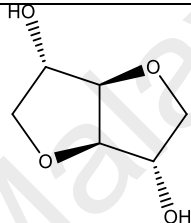
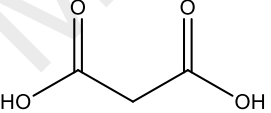
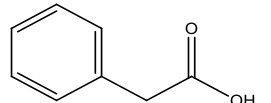
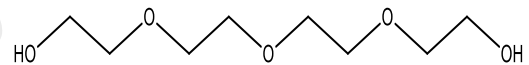
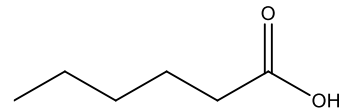
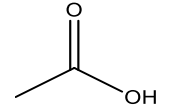
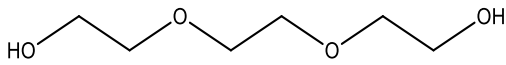
Type	Name	Structure	Molecular Formula
	D-Isosorbide		$C_6H_{10}O_4$
	Malonic acid		$C_3H_4O_4$
	Phenylacetic acid		$C_8H_8O_2$
HBD	tetraethylene glycol		$C_8H_{18}O_5$
	Caproic acid (hexanoic acid)		$C_6H_{12}O_2$
	Acetic acid		$C_2H_4O_2$
	Triethylene glycol		$C_6H_{14}O_4$

Table 3.4: Full name and abbreviation of DESs screened using COSMO-RS

No.	Salt	HBD	Salt:HBD Molar Ratio	Abbreviation
Choline-based DESs				
1	Choline chloride	Urea	1:2	ChCl/Ur (1:2)
2	Choline chloride	Ethylene glycol	1:2	ChCl/EG (1:2)
3	Choline chloride	Glycerol	1:2	ChCl/Gly (1:2)
4	Choline chloride	2,2,2-Trifluoroacetamide	1:2	ChCl/TFA (1:2)
5	Choline chloride	Phenylpropionic acid	1:1	ChCl/PPA (1:1)
6	Choline chloride	Levulinic acid	1:2	ChCl/LA (1:2)
7	Choline chloride	Xylitol	1:1	ChCl/Xy (1:1)
8	Choline chloride	D-Sorbitol	1:1	ChCl/DS (1:1)
9	Choline chloride	D-Isosorbide	1:2	ChCl/DI (1:2)
10	Choline chloride	Malonic acid	1:1	ChCl/MA (1:2)
11	Choline fluoride	Urea	1:2	ChF/Ur (1:2)
12	ethylcholine chloride	Urea	1:2	EChC/Ur (1:2)
13	Acetylcholine chloride	Urea	1:2	ATCC/Ur (1:2)
14	Chlorocholine chloride	Urea	1:2	CChC/Ur (1:2)
15	N-benzyl-2-hydroxy-N,N-dimethylethanaminium chloride	Urea	1:2	BHDAC/Ur (1:2)
16	N,N diethyl ethanol ammonium chloride	Glycerol	1:2	DEAC/Gly (1:2)
17	N,N diethyl ethanol ammonium chloride	Glycerol	1:3	DEAC/Gly (1:3)
18	N,N diethyl ethanol ammonium chloride	Glycerol	1:4	DEAC/Gly (1:4)
19	N,N diethyl ethanol ammonium chloride	Ethylene glycol	1:2	DEAC/EG (1:2)
20	N,N diethyl ethanol ammonium chloride	Ethylene glycol	1:3	DEAC/EG (1:3)
21	N,N diethyl ethanol ammonium chloride	Ethylene glycol	1:4	DEAC/EG (1:4)
Tetramethyl-based DESs				
22	tetramethylammonium chloride	Glycerol	1:2	TMAC/Gly (1:2)
23	Tetramethylammonium chloride	Ethylene glycol	1:2	TMAC/EG (1:2)
24	Tetramethylammonium chloride	Phenylacetic acid	1:2	TMAC/PA (1:2)
25	Tetramethylammonium chloride	Malonic acid	1:2	TMAC/MA (1:2)
26	Tetramethylammonium chloride	tetraethylene glycol	1:2	TMAC/TEG (1:2)
27	Tetramethylammonium chloride	Caproic acid	1:2	TMAC/CA (1:2)
28	Tetramethylammonium chloride	Acetic acid	1:2	TMAC/AA (1:2)
29	Tetramethylphosphonium chloride	Glycerol	1:2	TMPC/Gly (1:2)

No.	Salt	HBD	Salt:HBD Molar Ratio	Abbreviation
30	Tetramethylphosphonium chloride	Ethylene glycol	1:2	TMPC/EG (1:2)
31	Tetramethylphosphonium chloride	Phenylacetic acid	1:2	TMPC/PA (1:2)
32	Tetramethylphosphonium chloride	Malonic acid	1:2	TMPC/MA (1:2)
33	Tetramethylphosphonium chloride	tetraethylene glycol	1:2	TMPC/TEG (1:2)
34	Tetramethylphosphonium chloride	Caproic acid	1:2	TMPC/CA (1:2)
35	Tetramethylphosphonium chloride	Acetic acid	1:2	TMPC/AA (1:2)
36	tetramethylammonium bromide	Glycerol	1:2	TMAB/Gly (1:2)
37	Tetramethylammonium bromide	Ethylene glycol	1:2	TMAB/EG (1:2)
38	Tetramethylammonium bromide	Phenylacetic acid	1:2	TMAB/PA (1:2)
39	Tetramethylammonium bromide	Malonic acid	1:2	TMAB/MA (1:2)
40	Tetramethylammonium bromide	tetraethylene glycol	1:2	TMAB/TEG (1:2)
41	Tetramethylammonium bromide	Caproic acid	1:2	TMAB/CA (1:2)
42	Tetramethylammonium bromide	Acetic acid	1:2	TMAB/AA (1:2)
43	Tetramethylphosphonium bromide	Glycerol	1:2	TMPB/Gly (1:2)
44	Tetramethylphosphonium bromide	Ethylene glycol	1:2	TMPB/EG (1:2)
45	Tetramethylphosphonium bromide	Phenylacetic acid	1:2	TMPB/PA (1:2)
46	Tetramethylphosphonium bromide	Malonic acid	1:2	TMPB/MA (1:2)
47	Tetramethylphosphonium bromide	tetraethylene glycol	1:2	TMPB/TEG (1:2)
48	Tetramethylphosphonium bromide	Caproic acid	1:2	TMPB/CA (1:2)
49	Tetramethylphosphonium bromide	Acetic acid	1:2	TMPB/AA (1:2)

Tetrabutyl-based DESs

50	tetrabutylammonium chloride	Malonic acid	1:2	TBAC/MA (1:2)
51	tetrabutylammonium chloride	Glycerol	1:2	TBAC/Gly (1:2)
52	tetrabutylammonium chloride	tetraethylene glycol	1:2	TBAC/TEG (1:2)
53	tetrabutylammonium chloride	Ethylene glycol	1:2	TBAC/EG (1:2)
54	tetrabutylammonium chloride	Phenylacetic acid	1:2	TBAC/PA (1:2)

No.	Salt	HBD	Salt:HBD Molar Ratio	Abbreviation
55	tetrabutylammonium chloride	Caproic acid	1:2	TBAC/CA (1:2)
56	tetrabutylammonium chloride	Acetic acid	1:2	TBAC/AA (1:2)
57	tetrabutylphosphonium chloride	Malonic acid	1:2	TBPC/MA (1:2)
58	tetrabutylphosphonium chloride	Glycerol	1:2	TBPC/Gly (1:2)
59	tetrabutylphosphonium chloride	tetraethylene glycol	1:2	TBPC/TEG (1:2)
60	tetrabutylphosphonium chloride	Ethylene glycol	1:2	TBPC/EG (1:2)
61	tetrabutylphosphonium chloride	Phenylacetic acid	1:2	TBPC/PA (1:2)
62	tetrabutylphosphonium chloride	Caproic acid	1:2	TBPC/CA (1:2)
63	tetrabutylphosphonium chloride	Acetic acid	1:2	TBPC/AA (1:2)
64	tetrabutylammonium bromide	Malonic acid	1:2	TBAB/MA (1:2)
65	tetrabutylammonium bromide	Glycerol	1:2	TBAB/Gly (1:2)
66	tetrabutylammonium bromide	tetraethylene glycol	1:2	TBAB/TEG (1:2)
67	tetrabutylammonium bromide	Ethylene glycol	1:2	TBAB/EG (1:2)
68	tetrabutylammonium bromide	Phenylacetic acid	1:2	TBAB/PA (1:2)
69	tetrabutylammonium bromide	Caproic acid	1:2	TBAB/CA (1:2)
70	tetrabutylammonium bromide	Acetic acid	1:2	TBAB/AA (1:2)
71	tetrabutylphosphonium bromide	Ethylene glycol	1:2	TBPB/EG (1:2)
72	tetrabutylphosphonium bromide	Malonic acid	1:2	TBPB/MA (1:2)
73	tetrabutylphosphonium bromide	Glycerol	1:2	TBPB/Gly (1:2)
74	tetrabutylphosphonium bromide	tetraethylene glycol	1:2	TBPB/TEG (1:2)
75	tetrabutylphosphonium bromide	Phenylacetic acid	1:2	TBPB/PA (1:2)
76	tetrabutylphosphonium bromide	Caproic acid	1:2	TBPB/CA (1:2)

Phenylammonium & Phenylphosphonium –based DESs

77	Methyltriphenylphosphonium bromide	Glycerol	1:2	MTPPB/Gly (1:2)
78	Methyltriphenylphosphonium bromide	Glycerol	1:3	MTPPB/Gly (1:3)
79	Methyltriphenylphosphonium bromide	Glycerol	1:4	MTPPB/Gly (1:4)

No.	Salt	HBD	Salt:HBD Molar Ratio	Abbreviation
80	Methyltriphenylphosphonium bromide	Ethylene glycol	1:2	MTPPB/EG (1:2)
81	Methyltriphenylphosphonium bromide	Ethylene glycol	1:3	MTPPB/EG (1:3)
82	Methyltriphenylphosphonium bromide	Ethylene glycol	1:4	MTPPB/EG (1:4)
83	Methyltriphenylphosphonium bromide	Ethylene glycol	1:5	MTPPB/EG (1:5)
84	Methyltriphenylphosphonium bromide	Triethylene glycol	1:3	MTPPB/TrEG (1:3)
85	Methyltriphenylphosphonium bromide	Triethylene glycol	1:4	MTPPB/TrEG (1:4)
86	Methyltriphenylphosphonium bromide	Triethylene glycol	1:5	MTPPB/TrEG (1:5)
87	tetrabutylphosphonium bromide	Ethylene glycol	1:2	TBPB/EG (1:2)
88	ethyltriphenylphosphonium bromide	ethylene glycol	1:2	ETPPB/EG (1:2)
89	Phenyltrimethylammonium chloride	Glycerol	1:2	PTMAC/Gly (1:2)
90	Phenyltrimethylammonium chloride	Ethylene glycol	1:2	PTMAC/EG (1:2)
91	Phenyltrimethylammonium chloride	Triethylene glycol	1:2	PTMAC/TrEG (1:2)
92	N,N,N-Trimethyl-1-phenylethanaminium bromide	Glycerol	1:2	TPENB/Gly (1:2)
93	N,N,N-Trimethyl-1-phenylethanaminium bromide	Ethylene glycol	1:2	TPENB/EG (1:2)
94	N,N,N-Trimethyl-1-phenylethanaminium bromide	Triethylene glycol	1:2	TPENB/TrEG (1:2)

Table 3.4, continued.

3.1.2 Expressions of Selectivity, Capacity and Performance Index at Infinite Dilution

Important criteria in choosing a solvent for a separation process include its selectivity, distribution ratio or capacity, its insolubility in the raffinate phase, its recovery, safety and environmental factors such as flammability and toxicity and finally its cost and availability.

Similar to ILs, DESs are insoluble in the raffinate phase as proven by previously reported experimental data of ternary liquid-liquid equilibria for systems with DES (Kareem, Mjalli, Hashim, & AlNashef, 2012) (Kareem, Mjalli, Hashim, Hadj-Kali, et al., 2012) (Kareem, et al., 2013) . It has also been proven that DES can be regenerated relatively easily and without any degradation in the quality and performance of the DES (Li, et al., 2013). Having negligible vapour pressure and high thermal stability, DESs are non-flammable and non-volatile therefore minimising its environmental impact through zero volatile compounds emission. DESs are also said to be less toxic than ILs, although this subject is yet to be validated through further studies. Finally, the cost of DESs is generally much lower than ILs due to their abundant raw materials and simpler synthesis route than that of ILs. Thus, it can safely be concluded that DESs fulfil most of the important criteria mentioned above. Hence, it is reasonable to screen the potential DES as solvent based on its selectivity and capacity.

It is desirable to have a DES with high selectivity towards the nitrogen compounds as this means less number of stages needed to remove them and thus lower capital cost. Higher selectivity means that the DES has a more favourable interaction towards the nitrogen compounds as compared to diesel. Besides, a high capacity is also desirable as this can lower the solvent to feed ratio and also requires smaller diameter for the extraction column and thus lower operating cost.

In this work, γ_i^∞ values were used to estimate the maximum selectivity and capacity of screened DESs. γ_i^∞ is essential because it describes the interaction between the solvent and solute at a very miniscule concentration of solute present. γ_i^∞ is defined as the limit of activity coefficient of a solute i as the concentration of i approaches zero. The mathematical expression is given in Equation 3.6:

$$\gamma_i^\infty = \lim_{x_i \rightarrow 0} \gamma_i \quad (\text{Eq. 3.6})$$

The composition of diesel fuel varies from the source but in general diesel fuels are comprised of paraffinic, iso-paraffinic, aromatic, naphthenic and olefinic (PIANO) compounds, with paraffinic compounds constituting most of the hydrocarbon composition i.e. at least 40 wt. %. According to Diesel Fuels Technical Review by Chevron, hydrocarbons in diesel fuels are those with carbon number between 9 and 23, with hydrocarbons containing 15 to 17 carbon number having the highest mass percent in the composition (Bacha et al., 2007). Yang et al. reported the chemical composition of diesel from various samples determined using liquid chromatography and gas-chromatography mass spectrometry (GC-MS) (Yang et al., 2002). Based on these reports, the composition of diesel fuel was formulated as presented in Table 3.5. *n*-hexadecane, isododecane, phenylnonane, butylcyclohexane and 1-dodecene were used as representative PIANO compounds because these compounds are easily available as pure chemicals for possible use in experimental work.

In COSMO-RS, the simulated diesel oil is treated as one single compound where the σ -profile is added linearly according to the composition as expressed in Equation 3.7, where x_i and p^{x_i} represent the composition and σ -profile of each diesel constituent, respectively.

$$p_S(\sigma) = \sum_{i \in S} x_i p^{x_i}(\sigma) \quad (\text{Eq. 3.7})$$

Table 3.5: Composition of Simulated Diesel

Diesel constituent	Molecular formula	wt %
<i>n</i> -hexadecane	C ₁₆ H ₃₄	42.55
isododecane	C ₁₂ H ₂₆	17.02
phenylnonane	C ₁₅ H ₂₄	24.47
butylcyclohexane	C ₁₀ H ₂₀	10.64
1-dodecene	C ₁₂ H ₂₄	5.32

Selectivity of nitrogen compounds can be defined as the ratio of concentration of nitrogen compounds in the extract phase to its concentration in the raffinate phase. At infinite dilution, estimation of the maximum selectivity, $S_{12, \max}$ can be done through the ratio between γ_i^∞ for diesel to that of nitrogen compound in the DES. This can be expressed by Equation 3.8 where S_{12}^∞ is the selectivity at infinite dilution whereas subscripts 1 and 2 refer to the nitrogen compound and simulated diesel, respectively.

$$S_{12, \max} = S_{12}^\infty = \left(\frac{\gamma_2^\infty}{\gamma_1^\infty} \right)_{\text{DES phase}} \quad (\text{Eq. 3.8})$$

Capacity at infinite dilution can be used as an estimate for the amount of DES needed for removing the nitrogen compounds. Operationally, it defines the maximum amount of nitrogen compounds that can be dissolved in the DES. The maximum capacity, $C_{1, \max}$ can be approximated by the capacity at infinite dilution for nitrogen compound, C_1^∞ where it is estimated as the inverse of activity coefficient at infinite dilution of the nitrogen compound in the DES as shown in Equation 3.9:

$$C_1^\infty = \left(\frac{1}{\gamma_1^\infty} \right)_{\text{DES phase}} \quad (\text{Eq. 3.9})$$

Finally, the performance index can be defined as the product of maximum selectivity and maximum capacity, i.e. the product of S_{12}^∞ and C_1^∞ :

$$PI = S_{12}^\infty \times C_1^\infty = \left(\frac{\gamma_2^\infty}{\gamma_1^\infty} \right)_{\text{DES phase}} \times \left(\frac{1}{\gamma_1^\infty} \right)_{\text{DES phase}} = \left(\frac{\gamma_2^\infty}{(\gamma_1^\infty)^2} \right)_{\text{DES phase}} \quad (\text{Eq. 3.10})$$

3.2 Step 2: Quantum Chemical Calculation

3.2.1 Geometry Optimization

The geometry optimization procedure was mentioned in section 3.1.1. Geometry optimization job was performed for each individual species (each heterocyclic nitrogen compound, cation and anion), whole ionic liquid complex (cation + anion) and complexes of heterocyclic nitrogen compound with whole ionic liquids. Calculation of geometry optimization at Hartree-Fock level gives more meaningful and accurate values for the orbital energy (Lin et al., 2008) while the 6-31G* basis set accounts for polarization effect of the species in the complexes. However, regarding the partial charge estimation, NBO population analysis is performed for the complexes at the same level and basis set as the optimized geometry of each complex.

3.2.2 Calculation of Orbital Energy Values, Global Scalar Properties and Interaction Energy

From the optimized geometries, the orbital energy values are retrieved and used for the determination of highest occupied molecular orbitals (HOMO) and lowest unoccupied molecular orbitals (LUMO). These HOMO and LUMO energy values are then used to calculate the global scalar properties which are the global hardness (η), global softness (S), electronegativity (χ) and electrophilicity index (ω). The total energy values of the optimized geometry of complexes and individual molecules were used to compute the interaction energy as detailed in Chapter II.

3.3 Step 3: Liquid-liquid Equilibria Experiment

3.3.1 Materials

The list of chemicals used in this study was given in the Tables 3.6 to 3.10 as follows. The ILs, DESs' constituents, aromatic nitrogen compounds and model diesel compound are used as received without any further purification. The selection of ILs is based on the calculation results where it was recommended to select ILs where the cation has aromatic ring, combined with either [EtSO₄] or [Ac] anions. It was originally planned to measure LLE with the IL [EPY][EtSO₄] but this IL is not available in the market thus the IL [EMPY][EtSO₄] was chosen as the closest substitute. Also, ILs with [Ac] anion is highly priced thus ILs with [EtSO₄] and [MeSO₃] anion were chosen instead. As for the DESs, it was originally planned to compare the LLE result between ChCl/EG (1:2) (predicted to have high selectivity but lower distribution ratio) and TBAB/EG (1:2) (predicted to have high distribution ratio but lower selectivity). But because the mixture ChCl/EG (1:2) could not be analysed using deuterated chloroform (CDCl₃) as the solvent for NMR spectroscopy, another DES which is TBPB/EG (1:2) was used instead to compare against TBAB/EG (1:2). This was done in the interest of time and cost involved if a new NMR solvent were to be purchased and tested for solubility with the DES ChCl/EG (1:2).

Table 3.6: Ionic Liquids used in this work

Name	Abbreviation	Chemical Formula	Purity (%)	Supplier	Country of Origin
1-ethyl-3-methylimidazolium ethylsulfate	[EMIM][EtSO ₄]	C ₈ H ₁₆ N ₂ O ₄ S	≥95%	Sigma-Aldrich, produced by BASF	Germany
1-ethyl-3-methylimidazolium methanesulfonate	[EMIM][MeSO ₃]	C ₇ H ₁₄ N ₂ O ₃ S	≥95%	Sigma-Aldrich, produced by BASF	Germany
1-ethyl-3-methylpyridinium ethylsulfate	[EMPY][EtSO ₄]	C ₁₀ H ₁₇ NO ₄ S	≥95%	Merck Chemicals	Germany

Table 3.7: DES constituents used in this work

Name	Abbreviation	Chemical Formula	Purity (%)	Supplier	Country of Origin
Tetrabutylammonium bromide	TBAB	C ₁₆ H ₃₆ BrN	≥98%	Sigma-Aldrich	India
Tetrabutylphosphonium bromide	TBPB	C ₁₆ H ₃₆ BrP	≥ 98.0	Sigma-Aldrich	India
Ethylene glycol	EG	HOCH ₂ CH ₂ OH	99.8%	Sigma-Aldrich	USA

Table 3.8: Aromatic nitrogen compounds used in this work

Name	Abbreviation	Chemical Formula	Purity (%)	Supplier	Country of Origin
Pyrrrole	PYR	C ₄ H ₅ N	98%	Aldrich	Germany
Pyridine	PY	C ₅ H ₅ N	99.8%	Sigma-Aldrich	Germany
Indoline	IND	C ₈ H ₉ N	99%	Aldrich	China
Quinoline	QU	C ₉ H ₇ N	98%	Aldrich	Germany

Table 3.9: Model diesel compound used in this work

Name	Chemical Formula	Purity (%)	Supplier	Country of Origin
<i>n</i> -hexadecane	CH ₃ (CH ₂) ₁₄ CH ₃	≥99%	Sigma-Aldrich	Germany

Table 3.10: Solvent for NMR spectroscopy used in this work

Name	Chemical Formula	Purity (%)	Supplier	Country of Origin
Chloroform-D1	CDCl ₃	Deuteration degree ≥99.8%	Merck Chemicals	Germany

3.3.2 Synthesis of DESs

DESs were synthesized using similar approach reported by Abbott et al. where the salt and HBD are mixed according to specified salt:HBD molar ratio at a particular temperature and mixing speed until a homogeneous liquid phase is formed (Abbott, et al., 2004). There are two DESs synthesized in this study: i) tetrabutylammonium bromide + ethylene glycol at molar ratio 1:2 and ii) tetrabutylphosphonium bromide + ethylene glycol at molar ratio 1:2.

First, the salt and HBD were weighed accordingly to give a final mixture with molar ratio 1:2. The weighing was done using the Mettler Toledo weighing balance with an accuracy of $\pm 1 \times 10^{-4}$ g. The salt and HBD were then mixed in a blue cap bottle and placed on a hot plate magnetic stirrer, where the stirring took place at 80°C and 500 rpm for at least 3 hours until a homogeneous liquid phase is formed. The resulting DESs were in the form of clear, colourless liquids. A fresh batch of DES was made for each ternary LLE experiment performed to avoid any contamination prior to the experiment.

3.3.3 Liquid-liquid Equilibrium Experiment

Feed mixtures of *n*-hexadecane (used as a model diesel compound) and nitrogen compounds were prepared with the concentration of nitrogen compound ranging between 5 and 50 wt%. Thereafter, the solvent (IL or DES) was added so that the feed to solvent mass ratio was 1:1. All weighing were done using Mettler Toledo weighing balance with an accuracy of $\pm 1 \times 10^{-4}$ g. The total mass of each of the mixture was set to 6 g. Screw-capped vials with total capacity of 20 ml were used to hold the mixtures to ensure sufficient agitation was employed in order to achieve equilibrium. The vials were sealed with Parafilm M tapes to avoid loss of components by evaporation and moisture contamination. The vials were then placed in an incubator-shaker at room temperature (298.15 K), where they were allowed to shake for at least 5 hours at a speed of 200 rpm to achieve equilibrium. The mixtures were then left to settle for at least 12 hours in order to ensure the phases were fully separated.

The systems are separated into 6 different sets based on the solvent used to separate the aromatic nitrogen compound from the model diesel compound, *n*-hexadecane. Pyrrole and indoline were used as representative of 5-membered nitrogen compounds whereas pyridine and quinoline for 6-membered compounds. All nitrogen compounds used are liquid at room temperature. The ILs used are [EMIM][EtSO₄], [EMPY][EtSO₄] and [EMIM][MeSO₃] whereas the DESs used are TBAB/EG (1:2) and

TBPB/EG (1:2). In total, there were 22 sets of ternary LLE experiments conducted which are listed as follows:

1) Systems with [EMIM][EtSO₄]

- [EMIM][EtSO₄] + pyrrole + *n*-hexadecane
- [EMIM][EtSO₄] + pyridine + *n*-hexadecane
- [EMIM][EtSO₄] + indoline + *n*-hexadecane
- [EMIM][EtSO₄] + quinoline + *n*-hexadecane

2) Systems with [EMPY][EtSO₄]

- [EMPY][EtSO₄] + pyrrole + *n*-hexadecane
- [EMPY][EtSO₄] + pyridine + *n*-hexadecane
- [EMPY][EtSO₄] + indoline + *n*-hexadecane
- [EMPY][EtSO₄] + quinoline + *n*-hexadecane

3) Systems with [EMIM][MeSO₃]

- [EMIM][MeSO₃] + pyrrole + *n*-hexadecane
- [EMIM][MeSO₃] + pyridine + *n*-hexadecane
- [EMIM][MeSO₃] + indoline + *n*-hexadecane
- [EMIM][MeSO₃] + quinoline + *n*-hexadecane

4) Systems with mixed IL [EMIM][EtSO₄] + [EMPY][EtSO₄]

- ([EMIM][EtSO₄] + [EMPY][EtSO₄]) + indoline + *n*-hexadecane
- ([EMIM][EtSO₄] + [EMPY][EtSO₄]) + quinoline + *n*-hexadecane

5) Systems with tetrabutylammonium bromide + ethylene glycol DES at 1:2 molar ratio

- TBAB/EG (1:2) + pyrrole + *n*-hexadecane

- TBAB/EG (1:2) + pyridine + *n*-hexadecane
- TBAB/EG (1:2) + indoline + *n*-hexadecane
- TBAB/EG (1:2) + quinoline + *n*-hexadecane

6) Systems with tetrabutylphosphonium bromide + ethylene glycol DES at 1:2 molar ratio

- TBPB/EG (1:2) + pyrrole + *n*-hexadecane
- TBPB/EG (1:2) + pyridine + *n*-hexadecane
- TBPB/EG (1:2) + indoline + *n*-hexadecane
- TBPB/EG (1:2) + quinoline + *n*-hexadecane

3.3.4 Compositional Analysis

Before the compositional analysis was performed for the LLE mixtures, the NMR spectra of all pure components were analysed to be used as references for identification peak of each component. The NMR analysis was also used to ascertain the purity of each compound. A drop of each pure compound was dissolved in 0.5 ml of CDCl₃ in an NMR tube (300 MHz). The NMR spectrometer Bruker Ultrashield Plus (600 MHz) was used to conduct the ¹H NMR spectral analysis for the measurement of the peak areas of the hydrogen molecule of each component.

For the analysis of the LLE mixture, the samples from the extract and raffinate phases were taken from each mixture using 1 ml syringes and dissolved in 0.5 ml of CDCl₃ for NMR analysis similar to what was done towards the pure compounds.

From the NMR analysis of the pure compounds, the identification peak for pyrrole is between 6.2 and 8.2. The H atom attached to the N atom in pyrrole showed peak at 8.2, whereas the other two H atoms attached to the carbon ring showed peak between 6.76 and 6.24. For pyridine, the two H atoms connected to C atoms nearest to the N atom showed peaks at 8.61, the neighbouring two H atoms 7.27 and the H atom connected to

the C atom adjacent to the N atom at 7.66. The identification peak for indoline is through H atom connected to N atom which shows peak at 3.49. For quinoline, the peak ranges from 7.31 to 8.89, with the H atom connected to C atom nearest to the N atom shows peak at 8.89.

For the ILs used in this work, only identification peaks shown by the cations are necessary to indicate the presence and concentration of ILs in the extract phase. The peaks shown by H atoms nearest to the N atoms in both [EMIM] and [EMPY] cations were used as identification peaks. In [EMIM] cation, the H atom connected to the C atom in between the two N atoms shows peak at 9.42 whereas the two H atoms connected near the N atom in the [EMPY] cation shows two peaks at 9.10 and 9.20, respectively.

For the DES tetrabutylammonium bromide + ethylene glycol, identification peaks were taken at the H atoms connected nearest to the tetrabutylammonium cation and the H atoms in the –OH groups in ethylene glycol, which show peaks at 3.32 and 3.70, respectively. Whereas for TBPB/EG (1:2), the identification peak for tetrabutylphosphonium cation is around 2.3.

Finally, *n*-hexadecane, considered as the model diesel compound, shows peak between 0.88 and 1.31 due to its nature as a straight-chain alkane.

These identification peaks from each pure compound are used to identify their presence in the extract and raffinate phases. Appendix D shows the NMR spectra for each pure compounds. The integral area computed using the NMR processing software (TopSpin) was used to calculate the concentration using Equation 3.11:

$$x_i = \frac{H_i}{\sum_{i=1}^3 H_i} \quad (\text{Eq. 3.11})$$

where x_i is the concentration of a component i in mole fraction and H_i is the peak area of a single hydrogen atom in component i .

3.3.5 Consistency test using Othmer-Tobias and Hand correlations

The reliability of the experimental results were ascertained using the Othmer–Tobias (Othmer et al., 1942) and Hand (Hand, 1929) correlations obtained using Equations 3.12 and 3.13, respectively:

$$\ln\left(\frac{1-x_{hex}^I}{x_{hex}^I}\right) = a + b \ln\left(\frac{1-x_{IL/DES}^{II}}{x_{IL/DES}^{II}}\right) \quad (\text{Eq. 3.12})$$

$$\ln\left(\frac{x_{NC}^I}{x_{hex}^I}\right) = c + d \ln\left(\frac{x_{aro}^{II}}{x_{IL/DES}^{II}}\right) \quad (\text{Eq. 3.13})$$

x_{hex} , x_{NC} and $x_{IL/DES}$ refers to the concentrations of *n*-hexadecane, aromatic nitrogen compounds and IL or DES, respectively, whereas superscript I and II refers to the raffinate and extract phases, respectively. a and b are the fitting parameters of the Othmer–Tobias correlation whereas c and d are those of the Hand correlation. The linearity of each plot indicates the degree of consistency of the data. The fitting parameters of the Othmer-Tobias and Hand correlations vary with each system and are shown in the next chapter.

3.3.6 Prediction of Ternary LLE using COSMO-RS model

The ternary phase diagrams for each system is predicted by COSMO-RS model using the COSMOthermX software package at TZVP basis set and parameterization file BP_TZVP_C30_1301.ctd. Calculations were performed using the *.cosmo* files generated which were previously used in the screening process and quantum chemical calculations. The feed composition is used as the only input from the experiment in order to search for LLE points at 25°C and atmospheric pressure. A more detailed procedure on using COSMOthermX to predict ternary LLE can be referred to in its user guide (KG, December 12th 2012).

3.3.7 Correlation of LLE data

The phase compositions in a liquid-liquid equilibrium calculation are obtained by solving an isothermal liquid-liquid flash at a given temperature and pressure. The following system of equations makes up the flash calculation:

Material Balance:

$$x_i - (1 - \omega)x_i^{L1} - \omega x_i^{L2} = 0, \quad i = 1, N_c \quad (\text{Eq. 3.14})$$

Equilibrium Equation:

$$x_i^{L1} \gamma_i^{L1} - x_i^{L2} \gamma_i^{L2} = 0, \quad i = 1, N_c \quad (\text{Eq. 3.15})$$

Equation of Summation:

$$\sum_i x_i^{L1} - \sum_i x_i^{L2} = 0 \quad (\text{Eq. 3.16})$$

Where ω is the liquid-liquid splitting ratio, x_i the amount of component i in the mixture, x_i^{L1} the amount of component i in liquid phase $L1$, x_i^{L2} the amount of component i in liquid phase $L2$, and N_c the number of constituents of the liquid phases. The parameters γ_i^{L1} and γ_i^{L2} are the activity coefficients of component i in $L1$ and $L2$, respectively.

Many equations were developed to correlate activity coefficients, but the equations which are in common use are those based on the concept of local composition introduced by Wilson in 1964 (Wilson, 1964) such as the NRTL (Non-Random Two Liquid) equation by Renon and Prausnitz (Renon et al., 1968), the UNIQUAC (UNIversal QUAsi-Chemical) equation by Abrams and Prausnitz (Abrams et al., 1975) and the UNIFAC (UNIversal Functional Activity Coefficient) method in which activity coefficients are calculated from group contributions (Fredenslund et al., 1975).

In this study, the activity coefficients were evaluated using the NRTL model. This model was found to be useful for correlating the experimental LLE data of systems containing ILs and DESs (Ravilla, et al., 2012) (Anantharaj et al., 2011b) (Kareem, et al.,

2013). For a multicomponent system, the activity coefficient of component i is given by the general expression

$$\ln \gamma_i = \frac{\sum_j \tau_{ji} G_{ji} x_j}{\sum_j G_{ji} x_j} + \sum_j \frac{G_{ji} x_j}{\sum_k G_{kj} x_k} \left(\tau_{ij} - \frac{\sum_k \tau_{kj} G_{kj} x_k}{\sum_k G_{kj} x_k} \right) \quad (\text{Eq. 3.17})$$

$$\text{with } \ln G_{ij} = -\alpha_{ij} \tau_{ij}, \alpha_{ij} = \alpha_{ji} \text{ and } \tau_{ii} = 0$$

where τ_{ij} and τ_{ji} are binary interaction parameters and α_{ij} is the nonrandomness parameter which measures the non-randomness of the mixture; when α_{ij} is zero, the mixture is said to be completely random. This parameter gives an additional degree of freedom to the NRTL equation where it can be applied to a large variety of binary and ternary mixtures and at the same time allows an excellent prediction of liquid-liquid equilibria.

Tassios has eliminated any physical significance attributed to the parameter and has stated that the nonrandomness parameter is mainly an empirical parameter obtained by fitting the experimental data and may not follow the rules set out by Renon (Tassios, 1976). He has even showed that $\alpha_{ij} = -1$ works in many cases. However, when the NRTL equation was derived, Renon and Prausnitz have suggested a relationship between the non-randomness parameter and Guggenheim's quasichemical approximation (Renon, et al., 1968). They have shown that α is related to the inverse of the coordination number $1/z$ that appeared in Guggenheim's expression. Since the coordination number was typically found to be between 6 and 12, the non-randomness parameter was expected to vary in the range of 0.1 – 0.3, which was revised to 0.2 – 0.47 later on.

Simulis[®] environment was utilized to achieve the model development (Simulis[®] et al.) where the third non-randomness parameter α_{ij} was fixed at 0.20 and the interaction parameters τ_{ij} and τ_{ji} were estimated from “6M” experimental data points (where M

represents the number of tie lines) by minimizing the root mean square deviation (RMSD) between calculated and experimental solubilities of each constituent in each phase:

$$\text{RMSD (\%)} = 100 \times \left(\frac{1}{6M} \sum_i \sum_j \sum_k (s_{ijk}^{\text{exp}} - s_{ijk}^{\text{cal}})^2 \right)^{1/2} \quad (\text{Eq. 3.18})$$

Where s is the solubility expressed in mole fraction and the subscripts i, j and k designate the component, phase and tie line, respectively.

University of Malaya

CHAPTER 4: RESULTS AND DISCUSSION

In this chapter, the results will be discussed in three different sections: COSMO-RS screening, quantum chemical calculation results and ternary LLE experimental results.

4.1 COSMO-RS Screening

4.1.1 Qualitative screening of ionic liquids using σ -profiles and σ -potentials

The σ -profiles and σ -potentials for cations, anions and heterocyclic nitrogen compounds involved in this work are shown in Figures 4.1 and 4.2. The dashed vertical lines show the threshold for hydrogen bond σ value ($\sigma_{hb} = \pm 0.0085 \text{ e \AA}^{-2}$). The overall positive charge of the cations is implied by the peaks on the negative side of the σ -profiles while the overall negative charge of the anions is distinguished by the peaks on the positive side of the σ -profiles.

As shown in Figure 4.1 a), the σ -profiles of cations are similar in shape and only differ in the height of peaks. All cations have two peaks, the lower one around $\sigma = -0.01 \text{ e \AA}^{-2}$ due to hydrogen atoms while the slightly higher peak between $\sigma = 0$ and $\sigma = -0.01 \text{ e \AA}^{-2}$ is due to polarized carbon atoms. The cations also show peaks at outside the threshold for hydrogen bond σ value ($\sigma_{hb} = -0.0085 \text{ e \AA}^{-2}$) which indicates the presence of HBDs. [EMMOR] cation has a tiny peak at around $\sigma = +0.012 \text{ e \AA}^{-2}$ due to presence of oxygen atom.

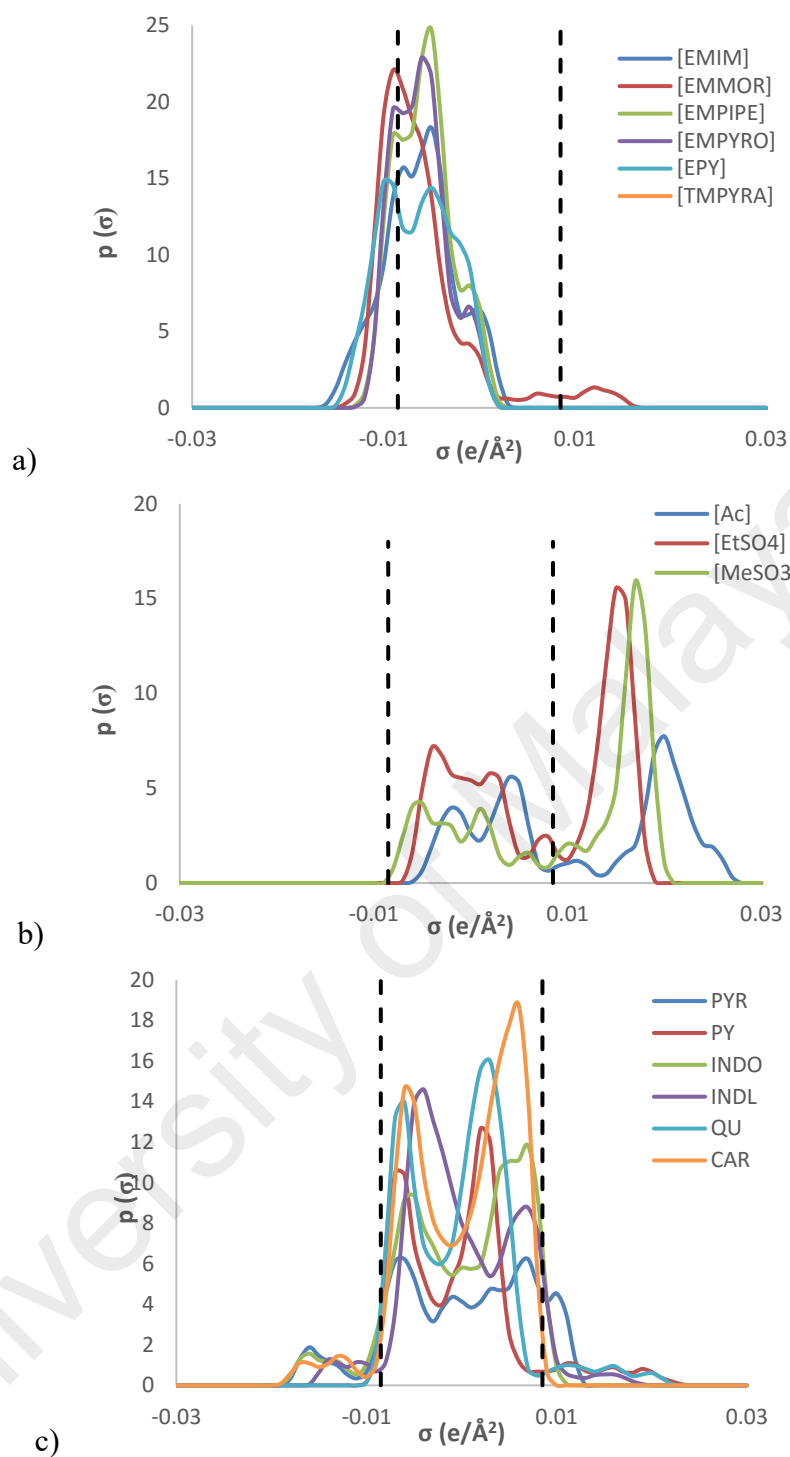


Figure 4.1: σ -profiles for all (a) cations, (b) anions and (c) heterocyclic nitrogen compounds studied. Dashed straight lines indicate the threshold value for hydrogen bond ($\sigma_{hb} = \pm 0.0085 e \text{\AA}^{-2}$)

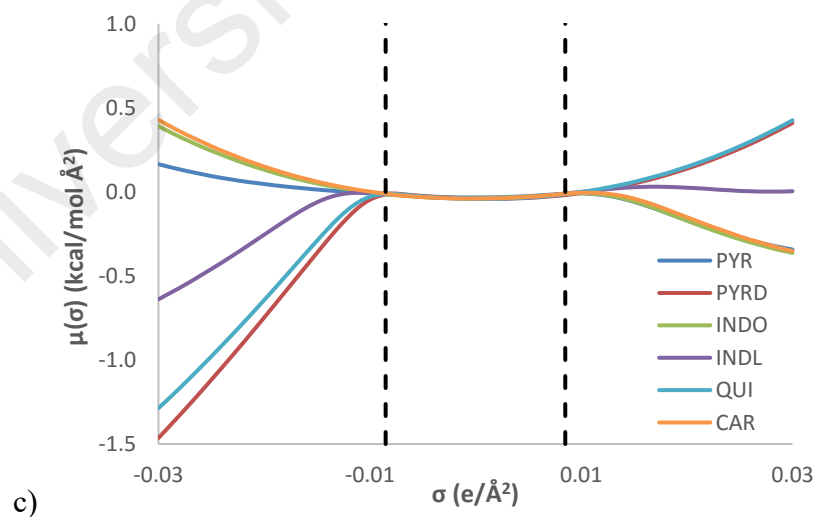
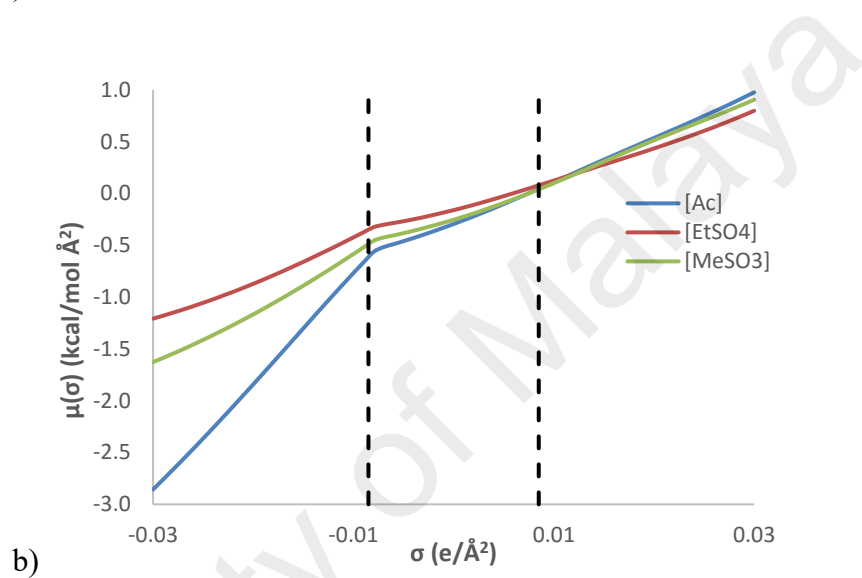
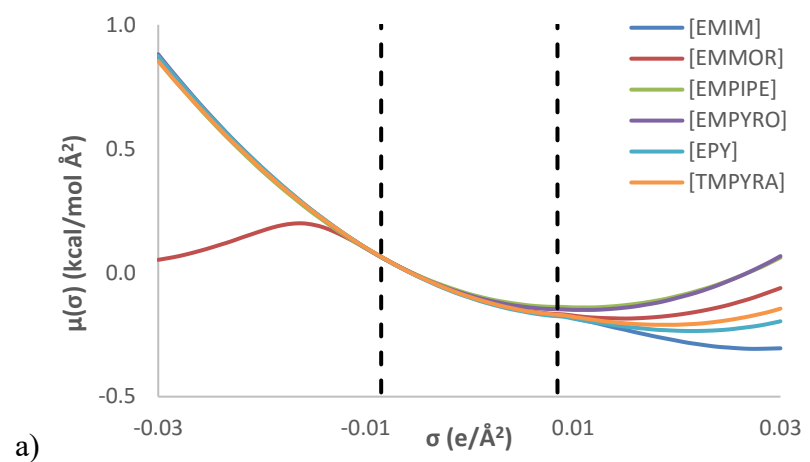


Figure 4.2: σ -potential for all (a) cations, (b) anions and (c) heterocyclic nitrogen compounds studied. Dashed straight lines indicate the threshold value for hydrogen bond ($\sigma_{hb} = \pm 0.0085 \text{ e \AA}^{-2}$)

Similarly for the σ -potential curves as shown in Figure 4.2 a), the shape looks the same for all cations except for [EMMOR] where it marks a downward curve at the negative side of the σ . The σ -potential curves for cations is a skewed parabola overlapping each other on the negative side of σ except for [EMMOR] and heading for different individual direction at the positive side of σ . σ -potentials of the cations show that they have low affinity towards HBD as shown by the positive values of $\mu(\sigma)$ at outside σ_{hb} . However, they show affinity towards non-polar surfaces and even more affinity towards hydrogen-bond acceptors as marked by the negative values of $\mu(\sigma)$ at these region and as indicated in the σ -profiles by the presence of HBDs. From the negative slope of the σ -potential at the right hand side of the curves, cations with aromatic ring i.e. [EMIM], [EPY] and [TMPYRA] appear to have better capacity as HBDs compared to those without aromatic rings i.e. [EMMOR], [EMPIPE] and [EMPYRO]. Nevertheless, all of the cations are weak HBDs since the value of $\mu(\sigma)$ only becomes slightly negative as it approaches region σ_{hb} . Figure 4.1 b) also presents the σ -profiles for the anions studied.

Contrary to the cations, σ -profiles of anions show peaks at positive side of the σ , indicating the overall negative charge of the anions. The peaks between $\sigma=-0.01e \text{ \AA}^{-2}$ and $\sigma=+0.01e \text{ \AA}^{-2}$ arise from the CH_3 groups in the anions. [Ac] has a peak at around $\sigma=+0.02 e \text{ \AA}^{-2}$ due to the oxygen atoms while [EtSO₄] and [MeSO₃] have almost similar shape and height of peaks due to presence of sulfur and oxygen atoms i.e. SO₄ and SO₃, respectively. The peak for [EtSO₄] is skewed more towards zero as it contains an extra methyl group and this is indicated by the higher peak at between $\sigma=-0.01e \text{ \AA}^{-2}$ and $\sigma=+0.01 e \text{ \AA}^{-2}$. In contrast to the cations, anions show peaks at the hydrogen-bond acceptor region. This is confirmed by the σ -potentials of the anions as shown in Figure 4.4 where it is observed that anions do not have affinity towards hydrogen bond acceptors indicated by the positive values of $\mu(\sigma)$ at outside σ_{hb} . Whereas, anions show affinity towards non-polar surfaces

and even more for HBDs as indicated by the negative values of $\mu(\sigma)$ at outside σ_{hb} at the negative side. [Ac] anion appears to have better affinity towards HBDs compared to [EtSO₄] and [MeSO₃], as the value of $\mu(\sigma)$ quickly becomes negative at outside σ_{hb} region.

The σ -profiles for heterocyclic nitrogen compounds have similar shape with some small peaks at the hydrogen-bond donor and hydrogen-bond acceptor regions. It is observed that the peaks and areas of the curves become higher with increasing carbon atoms in the molecule. Pyrrole has a relatively more symmetrical σ -profile compared to the other heterocyclic nitrogen compounds. Because their shapes are almost similar to each other, one can actually choose any of these compounds as a model heterocyclic nitrogen compound when studying denitrogenation of fuels. However, as shown by Figure 4.2, the σ -potential curve shows a more apparent difference amongst the nitrogen compounds although a common trait is that all heterocyclic nitrogen compounds in this study show an almost flat region in the range $-0.01 < \sigma < +0.01 \text{ e \AA}^{-2}$, with the value of $\mu(\sigma)$ at almost zero.

Pyrrole shows a slight affinity towards hydrogen-bond acceptors whereas indole and carbazole show almost identical σ -potential curve which overlaps each other and also have the same slight affinity for hydrogen-bond acceptors like pyrrole. Pyridine and quinoline demonstrate almost similar affinity for hydrogen-bond donors with values of $\mu(\sigma)$ which quickly become negative at outside σ_{hb} region. They also show the same lack of affinity for hydrogen-bond acceptors as indicated by the parabolic curve at the positive side of σ_{hb} . Indoline has a slight affinity for hydrogen-bond donors and maintains a value of $\mu(\sigma) = 0 \text{ e \AA}^{-2}$ at the positive side of σ_{hb} . Generally, non-basic aromatic nitrogen compounds have better affinity for hydrogen-bond acceptors due to themselves having –NH bond at the end of the five-membered ring which functions as hydrogen-bond donor.

Basic nitrogen compounds have better affinity for HBD species due to the absence of HBD groups in their structure and thus are keener to be hydrogen bond acceptors.

Figures 4.3 and 4.4 show the σ -profile and σ -potential of [EPY][EtSO₄] as the representative IL with nitrogen compounds plotted together to illustrate the interaction between the IL and the nitrogen compounds. It can be observed that the σ -profiles of [EPY] cation, [EtSO₄] anion and nitrogen compounds are complementary which indicates mutual interaction among the three species.

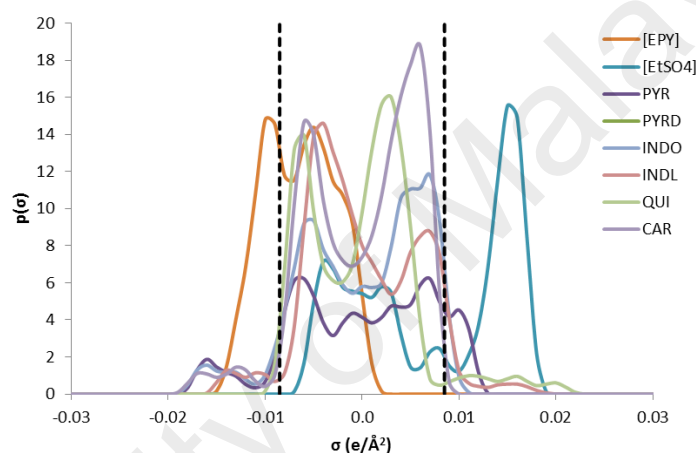


Figure 4.3: σ -profiles for the ionic liquid [EPY][EtSO₄] and heterocyclic nitrogen compounds. Dashed straight lines indicate the threshold value for hydrogen bond ($\sigma_{hb} = \pm 0.0085 \text{ e } \text{Å}^{-2}$)

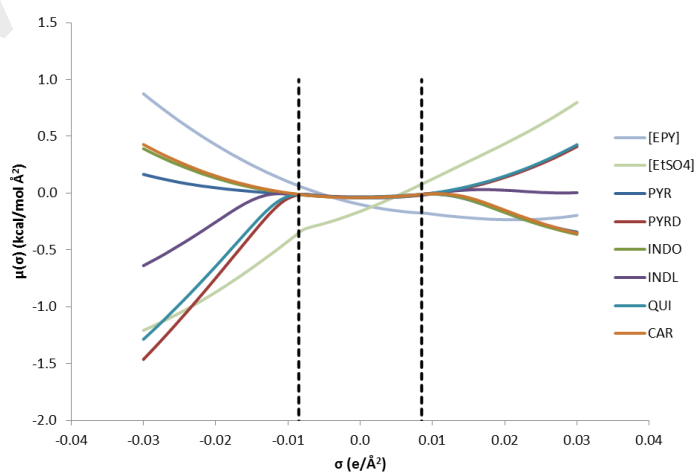


Figure 4.4: σ -potential for the ionic liquid [EPY][EtSO₄] and heterocyclic nitrogen compounds. Dashed straight lines indicate the threshold value for hydrogen bond ($\sigma_{hb} = \pm 0.0085 \text{ e } \text{Å}^{-2}$)

In summary, the σ -profiles and σ -potentials of cations, anions and nitrogen compounds studied being complementary, confirms the report that nitrogen compounds interact with cations via CH- π interaction while the interaction between nitrogen compounds with anions is mainly through hydrogen bonding. Based on the σ -profile and σ -potential, it is recommended to select ILs based on a combination of cation with aromatic ring and either [Ac] or [EtSO₄] anion.

4.1.2 Quantitative and Qualitative Screening of DESs

The effects of heterocyclic structure of nitrogen compounds, salt cations, salt anions, HBD choice and salt:HBD molar ratio towards the selectivity, capacity and performance index at infinite dilution is discussed in this section. σ -profile and σ -potential are used to facilitate understanding of intermolecular interaction between the species involved.

Li et al. reported that the extraction of benzothiophene from *n*-octane using ammonium-based DES is mainly driven by the hydrogen bond interaction between the active hydrogen in the DES and the sulfur atom in benzothiophene where the presence of benzothiophene weakens or destroys the hydrogen bonding between the halide anion and the active hydrogen in the DESs' HBD (Li, et al., 2013). If the interaction between DES and nitrogen compounds is to be assimilated to that between DES and sulfur compounds, it could be illustrated by Figure 4.5 where the intermolecular interactions are dominated by hydrogen bonding. In this figure, tetramethyl-ammonium chloride salt + two molecules of ethylene glycol are taken as a model DES whereas pyrrole and pyridine represent the model neutral and basic nitrogen compounds. The interaction between tetramethylammonium cation and chloride is via electrostatic interaction which is somehow weakened by the presence of ethylene glycol by forming a hydrogen bond between the free hydrogen and the chloride anion. When a weak HBD (like pyrrole) is present, it interacts with chlorine ion to form another hydrogen bond in the mixture;

weakening the existing hydrogen bonding between ethylene glycol and chloride ion. In the case where a weak hydrogen bond acceptor (like pyridine) is present, it creates hydrogen bonding with ethylene glycol and so weakened the hydrogen bonding between ethylene glycol and chloride ion.

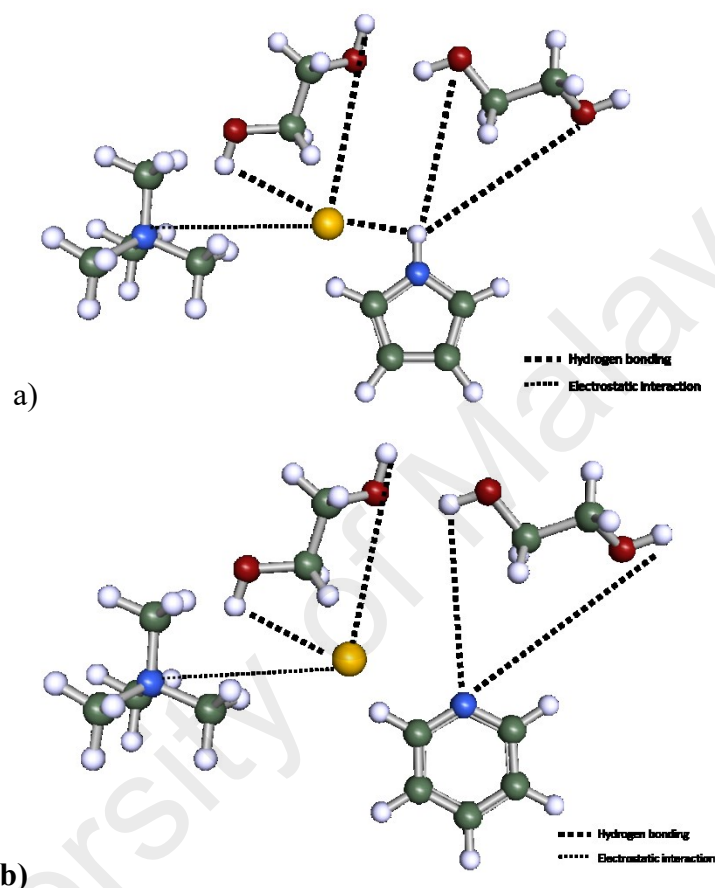


Figure 4.5: Depiction of molecular interaction between salt cation, anion, HBD and nitrogen compound. The DES TMAC/EG (1:2) is taken as model DES while pyrrole (a) and pyridine (b) as representative neutral and basic nitrogen compounds, respectively. Thick dash represents hydrogen bonding while small dots represent electrostatic interaction.

Calculated Selectivity, Capacity and Performance Index at Infinite Dilution

The DESs investigated in this work were divided into six categories:

1. choline-based DESs where the salt cations are different forms of choline cation,
2. tetramethyl –based DES where the salt cations are tetramethylammonium and tetramethylphosphonium cations with chloride anions,

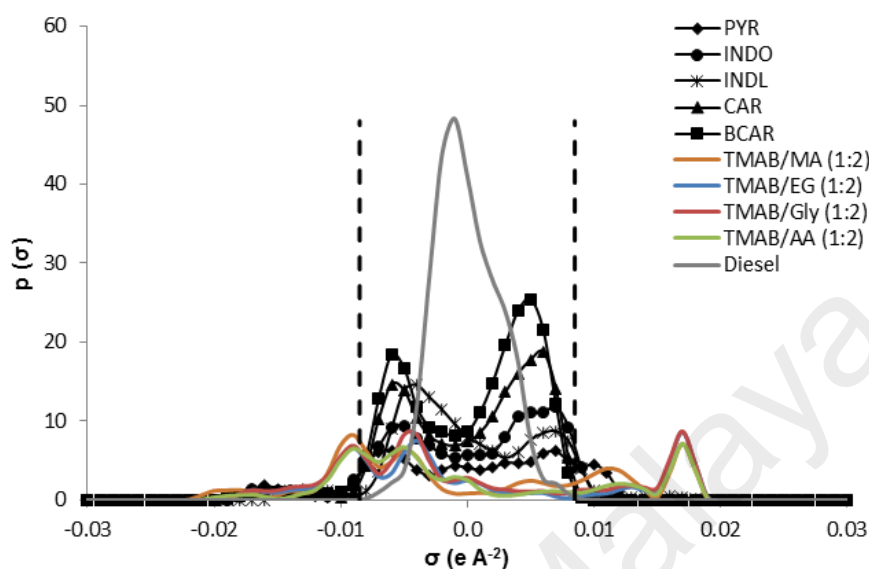
3. tetramethyl –based DES where the salt cations are tetramethylammonium and tetramethylphosphonium cations with bromide anions
4. tetrabutyl –based DES where the salt cations are tetrabutylammonium and tetrabutylphosphonium cations with chloride anion,
5. tetrabutyl –based DES where the salt cations are tetrabutylammonium and tetrabutylphosphonium cations with bromide anion and
6. DESs based on salts with phenylammonium and phenylphosphonium cations, both with chloride or bromide anion.

In the next sub sections, the effects of different parameters on the selectivity, capacity and performance index of these DESs towards the nitrogen compounds are discussed.

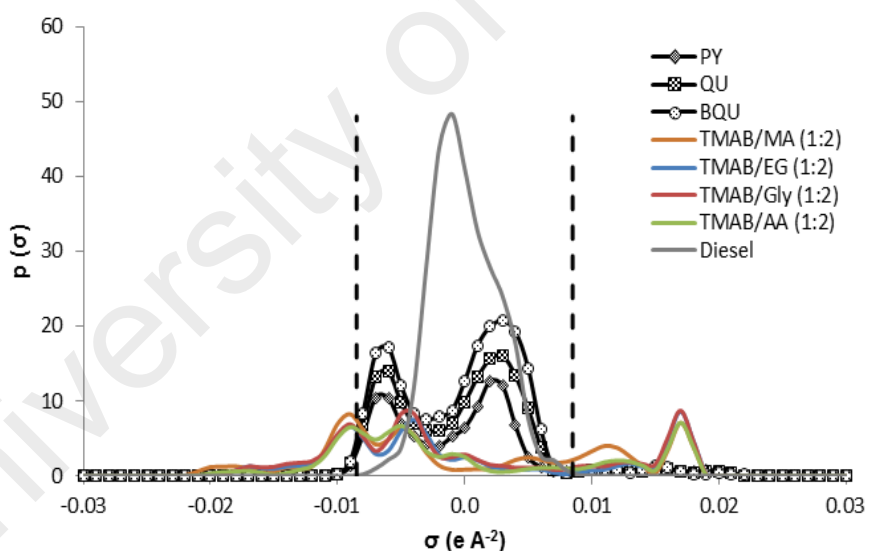
Effect of heterocyclic structure of nitrogen compounds

In general, neutral nitrogen compounds are weak HBDs whereas basic nitrogen compounds are weak hydrogen bond acceptors. This can be proven by looking at the σ -profiles and σ -potentials of each nitrogen heterocycles as presented by Figures 4.6 and 4.7. The dashed vertical lines in the σ -profile and potential diagrams represent the threshold value for the hydrogen bond interaction, $\sigma_{hb} = \pm 0.0084 \text{ e A}^{-2}$. In σ -profiles, peaks at $\sigma < -\sigma_{hb}$ show capability of HBD while peaks on the right hand side at $\sigma > +\sigma_{hb}$ show capability for hydrogen bond acceptor. The σ -profiles for the neutral compounds generally show peaks at the left hand side of the dashed line, which indicates the presence of HBD while in their σ -potentials, the values of $\mu(\sigma)$ are negative at $\sigma > +\sigma_{hb} = 0.0084 \text{ e A}^{-2}$ which indicates affinity for hydrogen bond acceptor. On the other hand, σ -profiles for the basic compounds show peak at $\sigma > +\sigma_{hb}$ indicating presence of hydrogen bond acceptor and similarly their σ -potential have negative values of $\mu(\sigma)$ at $\sigma < -\sigma_{hb} = -0.0084 \text{ e A}^{-2}$ indicating affinity for HBD. An exception to this

generalization is indoline, a five-membered compound which exhibits σ -potential like those of six-membered compounds, i.e. being a weak hydrogen bond acceptor.



a)



b)

Figure 4.6: σ -profiles of selected DESs and simulated diesel with a) neutral compounds and b) basic compounds. Vertical dashed lines represent the threshold value for the hydrogen bond interaction, ($\sigma_{hb} = \pm 0.0085 \text{ e \AA}^{-2}$)

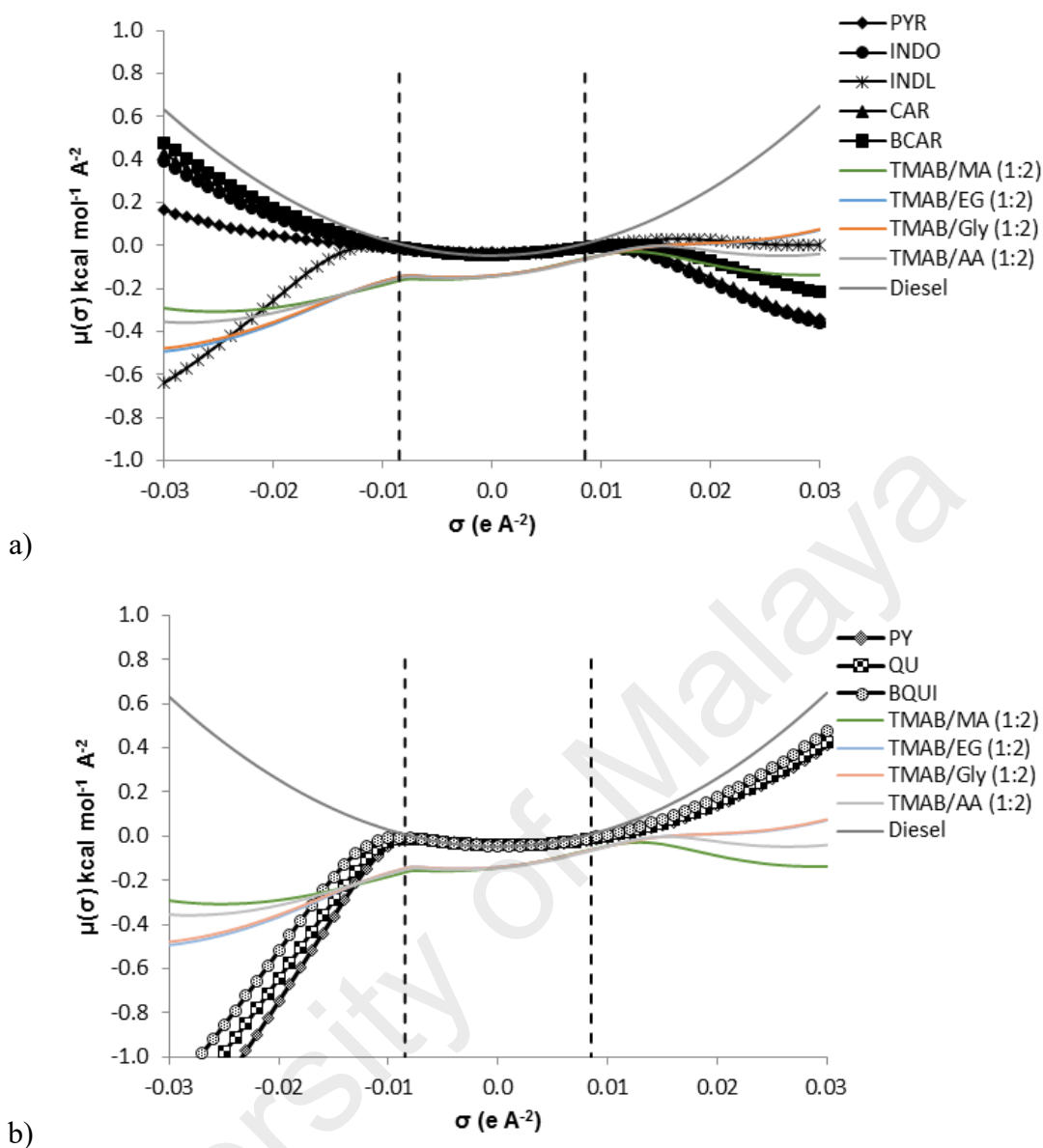
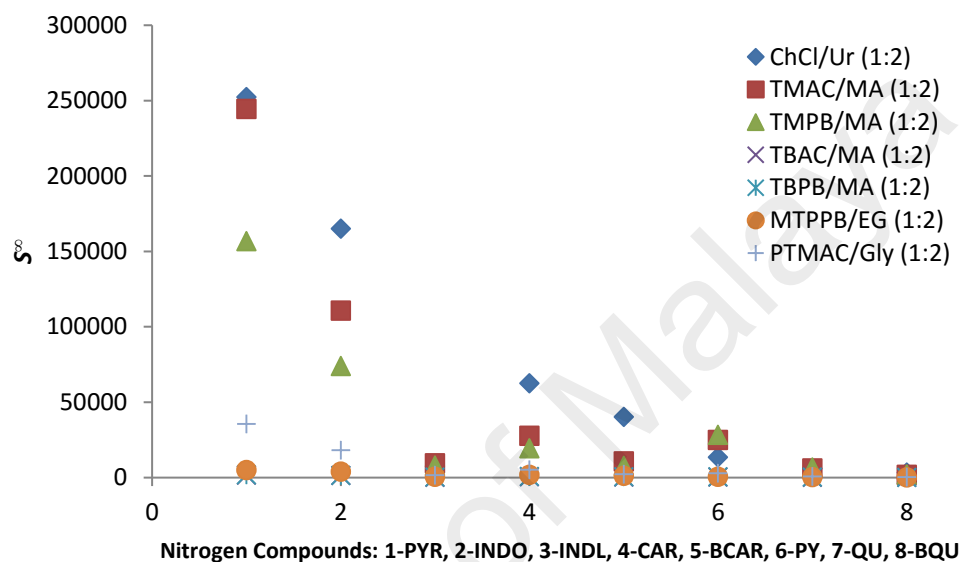


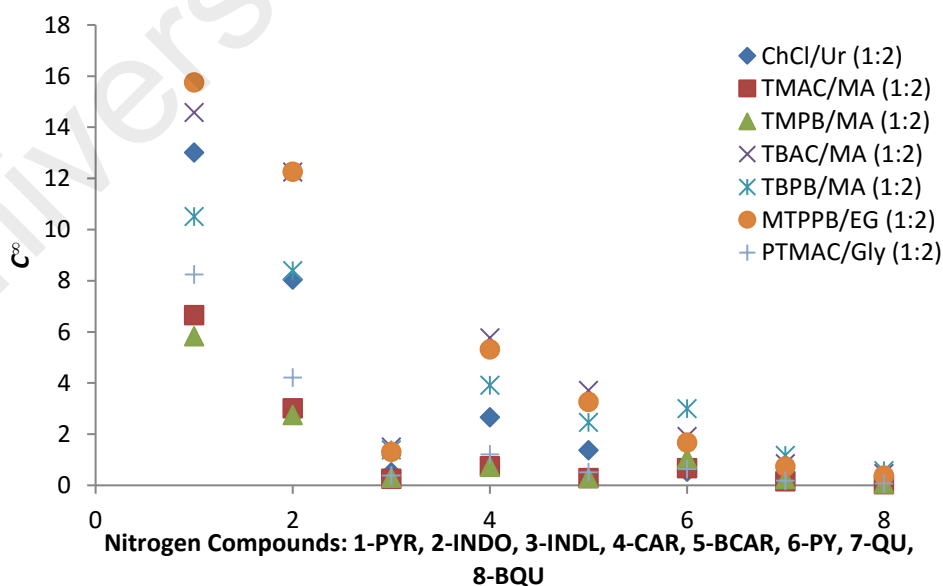
Figure 4.7: σ -potentials of selected DESs and simulated diesel with a) neutral compounds and b) basic compounds. Vertical dashed lines represent the threshold value for the hydrogen bond interaction, ($\sigma_{hb} = \pm 0.0085 \text{ e \AA}^{-2}$)

Figures 4.6 and 4.7 qualitatively demonstrate the interaction between the DESs, diesel and aromatic nitrogen compounds. Figures 4.6 a) and b) show the σ -profiles of some representative DESs, diesel and nitrogen compounds, respectively while Figures 4.7 a) and b) show the σ -potentials of the said compounds. In these figures the σ -profile and σ -potential of the DESs are represented as a whole DES instead of its individual constituents. As shown in the figures, the DESs have a hydrogen bond donor side and a hydrogen bond acceptor side. It can be observed from Figures 4.6 a) and 4.7 a) that neutral

nitrogen compounds show slight affinity towards the DESs' side of hydrogen bond acceptor. Meanwhile, Figures 4.6 b) and 4.7 b) elucidate the interaction between DESs, diesel and basic nitrogen compounds where it can be observed from Figure 4.7 b) that the basic nitrogen compounds interact with DES only by having affinity towards the hydrogen bond donor side of the DESs.



a)



b)

Figure 4.8: Selectivity (a) and capacity (b) at infinite dilution for representative DESs towards nitrogen compounds in comparison of the effect of nitrogen heterocyclic structure.

Figures 4.8 a) and b) show the values of selectivity and capacity at infinite dilution for non-basic and basic nitrogen compounds in several representative DESs, i.e. ChCl/Ur (1:2), TMAC/MA (1:2), TMPB/MA (1:2), TBAC/MA (1:2), TBPB/MA (1:2), MTPPB/EG (1:2) and PTMAC/Gly (1:2). It was observed that DESs report higher values for selectivity and capacity at infinite dilution and hence performance index (S^∞ , C^∞ and PI, respectively) for neutral nitrogen compounds compared to the basic ones. A possible explanation for this observation is due to neutral compounds being weak hydrogen bond donors, when present in the DES mixture they will increase the hydrogen bonding in the mixture through bonding of the halide anion and the pyrrolic compounds' $-NH$ atoms. Whereas, basic compounds as weak hydrogen bond acceptor when present in DES mixture will cause the hydrogen bonding between the halide anion and the HBD to be weakened, due to the need to share the same amount of hydrogen bond donor to two species now, i.e. the halide anion and the pyridinic compounds.

Table 4.1 shows the summary of results according to the maximum and minimum values of S^∞ , C^∞ and PI for each aromatic nitrogen heterocycles. For the five-membered compounds, the maximum S^∞ values goes by the order as follows: PYR> INDO> CAR> BCAR>INDL while the maximum values of C^∞ is of the following order: BCAR> INDO> CAR> PYR> INDL. Indoline reports the lowest selectivity and capacity compared to the rest of five-membered nitrogen compounds. This result is similar to the findings by Anantharaj & Banerjee and it is explained due to indoline's lack of aromatic rings in its structure, which inhibits the delocalization of π -electrons inside the rings (Anantharaj, et al., 2010a).

Table 4.1: Maximum and minimum values for S^∞ , C^∞ and PI reported by DESs for each nitrogen heterocycles.

Nitrogen Compound	Value	S^∞	DES	C^∞	DES	PI	DES
PYR	max	980618.5	CChC/ Ur	96.6	ChF/Ur	9036159.4	CChC/ Ur
	min	207.0	TBAB/ CA	4.2	TMAB/ MA	5097.1	TBAB/ CA
INDO	max	502663.7	CChC/ Ur	146.6	ChF/Ur	2374316.8	CChC/ Ur
	min	248.1	TBAB/ CA	0.6	PTMAC /EG	1419.1	PTMA C/EG
INDL	max	24081.6	CChC/ Ur	4.8	ChF/Ur	5449.5	CChC/ Ur
	min	32.2	TBAB/ CA	0.2	TMAB/ MA	123.4	TBAC/ CA
CAR	max	154693.8	CChC/ Ur	121.3	ChF/Ur	640260.0	ChF/Ur
	min	165.2	TBAB/ CA	0.35	TMAB/ MA	1184.4	DEAC/ Gly
BCAR	max	82588.4	CChC/ Ur	173.8	ChF/Ur	1315198.7	ChF/Ur
	min	130.85	MTPPB/ TrEG	0.1	TMAB/ MA	139.2	DEAC/ Gly
PY	max	96702.9	TBAB/ MA	6.0	MTPPB/ TrEG	75330.2	TMAB /MA
	min	15.2	TBAC/ CA	0.3	ChCl/ Xy	30.1	TBAC/ CA
QU	max	20568.7	CChC/ Ur	3.6	ChF/Ur	3975.5	CChC/ Ur
	min	11.1	TBAB/ CA	0.1	ChCl/ Xy	16.1	TBAC/ CA
BQU	max	8781.8	CChC/ Ur	4.5	ChF/Ur	873.9	ChF/Ur
	min	9.4	TBAB/ CA	0.03	ChCl/ Xy	8.2	TBAC/ Gly

This leads to the lack of interaction between the halide anion and the –NH atoms of indoline, thus the lower selectivity and capacity. Unlike indoline, other neutral compounds have similar order of magnitude in maximum selectivity and capacity due to their similarity in the π -electron density. For the basic compounds, the order of maximum S^∞ is as follows: PY > QU > BQU and the maximum C^∞ values follows the same order. It is observed that S^∞ and C^∞ values decreases with increasing benzene ring attached to the pyridinic compounds. Overall in terms of S^∞ , the DES CChC/Ur (1:2) gives the highest

value for all nitrogen compounds. The DES ChF/Ur (1:2) gives the highest values of C^∞ for all of the nitrogen compounds except for pyridine of which the highest C^∞ value is given by the DES MTPPB/TrEG. Mixed results is observed for the PI for each nitrogen compound where there is no clear trend on which DES excels in the value of PI for all of the aromatic nitrogen compounds. However, generally DESs with high S^∞ will give high PI as well due to PI being the product of S^∞ and C^∞ .

Effect of cation choice

The effect of cation choice on selectivity, capacity and performance index at infinite dilution was also explored. Choline-based cations, tetramethylammonium, tetramethylphosphonium, tetrabutylammonium, tetrabutylphosphonium, phenylammonium and phenylphosphonium cations were compared. Figure 4.9 a) shows the values of S^∞ for choline-based DESs towards all nitrogen compounds. For the same anion (Cl), HBD (Urea) and salt:HBD molar ratio (1:2), the selectivity of the DESs chlorocholine chloride/urea (CChCl/Ur (1:2)), choline chloride/urea (ChCl/Ur (1:2)), ethylcholine chloride/urea (EChCl/Ur (1:2)), acetylcholine chloride/urea (ATCC/Ur (1:2)) and N-benzyl-2-hydroxy-N,N-dimethylethanaminium chloride/urea (BHDAC/Ur (1:2)) can be compared. DES with chlorocholine cation gives the highest S^∞ most probably due to the presence of Cl atom attached to the choline cation, thereby increasing the polarity of the DES as a whole and thus enabling it to be more selective towards the nitrogen compounds than towards diesel compounds. To simplify the comparison, pyrrole and pyridine are taken as benchmark for neutral and basic compounds, respectively.

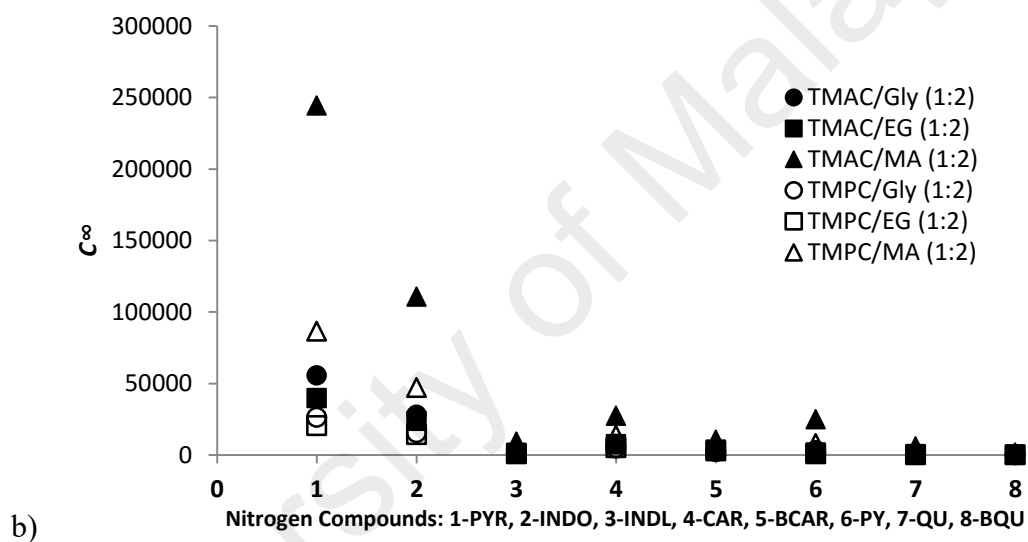
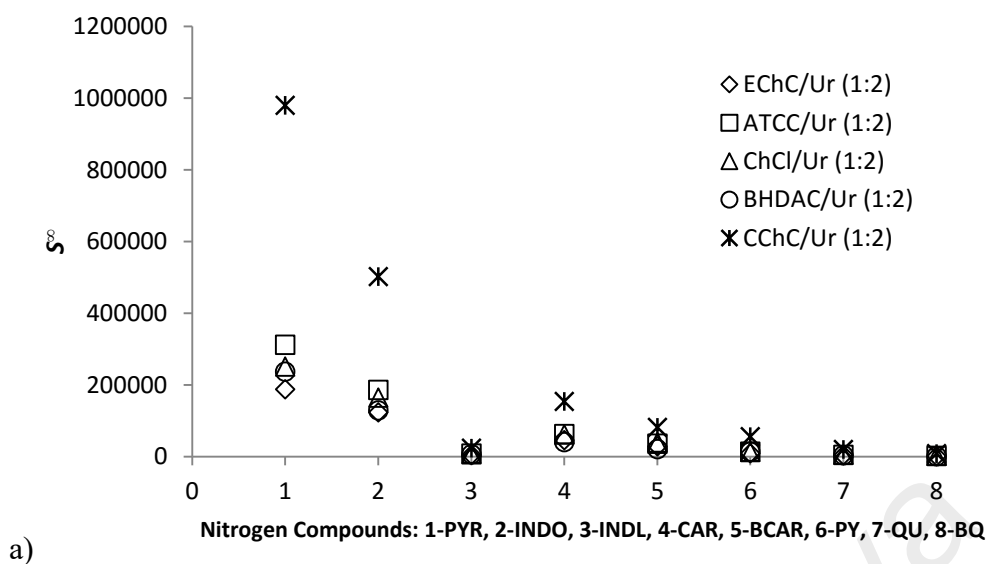
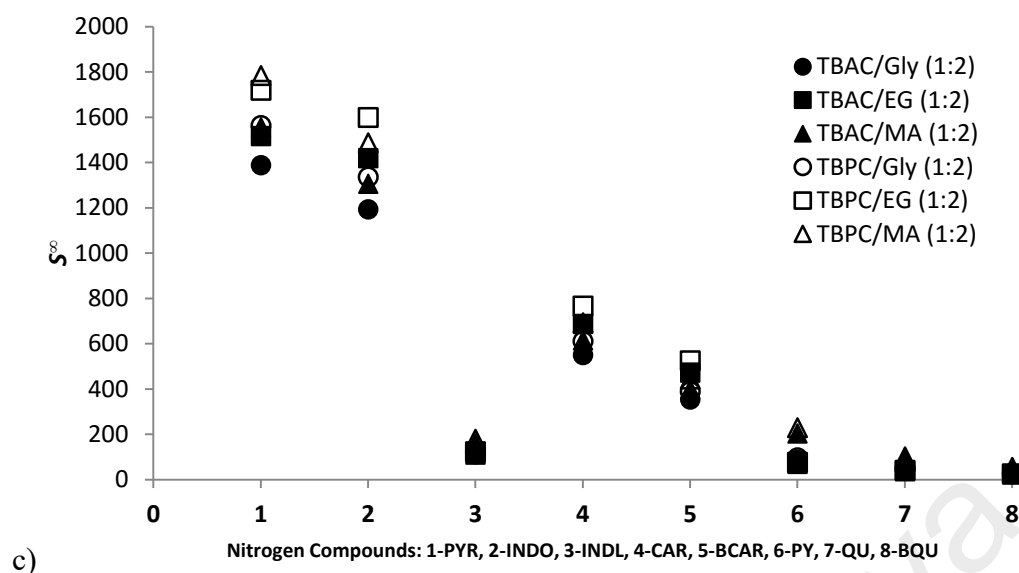
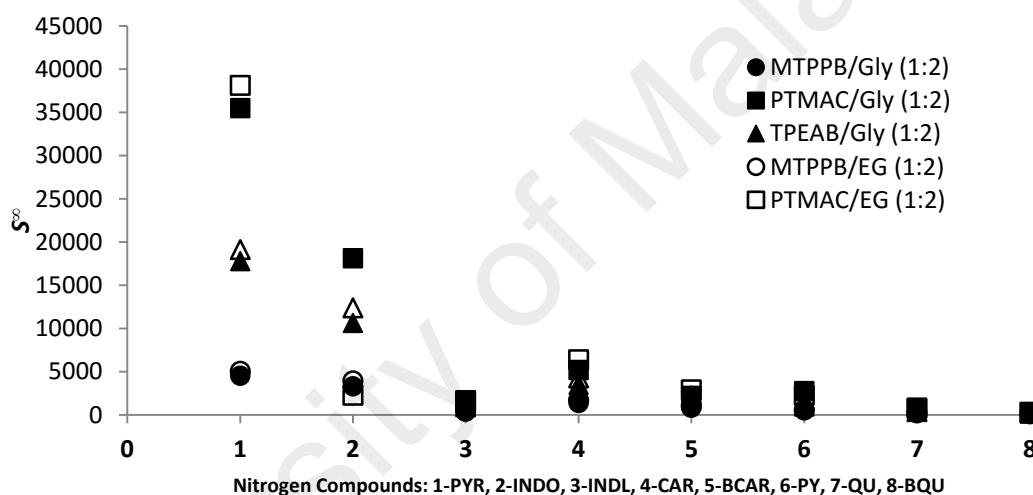


Figure 4.9: Selectivity at infinite dilution for nitrogen compounds according to different types of DESs in comparison of the effect of cation choice. a) Choline-based DESs, b) tetramethyl-based DESs, c) tetrabutyl-based DESs, d) phenylammonium and phenylphosphonium-based DESs.



c)



d)

Figure 4.9, continued.

The values of S^{∞} for pyrrole decreases for DESs in the following cations order: chlorocholine > acetylcholine > choline > N-benzyl-2-hydroxy-N,N-dimethylethanaminium > ethylcholine; with the values for both N-benzyl-2-hydroxy-N,N-dimethylethanaminium and choline close to each other. Whereas, for pyridine as representative of basic compounds, the S^{∞} values decreases for DESs with cations as follows: chlorocholine > acetylcholine > N-benzyl-2-hydroxy-N,N-dimethylethanaminium > choline > ethylcholine; with the value of S^{∞} for N-benzyl-2-hydroxy-N,N-dimethylethanaminium only slightly higher than that of choline.

Similar comparison can be made for DESs with tetramethylammonium (TMA) and tetramethylphosphonium (TMP) salts by keeping the anion and HBD constant for consistent comparison. This is illustrated in Figure 4.9 b) which presents the values of S^∞ by TMA- and TMP-based DESs towards nitrogen compounds. When comparing DESs with tetramethyl-based salt with chloride anion and malonic acid as the HBD, it was observed that DESs with TMA cation give significantly higher selectivity than DESs with TMP cation for both neutral ($S_{TMA}^\infty = 244425$ and $S_{TMP}^\infty = 86698$) and basic nitrogen compounds ($S_{TMA}^\infty = 25017$ and $S_{TMP}^\infty = 8161$). Similar trend was observed for tetramethyl-based salt DESs with bromide anion and the same HBD, where DESs with TMA cation give higher selectivity for both types of nitrogen compounds. The trend is further confirmed when comparing the DESs of TMA and TMP cations with different HBDs, e.g. glycerol and ethylene glycol, where in all cases DESs with TMA cation report higher selectivity. σ -profile of TMA and TMP cations show that TMA is slightly more polar than TMP, with TMA having more surface segments positively charged (σ values negative) than TMP. σ -profile of TMA is skewed to the left compared to σ -profile of TMP which is closer to the centre ($\sigma=0$) indicating TMP have more surface segments closer to neutral charge. Another possible explanation for TMA having higher selectivity towards nitrogen compounds is because the N atom attached to the tetramethyl chain in tetramethylammonium cation is more electronegative than the P atom attached to tetramethylphosphonium cation.

For DESs with tetrabutyl-based salts, it was generally observed that DESs with tetrabutylphosphonium (TBP) cations give higher values of S^∞ for both basic and neutral nitrogen compounds than those with tetrabutylammonium (TBA) cations with the anion and HBD kept constant for comparison as shown in Figure 4.9 c). However, the difference in values is not as large as compared to the difference in S^∞ values between DESs with TMA and TMP cations. For example, the DES tetrabutylphosphonium chloride/malonic

acid (TBPC/MA (1:2)) reports S^∞ value of 1784 for pyrrole while the S^∞ value for pyrrole by DES tetrabutylammonium chloride/malonic acid (TBAC/MA (1:2)) is 1557. Also, for pyridine, S^∞ by the DES TBPC/MA (1:2) is 229 while the DES TBAC/MA (1:2) reports S^∞ value of 204. This is also true for other DESs with TBA and TBP cations with bromide anion and with other HBDs, e.g. with glycerol and ethylene glycol. When comparing the σ -profile between TBA and TBP cations, TBA is slightly less polar than TBP in a way that TBA has more surface segments with charges close to neutral ($\sigma=0$) than TBP. However, both σ -profile and σ -potential of TBA and TBP looks very similar and this explains the close values of S^∞ obtained by the DESs with those cations. DESs with TBA and TBP cations have lower selectivity than those with choline-based or tetramethyl-based cations because the σ -profiles of TBA and TBP resemble that of diesel compounds, which means that DESs with TBA and TBP is also miscible entropically with the diesel compounds.

Figure 4.9 d) shows the values of S^∞ for phenylammonium and phenylphosphonium-based DESs towards nitrogen compounds. Comparing DESs with phenylammonium and phenylphosphonium cations, in general phenylammonium salt DESs report higher S^∞ than phenylphosphonium DESs. For example, the DES methyltriphenylphosphonium bromide/glycerol (MTPPB/Gly (1:2)) reports S^∞ values of 4509 and 600 for pyrrole and pyridine respectively, while the DES N,N,N-Trimethyl-1-phenylethanaminium bromide/glycerol (TPEAB/Gly (1:2)) give higher S^∞ values for pyrrole and pyridine (17783 and 1218, respectively). Comparing the σ -profiles of MTPPB and TPEA cations, MTPPB is less polar than TPEA as it can be observed that TPEA have a broader profile and less surface segments with neutral charge; whereas the σ -profile for MTPPB is narrow and have more surface segments close to neutral charge.

To summarize, the selectivity at infinite dilution of the nitrogen compounds in decreasing order based on the influence of cation is as follows: choline-based >

tetramethylammonium > phenylammonium > tetramethylphosphonium > phenylphosphonium > tetrabutylphosphonium > tetrabutylammonium, where DESs with the last two cations report almost similar values of S^∞ .

Similar approach of comparison was adopted to investigate the effect of cation choice towards capacity at infinite dilution, C^∞ . Overall, the DES choline fluoride/urea (ChF/Ur (1:2)) reports the highest value of C^∞ for all nitrogen compounds except for pyridine.

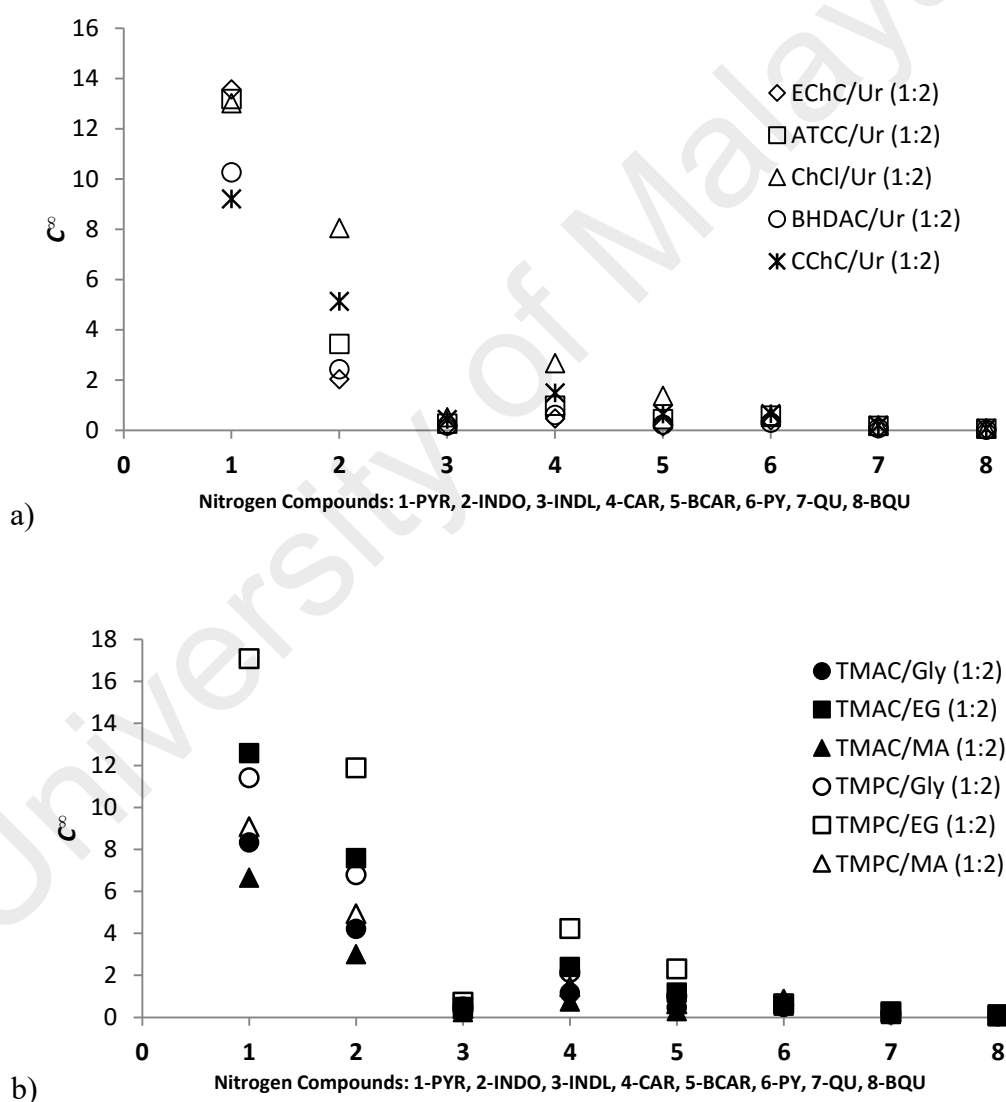


Figure 4.10: Capacity at infinite dilution for nitrogen compounds according to different types of DESs in comparison of the effect of cation choice. a) Choline-based DESs, b) tetramethyl-based DESs, c) tetrabutyl-based DESs, d) phenylammonium and phenylphosphonium-based DESs.

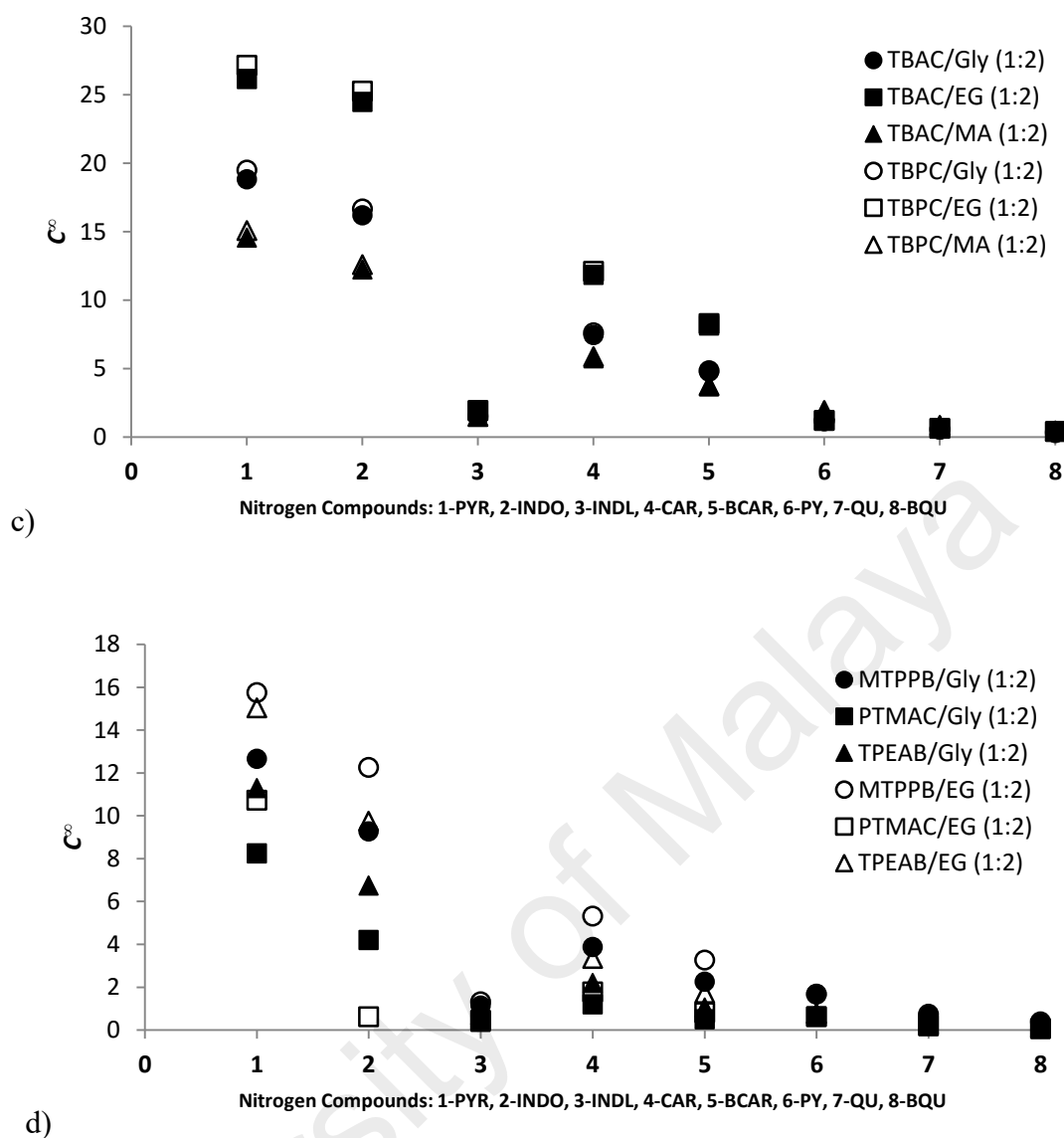


Figure 4.10, continued.

Comparing other choline-based DESs with the Cl anion and urea as the HBD with salt:HBD ratio 1:2 as shown in Figure 4.10 a), the trend for C^∞ of pyrrole in the DES follows the order: ethylcholine (14) > acetylcholine (13.2) > choline (13) > N-benzyl-2-hydroxy-N,N-dimethylethanaminium (10) > chlorocholine (9); where a very small difference in value can be observed between DESs with acetylcholine and choline cations. Meanwhile for pyridine, the values of C^∞ follows the order chlorocholine (0.65) > acetylcholine (0.59) > choline (0.53) > ethylcholine (0.40) > N-benzyl-2-hydroxy-N,N-dimethylethanaminium (0.30). The values of C^∞ by choline-based DESs are less than unity for pyridine and the difference between them are not so significant.

The values of C^∞ for DESs with TMA and TMP cations are also compared by keeping the anion and HBD constant for consistent comparison and this is shown in Figure 4.10 b). It is observed that DESs with TMP cation give higher values of C^∞ for both neutral and basic nitrogen compounds. Similarly for tetrabutyl- cations, Figure 4.10 c) shows that DESs with TBP cation have higher capacity for nitrogen compounds than those with TBA cations.

On the other hand, it is observed from Figure 4.10 d) that DESs with phenylphosphonium cation have slightly higher values of C^∞ for neutral compounds than those with phenylammonium cation by about 4 to 10%. However, for basic compounds, DESs with phenylphosphonium cation report significantly higher values of C^∞ by about twice the values of C^∞ reported by DESs with phenylammonium cation. As the definition C^∞ is the inverse of γ^∞ of nitrogen compound in the DES, higher values of C^∞ indicate that the solute have smaller values of γ^∞ in the solvent, thereby indicating a more favourable interaction. Thus, based on the higher values of C^∞ of nitrogen compounds in DESs with phosphonium-based cations, the nitrogen compounds have better interaction with DESs with phosphonium cations than those with ammonium cations.

Overall, in terms of capacity, the DESs with the following cations are arranged in the order of decreasing values of C^∞ : tetrabutylphosphonium \geq tetrabutylammonium $>$ tetramethylphosphonium $>$ tetramethylammonium $>$ phenylphosphonium $>$ phenylammonium $>$ choline-based cations. Finally, regarding the performance index (PI), it generally follows the same trend of selectivity because DESs with high values of S^∞ usually have high PI.

Effect of halide anion

In this section, the influence of anion choice for the salt making up the DESs will be discussed. The effect of chloride (Cl^-) and bromide (Br^-) anions based on the performance of DESs with the salts tetramethylammonium chloride (TMAC), tetramethylammonium bromide (TMAB), tetramethylphosphonium chloride (TMPC), tetramethylphosphonium bromide (TMPB), tetrabutylammonium chloride (TBAC), tetrabutylammonium bromide (TMAB), tetrabutylphosphonium chloride (TBPC) and tetrabutylphosphonium bromide (TBPB); combined with a few HBDs such as malonic acid (MA), glycerol (Gly) and ethylene glycol (EG) with salt:HBD ratio of 1:2 is discussed. This is to enable consistent comparison on the effects on anion alone where the cation, HBD and salt:HBD ratio are made constant.

Figures 4.11 a) and b) are referred for observation towards the selectivity at infinite dilution. In terms of selectivity, DESs with TMA/TMP salts with Br^- anion give higher values of S^∞ compared to those with Cl^- anion for both neutral and basic nitrogen compounds. For example, with MA kept constant as the HBD, the DES TMAC/MA gives S^∞ of 244425 and 25017 for pyrrole and pyridine, respectively, while the DES TMAB/MA gives S^∞ of 511510 and 96073 for pyrrole and pyridine, respectively. The values of S^∞ are also higher for DES TMAB/MA towards other neutral (i.e. indole, indoline, carbazole, benzocarbazole) and basic compounds (i.e. quinoline, benzoquinoline). This trend is also true for DESs with TMP salts, where the values of S^∞ for pyrrole and pyridine by TMPC/MA are 86698 and 8161, respectively, compared to 159742 and 28328, respectively by the DES TMPB/MA. Again, DESs with TMPB salts also report higher values of S^∞ towards all other neutral and basic compounds compared to DESs with TMPC salts.

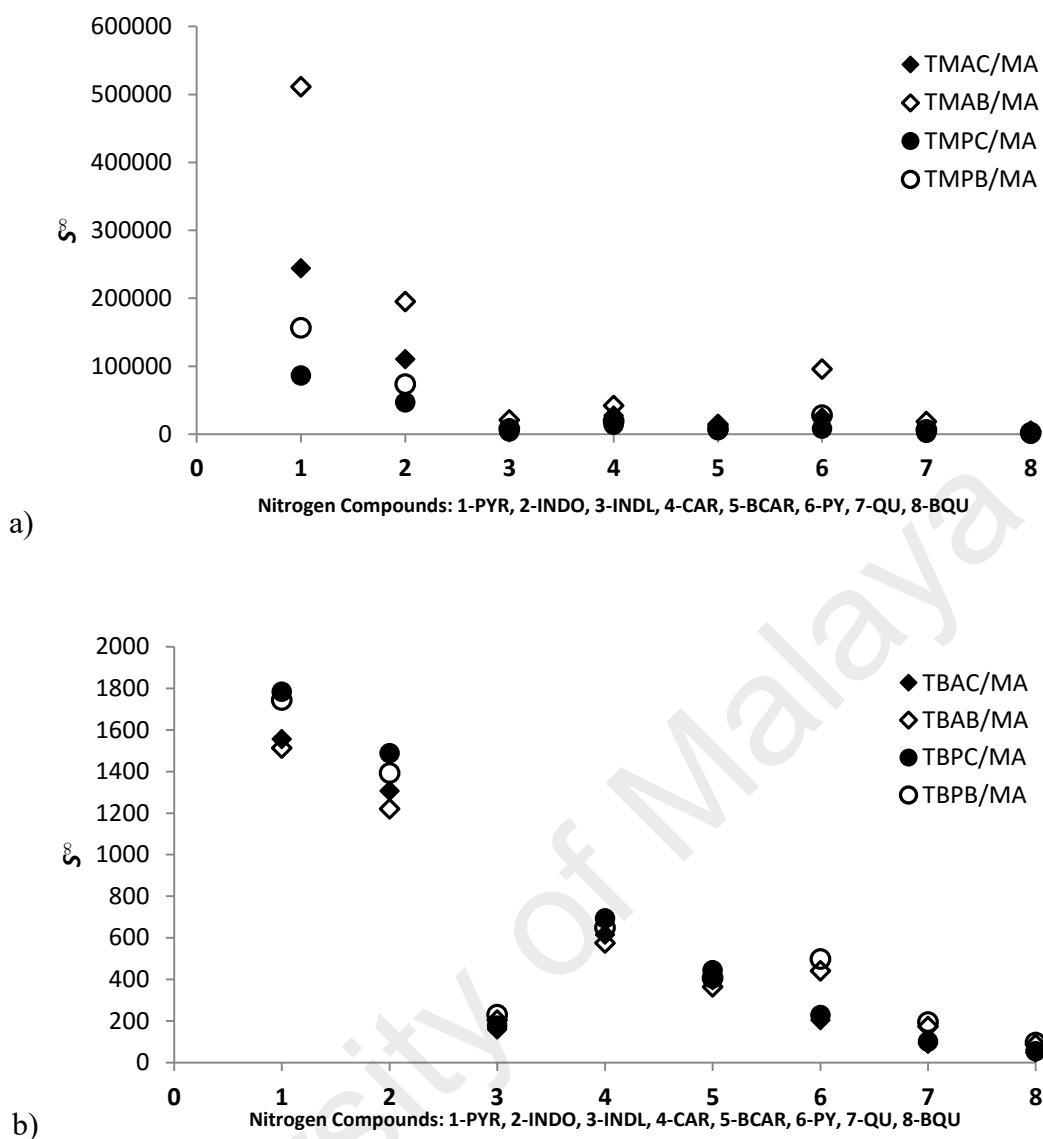


Figure 4.11: Selectivity at infinite dilution in comparison of anion choice. a) tetramethyl-based DESs. b) tetrabutyl-based DESs.

Whereas for DESs with TBA/TBP salts, mixed trend was obtained for the values of S^∞ for neutral and basic compounds. DESs with TBA/TBP cation report higher values of S^∞ for neutral compounds when there is Cl^- anion versus those with Br^- anion. However the difference in values is very small, i.e. around 2-10%. For instance, the DES TBAC/MA reports S^∞ values for pyrrole of 1557 while the DES TBAB/MA reports 1514. Similarly for phosphonium-based DES, TBPC/MA reports S^∞ for pyrrole of 1784 while TBPB/MA reports 1745. For the other neutral compounds, the DES TBAC/MA reports S^∞ values of 1308, 160, 616, 397 for indole, indoline, carbazole and benzocarbazole, respectively while the DES TBAB/MA reports S^∞ values of 1221, 205, 575, 365 for the

respective compounds. Similar trend is also shown by the DES TBPC/MA and TBPB/MA towards the rest of the neutral compounds. The only exception from this trend is indoline, which as discussed in a previous section shows behaviour similar to basic compounds instead.

For basic nitrogen compounds, DESs with TBA/TBP cation report higher values of S^∞ when combined with Br^- anion, but lower values of S^∞ are reported when combined with Cl^- anion. The DES TBAB/MA has $S^\infty=441$ vs. $S^\infty=204$ by the DES TBAC/MA for pyridine. Similarly, TBPB/MA reports higher S^∞ for pyridine, i.e. 499 vs. 229 by TBPC/MA. For the rest of the basic compounds, the DES TBAC/MA reports S^∞ values of 90 and 49 for quinoline and benzoquinoline, respectively, while the DES TBAB/MA reports S^∞ values of 173 and 87 for the respective compounds. The difference in values of S^∞ for DESs with TBA/TBP cation with Cl^- or Br^- anion towards basic compounds is more significant than that towards neutral compounds.

In terms of capacity as shown by Figures 4.12 a) and b), there is a mixed trend between DESs with Cl^- and Br^- anion. With the same salt cation and HBD, DESs with Cl^- anion generally give higher C^∞ for neutral compounds but DESs with Br^- anion give higher C^∞ for basic compounds. However, for basic compounds, the values of C^∞ is small (≤ 1) and the difference in the values of C^∞ reported by DESs with Br^- and Cl^- anion is also very small; in some cases similar values of C^∞ were obtained for the DESs. For example, for pyrrole, the DES TMAC/MA reports $C^\infty=6.65$ while the DES TMAB/MA reports $C^\infty=4.17$. On the other hand, the same DESs report C^∞ values for pyridine as 0.68 and 0.78, respectively. C^∞ values for the rest of neutral compounds by the TMAC/MA are 3.01, 0.26, 0.75 and 0.29 for indole, indoline, carbazole and benzocarbazole, respectively while the values reported by TMAB/MA are 1.60, 0.17, 0.35 and 0.12 for the respective compounds. Similar trend was observed for DESs with phosphonium salts, where the DES TMPC/MA reports $C^\infty=9.08$ and the DES TMPB/MA reports $C^\infty=5.83$

for pyrrole. For pyridine, TMPC/MA reports $C^\infty=0.86$ while TMPB/MA reports $C^\infty=1.05$. Similarly for DESs with tetrabutyl-based salts with the same HBD (MA), C^∞ for pyrrole by the DES TBAC/MA is 14.58 while the DES TBAB/MA reports $C^\infty=10.24$. For pyridine, TBAC/MA reports $C^\infty=1.91$ and TBAB/MA reports $C^\infty=2.98$. DESs with tetrabutylphosphonium salt also exhibit the same trend, where TBPC/MA and TBPB/MA reports C^∞ values of 15.11 and 10.52, respectively for pyrrole and the same DESs reports C^∞ values of 1.94 and 3.01, respectively for pyridine.

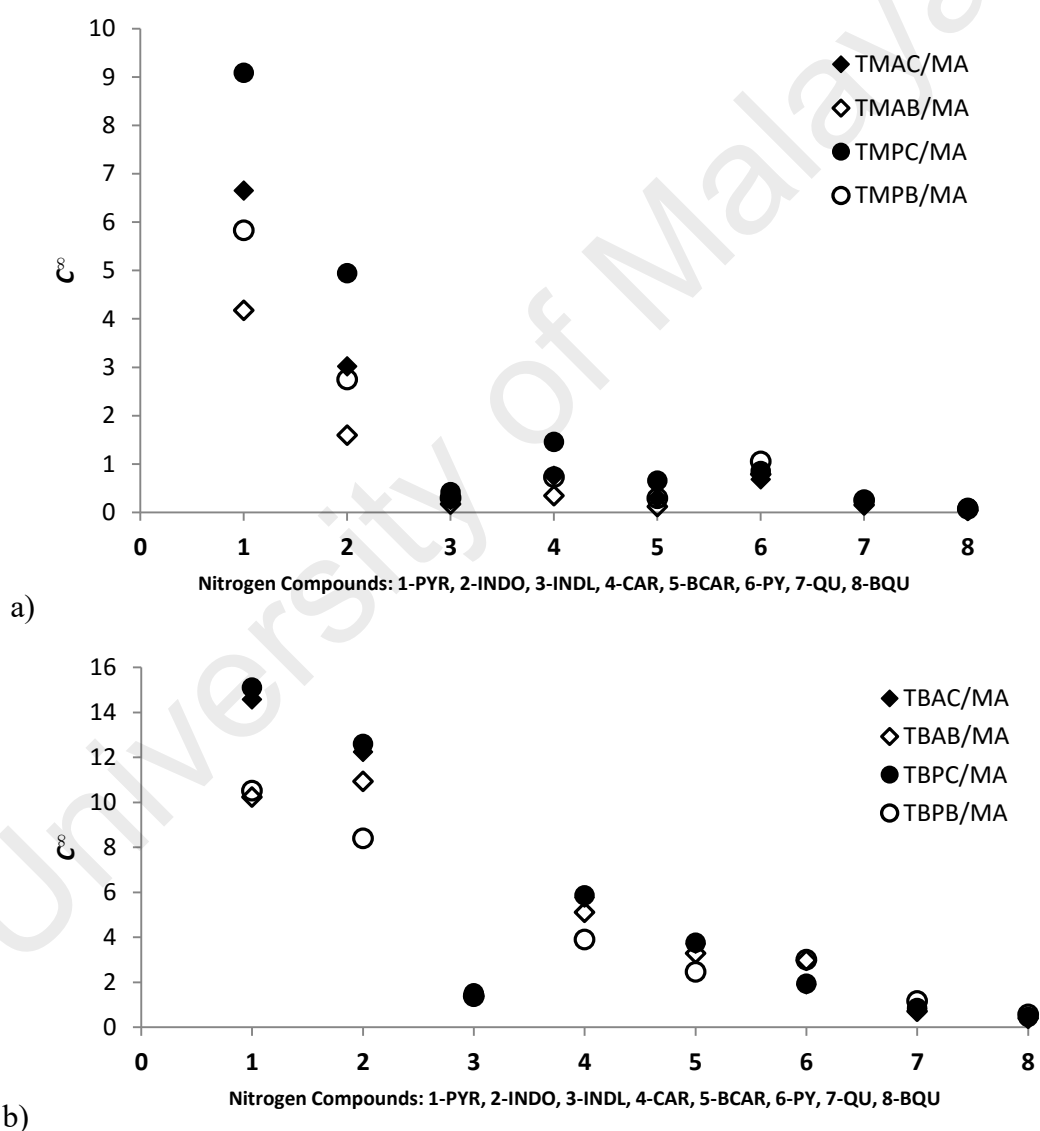


Figure 4.12: Capacity at infinite dilution in comparison of anion choice. a) tetramethyl-based DESs. b) tetrabutyl-based DESs. Nitrogen Compounds: 1-PYR, 2-INDO, 3-INDL, 4-CAR, 5-BCAR, 6-PY, 7-QU, 8-BQU

When observing the effect of halide anion towards the selectivity and capacity at infinite dilution of the DESs for aromatic nitrogen compounds, it should be noted that the difference in values of S^∞ for DESs with Cl^- and Br^- is more significant than the difference in values of C^∞ . In other words, the choice of halide anion has a greater impact towards the selectivity at infinite dilution than it has for capacity at infinite dilution. Observation of the trend on the effect of halide anion towards the performance index (PI) of the DESs indicates that the DESs with Cl^- anion give higher values of PI for neutral nitrogen compounds while higher PI values were reported for basic nitrogen compounds by DESs with Br^- anion. This is expected since PI is largely influenced by the values of selectivity than capacity; and it was observed that in general DESs with Cl^- anion give higher selectivity for neutral compounds and DESs with Br^- anion give higher selectivity for basic compounds.

From the σ -profile and σ -potential of the anions, Cl^- is a stronger hydrogen bond acceptor and it has a better affinity towards hydrogen bond donor compared to Br^- . This can be observed from its σ -potential where the values of $\mu(\sigma)$ of Cl^- becomes more negative at $\sigma < -0.0084 \text{ e \AA}^{-2}$. From the σ -profile, Br^- has more surface segments with $\sigma > +0.0084 \text{ e \AA}^{-2}$. Cl^- is a smaller ion than Br^- and it is more electronegative. The values of activity coefficient at infinite dilution (γ^∞) of nitrogen compounds are smaller in DESs with Cl^- anion. On the other hand, γ^∞ of diesel compound is also smaller in DESs with Cl^- anion than in those with Br^- anion. Smaller values of γ^∞ indicate that both nitrogen compounds and diesel compounds have favourable interaction with DESs with Cl^- anion than with those with Br^- anion.

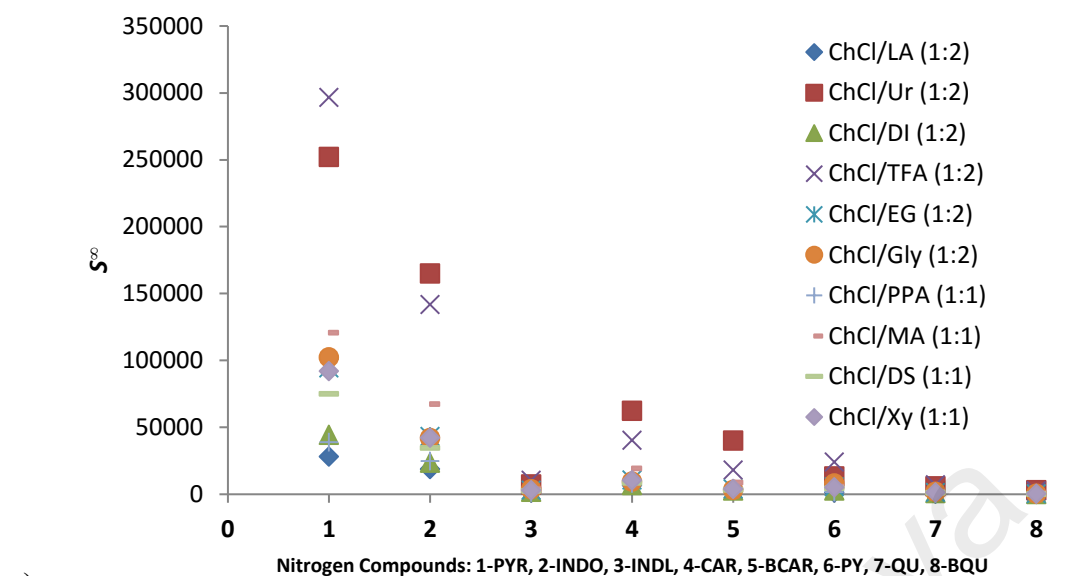
This explains why DESs with Cl^- anion report greater values of capacity but lower values of selectivity, especially for neutral nitrogen compounds. The higher values of C^∞ towards basic compounds reported by DESs with Br^- anion indicate that basic compounds have a better affinity with those DESs. A possible explanation based on the σ -profile and

potential analysis is that, the basic compounds are weak hydrogen bond acceptors and have affinity towards HBDs. Compared to Br⁻, Cl⁻ is a stronger hydrogen bond acceptor and has a better affinity towards HBD species. Thus, basic compounds would rather mix with Br⁻ compounds than with Cl⁻ compounds to reduce the competition of creating hydrogen bonding interaction with available HBD species.

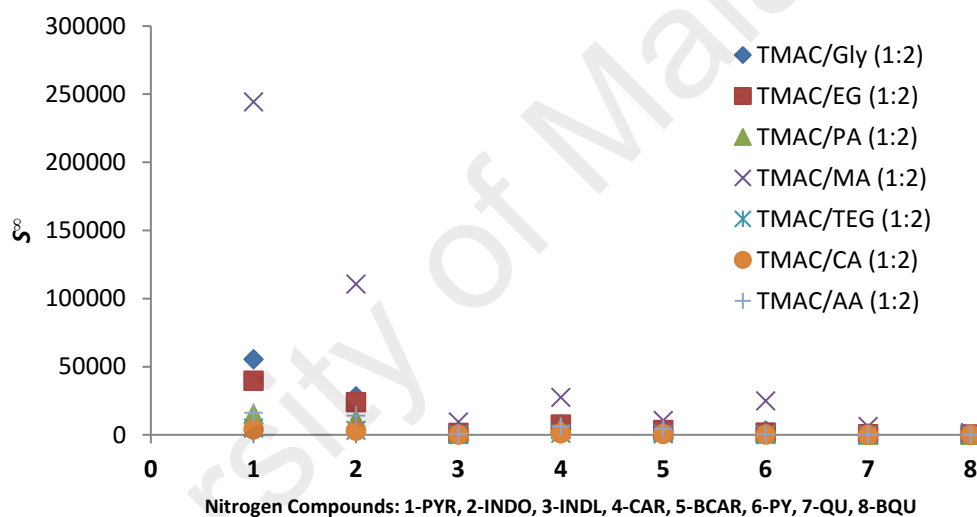
Effect of HBD

In this section, the influence of the choice of HBD towards the selectivity and capacity of the DESs for the nitrogen compounds at infinite dilution is discussed. The DESs can be divided into two categories: 1) ChCl-based DESs with different HBDs and 2) tetraalkyl salt-based DESs with different HBDs. Both categories of DESs were compared at the same salt:HBD molar ratio and it was observed that the choice of HBD has a significant effect towards the values of S^∞ , C^∞ and thus PI of the DESs for the nitrogen compounds.

For ChCl-based DESs, there are DESs with salt:HBD molar ratio of 1:1 and 1:2; those with salt:HBD molar ratio 1:1 are ChCl/MA, ChCl/Xy, ChCl/DS and ChCl/PPA; while those with 1:2 salt to HBD molar ratio are ChCl/Ur, ChCl/TFA, ChCl/Gly, ChCl/EG, ChCl/DI and ChCl/LA. The DESs were selected at these particular molar ratios because they have been reported in the literature as liquid at room temperature. For ChCl-based DESs with salt:HBD ratio 1:1 (Figure 4.13 a)), the values of S^∞ for neutral and basic nitrogen compounds according to HBD is as follows: MA>Xy>DS>PPA; i.e. ChCl combined with malonic acid reports the highest value of S^∞ , followed by ChCl combined with xylitol, *D*-sorbitol and phenylpropionic acid. For ChCl-based DESs with salt:HBD ratio 1:2, the DESs which report the highest value of S^∞ are ChCl/Ur and ChCl/TFA, followed by ChCl/Gly, ChCl/EG, ChCl/DI and ChCl/LA in decreasing order of S^∞ values.



a)



b)

Figure 4.13: Selectivity at infinite dilution in comparison of HBD choice. a) ChCl-based DES b) TMAC-based DESs.

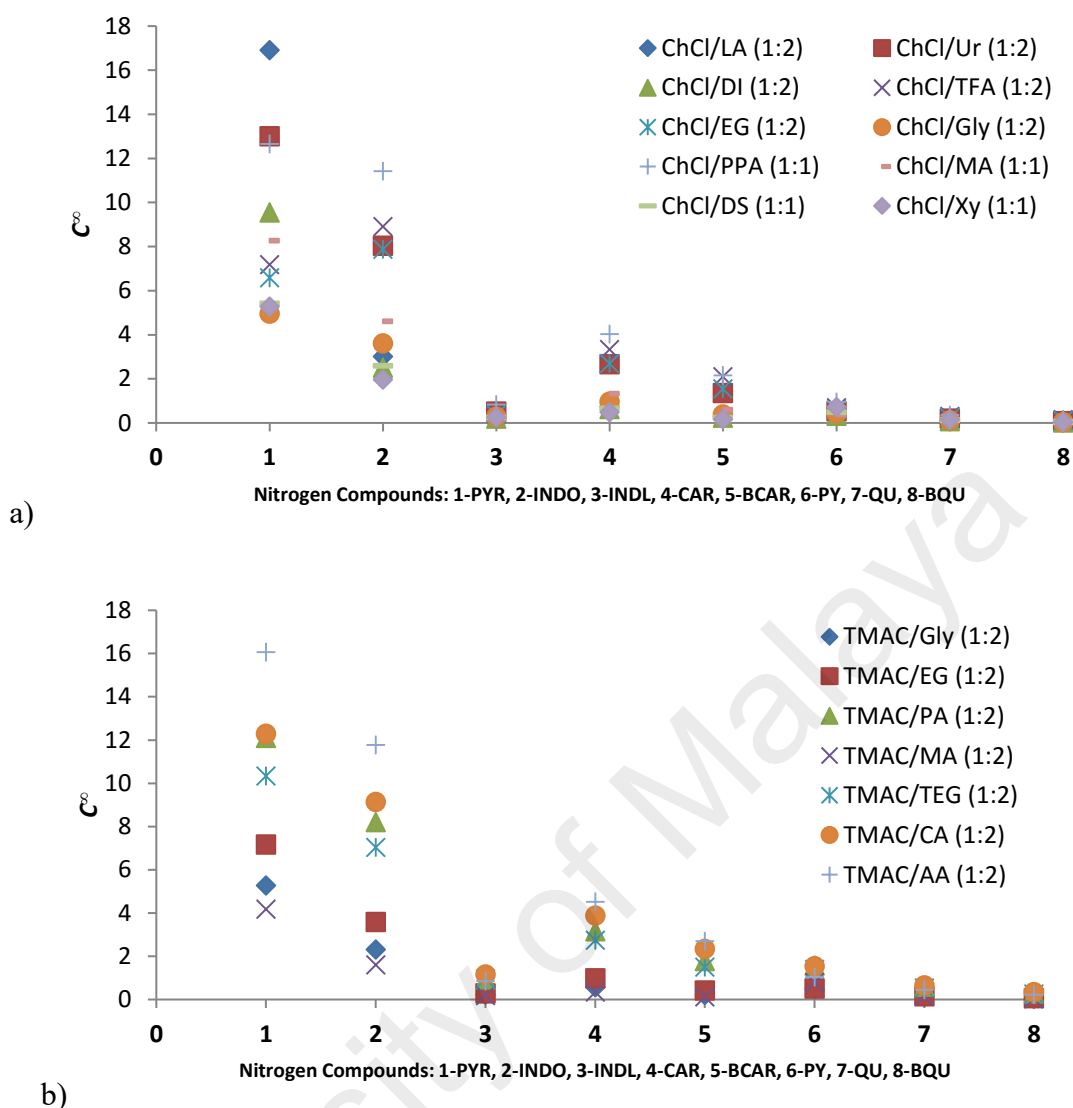


Figure 4.14: Capacity at infinite dilution in comparison of HBD choice. a)ChCl-based DES b) TMAC-based DESs.

In terms of C^∞ values, Figure 4.14 a) shows an opposite order of the DESs. For ChCl-based DESs with 1:1 salt:HBD ratio, ChCl/PPA reports the highest value of C^∞ for both neutral and basic nitrogen compounds, followed by ChCl/MA, ChCl/DS and lastly ChCl/Xy. ChCl-based DESs with 1:2 salt:HBD molar ratio report highest values of C^∞ for all nitrogen compounds by ChCl/LA, followed by ChCl/Ur, ChCl/DI, ChCl/TFA, ChCl/EG and lastly ChCl/Gly. From the trends, it was observed that ChCl-based DESs which give high selectivity report low values of capacity and those which report low

selectivity have high values of capacity. An exception to this observation is ChCl/Ur which reports high values of S^∞ and C^∞ for all aromatic nitrogen compounds.

Oliveria et al. reported the use of ChCl-based DESs for the separation of azeotropic mixture of ethanol and heptane (Oliveira, et al., 2013). The DESs used in their study are ChCl/Gly, ChCl/EG and ChCl/LA with salt:HBD ratio of 1:2. They reported that high selectivity with low distribution coefficient of ethanol was obtained with the DESs ChCl/Gly and ChCl/EG, whereas high distribution coefficient and low selectivity of ethanol was obtained with the DES ChCl/LA. The difference among the three HBDs (Gly, EG and LA) are in their functional groups, where Gly and EG contains 3 and 2 –OH groups respectively while LA have a carboxylic group (-COOH) and a carbonyl group (C=O). The presence of the carboxylic and carbonyl group in LA enhances the polarization of the –OH group present in LA than those of alcohols in Gly and EG. This enhances the dipole strength and allows for higher number and stronger dipoles which lead to larger number and stronger hydrogen bonding interaction to occur in the mixture of solute-DES. Furthermore, the total energy of hydrogen bonding interaction for carboxylic acid is greater than that observed for other organic compounds containing –OH and/or C=O dipoles, thus ChCl with LA can form stronger hydrogen bonding with ethanol which lead to higher solute-carrying capacity and thus higher distribution coefficient. Whereas for ChCl/Gly and ChCl/EG, the abundant number of –OH groups increases the capability of establishing hydrogen bonding with the –OH group of ethanol, thus they can extract ethanol more easily and this is reflected in the higher values of selectivity.

Analogous to the application in denitrogenation of diesel oil where the main driving force is also based on hydrogen bonding interaction as discussed previously, similar explanation can be adopted to elucidate the behaviour of ChCl-based DESs with different HBDs towards the selectivity and capacity for nitrogen compounds. For ChCl-

based DES with 1:1 molar ratio, ChCl with phenylpropionic acid reports highest capacity due to the presence of $-\text{COOH}$ and phenyl group which increases the dipole strength and enhances the hydrogen bonding interaction with the $-\text{N}$ and $-\text{NH}$ groups in the basic and neutral nitrogen compounds, respectively. However, due to the presence of seven $-\text{CH}$ groups in PPA, ChCl/PPA have relatively favourable interaction with the diesel compounds compared to other HBDs with less $-\text{CH}$ groups. This is reflected in the smaller value of γ^∞ of diesel compounds in ChCl/PPA than in other ChCl-based DESs with 1:1 ratio, which then resulted in the low value of selectivity towards aromatic nitrogen compounds exhibited by ChCl/PPA. Meanwhile, ChCl with malonic acid reports high selectivity and high capacity for nitrogen compounds because of the presence of two $-\text{COOH}$ groups in its dicarboxylic acid functional group. The presence of these carbonyl groups not only enhances the hydrogen bonding interaction with nitrogen compounds, but it also facilitates the extraction of nitrogen compounds via hydrogen bonding much easily. Besides, there are only three C atoms with only one $-\text{CH}$ group, thus it does not have a good interaction with diesel compound.

For ChCl-based DESs with 1:2 molar ratio, ChCl with TFA and Urea report high value of S^∞ due to the presence of $-\text{CF}_3$, $\text{C}=\text{O}$ and $-\text{NH}_2$ groups, which can all form hydrogen bonding with the nitrogen compounds. ChCl combined with TFA or Urea has more sites for hydrogen bonding, especially with non-basic nitrogen compounds. In TFA, $-\text{CF}_3$ group acts as a hydrogen bond acceptor while the $-\text{NH}_2$ group can be both HB acceptor and HB donor. In Urea, there are two $-\text{NH}_2$ groups, enabling more sites for HB interaction. The presence of $\text{C}=\text{O}$ group both in TFA and Urea enhances the dipole moment of molecules for stronger HB interaction. Thus, they can extract the nitrogen compounds more easily and therefore the high values of S^∞ . Similarly, MA and EG have two $-\text{OH}$ groups while Gly has three $-\text{OH}$ groups, which increase the number of sites for HB interactions and thus explain the high values of S^∞ reported. Compared to ChCl/LA

which reports the highest value of C^∞ but lowest value of S^∞ , LA is a keto acid (carboxylic acid + ketone). There are one C=O group and one –COOH group in LA, which are strong enough to induce high dipole moment for the –OH site for enhanced HB interaction with the nitrogen compounds. However, LA has 5 carbon atoms and three of them are –CH groups. Diesel compound has relatively more favourable interaction with compounds with longer carbon chain and thus the diesel compound has smaller values of γ^∞ in ChCl/LA DES compared to other DESs where the HBDs have shorter carbon chain length. Similarly, ChCl/PPA also reports high value of C^∞ for both basic and non-basic compounds but low values of S^∞ . Same explanation on the HB interaction strength due to the presence of –COOH group can be used and the presence of a phenyl group in the PPA molecule adds up the total carbon number to 8, making ChCl/PPA having a good interaction with diesel compounds which contributes to the low value of S^∞ .

ChCl-based DESs with sugar alcohols as HBD (DI, DS and Xy) do not have a good value of S^∞ and C^∞ as the hydrogen bonding formed with the –OH groups attached to the sugar alcohol is not as strong as those formed with the –OH groups attached to the other HBDs in different functional groups (e.g. carboxylic acids, amides, short-chained alcohols and keto acid). Meanwhile, it was observed that ChCl/Ur has high values of both S^∞ and C^∞ towards the nitrogen compounds. This is because, looking at the structure of urea, urea has many sites for HB interaction with both basic and non-basic compounds. There are two –NH₂ groups in urea which can both act as HB acceptor and donor due to the presence of a lone pair of electrons at the N atoms. Urea also has only one carbon atom, which makes the interaction with diesel compounds unfavourable. Thus, ChCl combined with urea can form strong and large number of HB interaction, while at the same time not having favourable interaction with the diesel compounds. This is ideal if the objective is to select a DES which can extract nitrogen compounds easily (high selectivity) and have large solute-carrying capacity (high capacity).

For DESs based on tetraalkyl salts, the DESs were compared with constant cation, anion and molar ratio. Comparison among the DESs with tetramethylammonium chloride (TMAC) salt combined with the HBDs glycerol (Gly), ethylene glycol (EG), phenylacetic acid (PA), malonic acid (MA), tetraethylene glycol (TEG), caproic acid (CA) and acetic acid (AA) at molar ratio 1:2 will be discussed in this section. From Figure 4.13 b) the highest value of S^∞ is reported when TMAC was combined with MA, followed by TMAC combined with Gly \geq EG>AA \geq PA>TEG>CA. In terms of capacity, Figure 4.14 b) shows that DESs combined with AA reports the highest value of C^∞ followed by DESs combined with CA>PA>TEG>EG>Gly>MA for neutral compounds. For basic compounds, the values of S^∞ follows the order of DESs combined with AA>CA>PA>TEG>EG>MA>Gly.

There is only a slight difference in the order for the last two HBDs (MA and Gly). Although in this section only TMAC-based DESs are discussed for the sake of simplicity, it should be noted that the same trend was observed for other tetraalkyl-salt-based DESs, i.e. DESs based on TMAB, TBAB, TMPC, TMPB, TBPC and TBPB. Further information on the specific numerical values of the S^∞ and C^∞ for each DES can be referred to in Appendix A.

As explained in the discussion regarding ChCl-based DESs, it was observed that the same trend is also exhibited by the tetraalkyl salt-based DESs. DESs which give high values of S^∞ report low values of C^∞ . TMAC and TBAC-based DESs combined with MA, Gly or EG give high values of S^∞ but low values of C^∞ for both basic and non-basic compounds. On the other hand, DESs with AA, CA or PA give high values of C^∞ and low values of S^∞ . DES with TEG sits somewhere in the middle but compared to EG. DES with TEG gives lower S^∞ and higher C^∞ . MA, Gly and EG, as previously discussed with regards to ChCl-based DESs, have 2 or 3 –OH groups in the molecule which enable more interactions with nitrogen compounds and can thus extract them more easily, yielding to

higher values of selectivity. Meanwhile, HBDs with carboxylic acid functional groups (AA, PA and CA) give higher values of C^∞ for the same previous reason with ChCl-based DESs (i.e. enhanced dipole strength due to $-\text{COOH}$ group enabling stronger HB interaction with aromatic nitrogen compounds). Among these three carboxylic acids, the order of S^∞ is $\text{AA} > \text{PA} > \text{CA}$; while the order of C^∞ is $\text{AA} > \text{CA} > \text{PA}$ for nitrogen compounds in all tetraalkyl-salt-based DESs. Overall, tetraalkyl salt-based DESs with AA as the HBD have highest value of S^∞ and C^∞ . This is because in acetic acid, there is a $-\text{COOH}$ group enhancing the HB interaction while at the same time acetic acid has relatively unfavourable interaction with diesel compounds, unlike its phenyl derivative (PA) and caproic acid (CA). Between PA and CA, CA has a higher capacity for aromatic nitrogen compound but it also has a more favourable interaction with diesel compounds due to the longer alkyl chain compared to the aromatic phenyl ring present in PA. It should also be noted that particularly for pyridine, DESs with PA have higher values of C^∞ due to the similarity between the 6-membered pyridine ring and the phenyl ring.

On the other hand, there is no explicit trend observed in the values of performance index (PI) of the DESs on the effect of HBD choice. Similar to the observation in the previous sections, DESs with high values of S^∞ tend to have high values of PI too.

Overall, it can be deduced that DESs with HBDs from alcohol (ethylene glycol, glycerol) and amide functional group (urea, trifluoroacetamide) will have high values of S^∞ but with low values of C^∞ . The only exception is ChCl/Urea which reports high values both in S^∞ and C^∞ . DESs with HBDs from carboxylic acid functional group (acetic acid, phenylpropanoic acid, phenylacetic acid, caproic acid, levulinic acid) generally have high values of C^∞ but low values of S^∞ . DESs with sugar alcohols as *D*-sorbitol, xylitol or *D*-isosorbide HBDs probably will not give good values of both S^∞ and C^∞ . The ability to establish strong network of hydrogen bonding and interaction with the diesel compounds are the main contributing factor towards the values of S^∞ and C^∞ for nitrogen compounds.

Effect of salt:HBD molar ratio

In this section, the effect of salt:HBD molar ratio will be discussed by comparing the DESs of the same cation, anion and HBD. The DESs examined in this section are methyltriphenylphosphonium bromide (MTPPB) combined with glycerol (Gly), ethylene glycol (EG) or triethylene glycol (TrEG) at molar ratios between 1:2 and 1:5.

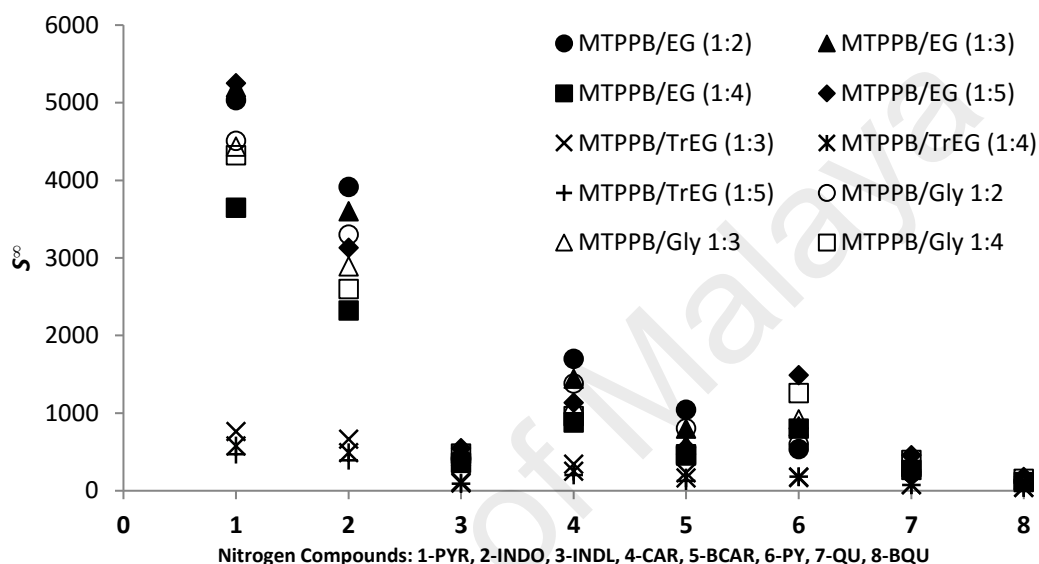


Figure 4.15: Selectivity at infinite dilution in comparison of salt:HBD molar ratio.

Figure 4.15 shows the values of S^∞ for nitrogen compounds by the DESs with varied molar ratio. In general, for non-basic compounds, DESs with lower salt:HBD molar ratio give higher values of S^∞ than those with higher salt:HBD molar ratio. For example, the order of S^∞ towards pyrrole for the DES MTPPB/Gly is highest at molar ratio 1:2 (4509), followed by molar ratios 1:3 (4434) and 1:4 (4324). This trend is also true for the DES MTPPB/TrEG where it follows the same order for the values of S^∞ towards pyrrole. However, there is no clear trend for the DESs MTPPB/EG at different molar ratios, although it can be mentioned that among the four molar ratios (1:2, 1:3, 1:4 and 1:5), DESs with molar ratios 1:2, 1:3 and 1:5 give good values of S^∞ while the DES at 1:4 molar ratio reports the lowest value of S^∞ . An exception for this trend is indoline,

where it exhibits a trend similar to the basic compounds instead. On the other hand, for basic compounds, DESs with higher salt:HBD molar ratio give higher values of S^∞ . However, the difference is very small especially for the DES MTPPB/TrEG where varying the molar ratio does not have a significant effect towards the values of S^∞ , especially for multi-aromatic basic nitrogen compounds (i.e. quinoline and benzoquinoline).

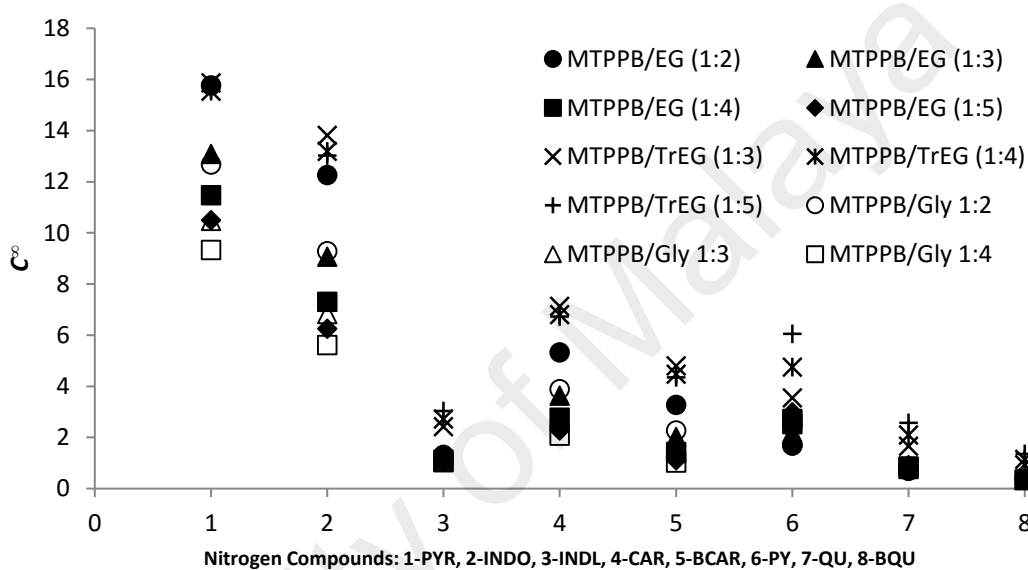


Figure 4.16: Capacity at infinite dilution in comparison of salt:HBD molar ratio.

Similarly in terms of capacity at infinite dilution, C^∞ , as presented in Figure 4.16 for neutral compounds, the DESs with lower molar ratios report higher values of C^∞ for all DESs and all non-basic compounds. Insignificant effect of changing the molar ratio is observed for DES MTPPB/TrEG where the values of S^∞ are very close for all the nitrogen compounds. For basic compounds, DESs with higher molar ratios report higher values of C^∞ . Similarly for selectivity, the values of C^∞ for quinoline and benzoquinoline are at plateau for DESs at different molar ratio.

In summary, increasing the salt:HBD molar ratio will lower the values of S^∞ and C^∞ for neutral compounds whereas for basic compounds, the increase in molar ratio will lead to higher values of S^∞ and C^∞ . This indicates that for neutral compounds, there is less favourable interaction when there is more HBD in the DES as the value of γ^∞ increases with increasing HBD ratio.

This is in concurrence with the nature of non-basic compounds which have better affinity towards hydrogen bond acceptor than with hydrogen bond donor due to their weak HBD ability. Meanwhile for basic compounds, there is more favourable interaction when there are more HBDs and this is reflected in the decreasing values of γ^∞ of basic compounds in the DES with higher ratios of HBDs. Moreover, as discussed beforehand, basic compounds are hydrogen bond acceptors and have better affinity for HBDs than neutral compounds due to the presence of $-\text{NH}$ group in their structure. Thus, having more HBDs will strengthen the hydrogen bond interaction with the DESs which subsequently gives higher values of S^∞ and C^∞ .

However from the observed trend, it should be noted that the salt:HBD molar ratio does not have a significant effect towards the values of S^∞ and C^∞ . Furthermore, although some increase or decrease is observed in the values of S^∞ and C^∞ when the molar ratio is varied, the change is not substantial in impacting the operating or capital cost when using such DESs as solvent for extractive denitrogenation. The same observation follows for the performance index values due to the insignificant effect of the salt:HBD molar ratio on both S^∞ and C^∞ values.

Table 4.2 summarizes the discussion on each factor affecting the values of S^∞ and C^∞ when selecting appropriate combination of DES constituent for extractive denitrogenation process.

Table 4.2: Summary of the factors affecting the values of S^∞ and C^∞ for denitrogenation using DESs

Factor	Effect on S^∞	Effect on C^∞
Heterocyclic structure of nitrogen compounds	Higher values of S^∞ and C^∞ for non-basic nitrogen compounds Due to increase H-bonding of halide anion and –NH atoms by non-basic compounds versus weakening of H-bonding between halide anion and HBD caused by basic compounds	
Cation choice	choline-based cations>TMA>PhA>TMP>PhP>TBP>TBA	TBP>TBA>TMP>TMA>PhP>PhA>choline-based cations
Halide anion choice	Cl>Br for non basic Br>Cl for basic	Cl>Br for non basic Br>Cl for basic
HBD choice	Functional group of HBD affects selectivity and capacity: HBDs from alcohol groups: high S^∞ , low C^∞ HBDs from carboxylic acid groups: high C^∞ , low S^∞ HBDs from sugar alcohols: low S^∞ and C^∞	
Salt:HBD molar ratio	For non-basic compounds, increasing ratios lead to lower S^∞ and C^∞ For basic compounds, higher S^∞ and C^∞ were obtained with increasing ratios	

4.2 Quantum Chemical Calculation Results

In any system of interacting molecules with ILs, the naturally existing molecular interactions include orbital interactions (with most likely interaction being between the highest occupied molecular orbitals or HOMO and the lowest unoccupied molecular orbitals or LUMO), charge-charge interactions, hydrogen bonding interaction with neutral molecules, interaction between heteroatom and hydrogen atoms of ILs and van der Waals forces between alkyl groups. These fundamental interactions are manifested at macro level in terms of CH- π interaction, π - π interaction and heteroatom- π interaction. In general, the interactions between heterocyclic nitrogen compounds with ILs occur through both the cation and anion. The interaction between heterocyclic nitrogen compound with cation is through CH (cation)- π (heterocyclic nitrogen compound) interaction while for heterocyclic nitrogen compound and anion, the interaction is mainly through hydrogen bonding between the hydrogen bonded to nitrogen heteroatom, and the anion heteroatom. At quantum level, the interactions between ILs and heterocyclic nitrogen compounds depend on π - π interaction, CH- π interaction and hydrogen bond interaction. These can be studied at electronic level based on information of their frontier orbital energy values and global scalar properties. In this section, the calculation results and their interpretation in identifying ILs for use in extractive denitrogenation of liquid fuels is discussed.

4.2.1 Orbital energy values

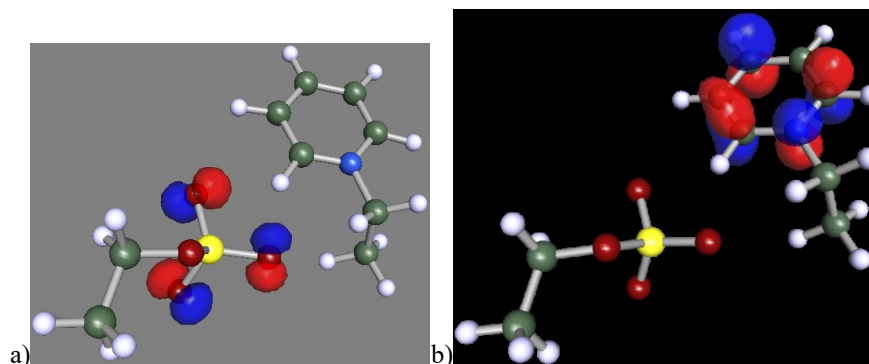


Figure 4.17: HOMO and LUMO of [EPY][EtSO₄]. a) HOMO, b) LUMO.

Figure 4.17 shows the optimized structure of [EPY][EtSO₄] IL. It is observed that the HOMO comes from the anion heteroatoms (oxygen atoms) while the LUMO comes from the cations. This is consistent with findings from Nishi et al. and Lu et al. who have reported that the HOMO and LUMO of ILs come from anion and cation, respectively (Nishi et al., 2008) (Lü, et al., 2013). For ILs with aromatic cations, the LUMO comes from the N₁-C₂-N₃ atoms in the aromatic ring, while for ILs with saturated cations, the LUMO are spread over the ring face and alkyl chain of the cations. Although the electrostatic (Coulombic) interaction is the dominant interaction in ILs, there also exist hydrogen bonds between oxygen atoms of the anion and the C-H of cation ring and C-H of cation alkyl chain as observed in the optimized structure.

On the other hand, for the optimized structure of complexes with ILs and heterocyclic nitrogen compounds, the most common observation is that HOMO comes from heterocyclic nitrogen compounds with the LUMO from cations, as shown by the optimized structure of pyrrole complex with [EPY][EtSO₄] IL in Figure 4.18.

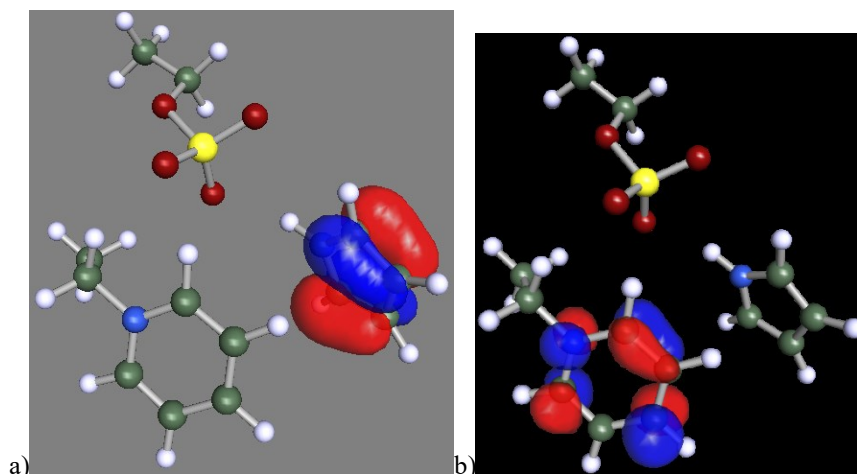
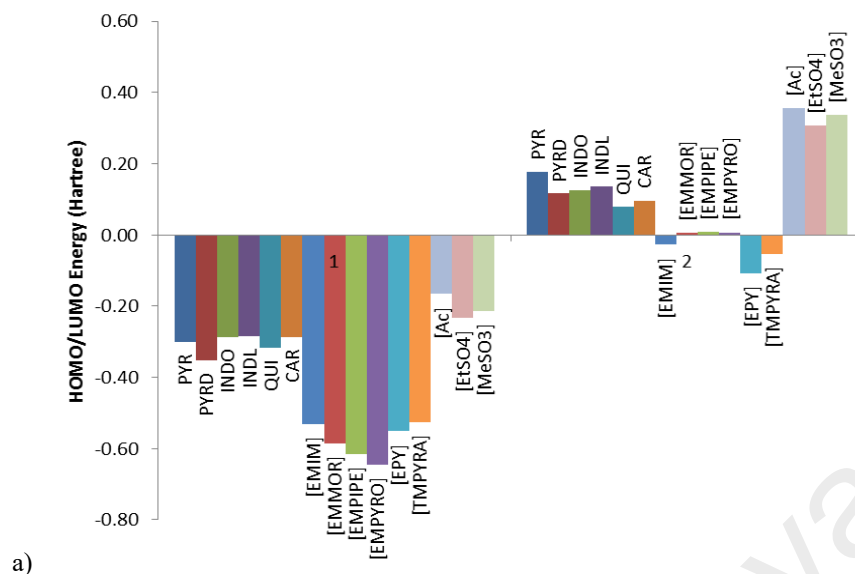


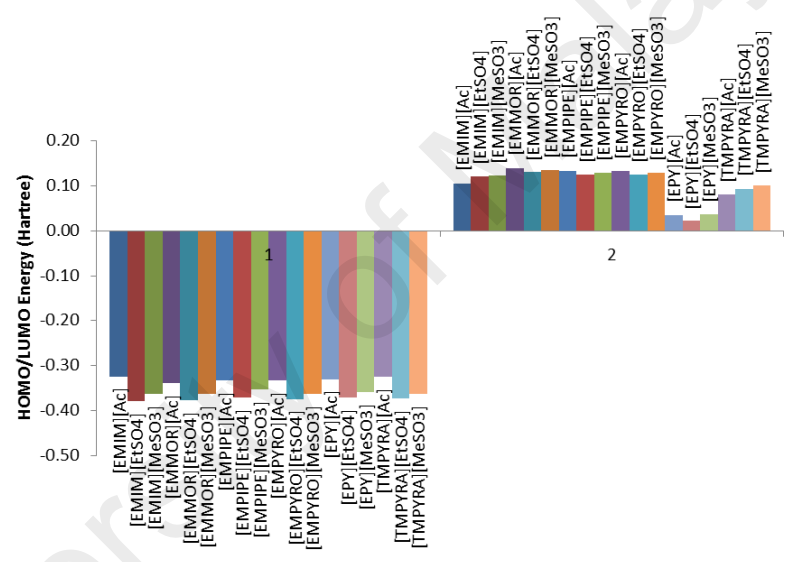
Figure 4.18: HOMO and LUMO location of PYR-[EPY][EtSO₄] complex. a) HOMO, b) LUMO.

In some structures containing pyridine, HOMO comes from the anion while the LUMO comes from heterocyclic nitrogen compound. In complexes of PYR-[EPY][Ac], PY-[EMIM][Ac], PY-[EPY][EtSO₄], PY-[EPY][MeSO₃] and PY-[TMPYRA][Ac], the HOMO comes from anion while the LUMO from cation, which indicates strong interaction between the ion pairs of ILs and less interaction with the heterocyclic nitrogen compound. There are also cases where both the HOMO and LUMO comes from heterocyclic nitrogen compounds which indicates weak orbital interaction between the nitrogen compounds with ILs as manifested by complexes of QU and CAR with ILs with saturated cations. However, in complexes of QU and CAR combined with aromatic-cation-based ILs, HOMO comes from either QU, CAR, or anion, while LUMO comes from either the cation, QU or CAR. This indicates weak interaction between the IL and the nitrogen compounds.

The calculated orbital energy values for HOMO and LUMO of individual species, ILs and complexes of IL-PYR and IL-PY are presented in Figure 4.19 a) – d).



a)



b)

Figure 4.19: HOMO and LUMO energy values for individual species (a), ionic liquids (b) and its complexes with PYR (c) and PY (d)

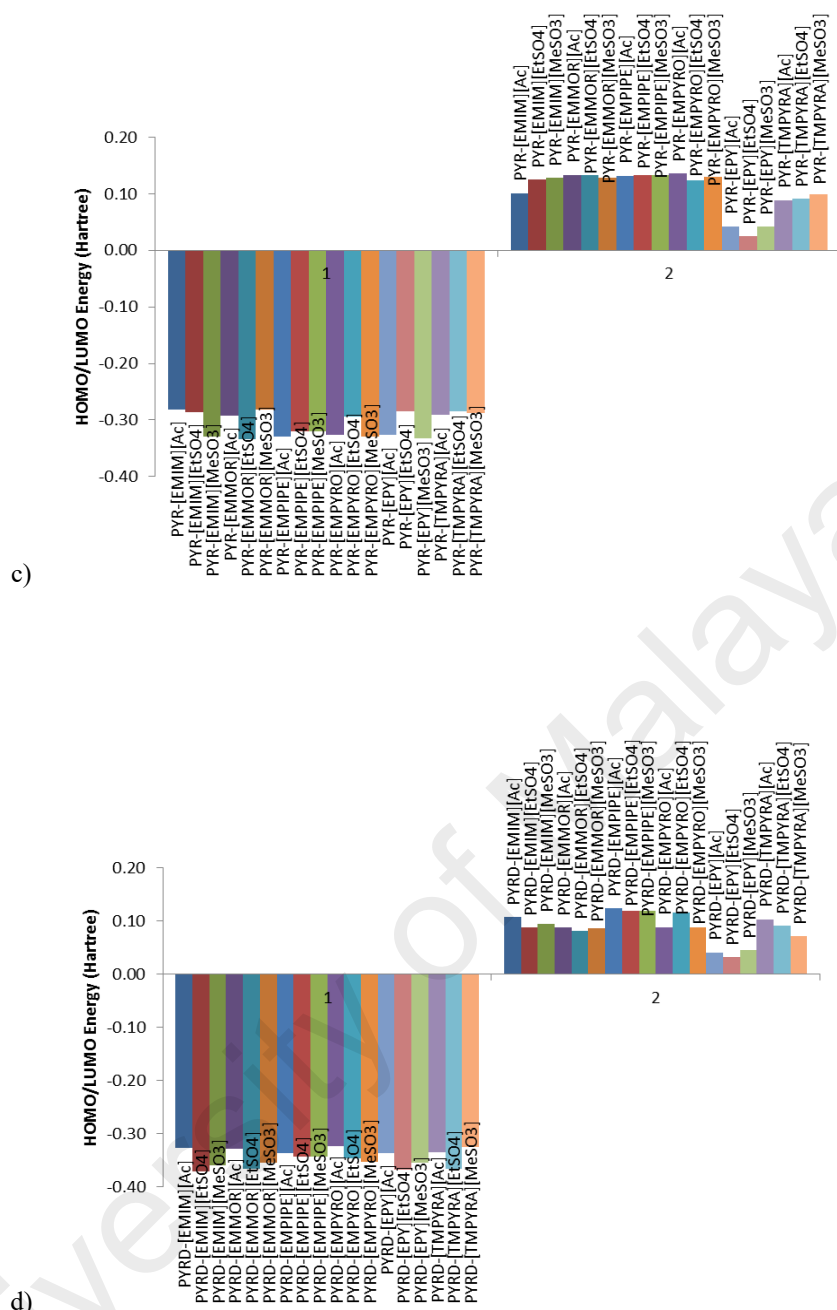


Figure 4.19, continued.

Results for complexes with INDO, INDL, QU and CAR are shown in Appendix C.. As mentioned in previous section, HOMO and LUMO are the most likely locations for interaction between two species. In the case of ILs, external connection will occur through the cation and anion. The external connection will be made by electrons in the HOMO having the highest energy and therefore able to make external interaction with the heterocyclic nitrogen compounds. Incoming electrons from other molecules will most likely fill into the LUMO and therefore form a bond in this orbital. From Figure 4.19 a),

the HOMO and LUMO energy values for each heterocyclic nitrogen compounds, cations and anions are presented. There is little difference in the values of HOMO and LUMO energies for heterocyclic nitrogen compounds. It is observed that basic nitrogen compounds (PY and QU) have more negative HOMO energy values compared to the non-basic nitrogen compounds. This means that basic nitrogen compounds have higher ionization potential and have better capability to donate electron than non-basic nitrogen compounds. The LUMO energy values decreases with the order $\text{PYR} > \text{INDL} > \text{INDO} > \text{PY} > \text{CAR} > \text{QU}$. The electron affinity of heterocyclic nitrogen compounds also follows this order since it is directly related to LUMO energy values. All nitrogen compounds have more HOMO than LUMO energy, which makes them more of electron donors than acceptors.

As for the cations, those with aromatic ring ([EMIM], [EPY], [TMPYRA]) have a lesser negative HOMO energy values compared to those without aromatic ring ([EMMOR], [EMPIPE], [EMPYRO]). Similar to the heterocyclic nitrogen compounds, all cations have more HOMO energy. Approximation of ionization potential with the HOMO energy value means that a high HOMO energy indicates higher amount of energy required to remove an electron from a ligand. Cations have high ionization potential since they have already released an electron. On the other hand, cations have small LUMO energy values, with aromatic cations having negative LUMO energy values (-0.02742, -0.10715, and -0.05434 for [EMIM], [EPY] and [TMPYRA], respectively) and saturated cations having slightly positive LUMO energy values (0.00647, 0.00752, and 0.00636 Hartrees for [EMMOR], [EMPIPE] and [EMPYRO], respectively). Electron affinity is approximated with the LUMO energy values, and a more positive value of electron affinity is indicative of electron acceptor. Higher LUMO energy values means more energy is released when an electron is accepted by a ligand and thus better electron affinity. In contrast to the cations, anions have more LUMO energy than HOMO energy.

The most stable anion is [EtSO₄] as it has the highest negative HOMO energy value, which indicates higher energy required to release an electron. [EtSO₄] also has the lowest LUMO energy value, which means the minimum electron affinity among the other two anions.

Figure 4.19 b) shows orbital energy values for IL complexes. In terms of its orbital energy values, [Ac]-based ILs have lower HOMO energy values followed by [MeSO₃]- and [EtSO₄]-based ILs, while [EPY]- and [TMPYRA]-based ILs have lower LUMO energy values, with [EPY][EtSO₄] having the lowest LUMO energy values amongst all ILs. [Ac]-based IL has the highest ionization potential with its lower HOMO energy values. While HOMO energy values and thus the ionization potential is influenced by the choice of anion, the choice of cation seems to have more influence in the LUMO energy values of ILs and hence their electron affinity. Since [EPY]- and [TMPYRA]-based ILs have small LUMO energy values, they have the least electron affinity among all ILs. It was observed that ILs with saturated cations ([EMMOR], [EMPIPE], [EMPYRO]) have better electron affinity than those with aromatic cations. This is probably due to the fact that saturated cations have localized charge on the nitrogen atoms of the saturated rings, which poses stronger electrostatic strength compared to delocalized charge in the aromatic rings in aromatic cations (Fernandes et al., 2011).

In complexes where the HOMO comes from nitrogen compounds and LUMO comes from the cations, the interaction between nitrogen compounds and ILs is through electron donation from the HOMO (i.e. the heterocyclic nitrogen compounds) to the LUMO (i.e. the cations) to form CH- π bond between them. However, in complexes where the HOMO comes from the anion and LUMO from the heterocyclic nitrogen compound, the interaction between nitrogen compounds and ILs is dominated by the hydrogen bonding between the anion heteroatom and the π face of the nitrogen compounds. Therefore, in complexes formed between ILs and heterocyclic nitrogen compounds, the

LUMO energies are more significant since the LUMO sites lead to the overlapping of the incoming HOMO orbitals. In determining favorable interaction between ILs and the heterocyclic nitrogen compounds based on the orbital energies, it is desirable to have the LUMO energies of the complexes in higher negative values. Figures 4.19 c) and d) show orbital energy values for IL-PYR and IL-PY complexes.

Based on these criteria, the most favorable ILs for removal of each heterocyclic nitrogen compound were identified and listed in Table 4.3. As can be seen, [EPY][EtSO₄] has the most favorable interaction with most of heterocyclic nitrogen compounds showing the smallest LUMO energy value in most of the complexes.

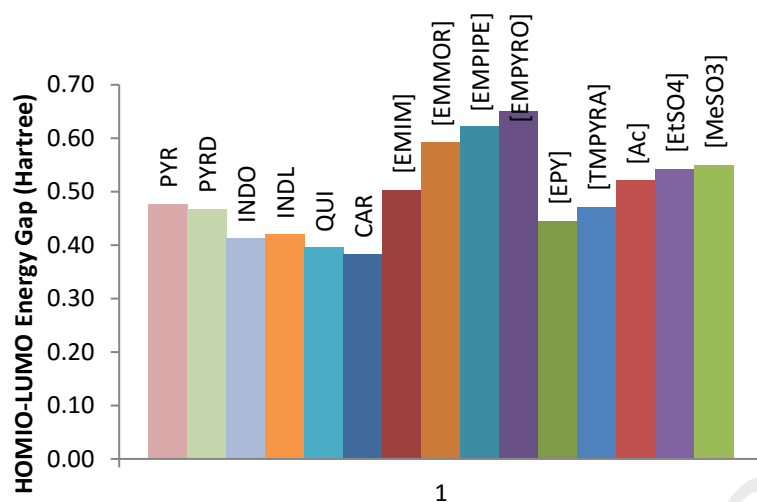
Table 4.3: The most favourable IL for each heterocyclic nitrogen compound according to different parameters

Nitrogen compound	The most favourable IL according to each parameter					
	LUMO Energy (lowest)	HOMO-LUMO Energy gap (smallest)	Global Softness (highest)	Electrophilicity Index (highest)	Interaction Energy (most negative value)	Charge Transfer (largest charge difference)
PYR	[EPY][EtSO ₄]	[EPY][EtSO ₄]	[EPY][EtSO ₄]	[EPY][MeSO ₃]	[TMPYRA][Ac]	[TMPYRA][Ac]
PY	[EPY][EtSO ₄]	[EPY][Ac]	[EPY][Ac]	[EPY][EtSO ₄]	[TMPYRA][Ac]	[EMMOR][MeSO ₃]
INDO	[EPY][Ac]	[EPY][Ac]	[EPY][Ac]	[EPY][Ac]	[TMPYRA][Ac]	[TMPYRA][Ac]
INDL	[EPY][EtSO ₄]	[EPY][EtSO ₄]	[EPY][EtSO ₄]	[EPY][EtSO ₄]	[EMPIPE][EtSO ₄]	[TMPYRA][Ac]
QU	[EPY][EtSO ₄]	[EPY][EtSO ₄]	[EPY][EtSO ₄]	[EPY][EtSO ₄]	[EMPIPE][MeSO ₃]	[TMPYRA][Ac]
CAR	[EPY][EtSO ₄]	[EPY][EtSO ₄]	[EPY][EtSO ₄]	[EPY][MeSO ₃]	[TMPYRA][Ac]	[EPY][Ac]
Overall	[EPY][EtSO ₄]	[EPY][EtSO ₄]	[EPY][EtSO ₄]	[EPY][EtSO ₄]	[TMPYRA][Ac]	[TMPYRA][Ac]

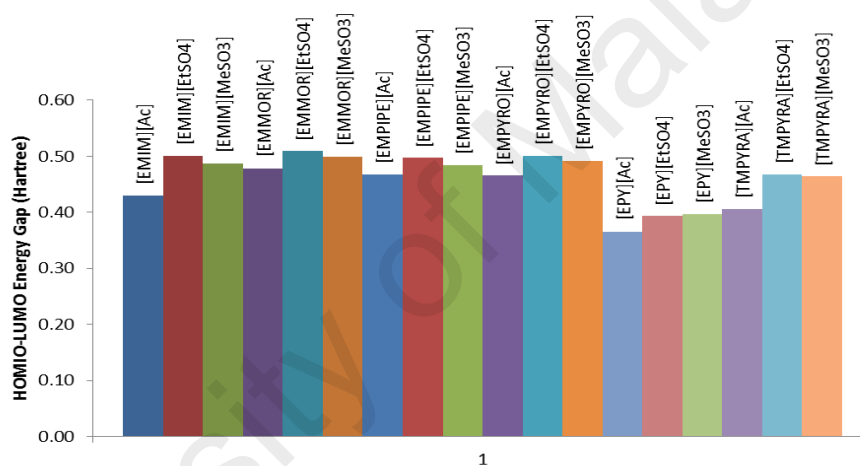
4.2.2 Orbital Energy Gap

The difference in the frontier orbital energy values (the HOMO-LUMO gap) corresponds to the lowest excitation energy. According to Fukui et al., the gap between HOMO and LUMO energy values indicates the electrical transport properties including electron carrier and mobility (Fukui, 1982). For individual species, the HOMO-LUMO gap indicates the stability of the species through the lowest electronic excitation energy, whereas for pairs of molecules (such as IL complexes), the HOMO-LUMO gap indicates the reactivity between the species involved through thermochemical electronic hopping energy amongst themselves (Martínez-Magadán et al., 2012). The HOMO-LUMO gap for individual species, ILs and their complexes with PYR and PY are presented in Figure 4.20 a) – d). Results for complexes with INDO, INDL, QU and CAR are shown in Appendix C.

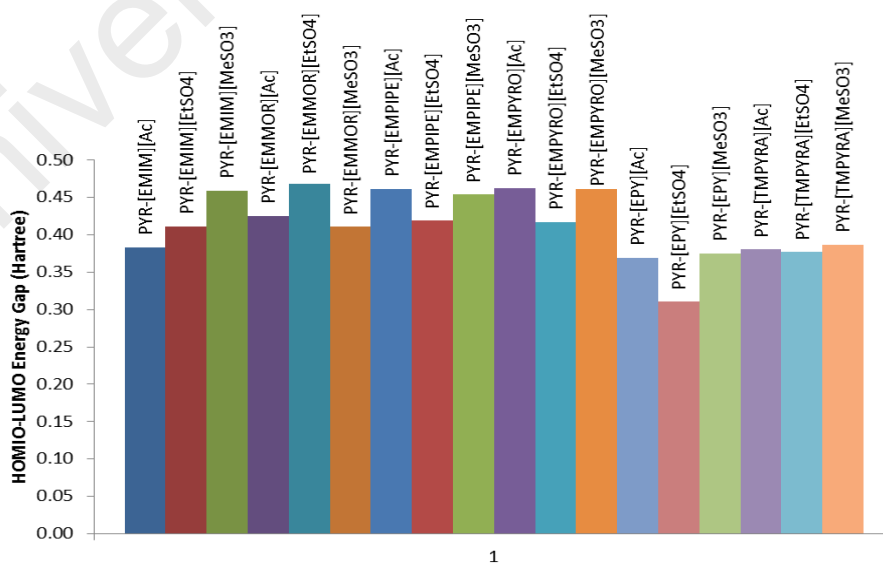
From Figure 4.20 a), the HOMO-LUMO gap for heterocyclic nitrogen compounds are of almost similar values, with PYR having the largest HOMO-LUMO gap. Cations with aromatic ring ([EMIM], [EPY], [TMPYRA]) have smaller HOMO-LUMO gap compared to cations without aromatic ring ([EMMOR], [EMPIPE], [EMPYRO]). Amongst the anions, [Ac] has the smallest gap, while [EtSO₄] and [MeSO₃] have almost similar HOMO-LUMO gap. In IL complexes as shown in Figure 4 b), the HOMO-LUMO energy gap for ILs complexes are lower than those of individual cations and anions. When combined together, the LUMO of the anions are lowered by the HOMO of the cations and thus resulting to smaller energy gaps. The energy gap between HOMO and LUMO of the ILs reports [EPY]- and [TMPYRA]-based ILs having the smallest gaps. Small HOMO-LUMO energy gap is indicative of soft molecules, which leads to better polarizability and reactivity.



a)



b)



c)

Figure 4.20: HOMO-LUMO Energy Gap for individual species (a), ionic liquids (b) and its complexes with PYR (c) and PY (d)

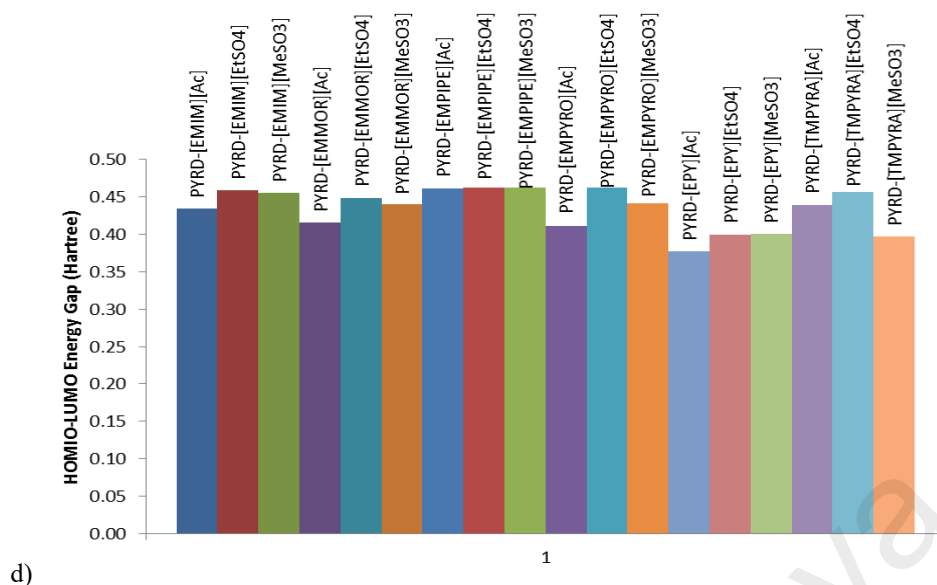


Figure 4.20, continued.

However, when investigating the interaction between ILs and other compounds, it is more important to observe the behavior of their complexes rather than evaluating them individually. The HOMO-LUMO gap of ILs can be compared with HOMO-LUMO gap of their complexes with nitrogen compounds to see if there is increase or decrease in the gap before and after IL addition. A decrease in HOMO energy value with an increase in LUMO energy value will lead to increase in HOMO-LUMO gap, whilst an increase in HOMO energy value with a decrease in LUMO energy value will lead to a decrease HOMO-LUMO gap (Wagle, et al., 2013). Figures 4.20 c) – d) present HOMO-LUMO gaps for IL complexes with PYR and PY. In general, there is increase in HOMO energy values combined with decrease in LUMO energy values, which resulted in the HOMO-LUMO gaps to be even smaller than those of neat IL complexes, which is indicative of favorable interaction between all the ILs and all the heterocyclic nitrogen compounds. This is consistent with the results obtained by Wagle et al. where the complexes of IL-polyaromatic hydrocarbons have reduced band gap compared to neat IL complexes (Wagle, et al., 2013).

It can be observed that in all of the complexes of heterocyclic nitrogen compounds with ILs, complexes with [EPY]- and [TMPYRA]-based ILs have smaller gaps compared to complexes with other ILs. Especially in complexes of ILs with quinoline and carbazole, little difference is observed in the HOMO-LUMO energy gap for all complexes with ILs, except for quinoline and carbazole complexes with [EPY]-based ILs. Having said so, when analyzing the band gap reduction between those of ILs and those of IL-heterocyclic nitrogen compound complexes, it was observed that although complexes with [EPY]-based ILs report the smallest HOMO-LUMO gap, they do not demonstrate the largest decrease in HOMO-LUMO band gap in IL before and after adsorption with nitrogen compounds. In fact, there are some cases where complexes with [EPY]-, [EMIM]- and [TMPYRA]-based ILs report slight increase in the band gap instead of reducing it. This occurs in complexes of PYR-[EPY][Ac], PY-[EMIM][Ac], PY-[EPY][MeSO₃], PY-[EPY][EtSO₄], PY-[EPY][Ac], and PY-[TMPYRA][Ac]. All other complexes show decrease in the HOMO-LUMO gap.

Although Wagle et al. explained that a larger decrease in band gap is desirable as this indicates stronger interaction between ILs and aromatic compounds, there is another perspective to look at the advantage of little decrease or slight increase in the band gap (Wagle, et al., 2013). In all of these cases with slight increase in band gap, the HOMO energy of the complex is decreased while the LUMO energy is increased. This means that the LUMO energy of the complex is not sufficiently lowered by the HOMO of the incoming electron donor by PYR and/or PY molecules, indicating there is room for potential extra lowering of LUMO energy by adding more HOMO by additional aromatic nitrogen molecules. In other words, these ILs can accommodate more nitrogen compounds than just PYR or PY alone. A small HOMO-LUMO energy gap in complexes indicates high polarizability and leads to better solubility. Based on this foundation, with regards to HOMO-LUMO gap, ILs with the most favorable interaction with heterocyclic

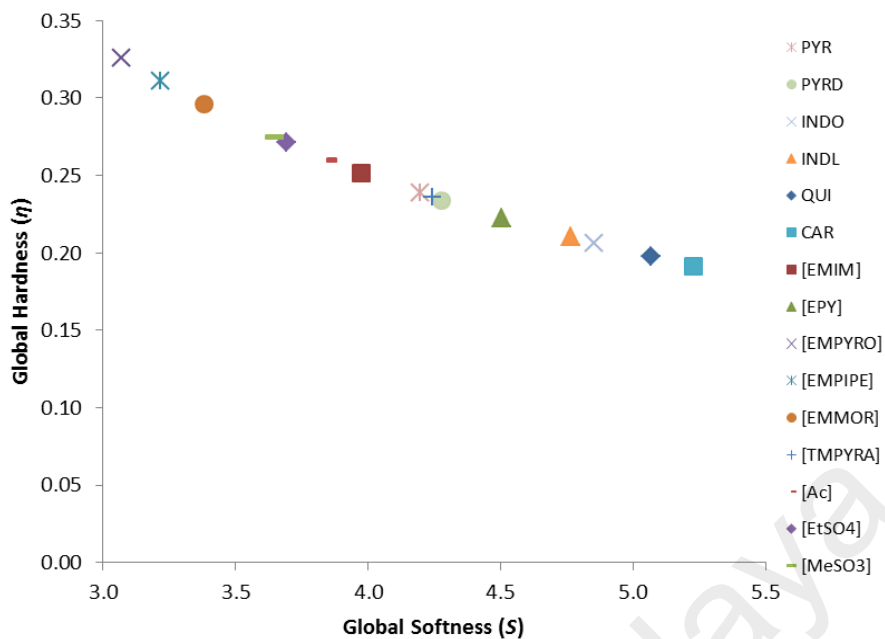
nitrogen compounds are the ones with the smallest gap and these are listed in Table 4.2. [EPY][EtSO₄] tops the ranks for most of the nitrogen compounds with smallest HOMO-LUMO energy gap in their complexes.

4.2.3 Global Scalar Properties

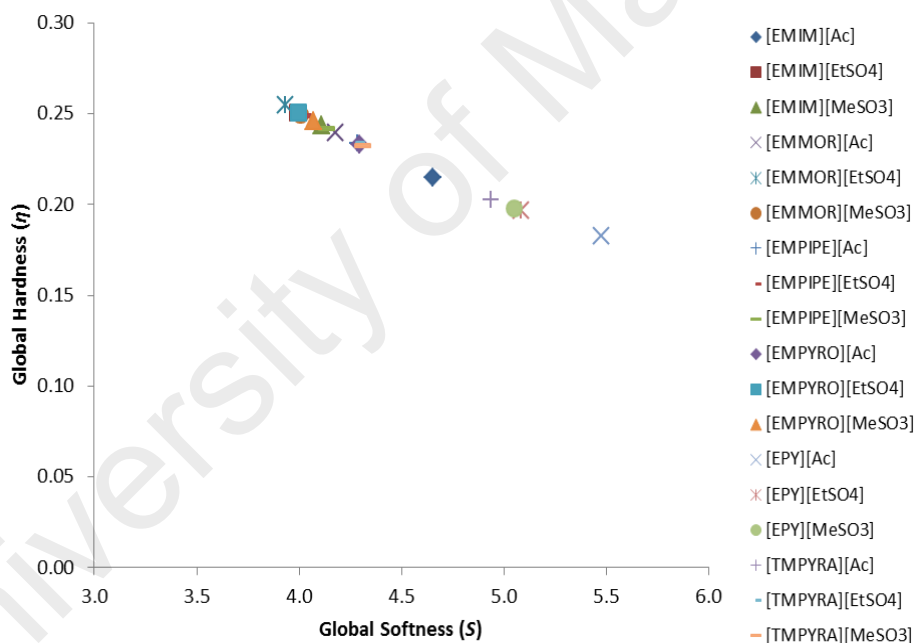
Global hardness, global softness, electronegativity and electrophilicity index are termed as global scalar properties because they characterize the complex species such as ionic liquids, and complexes of ionic liquids with heterocyclic nitrogen compounds. Hardness and softness are useful to characterize the stability and reactivity of a complex, and they are very much related to the HOMO-LUMO energy gap, as discussed in the computational details. Electronegativity and electrophilicity index are useful for measuring the extent of electron transfer within the complex.

Global Hardness and Global Softness

Figure 4.21 a) – d) presents the plot of hardness against softness of individual molecules, IL complexes and complexes of IL with PYR and PY. Results for complexes with INDO, INDL, QU and CAR are shown in Appendix C. From Figure 4.19 a), all individual species possess more softness than hardness, which means that the studied species are non-resistant to electron transfer. The heterocyclic nitrogen compounds possess softness than the cations and anions. It is observed that the global softness of IL increases with decreasing global hardness, which is expected since softness and hardness are inverse of each other by definition.

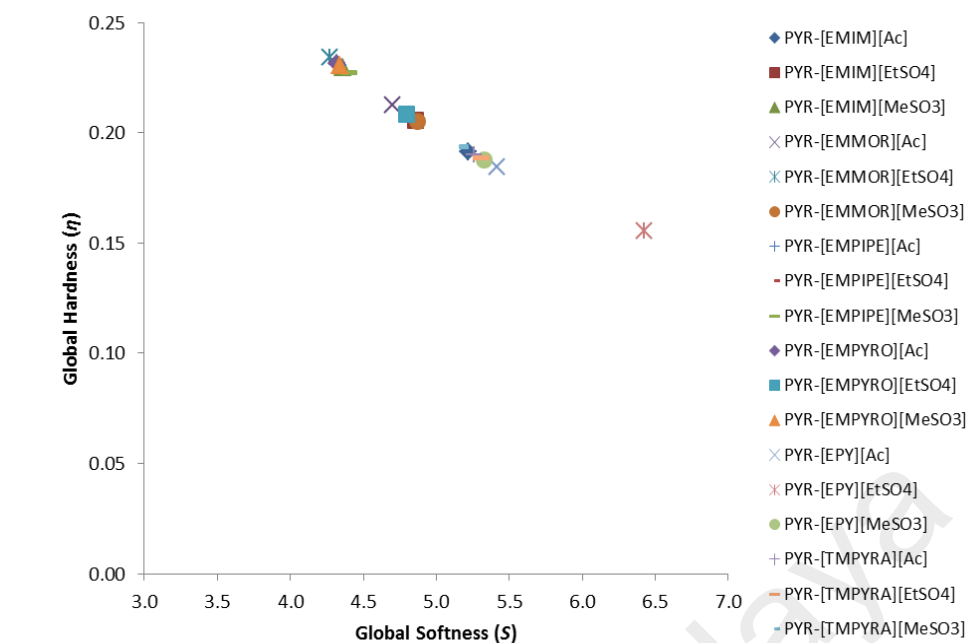


a)

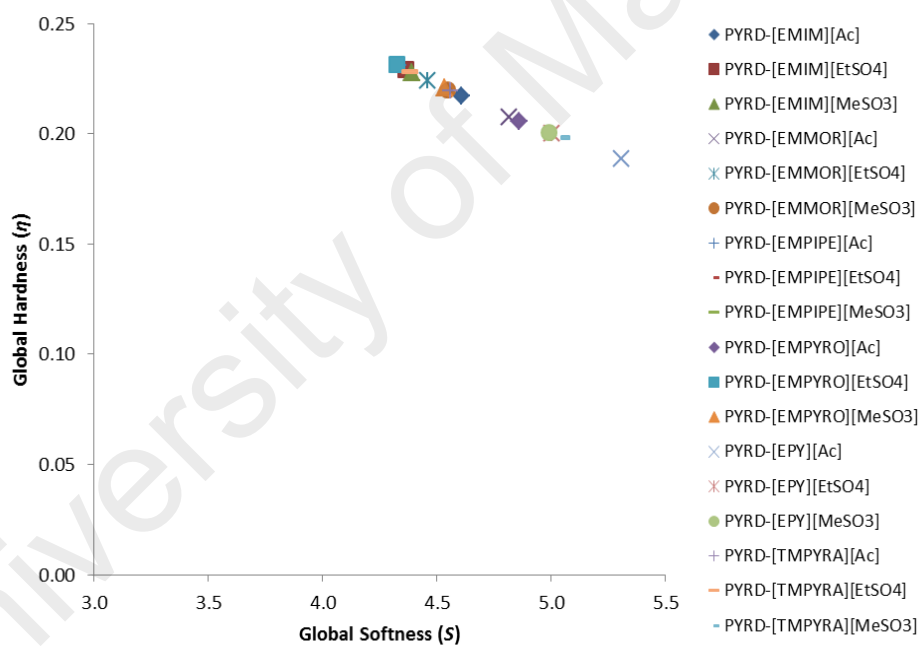


b)

Figure 4.21: Global hardness and global softness for individual species (a), ionic liquids (b) and its complexes with PYR (c) and PY (d)



c)



d)

Figure 4.21, continued.

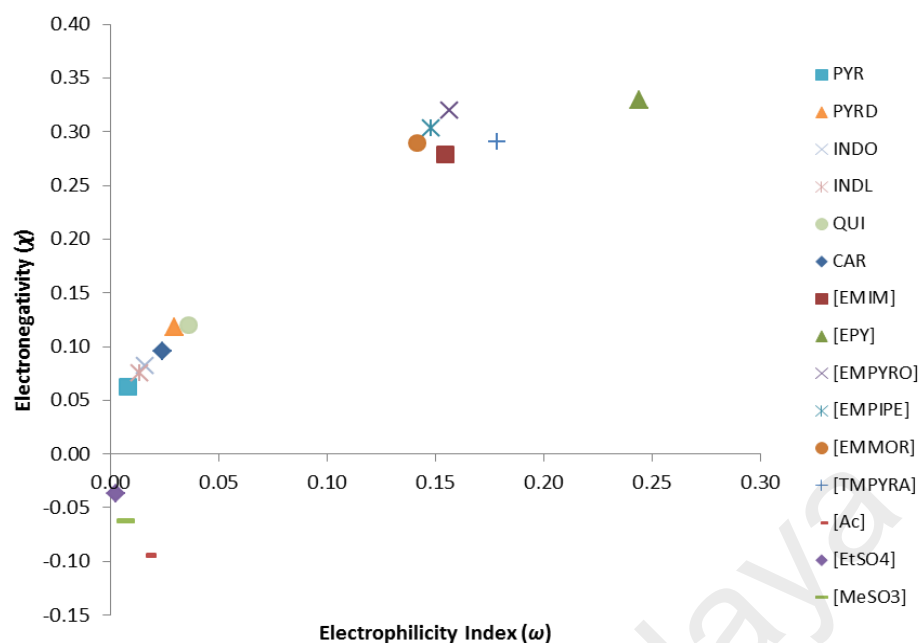
Complexes with IL and nitrogen compounds (Figure 4.21 c) – d)) also shows the same linear trend of increasing softness with decreasing hardness. Consistent with reduction in HOMO-LUMO gap between IL complexes and complexes with both IL and heterocyclic compounds, reduction in hardness and increase in softness in complexes of

IL-heterocyclic nitrogen compounds versus IL complexes are observed. Global softness and hardness of ionic liquids is presented in Figure 4.21 b), where it is observed that the hardness reduces with increasing softness. This trend is consistent with the result obtained by Anantharaj et al. where this was reasoned out by the fact that ILs are chemically less stable due to their relatively small HOMO-LUMO gap (Anantharaj, et al., 2010b). From this, compared to IL-PYR and IL-PY complexes, complexes of IL with INDO, INDL, QU and CAR have more softness and lower hardness. This indicates that the studied ILs have more affinity and better solubility for INDO, INDL, QU, and CAR, which is desired since most of the nitrogen compounds found in heavier petroleum fraction are present as heterocycles with multiple rings (Wiwel et al., 2000).

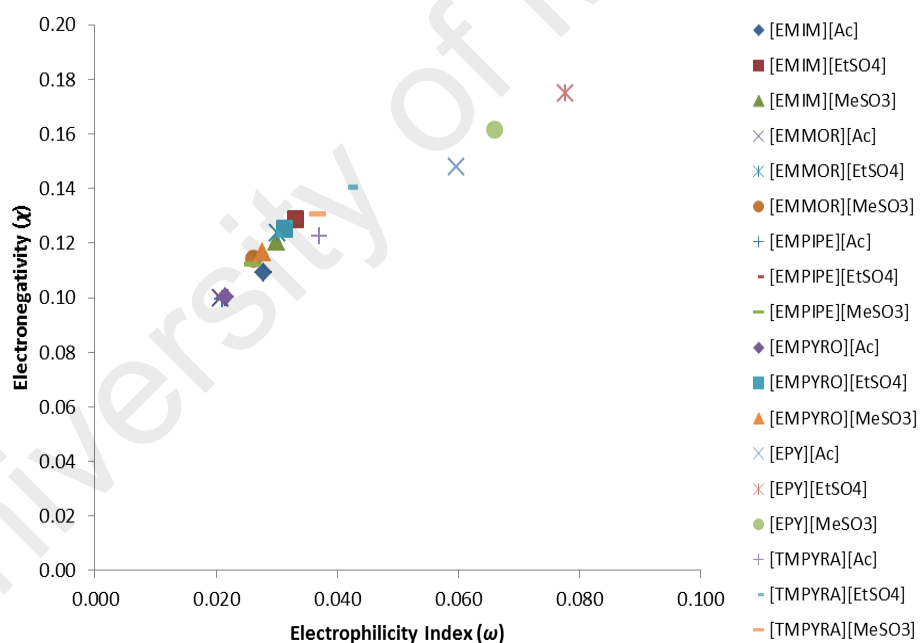
Based on the criteria of global softness, maximum softness is desirable because this can create an extended molecular interaction through hydrogen bond network or increase in π -electron density in aromatic compounds including the heterocyclic nitrogen compounds in this work. Higher softness in IL complexes with nitrogen compounds indicates high affinity and therefore better separation ability (Anantharaj, et al., 2010b). Thus, the most favorable ILs for each heterocyclic nitrogen compound are those with the highest softness and this is presented in Table 4.2. On this basis, [EPY]-based IL show better affinity towards all heterocyclic nitrogen compounds, especially [EPY][EtSO₄].

Electronegativity & Electrophilicity Index

Figure 4.22 a) – d) shows the plot of calculated electronegativity against electrophilicity index. With the exception of anions, it is observed that electronegativity increases with increasing electrophilicity index. Cations have higher electronegativity and electrophilicity index than heterocyclic nitrogen compounds.

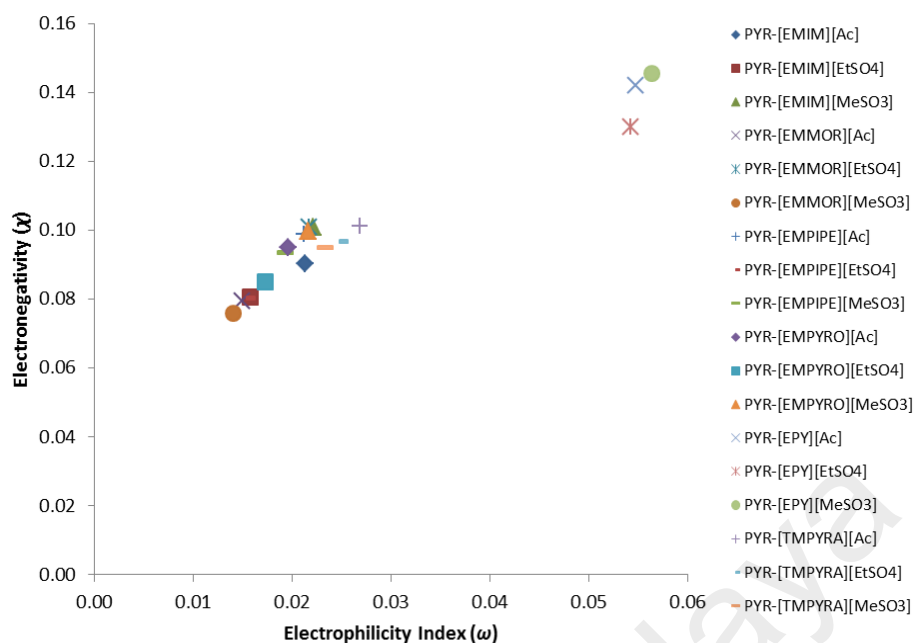


a)

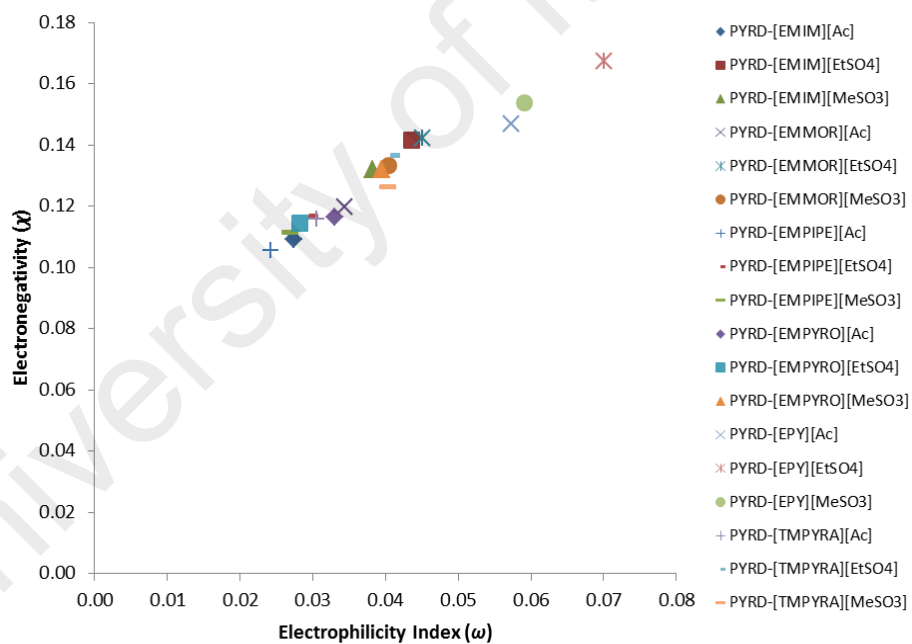


b)

Figure 4.22: Electronegativity and electrophilicity index for individual species (a), ionic liquids (b) and its complexes with PYR (c) and PY (d).



c)



d)

Figure 4.22, continued.

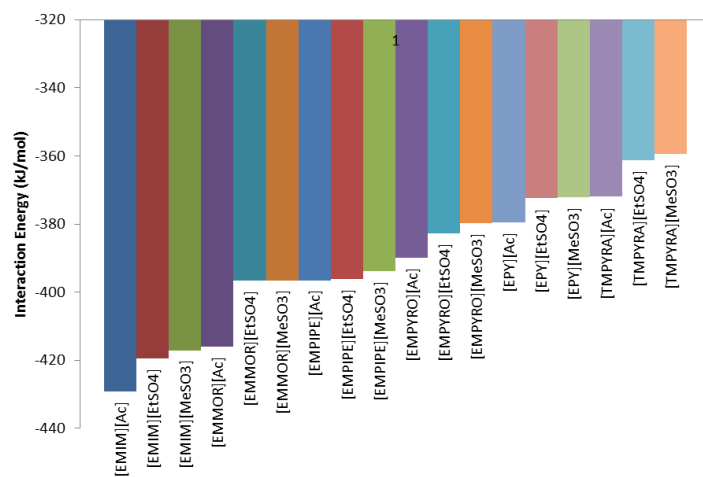
For anions, the electronegativity decreases with increasing electrophilicity index, and the values for electronegativity are negative. The ability of complexes to attract electrons to themselves is proportional to their ability to saturate itself with maximum

number of electrons. For ILs and complexes of ILs with heterocyclic nitrogen compounds, the trend is almost linear. The almost linear plot is most probably caused by strong interaction through electrophilic and nucleophilic attack (Anantharaj, et al., 2010b). Electronegativity and electrophilicity of ionic liquids are presented in Figure 4.22 b). It is observed that the ILs with aromatic cations have higher electrophilicity index and electronegativity compared to ILs with saturated cations, which means ILs with aromatic cations are more reactive in terms of attracting and saturating themselves with electrons from incoming compounds. [EPY]-based ILs report the highest electronegativity and electrophilicity index. Similar to other global properties, it is more meaningful to look at how the complexes with ILs and heterocyclic nitrogen compounds behave.

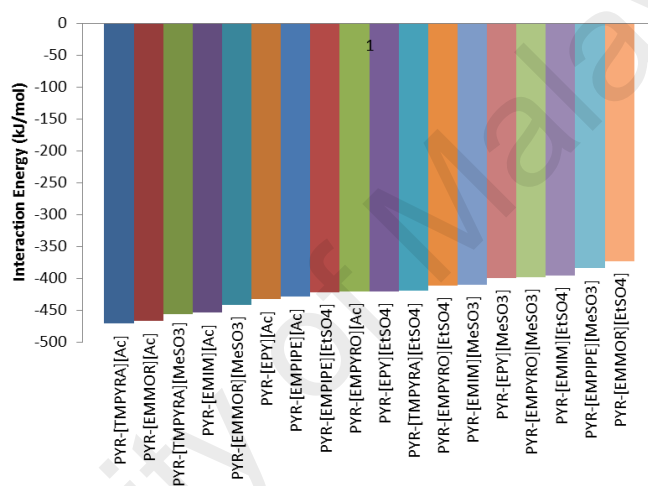
The electronegativity and electrophilicity index of complexes with IL and PYR and PY are shown in Figure 4.22 c) – d). Results for complexes with INDO, INDL, QU and CAR are shown in Appendix C. The electronegativity and electrophilicity index of IL decreases when combined with heterocyclic nitrogen compounds for all nitrogen compounds studied. The decrease in electronegativity and electrophilicity index in complexes with IL and heterocyclic nitrogen compound may be possibly due to electron transfer between the heterocyclic nitrogen compound and the cations via CH- π interaction when the HOMO of the nitrogen compounds overlap with the LUMO of cation in the IL. Based on electrophilicity index and electronegativity, it is desired to have maximum value for electrophilicity index in the complex which indicates better reactivity and ability for electron transfer. Generally, amongst all ILs, [EPY]-based ILs demonstrate higher electrophilicity index and electronegativity in all of the complexes with nitrogen compounds. High electrophilicity index even after adsorption with nitrogen compounds indicate that [EPY]-based ILs are able to accept more nitrogen compounds. The IL which reports the highest electrophilicity index in complexes with most of the nitrogen compound is presented in Table 4.2.

4.2.4 Interaction Energies

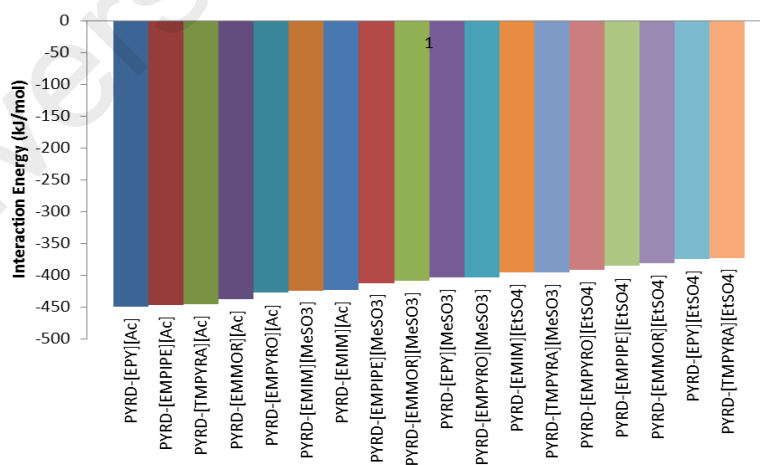
The distance between cation and anion in ionic liquids is an important consideration towards solubility of heterocyclic nitrogen compounds in the ionic liquids. Interaction energy (or binding energy) gives an indication of compactness of the ionic liquid and the distance between the ion pair. It is reported that, for ILs, the calculated interaction energy is almost inversely proportional to the distance between cation and anion, which is indicative of dominance of charge-charge interaction in ionic liquids (Tsuzuki, Tokuda, et al., 2007). Zhang et al. reported the performance of ILs 1-butyl-3-methylimidazolium tetrafluoroborate ([BMIM][BF₄]) and 1-methyl-3-methylimidazolium hexafluorophosphate ([BMIM][PF₆]) for dissolution with thiophene, where it was found that thiophene is more soluble in [BMIM][PF₆] than in [BMIM][BF₄] (Zhou, et al., 2008). Part of the explanation for this is due to the compactness of the IL, where [BMIM][PF₆] is less compact and have smaller interaction energy as compared to [BMIM][BF₄], which leads to facile restructuring of the cation and anion to accommodate thiophene molecules. Based on the calculated interaction energy of ionic liquids as presented in Figure 4.23 a) where the ILs are sorted according to its interaction energy, [EtSO₄]-based ILs report the lowest interaction energy compared to [MeSO₃]- and [Ac]-based ILs. Stronger interaction energy for the ILs is reported for [Ac]-based ILs. If cation factor is taken into account, it is observed that for each anion, ILs based on aromatic cation have smaller interaction energy than those with saturated cations.



a)



b)



c)

Figure 4.23: Interaction energies for ionic liquid complexes (a), and ionic liquid complexes with PYR (b) and PY (c).

Fernandes et al. reported that since electrostatic strength in aromatic rings is smaller than that of in saturated rings because of charge delocalization in aromatic rings as compared to localized charge on the heteroatom of the saturated rings, aromatic-based ILs present lower interaction strength values versus saturated-based ILs (Fernandes, et al., 2011). Apart from this, increase in cation size from five-membered to six-membered ring (for both aromatic and saturated cores) leads to increase in the distance between the charges and thus decrease in interaction energy (Fernandes, et al., 2011). This is why among the ILs with aromatic cations, [EPY]-based ILs have smaller interaction energy than [EMIM]- and [TMPYRA]-based ILs. The effect of anion on interaction strength is explained by Hunt et al. where ILs with small and higher symmetrical anion have low anion configurational variation and thus higher connectivity with the cations and results in relatively stronger interactions than ILs with larger and less symmetrical anion (Hunt et al., 2007). The sizes of anions in this study follow the order from smallest to largest: [Ac]<[MeSO₃]<[EtSO₄]. Therefore, ILs consisting six-membered aromatic cations combined with large anion are expected to have smaller interaction energy and may allow facile restructuring of the ion pairs to accommodate incoming molecules.

Ionic liquids interact with aromatic compounds through π - π interaction where a sandwich-like structure is formed when the aromatic solute is enclosed between the cations of the ILs (Holbrey et al., 2003). Due to higher π -electron density in sulfur-containing aromatic compounds, the interaction with ILs are stronger compared to aromatic compounds without heteroatom (Gao et al., 2008). This is also true for nitrogen-containing aromatic compounds. As a result, ILs report higher capacity for sulfur- and nitrogen-containing compounds compared to ordinary aromatic compounds. On the other hand, poly-aromatic compounds have stronger attraction with the cation of the ILs owing to stronger quadrupole moments of poly-aromatics compared to mono-aromatics which leads to closer packing between the poly-aromatic themselves and between the poly-

aromatics with the ILs' cation, thus better extraction capacity with ILs (Gao et al., 2009; Heard et al., 1997). Apart from the π - π interaction between aromatic compounds with ILs, the heteroatom in the aromatic compound may also form hydrogen bonding with the IL cation and/or anion. Interaction energy is an indication of the strength of hydrogen bonding between the heterocyclic nitrogen compound and ionic liquids (Ni et al., 2008).

The interaction energy of neat ILs was discussed earlier, where the interaction energy relates to compactness of the ILs, or, the distance between cation and anion. ILs with high interaction energy have higher compactness and closer distance between cation and anion, thus making it difficult for incoming molecules to restructure around the cation and anion. On the other hand, ILs with smaller interaction energy have lower compactness and larger distance between cation and anion, thus allowing for facile restructuring of incoming molecules. Thus, in choosing ILs for liquid-liquid extraction, a rule of thumb is to select those with smaller interaction energy so that it can provide better capacity for solute extraction. However, when looking at complexes with ILs and the aromatic solute, it is preferable to have higher interaction energy, since this indicates that extra amount of energy is required to disassemble the complex (Anantharaj, et al., 2011c).

Figure 4.23 a) – c) presents the interaction energy of complexes with ionic liquids and PYR and PY as representative neutral and basic nitrogen compounds, respectively, sorted by values. The values of the interaction energy are in reasonable accordance with the values obtained from literature, i.e. within the same order of magnitude. (Lü, Lin, et al., 2013; Lü et al., 2012). In all complexes except for complexes of IL with indoline and quinoline, complexes with the IL [TMPYRA][Ac] is seen to have the highest interaction energy compared to complexes with other ILs (with values of -77.05, -51.61, -83.14, -84.76 kJ mol⁻¹ for its complexes with PYR, PY, INDO, CAR, respectively).

Strangely, [TMPYRA][Ac] have the smallest or even negligible interaction energy with quinoline ($-2.27 \text{ kJ mol}^{-1}$). Except for indoline and quinoline, ILs with aromatic cation dominate the top three spot for highest interaction energy with nitrogen heterocycles. Cation with aromatic ring have a pronounce π -system, which enables the interaction with aromatic compounds through both π - π and cation- π interaction (Tsuzuki, Mikami, et al., 2007). However, indoline and quinoline reports interaction energy with ILs based on saturated cation is higher than those with ILs based on aromatic cations, at least in the top three spot. Table 4.2 shows the most favorable ILs for each nitrogen heterocycles based on the value of interaction energy.

4.2.5 Partial Charge Transfer

The partial charges of cation and anion before and after interaction with the heterocyclic nitrogen compounds are available in Table 4.4.

In PYR complexes, out of the eighteen ILs, nine of them show positive charge for PYR after interaction and nine shows negative. Complexes where PYR have negative charge are more significant in value than those with positive charge for PYR by an order of magnitude (10^{-2} vs. 10^{-3}). Charge transfer in [Ac] and [EtSO₄]-based ILs are more pronounce than [MeSO₃]-based ILs. [TMPYRA][Ac] has the largest charge transfer with pyrrole, with charge difference in pyrrole is -0.0281 a.m.u. In PY complexes, less significant charge transfer with ILs is observed where the values of PY charge are in the order of 10^{-3} . Charge difference is generally positive for PY, indicating charge transfer occurs from PY to IL. This is consistent with earlier result where it was observed that the HOMO comes from PY while the LUMO comes from IL cation.

Table 4.4: Partial charges (in a.m.u) from NBO analysis for ILs before and after interaction with each nitrogen compounds.

IL	Before interaction		After Interaction (PYR)			After Interaction (PY)		
	Cation	Anion	Cation	Anion	PYR	Cation	Anion	PY
[EMIM][Ac]	0.9338	-0.9338	0.9480	-0.9264	-0.0216	0.9385	-0.9393	0.00083
[EMIM][EtSO ₄]	0.9614	-0.9614	0.9548	-0.9591	0.0043	0.9485	-0.9567	0.00815
[EMIM][MeSO ₃]	0.9541	-0.9541	0.9498	-0.9551	0.0052	0.9472	-0.9553	0.00809
[EMMOR][Ac]	0.9323	-0.9323	0.9487	-0.9315	-0.0172	0.9251	-0.9331	0.00794
[EMMOR][EtSO ₄]	0.9578	-0.9578	0.9667	-0.9715	0.0049	0.9636	-0.9719	0.00821
[EMMOR][MeSO ₃]	0.9556	-0.9556	0.9574	-0.9374	-0.0199	0.9465	-0.9552	0.00872
[EMPIPE][Ac]	0.9304	-0.9304	0.9274	-0.9318	0.0045	0.9341	-0.9311	-0.0030
[EMPIPE][EtSO ₄]	0.9610	-0.9610	0.9619	-0.9442	-0.0177	0.9580	-0.9605	0.00246
[EMPIPE][MeSO ₃]	0.9602	-0.9602	0.9575	-0.9584	0.0009	0.9493	-0.9513	0.00197
[EMPYRO][Ac]	0.9440	-0.9440	0.9309	-0.9355	0.0045	0.9429	-0.9495	0.00658
[EMPYRO][EtSO ₄]	0.9609	-0.9609	0.9690	-0.9504	-0.0186	0.9602	-0.9584	-0.0018
[EMPYRO][MeSO ₃]	0.9511	-0.9511	0.9482	-0.9533	0.0052	0.9494	-0.9557	0.00630
[EPY][Ac]	0.9374	-0.9375	0.9336	-0.9394	0.0058	0.9320	-0.9322	0.00019
[EPY][EtSO ₄]	0.9631	-0.9631	0.9613	-0.9487	-0.0127	0.9627	-0.9669	0.00420
[EPY][MeSO ₃]	0.9542	-0.9542	0.9520	-0.9573	0.0052	0.9543	-0.9583	0.0040
[TMPYRA][Ac]	0.9463	-0.9463	0.9415	-0.9134	-0.0281	0.9418	-0.9414	-0.0003
[TMPYRA][EtSO ₄]	0.9793	-0.9793	0.9796	-0.9624	-0.0172	0.9642	-0.9674	0.0031
[TMPYRA][MeSO ₃]	0.9681	-0.9681	0.9731	-0.9523	-0.0209	0.9667	-0.9580	-0.0087
IL	Before interaction		After Interaction (INDO)			After Interaction (INDL)		
	Cation	Anion	Cation	Anion	INDO	Cation	Anion	INDL
[EMIM][Ac]	0.9338	-0.9338	0.9414	-0.9140	-0.0274	0.9404	-0.9387	-0.0017
[EMIM][EtSO ₄]	0.9614	-0.9614	0.9663	-0.9433	-0.0230	0.9593	-0.9603	0.0010
[EMIM][MeSO ₃]	0.9541	-0.9541	0.9637	-0.9396	-0.0241	0.9511	-0.9553	0.0041
[EMMOR][Ac]	0.9323	-0.9323	0.9343	-0.9288	-0.0055	0.9399	-0.9184	-0.0216
[EMMOR][EtSO ₄]	0.9578	-0.9578	0.9715	-0.9677	-0.0038	0.9607	-0.9621	0.0014
[EMMOR][MeSO ₃]	0.9556	-0.9556	0.9559	-0.9493	-0.0066	0.9602	-0.9517	-0.0086
[EMPIPE][Ac]	0.9304	-0.9304	0.9401	-0.9330	-0.0071	0.9351	-0.9359	0.0009
[EMPIPE][EtSO ₄]	0.9610	-0.9610	0.9652	-0.9446	-0.0205	0.9639	-0.9493	-0.0146
[EMPIPE][MeSO ₃]	0.9602	-0.9602	0.9572	-0.9319	-0.0253	0.9523	-0.9492	-0.0032
[EMPYRO][Ac]	0.9440	-0.9440	0.9338	-0.9285	-0.0053	0.9491	-0.9438	-0.0053
[EMPYRO][EtSO ₄]	0.9609	-0.9609	0.9725	-0.9556	-0.0169	0.9660	-0.9654	-0.0006
[EMPYRO][MeSO ₃]	0.9511	-0.9511	0.9540	-0.9480	-0.0060	0.9556	-0.9438	-0.0117
[EPY][Ac]	0.9374	-0.9375	0.9522	-0.9250	-0.0272	0.9255	-0.9221	-0.0034
[EPY][EtSO ₄]	0.9631	-0.9631	0.9766	-0.9562	-0.0204	0.9584	-0.9587	0.0003
[EPY][MeSO ₃]	0.9542	-0.9542	0.9609	-0.9560	-0.0050	0.9519	-0.9471	-0.0048
[TMPYRA][Ac]	0.9463	-0.9463	0.9585	-0.9220	-0.0364	0.9478	-0.9431	-0.0047
[TMPYRA][EtSO ₄]	0.9793	-0.9793	0.9827	-0.9599	-0.0227	0.9729	-0.9660	-0.0069
[TMPYRA][MeSO ₃]	0.9681	-0.9681	0.9786	-0.9522	-0.0263	0.9707	-0.9617	-0.0090
IL	Before interaction		After Interaction (QU)			After Interaction (CAR)		
	Cation	Anion	Cation	Anion	QU	Cation	Anion	CAR
[EMIM][Ac]	0.9338	-0.9338	0.9369	-0.9358	-0.0012	0.9416	-0.9298	-0.0119

[EMIM][EtSO ₄]	0.9614	-0.9614	0.9571	-0.9603	0.0031	0.9621	-0.9515	-0.0106
[EMIM][MeSO ₃]	0.9541	-0.9541	0.9607	-0.9646	0.0039	0.9570	-0.9492	-0.0079
[EMMOR][Ac]	0.9323	-0.9323	0.9318	-0.9307	-0.0011	0.9345	-0.9293	-0.0052
[EMMOR][EtSO ₄]	0.9578	-0.9578	0.9567	-0.9554	-0.0013	0.9751	-0.9512	-0.0239
[EMMOR][MeSO ₃]	0.9556	-0.9556	0.9515	-0.9521	0.0007	0.9696	-0.9435	-0.0261
[EMPIPE][Ac]	0.9304	-0.9304	0.9375	-0.9351	-0.0024	0.9474	-0.9183	-0.0292
[EMPIPE][EtSO ₄]	0.9610	-0.9610	0.9653	-0.9593	-0.0060	0.9673	-0.9458	-0.0215
[EMPIPE][MeSO ₃]	0.9602	-0.9602	0.9479	-0.9500	0.0020	0.9577	-0.9310	-0.0267
[EMPYRO][Ac]	0.9440	-0.9440	0.9356	-0.9327	-0.0030	0.9466	-0.9201	-0.0265
[EMPYRO][EtSO ₄]	0.9609	-0.9609	0.9576	-0.9601	0.0024	0.9677	-0.9481	-0.0196
[EMPYRO][MeSO ₃]	0.9511	-0.9511	0.9572	-0.9523	-0.0049	0.9604	-0.9339	-0.0265
[EPY][Ac]	0.9374	-0.9375	0.9369	-0.9352	-0.0017	0.9471	-0.9139	-0.0332
[EPY][EtSO ₄]	0.9631	-0.9631	0.9555	-0.9551	-0.0004	0.9763	-0.9545	-0.0218
[EPY][MeSO ₃]	0.9542	-0.9542	0.9676	-0.9652	-0.0024	0.9569	-0.9304	-0.0265
[TMPYRA][Ac]	0.9463	-0.9463	0.9524	-0.9613	0.0089	0.9569	-0.9283	-0.0286
[TMPYRA][EtSO ₄]	0.9793	-0.9793	0.9653	-0.9637	-0.0016	0.9827	-0.9587	-0.0240
[TMPYRA][MeSO ₃]	0.9681	-0.9681	0.9661	-0.9661	-3E-05	0.9680	-0.9400	-0.0280

Table 4.4, continued.

In PY, charge transfer with ILs based on [EtSO₄] and [MeSO₃] are more significant than in [Ac]-based ILs. Largest charge difference for PY is when combined with [EMMOR][MeSO₃] (+0.0087 a.m.u.). Meanwhile, all indole complexes report partial charges of indole to be negative, indicating charge transfer from ILs to indole. More significant charge transfer is observed between indole and ILs with aromatic cation combined with either [Ac] or [EtSO₄] anion; and the largest charge difference in indole is when combined with [TMPYRA][Ac], where the partial charge of indole is -0.0364 a.m.u. Indole complexes show more negative partial charges of indole in most ILs. Charge difference in indole is more significant in ILs with saturated cation compared to ILs with aromatic cations by an order of magnitude. Highest charge difference in indole is in INDO-[EMMOR][Ac] complex (-0.0216 a.m.u.). In quinoline complexes, two-third of the complexes report negative partial charge of quinoline and the rest positive. Charge differences in all quinoline complexes are small in magnitude, regardless of its sign. Some complexes report almost negligible charge difference (+0.0007, -0.0004, and -0.00003 a.m.u. for indole complexes with [EMMOR][MeSO₃], [EPY][EtSO₄], and [TMPYRA][MeSO₃], respectively). This indicates that charge transfer between IL and

quinoline is not as profound. Largest charge difference is in QUI-[TMPYRA][Ac] complex, with quinoline partial charge equals to +0.0089 a.m.u., albeit still relatively small in value as compared to IL complexes with other nitrogen compounds. On the other hand, all complexes of carbazole with ILs show negative partial charge in carbazole, indicating charge transfer from IL to carbazole. The charge difference in carbazole is quite encouraging, with most of them in the order of 10^{-2} . Small charge transfer is observed between carbazole and [EMIM] ILs and [EMMOR][Ac]. For complexes of carbazole with other ILs, more pronounced charge transfer is seen with [Ac]-based ILs, with the highest charge difference in carbazole is with the IL [EPY][Ac] (-0.0332 a.m.u.).

From the results of NBO analysis for investigation of charge transfer, it could be deduced that according to NBO analysis, charge transfer occurs mostly from IL to the nitrogen compounds, except for pyridine where the charge transfer is from pyridine to IL. In cases where charge transfer is from IL to nitrogen compound, anion plays a more significant role since the electron transfer is more significant through the anion, as demonstrated by the larger charge difference in anion (becoming more positive) before and after interaction with the nitrogen compounds. It is interesting to compare the results from NBO analysis with what have been obtained from the geometry optimization calculation. As an example, we take complex of PYR with [TMPYRA][Ac] as this complex reports the most significant charge transfer in PYR complexes. From the optimized geometry, the HOMO comes from PYR while the LUMO from the pyrazolium cation; which if based on molecular orbital theory, charge transfer or electron transfer generally proceeds in the direction of HOMO to LUMO. However, from the NBO analysis, it was observed that the partial charge of PYR in PYR-[TMPYRA][Ac] complex is negative, indicating charge transfer occurring from IL to PYR. This is also true for other complexes, where the NBO analysis result differ from the supposed electron or charge transfer between the frontier orbitals. Nevertheless, NBO analysis is still of good

use in gauging the magnitude of charge transfer within a complex. Larger charge difference in the nitrogen compound means more significant charge transfer, and the ILs are ranked according to this criteria for partial charge parameter as shown in Table 4.2. Thus, [TMPYRA][Ac] is the best IL for most of heterocyclic nitrogen compounds based on partial charge transfer.

4.2.6 Combination of parameters

The parameters studied in this work, i.e. orbital energy, global scalar properties, interaction energy and partial charge transfer cannot be related to one another, as they all have different definition and criteria at quantum level. However, based on the parameters discussed above, we can rank the ILs for denitrogenation purpose according to the objective by each parameter. For example, based on the global softness, the ILs are ranked based on the highest softness which indicates better reactivity and tendency for electron transfer. The ranking based on each parameter is this presented in Table 4.2. From Table 4.2, it is observed that the overall rank at each parameter is dominated by [EPY][EtSO₄] (for LUMO energy, HOMO-LUMO gap, global softness and electrophilicity index parameters) and [TMPYRA][Ac] (for interaction energy and charge transfer magnitude parameters). The choice of [EPY][EtSO₄] as having the most favorable interaction with nitrogen compounds are supported not only by the results of calculation in this work, but also has been confirmed by earlier works published (Ferro et al., 2012; Hansmeier, et al., 2011). It has been shown that pyridinium-based IL has better extraction capacity for aromatic compounds containing sulfur and nitrogen than imidazolium-based ILs with the same anion (Ferro, et al., 2012; Hansmeier, et al., 2011). Pyridinium cation enables better interaction with the aromatic components through both cation- π and π - π interaction due to its having a pronounce π system (Tsuzuki, et al., 2007). Besides, [EPY][EtSO₄] have among the smallest interaction energy in the neat IL complexes. As has been discussed, ILs with small interaction energy have lower packing and may allow for incoming

molecules to accommodate between the large distance of cation and anion thus better affinity and capacity for extraction.

University of Malaya

4.3 Ternary LLE Results

In order to validate the previous prediction results on the effectiveness of selected ILs and DES to extract non-basic and basic nitrogen compounds from a model diesel compound, ternary liquid-liquid equilibrium (LLE) experiments were conducted for mixtures of *n*-hexadecane (taken as a model diesel compound) and aromatic nitrogen compounds (pyrrole, pyridine, indoline, and quinoline) using three ILs and two DESs, namely, 1-ethyl-3-methylimidazolium ethyl sulfate ([EMIM][EtSO₄]), 1-ethyl-3-methylpyridinium ethyl sulfate ([EMPY][EtSO₄]), and 1-ethyl-3-methylimidazolium methanesulfonate ([EMIM][MeSO₃]) ILs and tetrabutylammonium bromide/ethylene glycol at molar ratio 1:2 (TBAB/EG (1:2)) and tetrabutylphosphonium bromide/ethylene glycol at molar ratio 1:2 (TBPB/EG (1:2)) DESs. These experimental LLE results are essential because of the lack of experimental ternary LLE data for extractive denitrogenation using ILs and DES available in the literature, especially for five-membered nitrogen compounds. The reliability of the experimental data was ascertained by performing a consistency test for each set of ternary LLE data using the Othmer-Tobias and Hand correlations as described in sub-section 3.3.5 in Chapter III (Methodology).

Evaluation on the extraction efficiency of ILs and DES used in the ternary LLE experiments was based on the distribution coefficient of aromatic nitrogen compounds and the selectivity towards the nitrogen compounds. The distribution coefficient of nitrogen compound at a given tie-line, D , was defined as the ratio of concentration of aromatic nitrogen compound in the solvent phase to that of in the hydrocarbon phase:

$$D = \frac{x_2''}{x_1'} \quad (\text{Eq. 4.1})$$

Where x_2'' and x_1' are the concentrations of aromatic nitrogen compound in the solvent and hydrocarbon phases, respectively.

Selectivity, S , is defined as the ratio of distribution ratios of aromatic nitrogen compound to that of n -hexadecane as the model diesel compound. Selectivity measures the extent of favourable interaction between the solvent and the solute. High values of selectivity indicate that the solvent has a more favourable interaction with the solute, i.e. the aromatic nitrogen compound than it has with the carrier, i.e. n -hexadecane as the model diesel compound. Mathematical expression of selectivity is given in Equation 4.2.

$$S = \frac{D_2}{D_1} = \frac{x_2''/x_2'}{x_1''/x_1'} \quad (\text{Eq. 4.2})$$

D_2 and D_1 are the distribution ratios of aromatic nitrogen compound and n -hexadecane, respectively, whereas x_2 and x_1 are the concentrations of aromatic nitrogen compound and n -hexadecane, respectively. Superscripts " and ' denote the solvent phase and the hydrocarbon phase, respectively.

In all of the ternary LLE experimental results, the extract phase is rich in IL or DES, whereas the raffinate phase is rich in n -hexadecane. The tie-lines of various ternary systems were plotted against a feed concentration of nitrogen compound ranging from 5% to 50% on a molar basis. In all of the LLE experiments, the presence of IL and DES solvents in the raffinate phase is found to be negligible showing concentrations below the detection limit of the NMR spectroscopy. It is also observed that the concentration of n -hexadecane present in the extract phase is very small, which indicates minimal cross-contamination between the extract and raffinate phases.

The experimental ternary LLE results are presented in the following subsections according to the respective solvents used in the experiments. For each solvent, there are four sets of ternary LLE systems as there are four aromatic nitrogen compounds used to compare the performance of each solvent in extracting five-membered and six-membered nitrogen compounds. NRTL correlations and COSMO-RS predictions were performed

for each ternary LLE system and the fitting goodness measured by the Relative Mean Square Deviation (RMSD) values was reported.

4.3.1 Consistency Test

The degree of consistency of the data is indicated by the linearity of each plot (value of R^2). The parameters of the Othmer–Tobias (a and b) and Hand correlation (c and d) are listed in Table 4.5, which also shows that the regression coefficients R^2 are very close to unity. This indicates that the degree of consistency of all experimental data reported is excellent.

Table 4.5: Parameters of Othmer-Tobias and Hand correlations for each ternary LLE system and the values of regression coefficient R^2 .

Ternary System	Othmer-Tobias			Hand		
	a	b	R^2	c	d	R^2
[EMIM][EtSO ₄] (1) + pyrrole (2) + <i>n</i> -hexadecane (3)	1.197	-5.233	0.981	1.186	-5.232	0.979
[EMIM][EtSO ₄] (1) + pyridine (2) + <i>n</i> -hexadecane (3)	0.965	-1.301	0.995	0.943	-1.319	0.996
[EMIM][EtSO ₄] (1) + indoline (2) + <i>n</i> -hexadecane (3)	0.762	-2.863	0.967	0.739	-2.884	0.962
[EMIM][EtSO ₄] (1) + quinoline (2) + <i>n</i> -hexadecane (3)	0.969	-1.110	0.999	0.921	-1.164	0.997
[EMPY][EtSO ₄] (1) + pyrrole (2) + <i>n</i> -hexadecane (3)	2.531	-3.986	0.946	2.409	-4.019	0.955
[EMPY][EtSO ₄] (1) + pyridine (2) + <i>n</i> -hexadecane (3)	1.022	-1.296	0.988	0.974	-1.333	0.986
[EMPY][EtSO ₄] (1) + indoline (2) + <i>n</i> -hexadecane (3)	1.126	-2.820	0.975	1.053	-2.886	0.974
[EMPY][EtSO ₄] (1) + quinoline (2) + <i>n</i> -hexadecane (3)	0.969	-1.659	0.990	0.913	-1.715	0.993
[EMIM][MeSO ₃] (1) + pyrrole (2) + <i>n</i> -hexadecane (3)	1.224	-5.828	0.986	1.158	-5.889	0.981
[EMIM][MeSO ₃] (1) + pyridine (2) + <i>n</i> -hexadecane (3)	1.406	-0.532	0.997	1.368	-0.568	0.997
[EMIM][MeSO ₃] (1) + indoline (2) + <i>n</i> -hexadecane (3)	1.007	-3.345	0.973	0.945	-3.404	0.987
[EMIM][MeSO ₃] (1) + quinoline (2) + <i>n</i> -hexadecane (3)	1.095	-1.399	0.997	1.043	-1.457	0.998
IL mixture 1* (1) + indoline (2) + <i>n</i> -hexadecane (3)	1.162	-3.275	0.989	1.111	-3.319	0.992
IL mixture 2** (1) + quinoline (2) + <i>n</i> -hexadecane (3)	1.063	-1.241	0.981	0.957	-1.362	0.992
TBAB/EG (1:2) (1) + pyrrole (2) + <i>n</i> -hexadecane (3)	1.470	-4.190	0.995	1.416	-4.197	0.995
TBAB/EG (1:2) (1) + pyridine (2) + <i>n</i> -hexadecane (3)	1.075	-1.859	0.992	1.019	-1.891	0.993
TBAB/EG (1:2) (1) + indoline (2) + <i>n</i> -hexadecane (3)	1.045	-2.319	0.992	1.018	-2.318	0.993
TBAB/EG (1:2) (1) + quinoline (2) + <i>n</i> -hexadecane (3)	1.046	-1.951	0.996	1.029	-1.966	0.996
TBPB/EG (1:2) (1) + pyrrole (2) + <i>n</i> -hexadecane (3)	1.495	-4.305	0.946	1.345	-4.246	0.961
TBPB/EG (1:2) (1) + pyridine (2) + <i>n</i> -hexadecane (3)	1.039	-2.121	0.996	0.929	-2.131	0.987
TBPB/EG (1:2) (1) + indoline (2) + <i>n</i> -hexadecane (3)	1.054	-2.428	0.992	0.968	-2.465	0.993
TBPB/EG (1:2) (1) + quinoline (2) + <i>n</i> -hexadecane (3)	1.307	-1.836	0.973	1.121	-1.887	0.963

* IL mixture 1: [EMIM][EtSO₄]+[EMPY][EtSO₄]

** IL mixture 2: [EMIM][EtSO₄]+[EMPY][EtSO₄]

4.3.2 Systems with IL [EMIM][EtSO₄]

The ternary LLE tie-lines [EMIM][EtSO₄] IL are presented in Tables 4.6 to 4.9 where the concentration of [EMIM][EtSO₄], aromatic nitrogen compounds (i.e. pyrrole, pyridine, indoline, or quinoline) and *n*-hexadecane were reported. In the tables, the experimental values of the tie-lines as obtained from the NMR spectroscopy were presented together with the tie-lines calculated using NRTL correlation and COSMO-RS prediction. The values of distribution coefficient, *D*, and selectivity, *S* at each tie-line were also calculated and presented.

Table 4.6: Ternary tie-lines for the system [EMIM][EtSO₄] (1) + pyrrole (2) + *n*-hexadecane (3) at T=25°C and P_{atm}

IL-rich phase			Hydrocarbon-rich phase			<i>D</i>	<i>S</i>
<i>x</i> ' ₁	<i>x</i> ' ₂	<i>x</i> ' ₃	<i>x</i> '' ₁	<i>x</i> '' ₂	<i>x</i> '' ₃		
Experimental tie-lines							
0.8450	0.1543	0.0008	0.0000	0.0004	0.9996	385.75	481 995
0.7397	0.2582	0.0021	0.0000	0.0014	0.9986	184.43	87 700
0.6678	0.3297	0.0025	0.0000	0.0022	0.9978	149.86	59 814
0.5890	0.4074	0.0036	0.0000	0.0025	0.9975	162.96	44 135
0.5395	0.4577	0.0028	0.0000	0.0031	0.9969	147.65	52 567
0.4903	0.5085	0.0011	0.0000	0.0041	0.9959	124.02	112 287
0.4518	0.5470	0.0012	0.0000	0.0050	0.9950	109.1	90 711
0.4187	0.5802	0.0010	0.0000	0.0053	0.9947	109.47	108 891
0.3898	0.6083	0.0020	0.0000	0.0070	0.9930	86.90	43 146
0.3656	0.6339	0.0004	0.0000	0.0079	0.9921	80.24	199 017
NRTL-calculated tie-lines							
0.8442	0.1556	0.0002	0.0006	0.0012	0.9982	129.67	647 166
0.7378	0.2618	0.0004	0.0005	0.0022	0.9973	119.00	296 697
0.6532	0.3462	0.0006	0.0004	0.0032	0.9963	108.19	179 645
0.5866	0.4126	0.0008	0.0004	0.0041	0.9955	100.63	125 227
0.5323	0.4667	0.0010	0.0003	0.0048	0.9948	97.23	96 724
0.4869	0.5118	0.0012	0.0003	0.0055	0.9942	93.05	77 096
0.4479	0.5507	0.0014	0.0003	0.0061	0.9936	90.28	64 072
0.4159	0.5825	0.0016	0.0003	0.0066	0.9932	88.26	54 786
0.3867	0.6115	0.0018	0.0002	0.0070	0.9927	87.36	48 177
0.3629	0.6352	0.0019	0.0002	0.0074	0.9924	85.84	44 834
COSMO-RS predicted tie-lines							
0.8457	0.1541	0.0002	0.0001	0.0015	0.9984	102.73	512 845
0.7367	0.2632	0.0001	0.0001	0.0033	0.9966	79.76	794 864
0.6445	0.3554	0.0001	0.0001	0.0055	0.9944	64.62	642 563
0.5779	0.4220	0.0001	0.0001	0.0077	0.9922	54.81	543 777
0.5296	0.4703	0.0001	0.0001	0.0098	0.9902	47.99	475 195
0.4778	0.5222	0.0001	0.0000	0.0125	0.9875	41.78	412 538
0.4461	0.5538	0.0001	0.0000	0.0145	0.9855	38.19	376 393
0.4085	0.5914	0.0001	0.0000	0.0172	0.9827	34.38	337 889
0.3937	0.6062	0.0001	0.0000	0.0185	0.9815	32.77	321 614
0.3537	0.6462	0.0001	0.0000	0.0223	0.9777	28.98	283 314

Table 4.7: Ternary tie-lines for the system [EMIM][EtSO₄] (1) + pyridine (2) + *n*-hexadecane (3) at T=25°C and P_{atm}

IL-rich phase			Hydrocarbon-rich phase			<i>D</i>	<i>S</i>
x'_1	x'_2	x'_3	x''_1	x''_2	x''_3		
Experimental tie-lines							
0.8959	0.1011	0.0030	0.0000	0.0319	0.9681	3.17	1 023
0.8078	0.1907	0.0015	0.0000	0.0661	0.9339	2.89	1 796
0.7439	0.2550	0.0011	0.0000	0.0966	0.9034	2.64	2 168
0.6776	0.3211	0.0013	0.0000	0.1184	0.8816	2.71	1 839
0.6215	0.3768	0.0017	0.0000	0.1461	0.8539	2.58	1 295
0.5665	0.4299	0.0036	0.0000	0.1729	0.8271	2.49	571
0.5353	0.4622	0.0025	0.0000	0.2025	0.7975	2.28	728
0.4938	0.5047	0.0015	0.0000	0.2189	0.7811	2.31	1 201
0.4601	0.5389	0.0009	0.0000	0.2351	0.7649	2.29	1 948
0.4257	0.5737	0.0005	0.0000	0.2534	0.7466	2.26	3 381
NRTL-calculated tie-lines							
0.8923	0.1074	0.0003	0.0007	0.0331	0.9661	3.24	10 449
0.8057	0.1937	0.0007	0.0008	0.0652	0.9340	2.97	3 964
0.7329	0.2658	0.0012	0.0009	0.0958	0.9033	2.77	2 089
0.6746	0.3236	0.0019	0.0009	0.1230	0.8761	2.63	1 213
0.6182	0.3791	0.0027	0.0010	0.1512	0.8478	2.51	787
0.5707	0.4257	0.0036	0.0011	0.1761	0.8228	2.42	553
0.5290	0.4663	0.0046	0.0012	0.1984	0.8005	2.35	409
0.4916	0.5027	0.0057	0.0013	0.2183	0.7805	2.30	315
0.4577	0.5354	0.0069	0.0013	0.2357	0.7630	2.27	251
0.4273	0.5646	0.0081	0.0014	0.2501	0.7485	2.26	209
COSMO-RS predicted tie-lines							
0.8989	0.1011	0.0001	0.0000	0.0405	0.9595	2.50	23 952
0.8136	0.1863	0.0001	0.0001	0.0756	0.9244	2.46	22 780
0.7397	0.2602	0.0001	0.0001	0.1054	0.8945	2.47	22 082
0.6789	0.3210	0.0001	0.0001	0.1288	0.8711	2.49	21 710
0.6197	0.3801	0.0002	0.0001	0.1500	0.8500	2.53	10 770
0.5698	0.4300	0.0002	0.0001	0.1662	0.8337	2.59	10 785
No LLE							
0.4883	0.5113	0.0003	0.0001	0.1894	0.8105	2.70	7 293
No LLE							
0.4246	0.5749	0.0005	0.0001	0.2045	0.7954	2.81	4 472

Table 4.8: Ternary tie-lines for the system [EMIM][EtSO₄] (1) + indoline (2) + *n*-hexadecane (3) at T=25°C and P_{atm}

IL-rich phase			Hydrocarbon-rich phase			<i>D</i>	<i>S</i>
x'_1	x'_2	x'_3	x''_1	x''_2	x''_3		
Experimental tie-lines							
0.9114	0.0848	0.0039	0.0000	0.0129	0.9871	6.57	1 664
0.8343	0.1631	0.0026	0.0000	0.0150	0.9850	10.87	4 119
0.7766	0.2218	0.0016	0.0000	0.0233	0.9767	9.52	5 811
0.5747	0.4239	0.0014	0.0000	0.0290	0.9710	14.62	10 138
0.6779	0.3206	0.0015	0.0000	0.0373	0.9627	8.60	5 516
0.6474	0.3511	0.0015	0.0000	0.0417	0.9583	8.42	5 379
0.6084	0.3902	0.0013	0.0000	0.0512	0.9488	7.62	5 562
0.5711	0.4278	0.0011	0.0000	0.0564	0.9436	7.59	6 507
0.5429	0.4552	0.0019	0.0000	0.0625	0.9375	7.28	3 594
0.5059	0.4924	0.0017	0.0000	0.0635	0.9365	7.75	4 272
NRTL-calculated tie-lines							
0.9130	0.0870	0.0001	0.0007	0.0077	0.9917	11.30	112 049
0.8425	0.1574	0.00005	0.0007	0.0151	0.9843	10.42	205 204
0.7815	0.2184	0.00004	0.0007	0.0224	0.9769	9.75	238 119
0.7271	0.2729	0.00004	0.0006	0.0298	0.9696	9.16	221 983
0.6817	0.3182	0.00004	0.0006	0.0365	0.9629	8.72	209 859
0.6400	0.3600	0.00004	0.0006	0.0431	0.9562	8.35	199 671
0.6026	0.3973	0.00003	0.0006	0.0495	0.9499	8.03	254 138
0.5694	0.4306	0.00003	0.0006	0.0555	0.9439	8.70	273 699
0.5396	0.4603	0.00003	0.0006	0.0611	0.9383	7.53	235 624
0.5116	0.4884	0.00003	0.0006	0.0666	0.9329	7.33	228 042
COSMO-RS predicted tie-lines							
0.9286	0.0714	0.0001	0.0000	0.0256	0.9743	2.79	27 174
0.8686	0.1313	0.0001	0.0000	0.0506	0.9494	2.59	24 636
0.8143	0.1856	0.0001	0.0001	0.0749	0.9250	2.48	22 921
0.7633	0.2365	0.0001	0.0001	0.0984	0.9016	2.40	21 670
0.7188	0.2810	0.0001	0.0001	0.1187	0.8812	2.37	20 861
0.6762	0.3236	0.0002	0.0001	0.1377	0.8622	2.35	10 131
0.6366	0.3631	0.0002	0.0001	0.1546	0.8453	2.35	9 927
0.6003	0.3994	0.0003	0.0001	0.1693	0.8306	2.36	6 532
0.5671	0.4325	0.0004	0.0001	0.1820	0.8179	2.38	4 859
0.5354	0.4641	0.0005	0.0001	0.1934	0.8065	2.40	3 871

Table 4.9: Ternary tie-lines for the system [EMIM][EtSO₄] (1) + quinoline (2) + *n*-hexadecane (3) at T=25°C and P_{atm}

IL-rich phase			Hydrocarbon-rich phase			<i>D</i>	<i>S</i>
x'_1	x'_2	x'_3	x''_1	x''_2	x''_3		
Experimental tie-lines							
0.9285	0.0651	0.0064	0.0000	0.0280	0.9720	2.33	353
0.8701	0.1278	0.0021	0.0000	0.0473	0.9527	2.70	1 226
0.8239	0.1731	0.0030	0.0000	0.0693	0.9307	2.50	775
0.7771	0.2207	0.0021	0.0000	0.0886	0.9114	2.49	1 081
0.7341	0.2637	0.0021	0.0000	0.1084	0.8916	2.43	1 033
0.6888	0.3100	0.0013	0.0000	0.1298	0.8702	2.39	1 599
0.6565	0.3413	0.0021	0.0000	0.1498	0.8502	2.28	922
0.6193	0.3784	0.0024	0.0000	0.1637	0.8363	2.31	805
0.5917	0.4066	0.0017	0.0000	0.1841	0.8159	2.21	1 060
0.5578	0.4401	0.0021	0.0000	0.2051	0.7949	2.15	812
NRTL-calculated tie-lines							
0.9327	0.0672	0.0002	0.0007	0.0231	0.9761	2.91	14 198
0.8761	0.1236	0.0003	0.0008	0.0448	0.9545	2.76	8 778
0.8245	0.1750	0.0005	0.0008	0.0663	0.9329	2.64	4 925
0.7776	0.2216	0.0008	0.0009	0.0873	0.9118	2.54	2 893
0.7341	0.2647	0.0012	0.0009	0.1081	0.8910	2.45	1 818
0.6926	0.3058	0.0016	0.0010	0.1289	0.8701	2.37	1 290
0.6557	0.3423	0.0020	0.0010	0.1483	0.8507	2.31	982
0.6208	0.3766	0.0025	0.0011	0.1671	0.8318	2.25	750
0.5889	0.4080	0.0031	0.0012	0.1847	0.8142	2.21	580
0.5588	0.4375	0.0037	0.0012	0.2013	0.7975	2.17	468
COSMO-RS predicted tie-lines							
0.9403	0.0597	0.0001	0.0000	0.0314	0.9686	1.90	18 416
0.8893	0.1106	0.0001	0.0000	0.0607	0.9393	1.82	17 115
0.8413	0.1586	0.0001	0.0001	0.0890	0.9109	1.78	16 232
0.7960	0.2039	0.0001	0.0001	0.1152	0.8847	1.77	15 659
0.7524	0.2475	0.0001	0.0001	0.1388	0.8611	1.78	15 355
0.7090	0.2909	0.0001	0.0001	0.1599	0.8400	1.82	15 282
0.6691	0.3308	0.0002	0.0001	0.1764	0.8235	1.88	7 721
0.6307	0.3691	0.0002	0.0001	0.1892	0.8107	1.95	7 908
0.5952	0.4045	0.0002	0.0001	0.1982	0.8017	2.04	8 181
0.5621	0.4376	0.0003	0.0001	0.2042	0.7957	2.14	5 684

From Table 4.6, the concentration of *n*-hexadecane in the extract phase of the system [EMIM][EtSO₄] (1) + pyrrole (2) + *n*-hexadecane (3) ranges from 0.0004 to 0.0036, which is considered very small and is indicative of minimal cross-contamination between the extract and raffinate phases. Similarly for all other ternary systems, the concentration of *n*-hexadecane in the extract phase is minute, with the highest concentration of *n*-hexadecane in the extract phase being 0.0064 in the system [EMIM][EtSO₄] (1) + quinoline (2) + *n*-hexadecane (3); which again can be considered insignificant.

The values of *D* and *S* are all greater than unity for the four ternary systems, which indicates that the solvent has better affinity towards all of the aromatic nitrogen compounds than it has towards the model diesel compound, although the values are higher for neutral nitrogen compounds i.e. pyrrole and indoline compared to those of basic nitrogen compounds i.e. pyridine and quinoline. Values of *D* and *S* are exceptionally higher for pyrrole; with the values being two orders of magnitude greater than those reported for other nitrogen compounds (pyridine, indoline and quinoline). Based on the values of *D* and *S*, [EMIM][EtSO₄] is an effective solvent for use in separation of both neutral and basic aromatic nitrogen compounds from model diesel fuel, as expected based on the quantum chemical calculation results.

The ternary LLE phase diagrams for the four systems containing [EMIM][EtSO₄] were presented by Figures 4.24 a) – d) where the tie-lines are drawn from experimental values, NRTL correlation and COSMO-RS predicted values. All of the ternary phase diagrams exhibit the behaviour of Type 1 phase behaviour where there is only one immiscibility region and one of the binary systems exhibiting partial immiscibility.

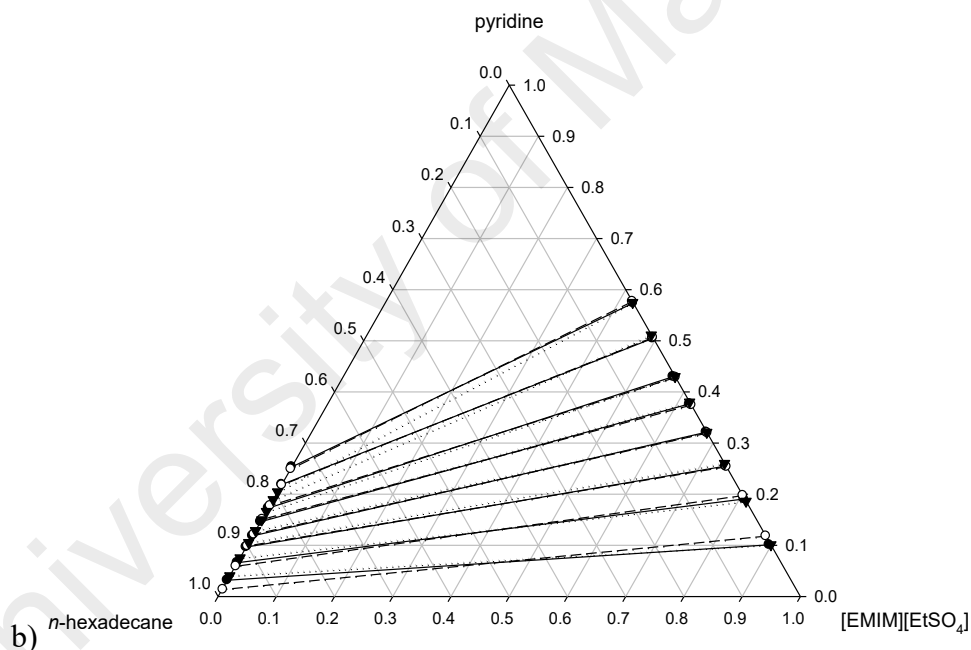
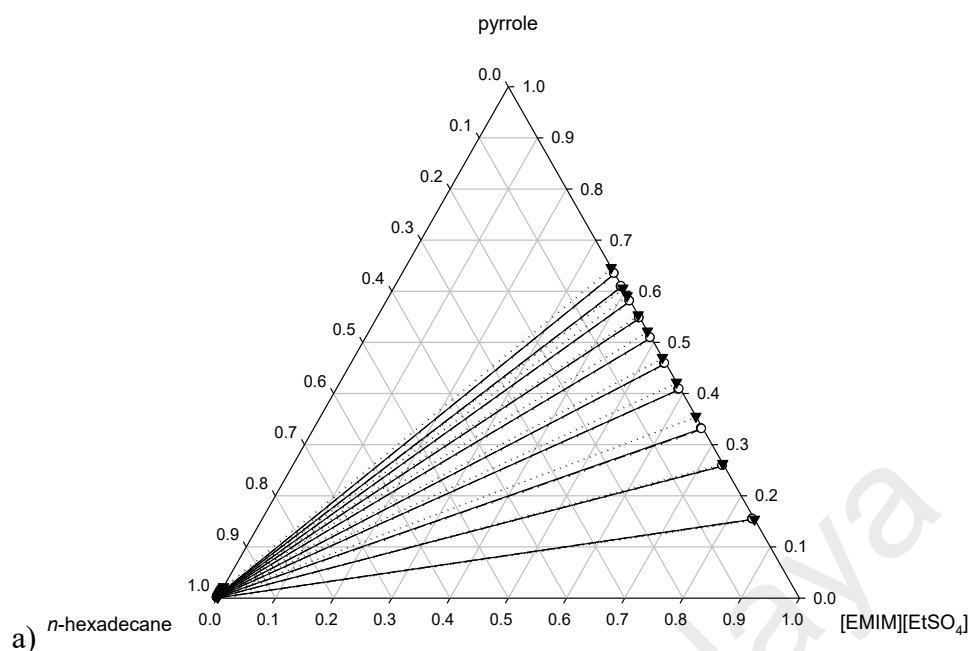


Figure 4.24: Tie-lines for the ternary systems a) [EMIM][EtSO₄] (1) + pyrrole (2) + *n*-hexadecane (3), b) [EMIM][EtSO₄] (1) + pyridine (2) + *n*-hexadecane (3), c) [EMIM][EtSO₄] (1) + indoline (2) + *n*-hexadecane (3) and d) [EMIM][EtSO₄] (1) + quinoline (2) + *n*-hexadecane (3) at $T=298.15$ K and P_{atm} . Full circle and solid lines indicate experimental tie-lines, empty circle and dashed lines indicate tie-lines from NRTL calculation, and full triangle and dotted lines indicate calculated tie-lines from COSMO-RS model.

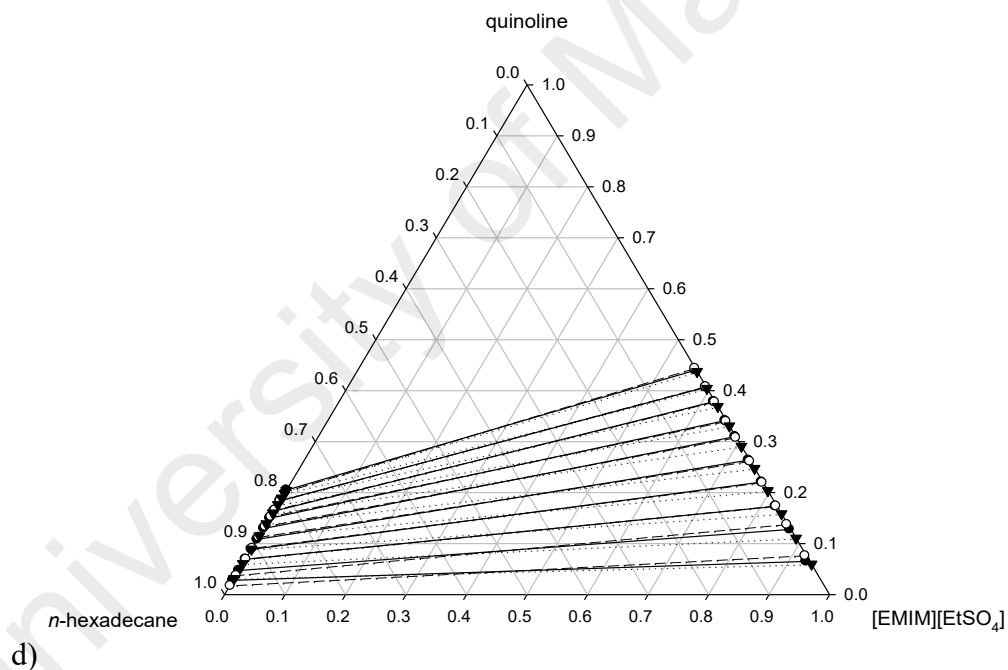
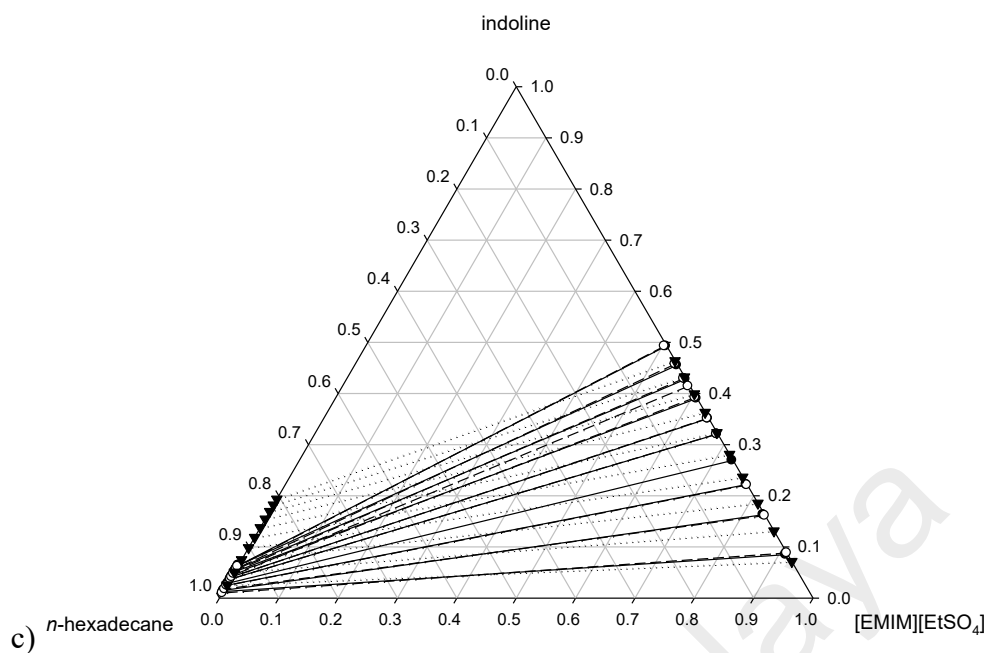


Figure 4.24, continued.

The slope of the tie-lines are positive in all ternary diagrams, indicating that small amount of solvent is sufficient to separate the nitrogen compounds from *n*-hexadecane as the model diesel compound. Comparing Figures 4.24 a) and c) to Figures 4.24 b) and d), it is observed that in the systems [EMIM][EtSO₄] (1) + pyrrole (2) + *n*-hexadecane (3) and [EMIM][EtSO₄] (1) + indoline (2) + *n*-hexadecane (3), the concentration of pyrrole

and indoline in the raffinate phase is smaller than the concentration of pyridine and quinoline in the raffinate phase for the systems [EMIM][EtSO₄] (1) + pyridine (2) + *n*-hexadecane (3) and [EMIM][EtSO₄] (1) + quinoline (2) + *n*-hexadecane (3). This indicates that as the concentration of pyridine and quinoline increases, higher amount of [EMIM][EtSO₄] is required to remove these basic nitrogen compounds from *n*-hexadecane, whereas for pyrrole and indole as the neutral nitrogen compounds, increase in the pyrrole and indole concentrations in the feed mixture from 5 to 50 wt % does not require significantly higher amount of [EMIM][EtSO₄] to remove them from *n*-hexadecane effectively.

The goodness of fit of NRTL correlation and COSMO-RS prediction with the experimental tie-lines were measured using the RMSD values (as previously described in Section 3.3.6 in Chapter III (Methodology)) and is presented in Table 4.10. The binary interaction parameters of NRTL correlation for systems containing [EMIM][EtSO₄] are shown in Table 4.11.

Table 4.10: RMSD values for NRTL correlation and COSMO-RS prediction of each ternary LLE system containing [EMIM][EtSO₄]

System	RMSD	
	NRTL	COSMO-RS
[EMIM][EtSO ₄] (1) + pyrrole (2) + <i>n</i> -hexadecane (3)	0.37%	0.85%
[EMIM][EtSO ₄] (1) + pyridine (2) + <i>n</i> -hexadecane (3)	0.38%	6.16%
[EMIM][EtSO ₄] (1) + indoline (2) + <i>n</i> -hexadecane (3)	0.32%	1.12%
[EMIM][EtSO ₄] (1) + quinoline (2) + <i>n</i> -hexadecane (3)	0.23%	1.53%

Table 4.11: The values of NRTL binary interaction parameters for each ternary systems containing the IL [EMIM][EtSO₄]

<i>i</i> – <i>j</i>	τ_{ij}	τ_{ji}
[EMIM][EtSO ₄] – pyrrole	-686.7	1050.1
[EMIM][EtSO ₄] – pyridine	-338.0	1249.4
[EMIM][EtSO ₄] – indoline	-661.9	941.1
[EMIM][EtSO ₄] – quinoline	-276.2	1229.5
[EMIM][EtSO ₄] – <i>n</i> -hexadecane	2352.2	1688.5
pyrrole – <i>n</i> -hexadecane	1073.9	824.7
pyridine – <i>n</i> -hexadecane	152.5	689.8
indoline – <i>n</i> -hexadecane	2937.8	186.8
quinoline – <i>n</i> -hexadecane	713.1	157.6

It can be visually deduced that the tie-lines obtained using NRTL and COSMO-RS models have good agreement with experimental data. An exception is the COSMO-RS prediction for the system [EMIM][EtSO₄] (1) + indoline (2) + *n*-hexadecane (3), where the COSMO-RS model predicted higher concentrations of indoline in the raffinate phase, when in actual experimental data the concentration of indoline in the raffinate phase is much lower. This explains the higher value of RMSD for COSMO-RS prediction for the system containing indoline (6.16%) compared to other systems which have RMSD than 2%. COSMO-RS is unable to compute LLE data for the system system [EMIM][EtSO₄] (1) + pyridine (2) + *n*-hexadecane (3) at feed concentrations of pyridine of 35 wt% and 45 wt%, hence the “No LLE” statement in the corresponding rows in Table 4.8. The values of *D* and *S* calculated from the NRTL correlation and COSMO-RS predicted tie lines vary significantly from those calculated from experimental data because the *D* and *S* values are sensitive towards the concentrations of nitrogen compounds and *n*-hexadecane in the extract and raffinate phases, and small changes in each point will lead to significant difference in the resulting *D* and *S* values.

Since the concentration of any nitrogen compound on real diesel feed mixture is typically less than 70 ppm, it is useful to compare the performance of [EMIM][EtSO₄] for the removal of aromatic nitrogen compounds at small concentration in the feed mixture, e.g. 5 wt%. The values of *D* and *S* for [EMIM][EtSO₄] towards aromatic nitrogen compounds follows the order: **pyrrole>indoline>pyridine>quinoline**.

4.3.3 Systems with IL [EMPY][EtSO₄]

Tables 4.12 to 4.15 present the ternary LLE tie-lines containing the IL [EMPY][EtSO₄] where the concentration of [EMPY][EtSO₄], aromatic nitrogen compounds (i.e. pyrrole, pyridine, indoline, or quinoline) and *n*-hexadecane were reported.

Table 4.12: Ternary tie-lines for the system [EMPY][EtSO₄] (1) + pyrrole (2) + *n*-hexadecane (3) at T=25°C and P_{atm}

IL-rich phase			Hydrocarbon-rich phase			<i>D</i>	<i>S</i>
x'_1	x'_2	x'_3	x''_1	x''_2	x''_3		
Experimental tie-lines							
0.8417	0.1487	0.0096	0.0000	0.0000	1.0000		
0.7372	0.2584	0.0044	0.0000	0.0006	0.9994	430.67	97 820
0.6486	0.3403	0.0111	0.0000	0.0013	0.9987	261.77	23 552
0.5828	0.4102	0.0071	0.0000	0.0018	0.9982	227.89	32 039
0.5329	0.4648	0.0024	0.0000	0.0027	0.9973	172.15	71 535
0.4814	0.5085	0.0101	0.0000	0.0026	0.9974	195.58	19 314
0.4501	0.5458	0.0041	0.0000	0.0043	0.9957	126.93	30 825
0.4132	0.5830	0.0038	0.0000	0.0058	0.9942	100.52	26 298
0.3941	0.5960	0.0099	0.0000	0.0040	0.9960	149.00	14 990
0.3602	0.6372	0.0026	0.0000	0.0057	0.9943	111.79	42 751
NRTL-calculated tie-lines							
0.8454	0.1544	0.0002	0.0006	0.0012	0.9982	128.67	642 175
0.7359	0.2636	0.0004	0.0005	0.0023	0.9972	114.61	285 719
0.6432	0.3561	0.0006	0.0004	0.0033	0.9962	107.91	179 165
0.5764	0.4227	0.0009	0.0004	0.0042	0.9954	100.64	111 311
0.5279	0.4711	0.0011	0.0003	0.0049	0.9947	96.14	86 939
0.4759	0.5228	0.0013	0.0003	0.0057	0.9940	91.72	70 130
0.4443	0.5543	0.0014	0.0003	0.0061	0.9936	90.87	64 491
0.4067	0.5917	0.0016	0.0003	0.0067	0.9930	88.31	54 810
0.3920	0.6062	0.0017	0.0002	0.0069	0.9928	87.86	51 307
0.3519	0.6461	0.0020	0.0002	0.0076	0.9922	85.01	42 175
COSMO-RS predicted tie-lines							
0.8457	0.1541	0.0002	0.0001	0.0015	0.9984	102.73	512 845
0.7367	0.2632	0.0001	0.0001	0.0033	0.9966	79.76	794 864
0.6445	0.3554	0.0001	0.0001	0.0055	0.9944	64.62	642 563
0.5779	0.4220	0.0001	0.0001	0.0077	0.9922	54.81	543 777
0.5296	0.4703	0.0001	0.0001	0.0098	0.9902	47.99	475 195
0.4778	0.5222	0.0001	0.0000	0.0125	0.9875	41.78	412 538
0.4461	0.5538	0.0001	0.0000	0.0145	0.9855	38.19	376 393
0.4085	0.5914	0.0001	0.0000	0.0172	0.9827	34.38	337 889
0.3937	0.6062	0.0001	0.0000	0.0185	0.9815	32.77	321 614
0.3537	0.6462	0.0001	0.0000	0.0223	0.9777	28.98	283 314

Table 4.13: Ternary tie-lines for the system [EMPY][EtSO₄] (1) + pyridine (2) + *n*-hexadecane (3) at T=25°C and P_{atm}

IL-rich phase			Hydrocarbon-rich phase			<i>D</i>	<i>S</i>
x'_1	x'_2	x'_3	x''_1	x''_2	x''_3		
Experimental tie-lines							
0.8892	0.1052	0.0055	0.0000	0.0323	0.9677	3.26	573
0.8006	0.1948	0.0046	0.0000	0.0554	0.9446	3.52	722
0.7412	0.2550	0.0038	0.0000	0.0824	0.9176	3.09	747
0.6662	0.3282	0.0056	0.0000	0.1154	0.8846	2.84	449
0.6011	0.3943	0.0046	0.0000	0.1303	0.8697	3.03	572
0.5645	0.4320	0.0036	0.0000	0.1505	0.8495	2.87	677
0.5199	0.4768	0.0033	0.0000	0.1683	0.8317	2.83	714
0.5017	0.4955	0.0028	0.0000	0.1944	0.8056	2.55	733
0.4664	0.5285	0.0051	0.0000	0.2404	0.7596	2.20	327
0.4492	0.5475	0.0033	0.0000	0.2540	0.7460	2.16	487
NRTL-calculated tie-lines							
0.8845	0.1152	0.0003	0.0007	0.0255	0.9738	4.52	14 664
0.7958	0.2035	0.0007	0.0007	0.0517	0.9476	3.94	5 328
0.7268	0.2720	0.0012	0.0007	0.0770	0.9223	3.53	2 715
0.6577	0.3404	0.0019	0.0007	0.1073	0.8920	3.17	1 489
0.6035	0.3938	0.0027	0.0008	0.1351	0.8642	2.91	933
0.5570	0.4395	0.0035	0.0008	0.1620	0.8372	2.71	649
0.5170	0.4786	0.0044	0.0008	0.1879	0.8113	2.55	470
0.4982	0.4969	0.0048	0.0009	0.2009	0.7983	0.50	83
0.4493	0.5444	0.0063	0.0009	0.2376	0.7615	2.29	277
0.4391	0.5543	0.0066	0.0010	0.2458	0.7533	2.26	257
COSMO-RS Predicted tie-lines							
0.8922	0.1075	0.0003	0.0001	0.0343	0.9655	3.13	10 087
0.8046	0.1951	0.0003	0.0001	0.0637	0.9361	3.06	9 557
0.7336	0.2660	0.0003	0.0001	0.0879	0.9120	3.03	9 200
0.6613	0.3383	0.0004	0.0002	0.1122	0.8876	3.02	6 691
0.6036	0.3960	0.0004	0.0002	0.1311	0.8687	3.02	6 560
0.5541	0.4454	0.0005	0.0002	0.1467	0.8531	3.04	5 180
0.5117	0.4877	0.0006	0.0002	0.1595	0.8403	3.06	4 282
No LLE							
No LLE							
0.4327	0.5664	0.0008	0.0002	0.1818	0.8181	3.12	3 186

Table 4.14: Ternary tie-lines for the system [EMPY][EtSO₄] (1) + indoline (2) + *n*-hexadecane (3) at T=25°C and P_{atm}

IL-rich phase			Hydrocarbon-rich phase			<i>D</i>	<i>S</i>
x'_1	x'_2	x'_3	x''_1	x''_2	x''_3		
Experimental tie-lines							
0.9038	0.0858	0.0104	0.0000	0.0044	0.9956	205.41	19 664
0.8311	0.1649	0.0040	0.0000	0.0066	0.9934	24.98	6 205
0.7693	0.2273	0.0034	0.0000	0.0153	0.9847	14.86	4 303
0.7168	0.2767	0.0065	0.0000	0.0198	0.9802	13.97	2 107
0.6571	0.3405	0.0024	0.0000	0.0242	0.9758	14.07	5 721
0.6388	0.3574	0.0038	0.0000	0.0292	0.9708	12.24	3 127
0.5789	0.4159	0.0051	0.0000	0.0323	0.9677	12.88	2 443
0.5635	0.4339	0.0026	0.0000	0.0368	0.9632	11.79	4 368
0.5136	0.4822	0.0042	0.0000	0.0401	0.9599	12.02	2 748
0.5031	0.4937	0.0032	0.0000	0.0449	0.9551	9.79	2 923
NRTL-calculated tie-lines							
0.9095	0.0904	0.0001	0.0007	0.0043	0.9950	21.02	209 181
0.8269	0.1731	0.00005	0.0006	0.0093	0.9900	18.61	368 535
0.7694	0.2305	0.00004	0.0006	0.0136	0.9858	16.95	417 697
0.7142	0.2857	0.00004	0.0006	0.0184	0.9810	15.53	380 804
0.6697	0.3302	0.00004	0.0005	0.0229	0.9765	14.42	352 009
0.6271	0.3729	0.00003	0.0005	0.0277	0.9717	13.46	436 037
0.5892	0.4108	0.00003	0.0005	0.0325	0.9669	12.64	407 387
0.5562	0.4438	0.00003	0.0005	0.0372	0.9624	11.93	382 718
0.5256	0.4744	0.00003	0.0005	0.0418	0.9577	11.35	362 307
0.4998	0.5002	0.00003	0.0004	0.0461	0.9535	10.85	344 860
COSMO-RS predicted tie-lines							
0.9219	0.0778	0.0003	0.0001	0.0185	0.9814	4.21	13 757
0.8484	0.1513	0.0003	0.0001	0.0392	0.9607	3.86	12 360
0.7950	0.2047	0.0003	0.0001	0.0558	0.9441	3.67	11 545
0.7417	0.2579	0.0004	0.0002	0.0732	0.9266	3.52	8 162
0.6973	0.3023	0.0004	0.0002	0.0882	0.9116	3.43	7 811
0.6542	0.3453	0.0005	0.0002	0.1030	0.8968	3.35	6 013
0.6139	0.3855	0.0006	0.0002	0.1168	0.8830	3.30	4 857
0.5790	0.4203	0.0007	0.0002	0.1288	0.8709	3.26	4 060
0.5456	0.4536	0.0009	0.0002	0.1403	0.8595	3.23	3 088
0.5181	0.4809	0.0010	0.0003	0.1496	0.8501	3.21	2 733

Table 4.15: Ternary tie-lines for the system [EMPY][EtSO₄] (1) + quinoline (2) + *n*-hexadecane (3) at T=25°C and P_{atm}

IL-rich phase			Hydrocarbon-rich phase			<i>D</i>	<i>S</i>
<i>x</i> ' ₁	<i>x</i> ' ₂	<i>x</i> ' ₃	<i>x</i> '' ₁	<i>x</i> '' ₂	<i>x</i> '' ₃		
Experimental tie-lines							
0.9174	0.0739	0.0087	0.0000	0.0170	0.9830	4.35	491
0.8555	0.1408	0.0037	0.0000	0.0326	0.9674	4.32	1 129
0.7951	0.2018	0.0031	0.0000	0.0457	0.9543	4.42	1 359
0.7581	0.2396	0.0023	0.0000	0.0603	0.9397	3.97	1 623
0.7066	0.2912	0.0022	0.0000	0.0774	0.9226	3.76	1 578
0.6585	0.3397	0.0018	0.0000	0.0867	0.9133	3.92	1 988
0.6155	0.3794	0.0051	0.0000	0.0936	0.9064	4.05	720
0.5832	0.4151	0.0017	0.0000	0.1066	0.8934	3.89	2 046
0.5620	0.4359	0.0021	0.0000	0.1201	0.8799	3.63	1 521
0.5350	0.4626	0.0023	0.0000	0.1423	0.8577	3.25	1 212
NRTL-calculated tie-lines							
0.9250	0.0748	0.0002	0.0007	0.0148	0.9845	5.05	24 879
0.8589	0.1407	0.0004	0.0007	0.0299	0.9694	4.71	11 404
0.8017	0.1977	0.0006	0.0007	0.0445	0.9547	4.44	7 069
0.7516	0.2474	0.0010	0.0008	0.0586	0.9407	4.22	3 971
0.7074	0.2913	0.0014	0.0008	0.0719	0.9273	4.05	2 684
0.6648	0.3334	0.0018	0.0008	0.0855	0.9137	3.90	1 979
0.6300	0.3677	0.0023	0.0008	0.0971	0.9020	3.79	1 485
0.5918	0.4053	0.0029	0.0008	0.1104	0.8888	3.67	1 125
0.5605	0.4360	0.0035	0.0009	0.1215	0.8776	3.59	900
0.5312	0.4647	0.0041	0.0009	0.1320	0.8671	3.52	745
COSMO-RS predicted tie-lines							
0.9332	0.0666	0.0003	0.0001	0.0238	0.9761	2.80	9 105
0.8729	0.1268	0.0003	0.0001	0.0472	0.9527	2.69	8 531
0.8186	0.1811	0.0003	0.0001	0.0689	0.9310	2.63	8 157
0.7696	0.2301	0.0003	0.0001	0.0882	0.9117	2.61	7 928
0.7249	0.2747	0.0003	0.0002	0.1050	0.8949	2.62	7 804
0.6809	0.3187	0.0004	0.0002	0.1203	0.8795	2.65	5 825
0.6441	0.3555	0.0004	0.0002	0.1320	0.8678	2.69	5 843
0.6036	0.3958	0.0005	0.0002	0.1435	0.8564	2.76	4 724
0.5702	0.4292	0.0006	0.0002	0.1517	0.8481	2.83	3 999
0.5390	0.4602	0.0007	0.0002	0.1584	0.8414	2.91	3 492

Similar to systems containing [EMIM][EtSO₄], the experimental values of the tie-lines as obtained from the NMR spectroscopy were presented together with the tie-lines calculated using NRTL correlation and COSMO-RS prediction. The values of distribution coefficient, *D*, and selectivity, *S* at each tie-line are also presented in tables 4.12 to 4.15. COSMO-RS was also unable to predict the tie lines for the system [EMPY][EtSO₄] (1) + pyridine (2) + *n*-hexadecane (3) at feed concentration of pyridine 40 and 45 wt%. This was indicated in Table 4.13 where it was noted with “No LLE”.

Minimal cross-contamination between the extract and raffinate phases was indicated by the minute concentration of hydrocarbon present in the extract phase in all of the ternary systems containing [EMPY][EtSO₄]. For example, the concentration of *n*-hexadecane in the extract phase of the system [EMPY][EtSO₄] (1) + pyrrole (2) + *n*-hexadecane (3) ranges between 0.0026 and 0.01 as shown in Table 4.11.

All four ternary systems report values of *D* and *S* greater than unity, indicating that [EMPY][EtSO₄] have better affinity towards all of the aromatic nitrogen compounds than it has towards the model diesel compound. Similar to system containing [EMIM][EtSO₄], the values of *D* and *S* are higher for neutral nitrogen compounds i.e. pyrrole and indoline in comparison to those of basic nitrogen compounds i.e. pyridine and quinoline. The values of *D* and *S* are also exceptionally higher for pyrrole, where they are two orders of magnitude greater than those reported for other nitrogen compounds. [EMPY][EtSO₄] is also an effective solvent for use in separation of both neutral and basic aromatic nitrogen compounds from model diesel fuel based on the reported values of *D* and *S*.

The ternary LLE phase diagrams for the systems containing [EMPY][EtSO₄] were presented by Figures 4.25 a) to d) where the tie-lines are drawn from experimental values, NRTL correlation and COSMO-RS predicted values. All of the ternary phase diagram exhibit Type 1 phase behaviour where there is only one immiscibility region and one of the binary systems exhibiting partial immiscibility.

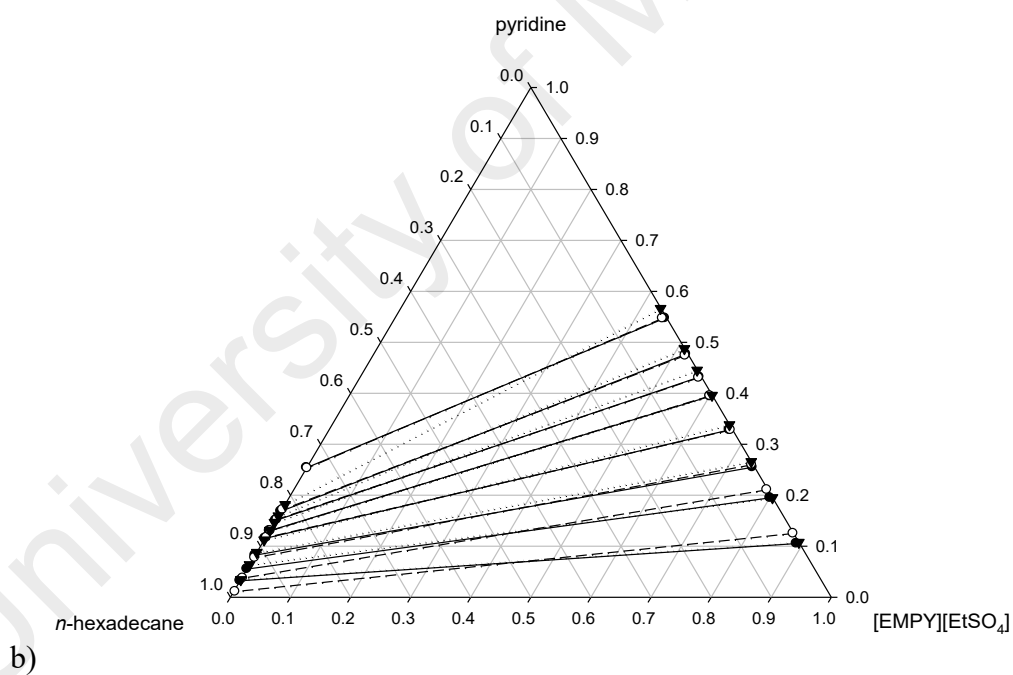
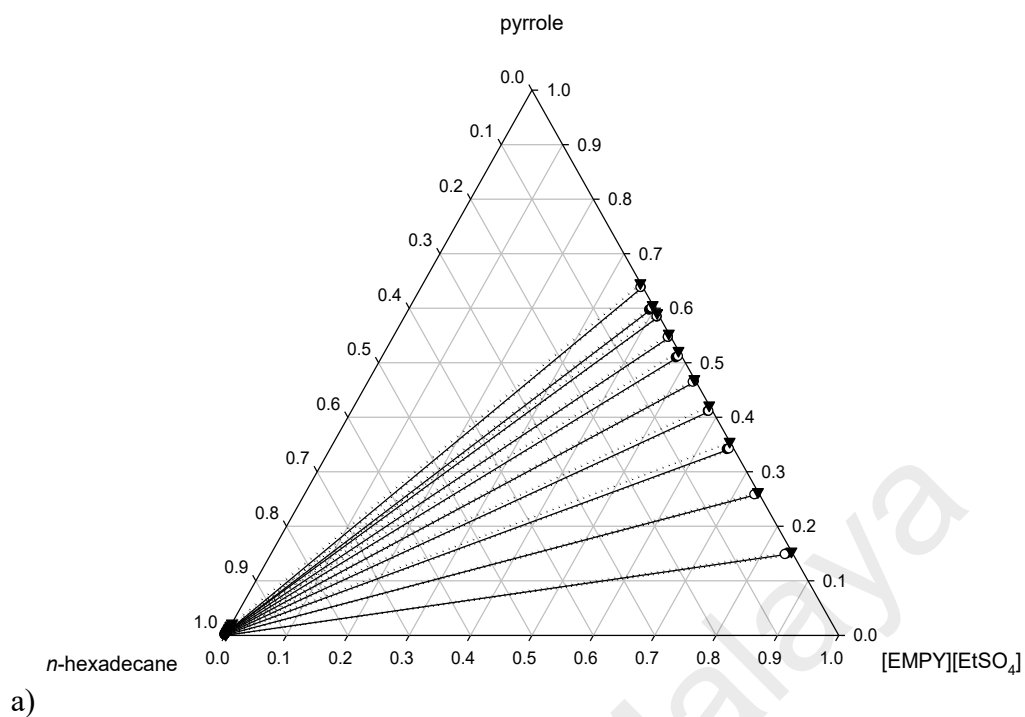


Figure 4.25: Tie-lines for the ternary system a) [EMPY][EtSO₄] (1) + pyrrole (2) + *n*-hexadecane (3), b) [EMPY][EtSO₄] (1) + pyridine (2) + *n*-hexadecane, c) [EMPY][EtSO₄] (1) + indoline (2) + *n*-hexadecane and d) [EMPY][EtSO₄] (1) + quinoline (2) + *n*-hexadecane at $T=298.15$ K and P_{atm} . Full circle and solid lines indicate experimental tie-lines, empty circle and dashed lines indicate tie-lines from NRTL calculation, and full triangle and dotted lines indicate calculated tie-lines from COSMO-RS model.

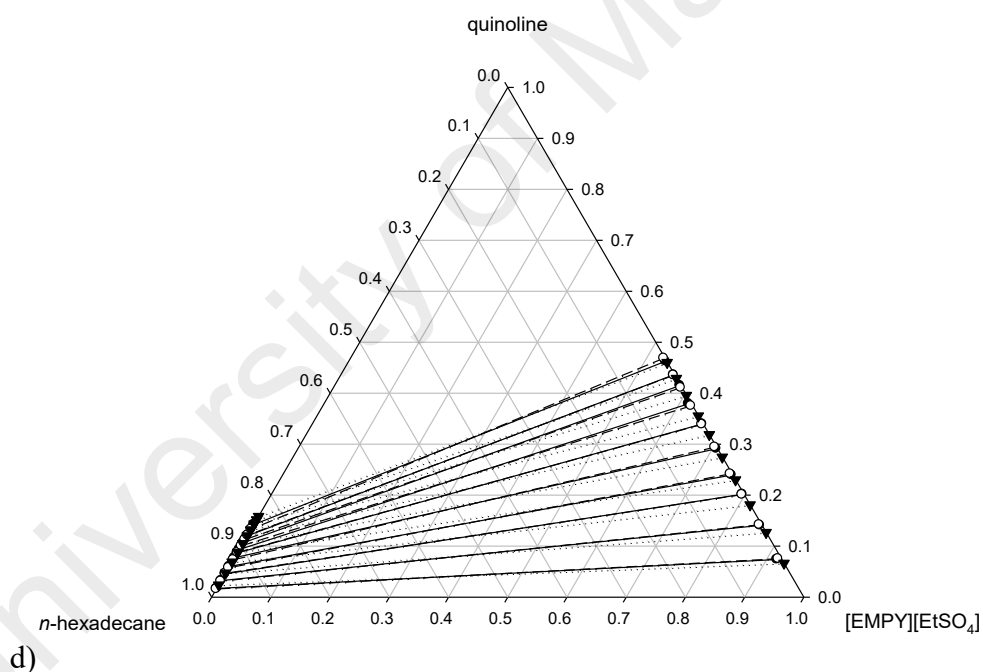
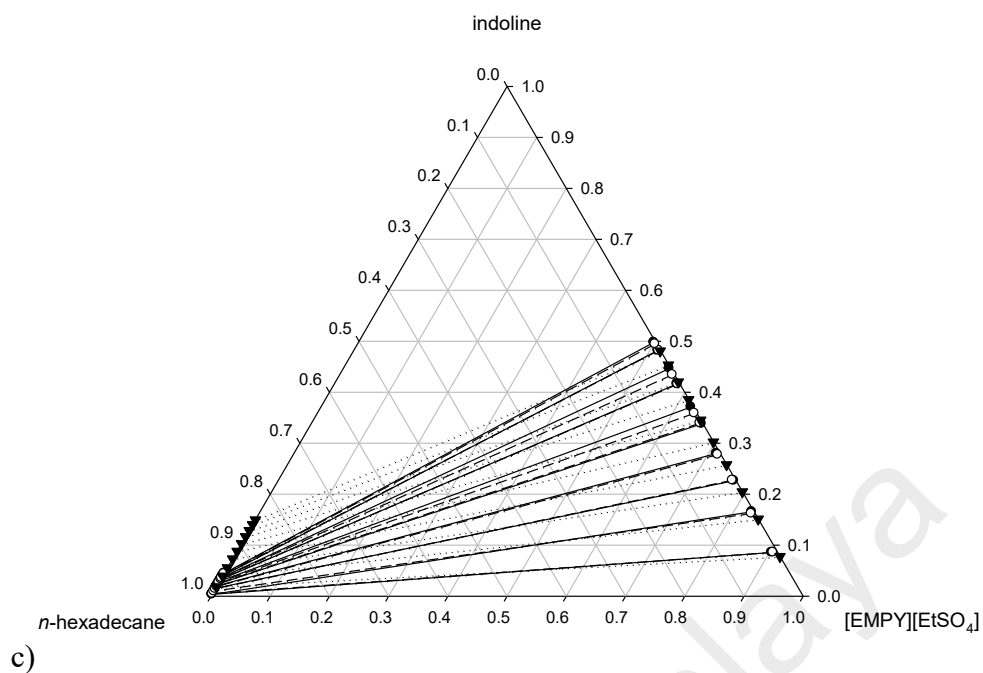


Figure 4.25, continued.

The positive slope of all of the tie-lines indicates that small amount of solvent is sufficient to separate the nitrogen compounds from *n*-hexadecane. Figures 4.25 shows that the concentration of pyrrole and indoline (Figures 4.25 a) and c)) in the raffinate phase is smaller than that of pyridine and quinolone (Figures 4.25 b) and d)) in the same phase. Consistent with the observation with [EMIM][EtSO₄], higher amount of

[EMPY][EtSO₄] is required to remove the basic nitrogen compounds from *n*-hexadecane as the concentration of pyridine and quinoline increases; whereas only small amount of the IL is needed to remove pyrrole and indoline as their concentration increases in the feed mixture.

Table 4.16: RMSD values for NRTL correlation and COSMO-RS prediction of each ternary LLE system containing [EMPY][EtSO₄]

System	RMSD	
	NRTL	COSMO-RS
[EMPY][EtSO ₄] (1) + pyrrole (2) + <i>n</i> -hexadecane (3)	0.56%	0.76%
[EMPY][EtSO ₄] (1) + pyridine (2) + <i>n</i> -hexadecane (3)	0.76%	1.44%
[EMPY][EtSO ₄] (1) + indoline (2) + <i>n</i> -hexadecane (3)	0.54%	4.39%
[EMPY][EtSO ₄] (1) + quinoline (2) + <i>n</i> -hexadecane (3)	0.47%	1.88%

Table 4.17: The values of NRTL binary interaction parameters between [EMPY][EtSO₄] and nitrogen compounds and *n*-hexadecane

<i>i-j</i>	τ_{ij}	τ_{ji}
[EMPY][EtSO ₄] – pyrrole	-686.7	1050.1
[EMPY][EtSO ₄] – pyridine	-463.9	1605.7
[EMPY][EtSO ₄] – indoline	-843.4	881.8
[EMPY][EtSO ₄] – quinoline	-444.3	1182.2
[EMPY][EtSO ₄] – <i>n</i> -hexadecane	2351.8	1689.8

Table 4.16 presents the goodness of fit of NRTL correlation and COSMO-RS prediction with the experimental tie-lines measured using the RMSD. The binary interaction parameters of NRTL correlation for systems containing [EMPY][EtSO₄] are shown in Table 4.17. The interaction parameters between nitrogen compounds and *n*-hexadecane obtained from the regression of ternary tie lines containing [EMIM][EtSO₄], reported in Table 4.11, are used without any adjustment and new parameters are obtained only for the interaction between [EMPY][EtSO₄] and nitrogen compounds and between [EMPY][EtSO₄] and *n*-hexadecane. This is done to preserve the coherence of the regression calculation when it would be used in the process simulation software for design calculations.

Based on visual observation, the tie-lines obtained using NRTL and COSMO-RS models have good agreement with experimental data except for the COSMO-RS prediction for the system [EMPY][EtSO₄] (1) + indoline (2) + *n*-hexadecane (3), where the COSMO-RS model predicted higher concentrations of indoline in the raffinate phase when experimental data of the concentration of indoline in the raffinate phase is actually much lower. This caused the higher value of RMSD for COSMO-RS prediction for the system containing indoline compared to other systems. Finally, the values of *D* and *S* for [EMPY][EtSO₄] towards aromatic nitrogen compounds at 5 wt.% solute concentration in the feed mixture follows the order: **pyrrole>indoline> quinoline>pyridine**.

4.3.4 Systems with IL [EMIM][MeSO₃]

The concentrations of [EMIM][MeSO₃], aromatic nitrogen compounds and *n*-hexadecane in the extract and raffinate phases were presented in Tables 4.18 to 4.21. Similarly, the experimental values of the tie-lines as obtained from the NMR spectroscopy were presented together with the tie-lines calculated using NRTL correlation and COSMO-RS prediction. The tables also included the values of distribution coefficient, *D*, and selectivity, *S* at each tie-line.

Table 4.18: Ternary tie-lines for the system [EMIM][MESO₃] (1) + pyrrole (2) + *n*-hexadecane (3) at T=25°C and P_{atm}

IL-rich phase			Hydrocarbon-rich phase			<i>D</i>	<i>S</i>
x'_1	x'_2	x'_3	x''_1	x''_2	x''_3		
Experimental tie-lines							
0.8579	0.1357	0.0064	0.0000	0.0003	0.9997	452.33	70 656
0.7620	0.2361	0.0018	0.0000	0.0005	0.9995	472.20	262 202
0.6806	0.3137	0.0057	0.0000	0.0012	0.9988	261.42	45 808
0.6182	0.3797	0.0022	0.0000	0.0015	0.9985	253.13	114 888
0.5624	0.4367	0.0008	0.0000	0.0019	0.9981	229.84	286 757
0.5130	0.4851	0.0019	0.0000	0.0026	0.9974	186.58	97 943
0.4789	0.5201	0.0010	0.0000	0.0029	0.9971	179.34	178 825
0.4472	0.5515	0.0013	0.0000	0.0032	0.9968	172.34	132 095
0.4126	0.5866	0.0008	0.0000	0.0036	0.9964	162.94	202 947
0.3890	0.6101	0.0009	0.0000	0.0041	0.9959	148.80	164 661
NRTL-calculated tie-lines							
0.8640	0.1358	0.0002	0.0006	0.0003	0.9991	452.67	2 261 296
0.7634	0.2363	0.0004	0.0005	0.0005	0.9989	472.60	1 180 200
0.6832	0.3162	0.0005	0.0004	0.0009	0.9987	351.33	701 753
0.6165	0.3827	0.0007	0.0004	0.0012	0.9984	318.92	454 866
0.5651	0.4340	0.0009	0.0003	0.0016	0.9981	271.25	300 816
0.5203	0.4787	0.0010	0.0003	0.0019	0.9978	251.95	251 393
0.4819	0.5169	0.0012	0.0002	0.0023	0.9975	224.74	186 814
0.4491	0.5495	0.0013	0.0002	0.0026	0.9972	211.35	162 119
0.4192	0.5793	0.0015	0.0002	0.0030	0.9969	193.10	128 334
0.3941	0.6043	0.0016	0.0001	0.0033	0.9965	183.12	114 050
COSMO-RS predicted tie-lines							
0.8607	0.1390	0.0003	0.0000	0.0007	0.9993	198.57	661 441
0.7613	0.2386	0.0001	0.0000	0.0017	0.9983	140.35	1 401 143
0.6841	0.3158	0.0001	0.0000	0.0029	0.9971	108.90	1 085 808
0.6199	0.3800	0.0001	0.0000	0.0043	0.9957	88.37	879 921
0.5673	0.4326	0.0000	0.0000	0.0058	0.9942	74.59	741 536
0.5209	0.4790	0.0000	0.0000	0.0075	0.9925	63.87	633 877
0.4828	0.5171	0.0000	0.0000	0.0091	0.9908	56.82	563 014
0.4498	0.5501	0.0000	0.0000	0.0109	0.9891	50.47	499 178
0.4208	0.5792	0.0000	0.0000	0.0126	0.9874	45.97	453 891
0.3953	0.6046	0.0001	0.0000	0.0144	0.9856	41.99	413 815

Table 4.19: Ternary tie-lines for the system [EMIM][MESO₃] (1) + pyridine (2) + *n*-hexadecane (3) at T=25°C and P_{atm}

IL-rich phase			Hydrocarbon-rich phase			<i>D</i>	<i>S</i>
x'_1	x'_2	x'_3	x''_1	x''_2	x''_3		
Experimental tie-lines							
0.8805	0.1159	0.0035	0.0000	0.0180	0.9820	6.46	1 800
0.8194	0.1787	0.0020	0.0000	0.0694	0.9306	2.57	1 225
0.7537	0.2445	0.0018	0.0000	0.1050	0.8950	2.33	1 134
0.6919	0.3070	0.0012	0.0000	0.1363	0.8637	2.25	1 643
0.6431	0.3558	0.0011	0.0000	0.1703	0.8297	2.09	1 636
0.5917	0.4074	0.0008	0.0000	0.2042	0.7958	2.00	1 891
0.5580	0.4413	0.0007	0.0000	0.2291	0.7709	1.93	1 989
0.5264	0.4728	0.0008	0.0000	0.2548	0.7452	1.86	1 661
0.5082	0.4905	0.0013	0.0000	0.2885	0.7115	1.70	897
0.4727	0.5265	0.0008	0.0000	0.3202	0.6798	1.64	1 412
NRTL-calculated tie-lines							
0.9026	0.0971	0.0002	0.0007	0.0336	0.9656	2.89	13 952
0.8262	0.1733	0.0005	0.0008	0.0657	0.9335	2.64	4 925
0.7622	0.2369	0.0010	0.0008	0.0970	0.9021	2.44	2 203
0.7054	0.2932	0.0015	0.0009	0.1288	0.8703	2.28	1 321
0.6559	0.3420	0.0021	0.0010	0.1599	0.8391	2.14	855
0.6101	0.3871	0.0028	0.0011	0.1922	0.8068	2.01	580
0.5708	0.4257	0.0035	0.0012	0.2231	0.7757	1.91	423
0.5353	0.4604	0.0043	0.0013	0.2543	0.7444	1.81	313
0.5033	0.4916	0.0051	0.0014	0.2863	0.7123	1.72	240
0.4745	0.5195	0.0060	0.0016	0.3204	0.6780	1.62	183
COSMO-RS predicted tie-lines							
0.9025	0.0970	0.0005	0.0000	0.0338	0.9662	2.87	5 546
0.8265	0.1731	0.0004	0.0000	0.0659	0.9341	2.63	6 134
0.7622	0.2375	0.0003	0.0000	0.0959	0.9041	2.48	7 463
0.7041	0.2956	0.0003	0.0000	0.1239	0.8761	2.39	6 967
0.6528	0.3469	0.0003	0.0000	0.1486	0.8514	2.33	6 625
0.6047	0.3951	0.0003	0.0000	0.1709	0.8290	2.31	6 388
0.5630	0.4367	0.0003	0.0000	0.1890	0.8110	2.31	6 246
0.5253	0.4744	0.0003	0.0000	0.2040	0.7960	2.33	6 170
0.4912	0.5084	0.0004	0.0000	0.2162	0.7838	2.35	4 608
0.4606	0.5390	0.0004	0.0000	0.2259	0.7740	2.39	4 617

Table 4.20: Ternary tie-lines for the system [EMIM][MESO₃] (1) + indoline (2) + *n*-hexadecane (3) at T=25°C and P_{atm}

IL-rich phase			Hydrocarbon-rich phase			<i>D</i>	<i>S</i>
<i>x</i> ' ₁	<i>x</i> ' ₂	<i>x</i> ' ₃	<i>x</i> '' ₁	<i>x</i> '' ₂	<i>x</i> '' ₃		
Experimental tie-lines							
0.9057	0.0841	0.0101	0.0000	0.0035	0.9965	24.03	2 371
0.8499	0.1468	0.0033	0.0000	0.0077	0.9923	19.06	5 733
0.7894	0.2094	0.0013	0.0000	0.0115	0.9885	18.21	13 846
0.7401	0.2579	0.0020	0.0000	0.0148	0.9852	17.43	8 584
0.6932	0.3032	0.0036	0.0000	0.0180	0.9820	16.84	4 595
0.6505	0.3484	0.0011	0.0000	0.0192	0.9808	18.15	16 179
0.6215	0.3771	0.0014	0.0000	0.0235	0.9765	16.05	11 193
0.5898	0.4087	0.0015	0.0000	0.0256	0.9744	15.96	10 371
0.5607	0.4385	0.0008	0.0000	0.0279	0.9721	15.72	1 736
0.5361	0.4626	0.0013	0.0000	0.0295	0.9705	15.68	11 707
NRTL-calculated tie-lines							
0.9189	0.0811	0.0001	0.0007	0.0026	0.9967	31.19	310 894
0.8538	0.1462	0.00005	0.0006	0.0052	0.9941	28.12	558 990
0.7978	0.2021	0.00004	0.0006	0.0080	0.9914	25.26	626 131
0.7463	0.2537	0.00004	0.0006	0.0110	0.9884	23.06	569 902
0.7019	0.2980	0.00004	0.0005	0.0141	0.9854	21.13	520 655
0.6630	0.3370	0.00004	0.0005	0.0172	0.9823	19.59	481 156
0.6276	0.3723	0.00003	0.0005	0.0203	0.9792	18.34	598 614
0.5962	0.4038	0.00003	0.0005	0.0235	0.9760	17.18	559 020
0.5665	0.4335	0.00003	0.0005	0.0268	0.9727	16.18	524 460
0.5415	0.4584	0.00003	0.0004	0.0299	0.9697	15.33	495 ,552
COSMO-RS predicted tie-lines							
0.9268	0.0727	0.0005	0.0000	0.0137	0.9863	5.31	10 468
0.8692	0.1305	0.0003	0.0000	0.0300	0.9700	4.35	14 065
0.8189	0.1808	0.0003	0.0000	0.0477	0.9523	3.79	12 032
0.7715	0.2283	0.0002	0.0000	0.0667	0.9332	3.42	15 971
0.7293	0.2705	0.0002	0.0000	0.0850	0.9150	3.18	14 559
0.6909	0.3089	0.0003	0.0000	0.1020	0.8979	3.03	9 064
0.6550	0.3447	0.0003	0.0000	0.1180	0.8819	2.92	8 587
0.6221	0.3776	0.0003	0.0000	0.1325	0.8675	2.85	8 241
0.5903	0.4093	0.0004	0.0001	0.1459	0.8540	2.81	5 989
0.5628	0.4367	0.0004	0.0001	0.1571	0.8428	2.78	5 857

Table 4.21: Ternary tie-lines for the system [EMIM][MESO₃] (1) + quinoline (2) + *n*-hexadecane (3) at T=25°C and P_{atm}

IL-rich phase			Hydrocarbon-rich phase			<i>D</i>	<i>S</i>
<i>x</i> ' ₁	<i>x</i> ' ₂	<i>x</i> ' ₃	<i>x</i> '' ₁	<i>x</i> '' ₂	<i>x</i> '' ₃		
Experimental tie-lines							
0.9323	0.0617	0.0060	0.0000	0.0148	0.9852	4.17	685
0.8807	0.1176	0.0017	0.0000	0.0280	0.9720	4.20	2 401
0.8407	0.1581	0.0012	0.0000	0.0414	0.9586	3.82	3 051
0.8058	0.1931	0.0011	0.0000	0.0576	0.9424	3.36	2 883
0.7516	0.2472	0.0012	0.0000	0.0719	0.9281	3.44	2 659
0.7122	0.2868	0.0010	0.0000	0.0876	0.9124	3.27	2 987
0.6783	0.3206	0.0012	0.0000	0.1055	0.8945	3.04	2 265
0.6427	0.3556	0.0017	0.0000	0.1197	0.8803	2.97	1 538
0.6163	0.3816	0.0020	0.0000	0.1294	0.8706	2.95	1 284
0.5949	0.4036	0.0015	0.0000	0.1422	0.8578	2.84	1 623
NRTL-calculated tie-lines							
0.9347	0.0651	0.0002	0.0007	0.0166	0.9826	3.92	19 267
0.8816	0.1181	0.0003	0.0008	0.0317	0.9675	3.73	12 015
0.8322	0.1673	0.0005	0.0008	0.0471	0.9521	3.55	6 764
0.7850	0.2142	0.0008	0.0008	0.0630	0.9362	3.40	3 979
0.7437	0.2552	0.0011	0.0008	0.0778	0.9214	3.28	2 748
0.7057	0.2929	0.0014	0.0009	0.0921	0.9070	3.18	2 060
0.6703	0.3279	0.0018	0.0009	0.1060	0.8931	3.09	1 535
0.6369	0.3609	0.0022	0.0009	0.1196	0.8795	3.02	1 206
0.6075	0.3898	0.0027	0.0010	0.1318	0.8672	2.96	950
0.5790	0.4178	0.0032	0.0010	0.1438	0.8552	2.91	776
COSMO-RS predicted tie-lines							
0.9383	0.0613	0.0005	0.0000	0.0215	0.9785	2.85	5 580
0.8906	0.1091	0.0003	0.0000	0.0446	0.9554	2.45	7 790
0.8467	0.1531	0.0003	0.0000	0.0703	0.9297	2.18	6 749
0.8045	0.1952	0.0002	0.0000	0.0979	0.9021	1.99	8 993
0.7669	0.2329	0.0002	0.0000	0.1242	0.8757	1.88	8 211
0.7313	0.2685	0.0002	0.0000	0.1497	0.8503	1.79	7 625
0.6971	0.3027	0.0002	0.0000	0.1738	0.8261	1.74	7 194
0.6635	0.3363	0.0002	0.0000	0.1964	0.8036	1.71	6 880
0.6328	0.3669	0.0002	0.0000	0.2151	0.7849	1.71	6 694
0.6022	0.3976	0.0003	0.0000	0.2313	0.7686	1.72	4 404

In all of the ternary systems containing [EMIM][MeSO₃], there were minimal cross-contamination between the extract and raffinate phases as indicated by the minute concentration of hydrocarbon present in the extract phase. For instance, Table 4.18 shows that the concentration of *n*-hexadecane in the extract phase of the system [EMIM][MeSO₃] (1) + pyrrole (2) + *n*-hexadecane (3) ranges between 0.0008 and 0.0064. The system [EMIM][MeSO₃] (1) + indoline (2) + *n*-hexadecane (3) reported the highest concentration of *n*-hexadecane in the extract phase i.e. 0.01 which can still be considered insignificant for cross-contamination.

Similar to [EMIM][EtSO₄] and [EMPY][EtSO₄], [EMIM][MeSO₃] reported greater than unity D and S values for all four nitrogen compounds, which indicates that it has better affinity towards all of the aromatic nitrogen compounds than towards the n -hexadecane. [EMIM][MeSO₃] is also an effective solvent for use in separation of both neutral and basic aromatic nitrogen compounds from model diesel fuel based on the reported values of D and S , with higher values of D and S reported for neutral nitrogen compounds and even exceptionally higher values reported for pyrrole in comparison to the rest of nitrogen compounds.

Figures 4.26 a) to d) presents the ternary LLE phase diagrams for systems containing [EMIM][MeSO₃] where the tie-lines are drawn from experimental values, NRTL correlation and COSMO-RS predicted values. All of the ternary phase diagrams exhibit Type 1 phase behaviour where there is only one immiscibility region and one of the binary systems exhibiting partial immiscibility.

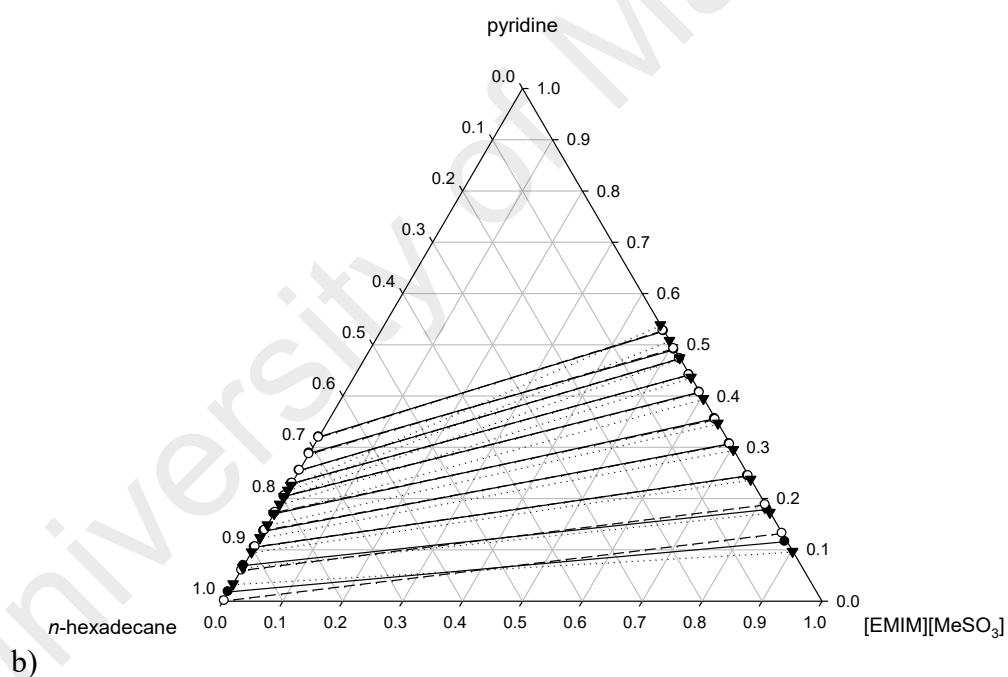
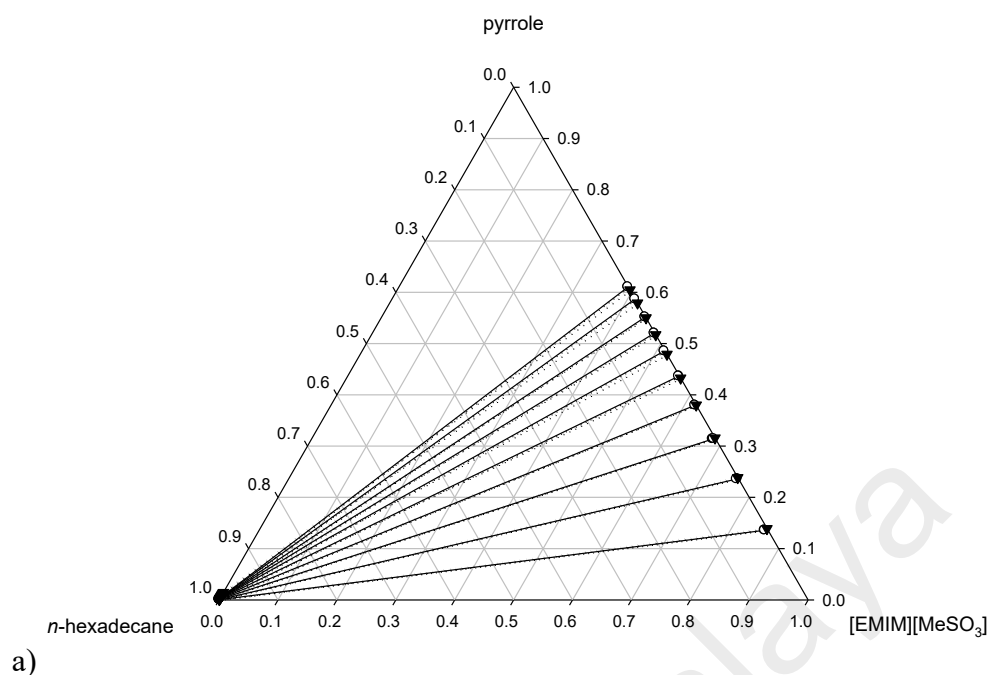


Figure 4.26: Tie-lines for the ternary system a) [EMIM][MeSO₃] (1) + pyrrole (2) + *n*-hexadecane (3), b) [EMIM][MeSO₃] (1) + pyridine (2) + *n*-hexadecane (3) c) [EMIM][MeSO₃] (1) + indoline (2) + *n*-hexadecane (3) and d) [EMIM][MeSO₃] (1) + quinoline (2) + *n*-hexadecane (3) at $T=298.15$ K and P_{atm} . Full circle and solid lines indicate experimental tie-lines, empty circle and dashed lines indicate tie-lines from NRTL calculation, and full triangle and dotted lines indicate calculated tie-lines from COSMO-RS model.

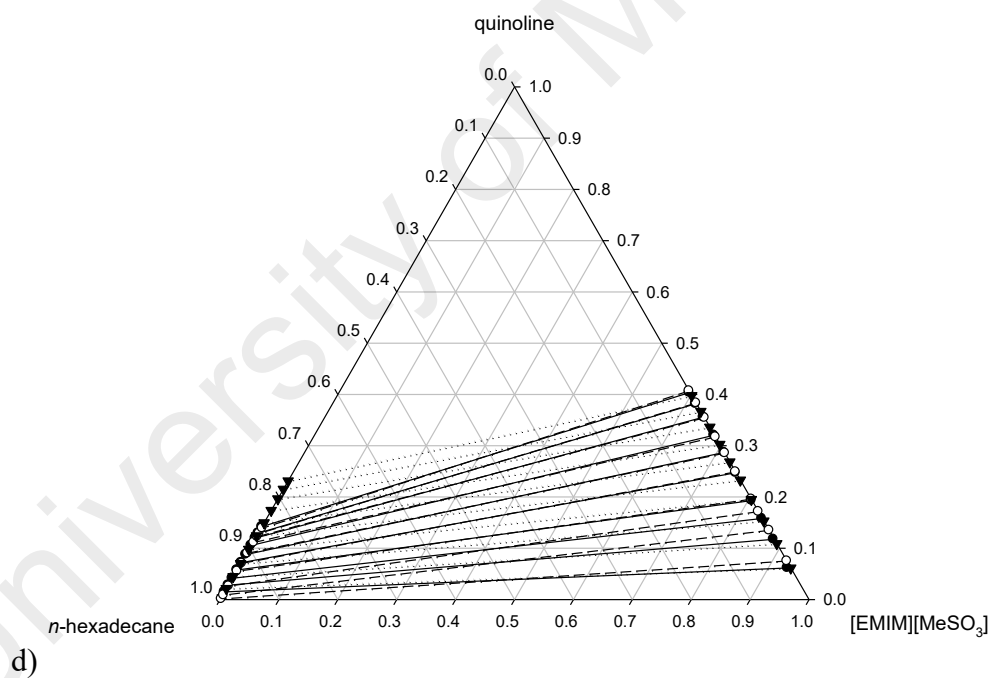
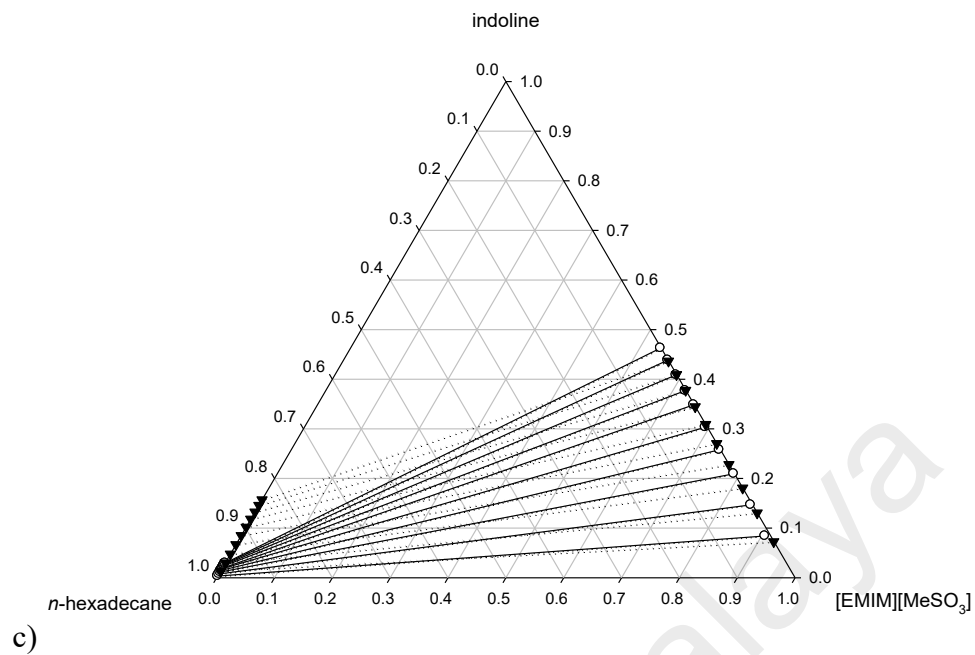


Figure 4.26, continued.

As indicated by the positive slope of all of the tie-lines, small amount of [EMIM][MeSO₃] is sufficient to separate the nitrogen compounds from *n*-hexadecane. As observed in Figures 4.26 a) and c) to Figures 4.26 b) and d), in the systems [EMIM][MeSO₃] (1) + pyrrole (2) + *n*-hexadecane (3) and [EMIM][MeSO₃] (1) +

indoline (2) + *n*-hexadecane (3), the concentration of pyrrole and indoline in the raffinate phase is smaller than the concentration of pyridine and quinoline in the raffinate phase for the systems [EMIM][MeSO₃] (1) + pyridine (2) + *n*-hexadecane (3) and [EMIM][MeSO₃] (1) + quinoline (2) + *n*-hexadecane (3). This indicates that higher amount of [EMIM][MeSO₃] is required to remove these basic nitrogen compounds from *n*-hexadecane as the concentration of pyridine and quinoline increases, whereas for pyrrole and indole as the neutral nitrogen compounds, increase in the pyrrole and indole concentrations in the feed mixture does not require significantly higher amount of [EMIM][MeSO₃] to remove them from *n*-hexadecane effectively.

RMSD values were used to evaluate the goodness of fit of NRTL correlation and COSMO-RS prediction with the experimental tie-lines and is presented in Table 4.22 whereas the binary interaction parameters of NRTL correlation for [EMIM][MeSO₃] and nitrogen compounds and *n*-hexadecane were shown in Table 4.23.

Table 4.22: RMSD values for NRTL correlation and COSMO-RS prediction of ternary LLE systems containing the IL [EMIM][MeSO₃]

System	RMSD	
	NRTL	COSMO-RS
[EMIM][MeSO ₃] (1) + pyrrole (2) + <i>n</i> -hexadecane (3)	0.27%	0.44%
[EMIM][MeSO ₃] (1) + pyridine (2) + <i>n</i> -hexadecane (3)	0.88%	2.69%
[EMIM][MeSO ₃] (1) + indoline (2) + <i>n</i> -hexadecane (3)	0.46%	5.02%
[EMIM][MeSO ₃] (1) + quinoline (2) + <i>n</i> -hexadecane (3)	0.64%	3.51%

Table 4.23: The values of NRTL binary interaction parameters between [EMIM][MeSO₃] and nitrogen compounds and *n*-hexadecane

<i>i</i> – <i>j</i>	τ_{ij}	τ_{ji}
[EMIM][MeSO ₃] – pyrrole	-1098.2	918.5
[EMIM][MeSO ₃] – pyridine	-312.1	1417.0
[EMIM][MeSO ₃] – indoline	-952.6	848.6
[EMIM][MeSO ₃] – quinoline	-364.7	1202.4
[EMIM][MeSO ₃] – <i>n</i> -hexadecane	2352.9	1682.4

The interaction parameters between nitrogen compounds and *n*-hexadecane were taken from the values obtained in the regression of ternary systems containing [EMIM][EtSO₄]. NRTL and COSMO-RS models provided ternary tie lines which are in good agreement with experimental data except for COSMO-RS prediction for the system [EMIM][MeSO₃] (1) + indoline (2) + *n*-hexadecane (3). In this system, COSMO-RS model predicted higher concentrations of indoline in the raffinate phase than what were obtained experimentally. Thus, higher value of RMSD for COSMO-RS prediction for the system containing indoline is reported in comparison to other systems. Based on the values of *D* and *S* for [EMIM][MeSO₃] towards aromatic nitrogen compounds, the extraction effectiveness follows the order: **pyrrole>indoline>pyridine >quinoline**.

4.3.5 Systems with IL [EMIM][EtSO₄] + [EMPY][EtSO₄]

The practice of mixing conventional solvents for extraction of aromatic compounds is commonly used in the industry (Lababidi et al., 2006). On the other hand, the concept of mixing ILs for aromatic extraction is rather new and was only introduced by Garcia et al. in 2012 where the performance of binary mixtures of N-butylpyridinium tetrafluoroborate and N-butylpyridinium bis(trifluoromethylsulfonyl)imide was investigated to extract aromatics from aliphatic hydrocarbons (Garcia et al., 2011). They reported that mixing of two ILs with different extractive properties led to selectivity and capacity values which are between the values obtained when using the pure ILs.

In this work, the ternary LLE experiments using the mixed ILs [EMIM][EtSO₄] and [EMPY][EtSO₄] at 1:1 mass ratio of each IL were conducted to investigate the effect of mixing ILs of 5-membered and 6-membered cation ring structure towards the extraction effectiveness of indoline and quinoline. Both indoline and quinoline have more than one ring their chemical structure. In indoline, a benzene ring is attached to the 5-membered ring of the heterocyclic nitrogen part whereas in quinoline, a benzene ring is attached to the 6-membered ring of the heterocyclic nitrogen part. The cation [EMIM] in

[EMIM][EtSO₄] is a 5-membered ring cation whereas the cation [EMPY] in [EMPY][EtSO₄] is a 6-membered ring cation. It was hypothesized that mixing of the ILs [EMIM][EtSO₄] and [EMPY][EtSO₄] would improve the extraction efficiency i.e. report higher values of *D* and *S* of indoline and quinoline due to similarity on the structures of these two nitrogen compounds to the cations of the mixed ILs. The ternary LLE results are presented in Tables 4.24 and 4.25 where the experimental ternary tie lines obtained from analysis of NMR spectroscopy were reported along with ternary tie lines obtained from NRTL correlation and COSMO-RS prediction. The calculated values of *D* and *S* were also included in the tables.

University of Malaya

Table 4.24: Ternary tie-lines for the system [EMIM][EtSO₄] + [EMPY][EtSO₄] (1) + indoline (2) + *n*-hexadecane (3) at T=25°C and P_{atm}

IL-rich phase			Hydrocarbon-rich phase			<i>D</i>	<i>S</i>
x'_1	x'_2	x'_3	x''_1	x''_2	x''_3		
Experimental tie-lines							
0.8867	0.1067	0.0066	0.0000	0.0026	0.9974	41.04	6 202
0.8231	0.1713	0.0056	0.0000	0.0057	0.9943	30.05	5 336
0.7726	0.2227	0.0047	0.0000	0.0082	0.9918	27.16	5 731
0.7134	0.2846	0.0020	0.0000	0.0119	0.9881	23.92	11 935
0.6720	0.3254	0.0026	0.0000	0.0152	0.9848	21.41	8 109
0.6266	0.3711	0.0023	0.0000	0.0178	0.9822	20.85	8 903
0.5831	0.4154	0.0015	0.0000	0.0200	0.9800	20.77	13 570
0.5540	0.4448	0.0012	0.0000	0.0229	0.9771	19.42	15,816
0.5243	0.4746	0.0011	0.0000	0.0275	0.9725	17.26	15 258
0.4971	0.5010	0.0019	0.0000	0.0285	0.9715	17.58	8 988
NRTL-calculated tie-lines							
0.9049	0.0950	0.0001	0.0006	0.0024	0.9970	39.58	394 646
0.8330	0.1669	0.00005	0.0006	0.0048	0.9947	34.77	691 731
0.7709	0.2291	0.00004	0.0005	0.0074	0.9921	30.96	767 872
0.7164	0.2835	0.00004	0.0005	0.0102	0.9893	38.31	947 522
0.6681	0.3318	0.00004	0.0005	0.0132	0.9863	27.79	685 ,333
0.6269	0.3731	0.00003	0.0004	0.0163	0.9833	22.89	750 244
0.5895	0.4104	0.00003	0.0004	0.0195	0.9801	21.05	687 578
0.5570	0.4430	0.00003	0.0004	0.0227	0.9769	19.52	635 487
0.5272	0.4728	0.00003	0.0004	0.0260	0.9736	18.18	590 151
0.5002	0.4998	0.00003	0.0003	0.0294	0.9703	17.00	549 837
COSMO-RS predicted tie-lines							
0.9224	0.0775	0.0002	0.0001	0.0226	0.9773	3.43	16 757
0.8610	0.1389	0.0002	0.0001	0.0435	0.9564	3.19	15,269
0.8051	0.1947	0.0002	0.0001	0.0641	0.9359	3.04	14 214
0.7536	0.2462	0.0002	0.0001	0.0838	0.9161	3.15	14 441
0.7060	0.2937	0.0003	0.0001	0.1023	0.8976	2.87	8 590
0.6633	0.3364	0.0003	0.0001	0.1188	0.8811	3.01	8 837
0.6237	0.3759	0.0004	0.0001	0.1338	0.8661	2.81	6 083
0.5881	0.4115	0.0005	0.0002	0.1469	0.8529	2.80	4 778
0.5548	0.4447	0.0006	0.0002	0.1589	0.8409	2.80	3 922
0.5242	0.4751	0.0007	0.0002	0.1696	0.8303	2.80	3 323

Table 4.25: Ternary tie-lines for the system [EMIM][EtSO₄] + [EMPY][EtSO₄] (1) + quinoline (2) + *n*-hexadecane (3) at T=25°C and P_{atm}

IL-rich phase			Hydrocarbon-rich phase			<i>D</i>	<i>S</i>
<i>x</i> ' ₁	<i>x</i> ' ₂	<i>x</i> ' ₃	<i>x</i> '' ₁	<i>x</i> '' ₂	<i>x</i> '' ₃		
Experimental tie-lines							
0.9205	0.0646	0.0149	0.0000	0.0186	0.9814	3.47	229
0.8598	0.1358	0.0044	0.0000	0.0401	0.9599	3.39	739
0.8076	0.1893	0.0032	0.0000	0.0536	0.9464	3.53	1 045
0.7601	0.2362	0.0038	0.0000	0.0796	0.9204	2.97	719
0.7219	0.2757	0.0023	0.0000	0.1014	0.8986	2.72	1 062
0.6820	0.3166	0.0013	0.0000	0.1069	0.8931	2.96	2 035
0.6360	0.3594	0.0046	0.0000	0.1269	0.8731	2.83	538
0.6075	0.3902	0.0023	0.0000	0.1378	0.8622	2.83	1 061
0.5751	0.4224	0.0025	0.0000	0.1485	0.8515	2.84	969
0.5490	0.4491	0.0019	0.0000	0.1605	0.8395	2.80	1 236
NRTL-calculated tie-lines							
0.9299	0.0699	0.0002	0.0007	0.0202	0.9791	3.46	16 940
0.8670	0.1327	0.0004	0.0008	0.0401	0.9591	3.31	7 935
0.8114	0.1880	0.0006	0.0008	0.0591	0.9401	3.18	4 984
0.7621	0.2369	0.0009	0.0009	0.0768	0.9223	3.08	3 161
0.7180	0.2807	0.0013	0.0009	0.0934	0.9057	3.01	2 094
0.6751	0.3231	0.0018	0.0009	0.1100	0.8891	2.94	1 451
0.6395	0.3582	0.0023	0.0010	0.1239	0.8751	2.89	1 100
0.6005	0.3966	0.0029	0.0010	0.1393	0.8597	2.85	844
0.5681	0.4283	0.0036	0.0011	0.1518	0.8471	2.82	664
0.5377	0.4580	0.0043	0.0011	0.1633	0.8355	2.80	545
COSMO-RS predicted tie-lines							
0.9391	0.0608	0.0001	0.0001	0.0261	0.9738	2.33	22 685
0.8797	0.1201	0.0001	0.0001	0.0539	0.9460	2.23	21 079
0.8311	0.1687	0.0002	0.0001	0.0772	0.9227	2.19	10 082
0.7804	0.2194	0.0002	0.0001	0.1010	0.8989	2.17	9 763
0.7358	0.2640	0.0002	0.0001	0.1206	0.8792	2.19	9 623
0.6951	0.3047	0.0002	0.0001	0.1370	0.8629	2.22	9 596
0.6535	0.3463	0.0003	0.0001	0.1517	0.8482	2.28	6 454
0.6154	0.3843	0.0003	0.0001	0.1631	0.8368	2.36	6 572
0.5820	0.4176	0.0004	0.0001	0.1714	0.8285	2.44	5 046
0.5511	0.4484	0.0005	0.0001	0.1776	0.8222	2.52	4 152

Similar to ternary systems with individual ILs [EMIM][EtSO₄] and [EMPY][EtSO₄], the concentration of *n*-hexadecane in the extract phase is minute indicating minimal cross contamination between the extract and raffinate phases. From the values of *D* and *S* reported for the mixed ILs, mixing the IL at 1:1 mass ratio of [EMIM][EtSO₄] and [EMPY][EtSO₄] does not give significant improvement of extraction performance. However, noticeable improvement can be observed for the

extraction of indoline using the mixed ILs, where the values of D and S reported using the mixed ILs [EMIM][EtSO₄] and [EMPY][EtSO₄] is noticeably higher than those using individual ILs. The values of D and S of indoline follows the order: mixed ([EMIM][EtSO₄] + [EMPY][EtSO₄]) > [EMPY][EtSO₄] > [EMIM][EtSO₄]. Whereas, mixing the ILs [EMIM][EtSO₄] and [EMPY][EtSO₄] for the extraction of quinoline only give the resulting D and S in the middle between those of [EMPY][EtSO₄] and [EMIM][EtSO₄], with the values of D and S following the order: [EMPY][EtSO₄] > mixed ([EMIM][EtSO₄] + [EMPY][EtSO₄]) > [EMIM][EtSO₄].

The ternary LLE phase diagrams for the systems containing mixed ILs [EMIM][EtSO₄] and [EMPY][EtSO₄] were presented by Figures 4.27 a) and b), where the tie-lines are drawn from experimental values, NRTL correlation and COSMO-RS predicted values. Both ternary phase diagrams exhibit the behaviour of Type 1 phase behaviour where there is only one immiscibility region and one of the binary systems exhibiting partial immiscibility.

The positive slope of all tie-lines indicates that small amount of solvent is sufficient to separate the nitrogen compounds from *n*-hexadecane. Table 4.26 shows the RMSD values which measures the goodness of fit of NRTL correlation and COSMO-RS prediction with the experimental tie-lines and Table 4.27 presents the binary interaction parameters of NRTL correlation between the mixed ILs and nitrogen compounds and *n*-hexadecane.

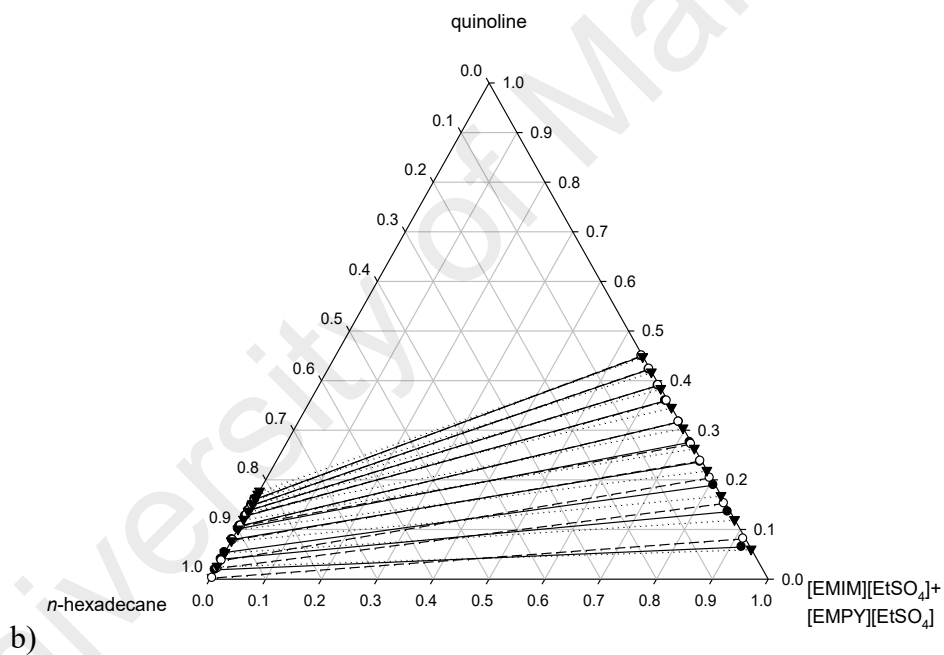
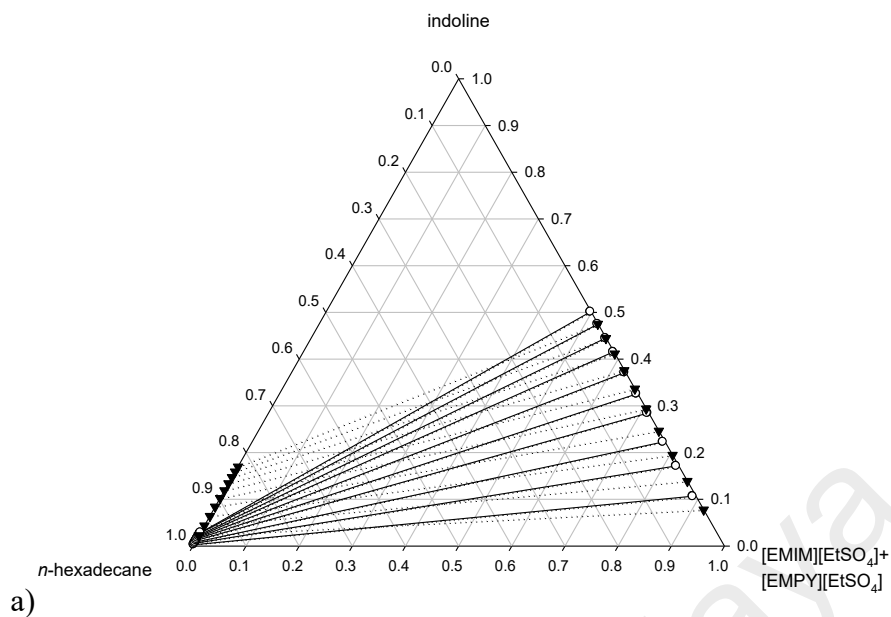


Figure 4.27: Tie-lines for the ternary system a) ([EMIM][EtSO₄] + [EMPY][EtSO₄] (1) + indoline (2) + *n*-hexadecane (3) and b) ([EMIM][EtSO₄] + [EMPY][EtSO₄] (1) + quinoline (2) + *n*-hexadecane (3) at $T=298.15$ K and P_{atm} . Full circle and solid lines indicate experimental tie-lines, empty circle and dashed lines indicate tie-lines from NRTL calculation, and full triangle and dotted lines indicate calculated tie-lines from COSMO-RS model.

Table 4.26: RMSD values for NRTL correlation and COSMO-RS prediction of ternary LLE system containing the mixed ILs [EMIM][EtSO₄]+[EMPY][EtSO₄]

System	RMSD	
	NRTL	COSMO-RS
[EMIM][EtSO ₄]+[EMPY][EtSO ₄] (1) + indoline (2) + <i>n</i> -hexadecane (3)	0.40%	5.92%
[EMIM][EtSO ₄]+[EMPY][EtSO ₄] (1) + quinoline (2) + <i>n</i> -hexadecane (3)	0.46%	1.50%

Table 4.27: The values of NRTL binary interaction parameters between the mixed ILs [EMIM][EtSO₄]+ [EMPY][EtSO₄] and nitrogen compounds and *n*-hexadecane

<i>i-j</i>	τ_{ij}	τ_{ji}
([EMIM][EtSO ₄] + [EMPY][EtSO ₄]) – indoline	-1029.8	824.0
([EMIM][EtSO ₄] + [EMPY][EtSO ₄]) – quinoline	-311.2	1076.0
([EMIM][EtSO ₄] + [EMPY][EtSO ₄]) – <i>n</i> -hexadecane	2349.5	1701.9

Again, the values of NRTL interaction parameters for nitrogen compounds and *n*-hexadecane are kept constant as obtained from previous regression of the ternary systems containing one IL. The tie-lines calculated using NRTL and COSMO-RS models have good agreement with experimental data. Similar to ternary systems in previous sections, the COSMO-RS prediction for the system ([EMIM][EtSO₄]+[EMPY][EtSO₄]) (1) + indoline (2) + *n*-hexadecane (3) shows greater deviation to the experimental tie-lines where the COSMO-RS model predicted higher concentrations of indoline in the raffinate phase than what was obtained experimentally. Therefore, higher value of RMSD for COSMO-RS prediction for the system containing indoline is obtained (5.29%) in comparison with the system containing quinoline (1.50%).

4.3.6 Systems with TBAB/EG (1:2) DES

Tables 4.28 to 4.31 present the ternary LLE tie-lines containing the DES TBAB/EG (1:2) where the concentration of TBAB/EG (1:2), aromatic nitrogen compounds and *n*-hexadecane were reported. The experimental values of the tie-lines as obtained from the NMR spectroscopy were presented together with the tie-lines calculated using NRTL correlation and COSMO-RS prediction along with the values of distribution coefficient, *D*, and selectivity, *S* at each tie-line. Table 4.28 shows the concentration of *n*-hexadecane in the extract phase of the system TBAB/EG (1:2) (1) +

pyrrole (2) + *n*-hexadecane (3) ranging between 0.0023 and 0.0071. It also confirms the absence of TBAB/EG (1:2) in the raffinate phase. This is indicative of minimal cross-contamination between the extract and raffinate phases. Similarly for all other ternary systems, the concentrations of *n*-hexadecane in the extract phase are minute with zero concentration of TBAB/EG (1:2) in the raffinate phase.

TBAB/EG (1:2) also has better affinity towards all of the aromatic nitrogen compounds than towards *n*-hexadecane as indicated by the values of *D* and *S* which are all greater than unity for all four ternary systems. However, *D* and *S* values are higher for neutral nitrogen compounds than for basic nitrogen compounds. These values are exceptionally higher for pyrrole; with the values being two orders of magnitude greater than those reported for other nitrogen compounds. Based on the values of *D* and *S*, TBAB/EG (1:2) is an effective solvent for use in separation of both neutral and basic aromatic nitrogen compounds from model diesel fuel, as expected based on the quantum chemical calculation results.

Table 4.28: Experimental tie-lines for the system TBAB/EG (1:2) (1) + pyrrole (2) + *n*-hexadecane (3) at T=25°C and P_{atm}

Extract phase			Raffinate phase			<i>D</i>	<i>S</i>
x'_1	x'_2	x'_3	x''_1	x''_2	x''_3		
Experimental tie-lines							
0.9035	0.0941	0.0023	0.0000	0.0006	0.9994	156.83	68 147
0.8220	0.1709	0.0071	0.0000	0.0019	0.9981	89.95	12 645
0.7438	0.2516	0.0046	0.0000	0.0032	0.9968	78.63	17 038
0.7009	0.2953	0.0038	0.0000	0.0047	0.9953	62.83	16 456
0.6577	0.3377	0.0046	0.0000	0.0066	0.9934	51.17	11 050
0.6204	0.3752	0.0043	0.0000	0.0088	0.9912	42.64	9 828
0.5763	0.4195	0.0042	0.0000	0.0105	0.9895	39.95	9 413
0.5452	0.4504	0.0044	0.0000	0.0124	0.9876	36.32	8 153
0.5124	0.4853	0.0023	0.0000	0.0157	0.9843	30.91	13 228
0.4878	0.5074	0.0049	0.0000	0.0151	0.9849	33.60	6 754
NRTL-calculated tie-lines							
0.9006	0.0991	0.0002	0.0006	0.0018	0.9976	55.06	274 617
0.8185	0.1809	0.0005	0.0006	0.0036	0.9958	50.25	100 078
0.7494	0.2497	0.0009	0.0005	0.0056	0.9939	44.59	49 241
0.6925	0.3061	0.0014	0.0005	0.0074	0.9921	41.36	29 313
0.6439	0.3543	0.0018	0.0005	0.0092	0.9904	38.51	21 190
0.5996	0.3980	0.0023	0.0004	0.0109	0.9886	36.51	15 695
0.5620	0.4352	0.0028	0.0004	0.0125	0.9871	34.82	12 274
0.5292	0.4674	0.0033	0.0004	0.0140	0.9856	33.39	9 971
0.4997	0.4965	0.0038	0.0004	0.0154	0.9843	32.24	8 351
0.4734	0.5222	0.0043	0.0003	0.0167	0.9830	31.27	7 148
COSMO-RS predicted tie-lines							
0.9011	0.0980	0.0009	0.0001	0.0037	0.9962	26.22	29 752
0.8199	0.1792	0.0009	0.0001	0.0076	0.9923	23.54	26 876
0.7514	0.2477	0.0009	0.0001	0.0116	0.9884	21.41	24 435
0.6950	0.3041	0.0009	0.0001	0.0154	0.9845	19.76	22 454
0.6466	0.3525	0.0009	0.0001	0.0191	0.9808	18.42	20 793
0.6026	0.3965	0.0009	0.0001	0.0230	0.9770	17.27	1 337
0.5651	0.4340	0.0009	0.0001	0.0266	0.9734	16.34	18 142
0.5324	0.4667	0.0009	0.0001	0.0299	0.9700	15.59	17 148
0.5029	0.4962	0.0009	0.0001	0.0332	0.9667	14.94	16 288
0.4766	0.5225	0.0009	0.0001	0.0363	0.9636	14.39	15 557

Table 4.29: Experimental tie-lines for the system TBAB/EG (1:2) (1) + pyridine (2) + *n*-hexadecane (3) at T=25°C and P_{atm}

Extract phase			Raffinate phase			<i>D</i>	<i>S</i>
x'_1	x'_2	x'_3	x''_1	x''_2	x''_3		
Experimental tie-lines							
0.9196	0.0758	0.0046	0.0000	0.0184	0.9816	4.12	879
0.8501	0.1452	0.0048	0.0000	0.0335	0.9665	4.33	873
0.7988	0.1981	0.0031	0.0000	0.0508	0.9492	3.90	1 194
0.7377	0.2572	0.0052	0.0000	0.0656	0.9344	3.92	705
0.7093	0.2879	0.0029	0.0000	0.0895	0.9105	3.22	1 010
0.6675	0.3292	0.0033	0.0000	0.1073	0.8927	3.07	527
0.6280	0.3668	0.0052	0.0000	0.1176	0.8824	3.12	529
0.5892	0.4049	0.0058	0.0000	0.1388	0.8612	2.92	433
0.5532	0.4437	0.0031	0.0000	0.1496	0.8504	2.97	814
0.5293	0.4675	0.0031	0.0000	0.1601	0.8399	2.92	791
NRTL calculated tie-lines							
0.9224	0.0773	0.0002	0.0007	0.0176	0.9817	4.39	21 558
0.8553	0.1442	0.0005	0.0007	0.0355	0.9638	4.06	7 830
0.7974	0.2018	0.0008	0.0008	0.0531	0.9461	3.80	4 494
0.7462	0.2525	0.0013	0.0008	0.0705	0.9287	3.58	2 559
0.6995	0.2986	0.0018	0.0008	0.0878	0.9114	3.40	1 722
0.6600	0.3376	0.0024	0.0008	0.1036	0.8955	3.26	1 216
0.6225	0.3744	0.0031	0.0009	0.1195	0.8796	3.13	889
0.5888	0.4074	0.0038	0.0009	0.1345	0.8646	3.03	689
0.5572	0.4382	0.0046	0.0009	0.1491	0.8500	2.94	543
0.5288	0.4658	0.0054	0.0010	0.1625	0.8365	2.87	444
COSMO-RS Predicted Tie-lines							
0.9261	0.0728	0.0011	0.0005	0.0258	0.9737	2.82	2 454
0.8597	0.1390	0.0014	0.0009	0.0465	0.9526	2.99	2 073
0.8005	0.1978	0.0017	0.0012	0.0628	0.9359	3.15	1 785
0.7475	0.2505	0.0019	0.0015	0.0761	0.9224	3.29	1 560
0.6990	0.2987	0.0023	0.0018	0.0873	0.9109	3.42	1 378
0.6579	0.3395	0.0026	0.0019	0.0962	0.9018	3.53	1 239
0.6193	0.3778	0.0029	0.0021	0.1042	0.8937	3.62	1 120
0.5850	0.4117	0.0032	0.0022	0.1111	0.8866	3.70	1 022
0.5532	0.4433	0.0035	0.0024	0.1174	0.8802	3.78	938
0.5249	0.4713	0.0039	0.0024	0.1230	0.8746	3.83	867

Table 4.30: Experimental tie-lines for the system TBAB/EG (1:2) (1) + indoline (2) + *n*-hexadecane (3) at T=25°C and P_{atm}

Extract phase			Raffinate phase			<i>D</i>	<i>S</i>
x'_1	x'_2	x'_3	x''_1	x''_2	x''_3		
Experimental tie-lines							
0.9447	0.0528	0.0025	0.0000	0.0075	0.9925	7.04	2 795
0.8952	0.1012	0.0036	0.0000	0.0154	0.9846	6.57	1 797
0.8656	0.1311	0.0033	0.0000	0.0252	0.9748	5.20	1 537
0.8079	0.1870	0.0051	0.0000	0.0331	0.9669	5.65	1 071
0.7601	0.2361	0.0038	0.0000	0.0413	0.9587	5.72	1 442
0.7248	0.2707	0.0045	0.0000	0.0482	0.9518	5.62	1 188
0.7016	0.2932	0.0052	0.0000	0.0597	0.9403	4.91	888
0.6749	0.3210	0.0041	0.0000	0.0654	0.9346	4.91	1 119
0.6430	0.3526	0.0044	0.0000	0.0747	0.9253	4.72	993
0.6179	0.3772	0.0049	0.0000	0.0833	0.9167	4.53	847
NRTL calculated tie-lines							
0.9439	0.0558	0.0002	0.0007	0.0074	0.9919	7.54	37 397
0.8933	0.1061	0.0006	0.0007	0.0153	0.9840	6.93	11 373
0.8502	0.1486	0.0011	0.0007	0.0230	0.9763	6.46	5 734
0.8087	0.1894	0.0019	0.0007	0.0313	0.9680	6.05	3 083
0.7724	0.2248	0.0027	0.0008	0.0394	0.9599	5.71	2 028
0.7393	0.2569	0.0038	0.0008	0.0475	0.9517	5.41	1 355
0.7044	0.2905	0.0051	0.0008	0.0569	0.9423	5.11	943
0.6745	0.3191	0.0064	0.0008	0.0657	0.9335	4.86	708
0.6487	0.3435	0.0078	0.0008	0.0739	0.9252	4.65	551
0.6209	0.3697	0.0094	0.0009	0.0835	0.9157	4.43	431
COSMO-RS Predicted tie-lines							
0.9551	0.0439	0.0010	0.0001	0.0279	0.9720	1.57	1 461
0.9128	0.0860	0.0012	0.0001	0.0540	0.9458	1.59	1 235
0.8748	0.1238	0.0014	0.0002	0.0768	0.9230	1.61	1 060
0.8365	0.1619	0.0016	0.0002	0.0990	0.9007	1.63	907
0.8016	0.1966	0.0019	0.0003	0.1187	0.8810	1.66	786
0.7686	0.2293	0.0021	0.0003	0.1367	0.8629	1.68	686
0.7335	0.2641	0.0024	0.0004	0.1552	0.8444	1.70	593
0.7026	0.2947	0.0027	0.0005	0.1710	0.8285	1.72	521
0.6750	0.3219	0.0031	0.0005	0.1846	0.8149	1.74	464
0.6455	0.3511	0.0035	0.0006	0.1987	0.8008	1.77	410

Table 4.31: Experimental tie-lines for the system TBAB/EG (1:2) (1) + quinoline (2) + *n*-hexadecane (3) at T=25°C and P_{atm}

Extract phase			Raffinate phase			<i>D</i>	<i>S</i>
x'_1	x'_2	x'_3	x''_1	x''_2	x''_3		
Experimental tie-lines							
0.9532	0.0454	0.0013	0.0000	0.0094	0.9906	4.83	3 680
0.9106	0.0888	0.0007	0.0000	0.0184	0.9816	4.83	6 768
0.8726	0.1264	0.0011	0.0000	0.0279	0.9721	4.53	4 004
0.8233	0.1757	0.0011	0.0000	0.0378	0.9622	4.65	4 066
0.8032	0.1960	0.0008	0.0000	0.0498	0.9502	3.94	4 675
0.7799	0.2195	0.0006	0.0000	0.0581	0.9419	3.78	5 931
0.7405	0.2585	0.0010	0.0000	0.0686	0.9314	3.77	3 510
0.7165	0.2829	0.0006	0.0000	0.0754	0.9246	3.75	5 782
0.6862	0.3129	0.0009	0.0000	0.0844	0.9156	3.71	3 772
0.6644	0.3348	0.0008	0.0000	0.0939	0.9061	3.57	4 038
NRTL calculated tie-lines							
0.9559	0.0440	0.0001	0.0007	0.0090	0.9903	4.89	48 415
0.9157	0.0841	0.0002	0.0007	0.0181	0.9812	4.65	22 795
0.8792	0.1205	0.0004	0.0007	0.0271	0.9721	4.45	10 806
0.8442	0.1553	0.0005	0.0007	0.0364	0.9628	4.27	8 216
0.8118	0.1875	0.0007	0.0007	0.0457	0.9536	4.10	5 589
0.7829	0.2162	0.0009	0.0008	0.0544	0.9448	3.97	4 172
0.7548	0.2441	0.0012	0.0008	0.0634	0.9358	3.85	3 002
0.7266	0.2719	0.0015	0.0008	0.0729	0.9263	3.73	2 303
0.7015	0.2967	0.0018	0.0008	0.0817	0.9175	3.63	1 851
0.6786	0.3193	0.0021	0.0008	0.0902	0.9090	3.54	1 532
COSMO-RS predicted tie-lines							
0.9629	0.0361	0.0010	0.0003	0.0243	0.9754	1.49	1 414
0.9273	0.0715	0.0012	0.0005	0.0450	0.9545	1.59	1 287
0.8928	0.1058	0.0014	0.0007	0.0621	0.9371	1.70	1 179
0.8582	0.1402	0.0016	0.0009	0.0768	0.9223	1.83	1 085
0.8250	0.1732	0.0018	0.0010	0.0887	0.9102	1.95	1 006
0.7946	0.2035	0.0020	0.0012	0.0979	0.9009	2.08	941
0.7646	0.2332	0.0022	0.0013	0.1056	0.8931	2.21	883
0.7344	0.2631	0.0025	0.0014	0.1121	0.8865	2.35	830
0.7075	0.2898	0.0028	0.0015	0.1171	0.8815	2.48	786
0.6828	0.3142	0.0030	0.0015	0.1209	0.8776	2.60	749

The tie-lines drawn from experimental values, NRTL correlation and COSMO-RS predicted values for the four systems containing TBAB/EG (1:2) were presented by Figures 4.28 a) to d). All of the ternary phase diagram exhibit Type 1 phase behaviour where there is only one immiscibility region and one of the binary systems exhibiting partial immiscibility.

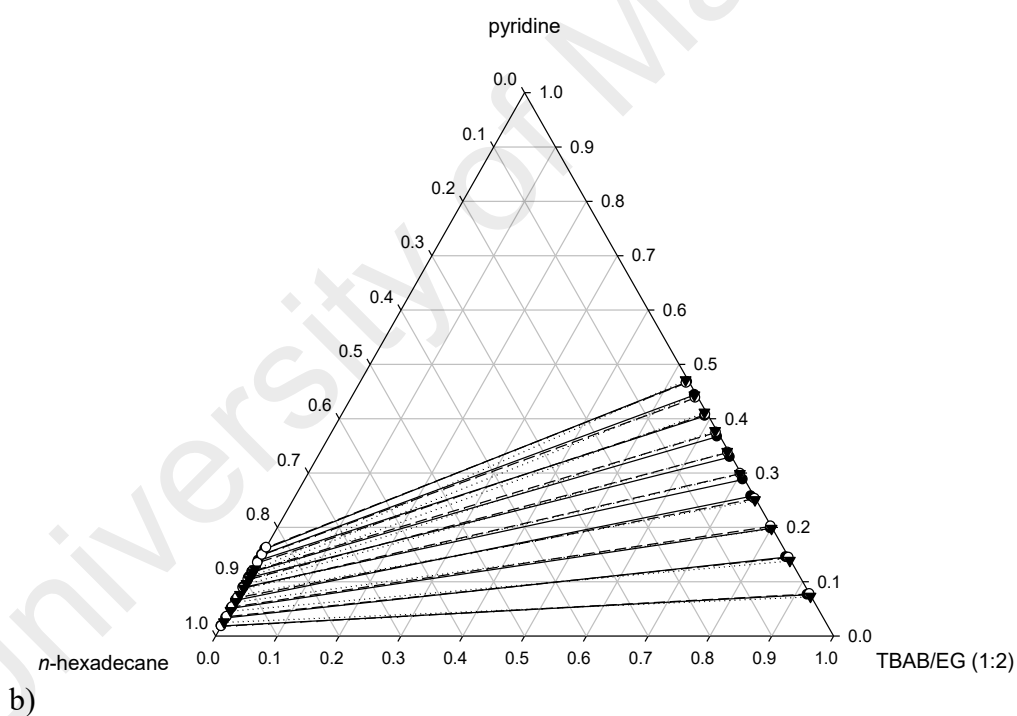
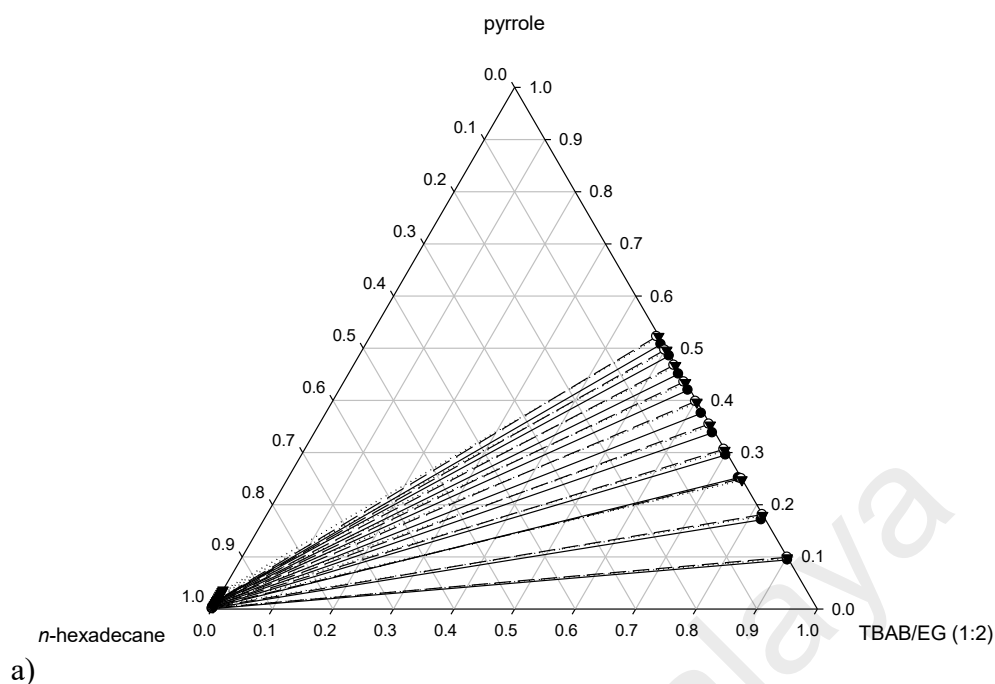


Figure 4.28: Tie-lines for the ternary system a) TBAB/EG (1:2) (1) + pyrrole (2) + *n*-hexadecane (3), b) TBAB/EG (1:2) (1) + pyridine (2) + *n*-hexadecane (3), c) TBAB/EG (1:2) (1) + indoline (2) + *n*-hexadecane (3) and d) TBAB/EG (1:2) (1) + quinoline (2) + *n*-hexadecane (3) at $T=298.15$ K and P_{atm} . Full circle and solid lines indicate experimental tie-lines, empty circle and dashed lines indicate tie-lines from NRTL calculation, and full triangle and dotted lines indicate calculated tie-lines from COSMO-RS model.

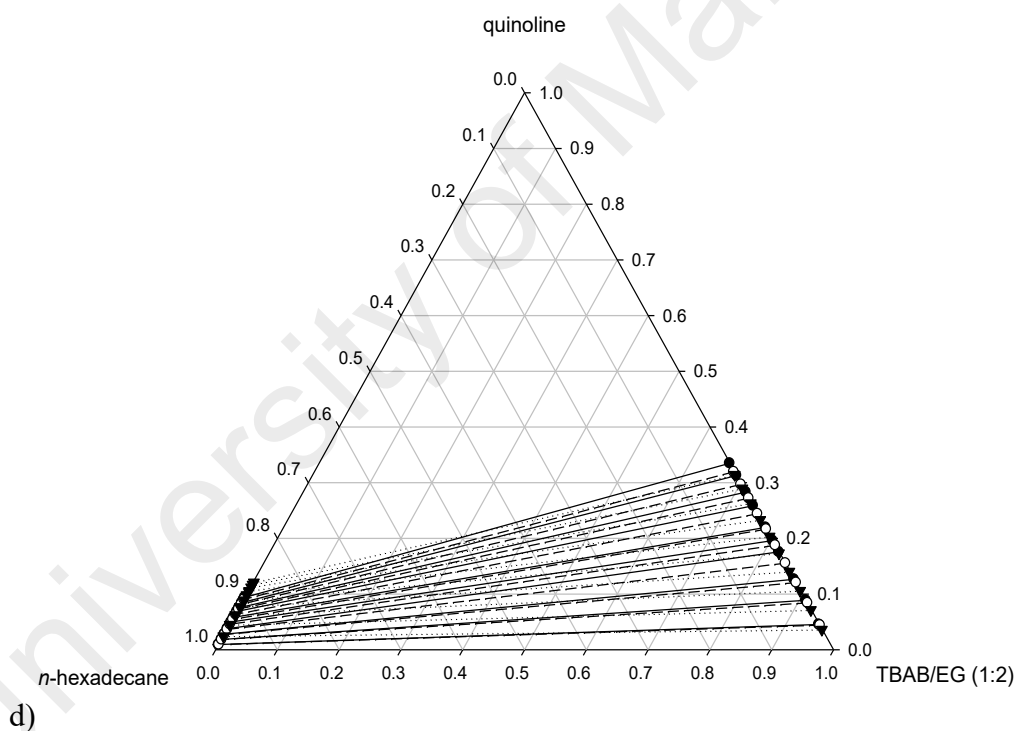
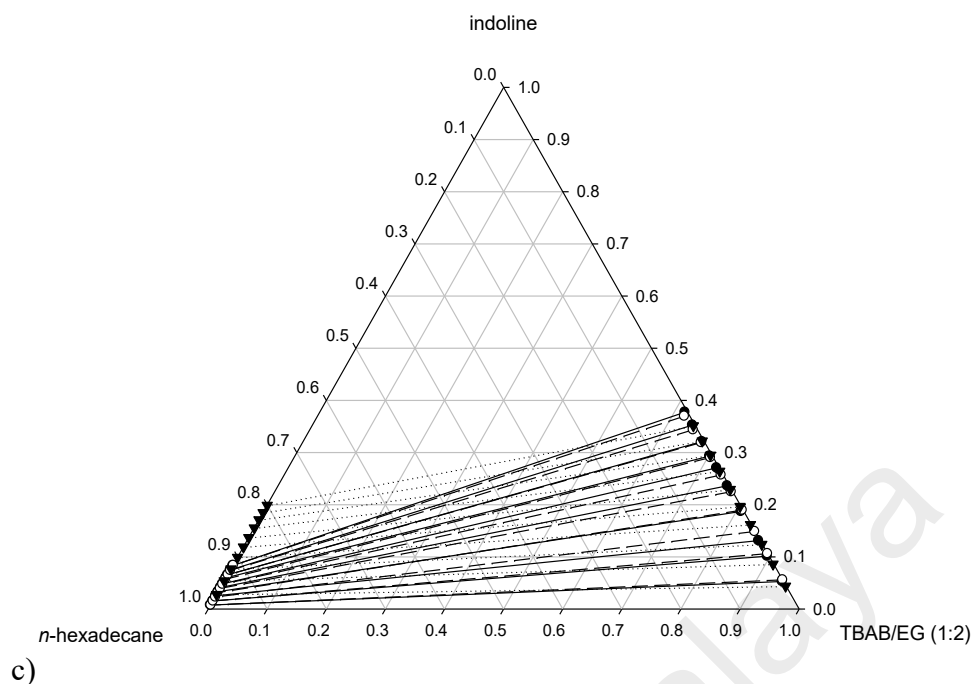


Figure 4.28, continued.

Similar to systems containing ILs, the slope of the tie-lines are positive for all of the ternary systems containing TBAB/EG (1:2) indicating that small amount of solvent is sufficient to separate the nitrogen compounds from *n*-hexadecane as the model diesel compound. Figures 4.28 a) and c) show that the systems TBAB/EG (1:2) (1) + pyrrole (2) + *n*-hexadecane (3) and TBAB/EG (1:2) (1) + indoline (2) + *n*-hexadecane (3) contains

smaller concentrations of pyrrole and indoline in the raffinate phase than those of pyridine and quinoline in the systems TBAB/EG (1:2) (1) + pyridine (2) + *n*-hexadecane (3) and TBAB/EG (1:2) (1) + quinoline (2) + *n*-hexadecane (3) as shown in Figures 4.28 b) and d). This means that as the concentration of basic nitrogen compound in the feed mixture increases, higher amount of TBAB/EG (1:2) is required to remove them from *n*-hexadecane, whereas for neutral nitrogen compounds, increase in concentrations in the feed mixture does not require significantly higher amount of TBAB/EG (1:2) to remove them from *n*-hexadecane effectively.

The goodness of fit of NRTL correlation and COSMO-RS prediction with the experimental tie-lines were measured using the RMSD values presented in Table 4.32. The binary interaction parameters of NRTL correlation for systems containing TBAB/EG (1:2) are shown in Table 4.33. The NRTL binary interaction parameters between nitrogen compounds and *n*-hexadecane were used as obtained in previous regression of the ternary systems containing ILs.

Table 4.32: RMSD values for NRTL correlation and COSMO-RS prediction of ternary LLE systems containing the DES TBAB/EG (1:2)

System	RMSD	
	NRTL	COSMO-RS
TBAB/EG (1:2) (1) + pyrrole (2) + <i>n</i> -hexadecane (3)	0.27%	0.44%
TBAB/EG (1:2) (1) + pyridine (2) + <i>n</i> -hexadecane (3)	0.88%	2.69%
TBAB/EG (1:2) (1) + indoline (2) + <i>n</i> -hexadecane (3)	0.46%	5.02%
TBAB/EG (1:2) (1) + quinoline (2) + <i>n</i> -hexadecane (3)	0.64%	3.51%

Table 4.33: The values of NRTL binary interaction parameters for each ternary systems containing the DES TBAB/EG (1:2). The value of α used is 0.2.

$i-j$	τ_{ij}	τ_{ji}
TBAB/EG (1:2) – pyrrole	-256.8	1409.9
TBAB/EG (1:2) – pyridine	-427.8	1307.4
TBAB/EG (1:2) – indoline	-562.6	1632.9
TBAB/EG (1:2) – quinoline	-433.3	1309.5
TBAB/EG (1:2) – <i>n</i> -hexadecane	2350.9	1689.9

Based on visual observation, the tie-lines obtained using NRTL and COSMO-RS models are in good agreement with experimental data except for COSMO-RS prediction for the system TBAB/EG (1:2) (1) + indoline (2) + *n*-hexadecane (3), where the COSMO-RS model predicted higher concentrations of indoline in the raffinate phase than what were obtained from experimental methods. This explains the highest value of RMSD for COSMO-RS prediction for the system containing indoline (5.02%) compared to other systems.

At concentration in the feed mixture of 5 wt.%, the values of *D* for TBAB/EG (1:2) towards aromatic nitrogen compounds follows the order: **pyrrole** > **indoline** > **quinoline** > **pyridine** whereas the values of *S* follows the order: **pyrrole** > **quinoline** > **indoline** > **pyridine**.

4.3.7 Systems with TBPB/EG (1:2) DES

Ternary LLE tie-lines containing TBPB/EG (1:2) DES were presented in Tables 4.34 to 4.37 where the concentrations of TBPB/EG (1:2), aromatic nitrogen compounds and *n*-hexadecane were reported. The presented tie lines comprised of values obtained from experimental work and those calculated using NRTL and COSMO-RS models, along with the values of distribution coefficient, *D*, and selectivity, *S* at each tie-line. Table 4.33 shows that the concentration of *n*-hexadecane in the extract phase ranges between 0.0111 and 0.0241 and that TBPB/EG (1:2) was absent in the raffinate phase. This indicates that cross-contamination between the extract phase and raffinate phase is negligible. All other ternary systems also reported minute concentrations of *n*-hexadecane in the extract phase and zero concentration of TBPB/EG (1:2) in the raffinate phase.

Based on *D* and *S* values greater than unity for all ternary systems, TBPB/EG (1:2) showed high affinity towards all aromatic nitrogen compounds than towards *n*-hexadecane. Likewise with the other solvents reported in previous section, the values of *D* and *S* are higher for neutral nitrogen compounds than for basic nitrogen compounds

and are higher for pyrrole; which are one order of magnitude greater than those reported for other nitrogen compounds.

Table 4.34: Experimental tie-lines for the system TBPB/EG (1:2) (1) + pyrrole (2) + *n*-hexadecane (3) at T=25°C and P_{atm}

Extract phase			Raffinate phase			<i>D</i>	<i>S</i>
x'_1	x'_2	x'_3	x''_1	x''_2	x''_3		
Experimental tie-lines							
0.8894	0.0981	0.0125	0.0000	0.0011	0.9989	89.18	7 614
0.7872	0.1868	0.0260	0.0000	0.0018	0.9982	103.78	4 504
0.7380	0.2509	0.0111	0.0000	0.0034	0.9966	73.79	6 938
0.6984	0.2892	0.0124	0.0000	0.0045	0.9955	64.27	5 468
0.6136	0.3630	0.0235	0.0000	0.0053	0.9947	68.49	3 244
0.5738	0.4021	0.0241	0.0000	0.0088	0.9912	45.69	2 107
0.5426	0.4413	0.0162	0.0000	0.0143	0.9857	30.86	2 028
0.5072	0.4701	0.0227	0.0000	0.0166	0.9834	28.32	1 365
0.4904	0.4921	0.0176	0.0000	0.0174	0.9826	28.28	1 726
0.4611	0.5202	0.0187	0.0000	0.0191	0.9809	27.24	1 562
NRTL calculated tie-lines							
0.8778	0.1004	0.0219	0.0005	0.0046	0.9949	21.83	992
0.7979	0.1820	0.0200	0.0005	0.0069	0.9926	26.38	1 309
0.7289	0.2525	0.0185	0.0005	0.0082	0.9913	30.79	1 650
0.6752	0.3074	0.0174	0.0005	0.0089	0.9906	34.54	1 966
0.6256	0.3580	0.0164	0.0005	0.0093	0.9902	38.49	2 324
0.5834	0.4011	0.0155	0.0005	0.0096	0.9900	41.78	2 669
0.5461	0.4392	0.0148	0.0005	0.0097	0.9898	45.28	3 028
0.5132	0.4727	0.0142	0.0005	0.0099	0.9897	47.75	3 328
0.4876	0.4988	0.0137	0.0005	0.0099	0.9896	50.38	3 639
0.4594	0.5274	0.0131	0.0005	0.0100	0.9895	52.74	3 984
COSMO-RS predicted tie-lines							
0.9011	0.0980	0.0009	0.0001	0.0037	0.9962	26.49	29 318
0.8199	0.1792	0.0009	0.0001	0.0076	0.9923	23.58	25 997
0.7514	0.2477	0.0009	0.0001	0.0116	0.9884	21.35	23 451
0.6950	0.3041	0.0009	0.0001	0.0154	0.9845	19.75	21 601
0.6466	0.3525	0.0009	0.0001	0.0191	0.9808	18.46	20 112
0.6026	0.3965	0.0009	0.0001	0.0230	0.9770	17.24	18 714
0.5651	0.4340	0.0009	0.0001	0.0266	0.9734	16.32	17 646
0.5324	0.4667	0.0009	0.0001	0.0299	0.9700	15.61	16 823
0.5029	0.4962	0.0009	0.0001	0.0332	0.9667	14.95	16 053
0.4766	0.5225	0.0009	0.0001	0.0363	0.9636	14.39	15 411

Table 4.35: Experimental tie-lines for the system TBPB/EG (1:2) (1) + pyridine (2) + *n*-hexadecane (3) at T=25°C and P_{atm}

Extract phase			Raffinate phase			<i>D</i>	<i>S</i>
x'_1	x'_2	x'_3	x''_1	x''_2	x''_3		
Experimental tie-lines							
0.8991	0.0862	0.0147	0.0000	0.0228	0.9772	3.78	270
0.8408	0.1494	0.0098	0.0000	0.0328	0.9672	4.55	474
0.7808	0.2071	0.0120	0.0000	0.0453	0.9547	4.57	386
0.7211	0.2676	0.0113	0.0000	0.0623	0.9377	4.30	376
0.6849	0.2971	0.0179	0.0000	0.0777	0.9223	3.82	214
0.6442	0.3392	0.0165	0.0000	0.0955	0.9045	3.55	211
0.6137	0.3677	0.0186	0.0000	0.1087	0.8913	3.38	177
0.5646	0.4178	0.0176	0.0000	0.1286	0.8714	3.25	176
0.5314	0.4536	0.0151	0.0000	0.1370	0.8630	3.31	204
0.5057	0.4783	0.0160	0.0000	0.1429	0.8571	3.35	194
NRTL calculated tie-lines							
0.8937	0.0831	0.0232	0.0006	0.0157	0.9838	5.29	224
0.8307	0.1467	0.0226	0.0006	0.0304	0.9691	4.83	207
0.7703	0.2075	0.0223	0.0006	0.0468	0.9526	4.43	189
0.7210	0.2569	0.0221	0.0006	0.0621	0.9373	4.14	175
0.6749	0.3029	0.0222	0.0006	0.0781	0.9213	3.88	161
0.6343	0.3433	0.0224	0.0006	0.0935	0.9058	3.67	148
0.5976	0.3797	0.0227	0.0007	0.1086	0.8908	3.50	137
0.5647	0.4123	0.0230	0.0007	0.1230	0.8763	3.35	128
0.5352	0.4414	0.0234	0.0007	0.1365	0.8628	3.23	119
0.5071	0.4690	0.0239	0.0007	0.1500	0.8493	3.13	111
COSMO-RS predicted tie-lines							
0.9206	0.0784	0.0010	0.0005	0.0267	0.9728	2.94	2 56
0.8568	0.1420	0.0012	0.0008	0.0456	0.9535	3.11	2 474
0.7937	0.2048	0.0015	0.0012	0.0623	0.9365	3.29	2 052
0.7414	0.2569	0.0017	0.0014	0.0749	0.9237	3.43	1 864
0.6922	0.3058	0.0020	0.0016	0.0858	0.9126	3.56	1 626
0.6488	0.3488	0.0023	0.0018	0.0948	0.9034	3.68	1 445
0.6100	0.3873	0.0026	0.0020	0.1026	0.8955	3.77	1 300
0.5754	0.4216	0.0029	0.0021	0.1093	0.8886	3.86	1 182
0.5448	0.4519	0.0032	0.0022	0.1152	0.8827	3.92	1 082
0.5160	0.4805	0.0036	0.0023	0.1207	0.8770	3.98	970

Table 4.36: Experimental tie-lines for the system TBPB/EG (1:2) (1) + indoline (2) + *n*-hexadecane (3) at T=25°C and P_{atm}

Extract phase			Raffinate phase			<i>D</i>	<i>S</i>
x'_1	x'_2	x'_3	x''_1	x''_2	x''_3		
Experimental tie-lines							
0.9355	0.0556	0.0089	0.0000	0.0083	0.9917	6.70	746
0.8872	0.1053	0.0076	0.0000	0.0172	0.9828	6.12	792
0.8485	0.1414	0.0101	0.0000	0.0195	0.9805	7.25	704
0.7937	0.2002	0.0060	0.0000	0.0291	0.9709	6.88	1 113
0.7595	0.2328	0.0077	0.0000	0.0399	0.9601	5.83	728
0.7287	0.2624	0.0089	0.0000	0.0449	0.9551	5.84	627
0.6953	0.2940	0.0107	0.0000	0.0512	0.9488	5.74	509
0.6665	0.3246	0.0090	0.0000	0.0617	0.9383	5.26	548
0.6341	0.3552	0.0107	0.0000	0.0661	0.9339	5.37	469
0.6123	0.3784	0.0093	0.0000	0.0752	0.9248	5.03	500
NRTL calculated tie-lines							
0.9224	0.0565	0.0212	0.0005	0.0071	0.9923	7.96	372
0.8748	0.1064	0.0187	0.0005	0.0145	0.9850	7.34	387
0.8320	0.1513	0.0167	0.0005	0.0221	0.9774	6.85	401
0.7907	0.1944	0.0149	0.0005	0.0302	0.9693	6.44	419
0.7553	0.2311	0.0135	0.0005	0.0378	0.9616	6.11	435
0.7224	0.2653	0.0123	0.0005	0.0455	0.9540	5.83	452
0.6911	0.2977	0.0112	0.0005	0.0533	0.9462	5.59	472
0.6620	0.3277	0.0103	0.0005	0.0610	0.9385	5.37	489
0.6361	0.3545	0.0095	0.0005	0.0682	0.9313	5.20	510
0.6105	0.3808	0.0087	0.0005	0.0755	0.9240	5.04	536
COSMO-RS predicted tie-lines							
0.9540	0.0451	0.0009	0.0001	0.0277	0.9722	1.63	1 759
0.9115	0.0875	0.0011	0.0001	0.0532	0.9467	1.64	1 416
0.8709	0.1279	0.0012	0.0002	0.0767	0.9231	1.67	1 283
0.8306	0.1679	0.0015	0.0002	0.0993	0.9004	1.69	1 015
0.7945	0.2038	0.0017	0.0003	0.1190	0.8807	1.71	887
0.7598	0.2382	0.0019	0.0003	0.1373	0.8624	1.73	787
0.7261	0.2717	0.0022	0.0004	0.1545	0.8452	1.76	676
0.6939	0.3035	0.0025	0.0004	0.1703	0.8293	1.78	591
0.6649	0.3323	0.0029	0.0005	0.184	0.8155	1.81	508
0.6358	0.3610	0.0032	0.0005	0.1974	0.8021	1.83	458

Table 4.37: Experimental tie-lines for the system TBPB/EG (1:2) (1) + quinoline (2) + *n*-hexadecane (3) at T=25°C and P_{atm}

Extract phase			Raffinate phase			<i>D</i>	<i>S</i>
x'_1	x'_2	x'_3	x''_1	x''_2	x''_3		
Experimental tie-lines							
0.9091	0.0780	0.0129	0.0000	0.0100	0.9900	7.80	757
0.8754	0.0957	0.0289	0.0000	0.0205	0.9795	4.67	181
0.8478	0.1344	0.0179	0.0000	0.0314	0.9686	4.28	253
0.8123	0.1667	0.0210	0.0000	0.0407	0.9593	4.10	207
0.7593	0.2124	0.0284	0.0000	0.0505	0.9495	4.21	160
0.7408	0.2436	0.0156	0.0000	0.0588	0.9412	4.14	269
0.7103	0.2684	0.0213	0.0000	0.0719	0.9281	3.73	163
0.6787	0.2992	0.0221	0.0000	0.0745	0.9255	4.02	187
0.6522	0.3312	0.0166	0.0000	0.0885	0.9115	3.74	223
0.6263	0.3637	0.0100	0.0000	0.0980	0.9020	3.71	349
NRTL calculated tie-lines							
0.9253	0.0513	0.0234	0.0005	0.0095	0.9899	5.40	228
0.8813	0.0958	0.0229	0.0006	0.0189	0.9805	5.07	217
0.8405	0.1370	0.0225	0.0006	0.0286	0.9708	4.79	207
0.8024	0.1754	0.0222	0.0006	0.0386	0.9608	4.54	197
0.7672	0.2109	0.0220	0.0006	0.0487	0.9507	4.33	187
0.7332	0.2449	0.0218	0.0006	0.0592	0.9402	4.14	178
0.7034	0.2748	0.0218	0.0006	0.0692	0.9302	3.97	169
0.6754	0.3028	0.0218	0.0006	0.0790	0.9204	3.83	162
0.6495	0.3287	0.0219	0.0006	0.0887	0.9107	3.71	154
0.6247	0.3533	0.0220	0.0006	0.0984	0.9010	3.59	147
COSMO-RS predicted tie-lines							
0.9575	0.0416	0.0009	0.0003	0.0269	0.9728	1.55	1 672
0.9176	0.0813	0.0011	0.0005	0.0487	0.9508	1.67	1 443
0.8776	0.1211	0.0013	0.0007	0.0670	0.9323	1.81	1 296
0.8384	0.1601	0.0015	0.0009	0.0819	0.9172	1.95	1 195
0.8006	0.1977	0.0017	0.0011	0.0936	0.9053	2.11	1 125
0.7632	0.2348	0.0020	0.0012	0.1031	0.8957	2.28	1 020
0.7299	0.2678	0.0023	0.0013	0.1100	0.8888	2.43	941
0.6985	0.2989	0.0026	0.0013	0.1153	0.8833	2.59	881
0.6696	0.3275	0.0029	0.0014	0.1195	0.8791	2.74	831
0.6422	0.3546	0.0032	0.0015	0.1228	0.8757	2.89	790

Figures 4.29 a) – d) present the tie-lines drawn from experimental values, NRTL correlation and COSMO-RS predicted values for the four systems containing TBPB/EG (1:2) which showed that all of the ternary phase diagram exhibit Type 1 phase behaviour.

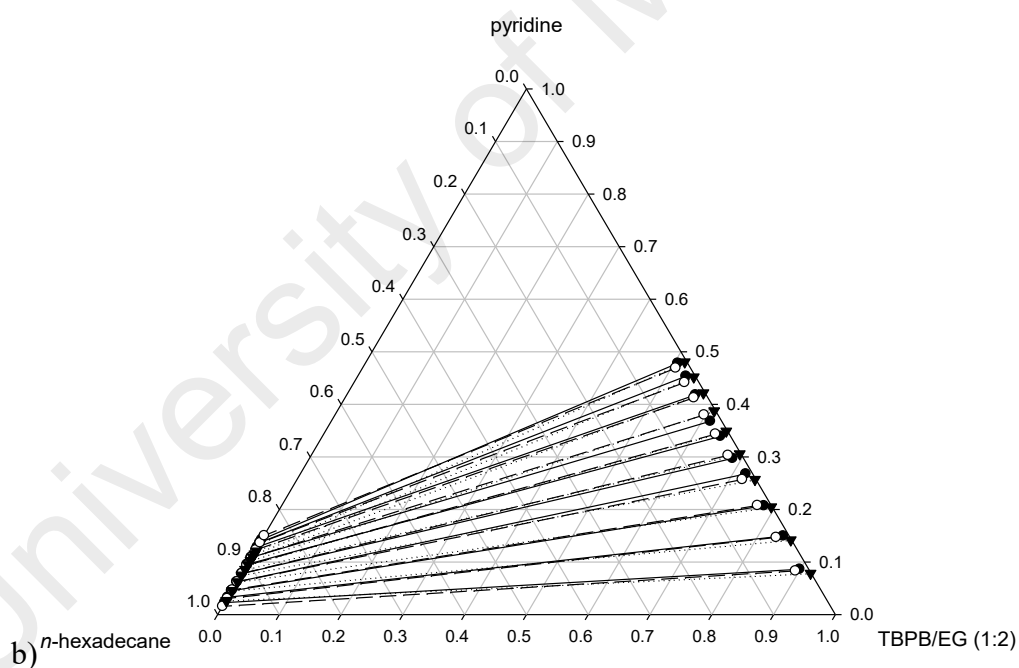
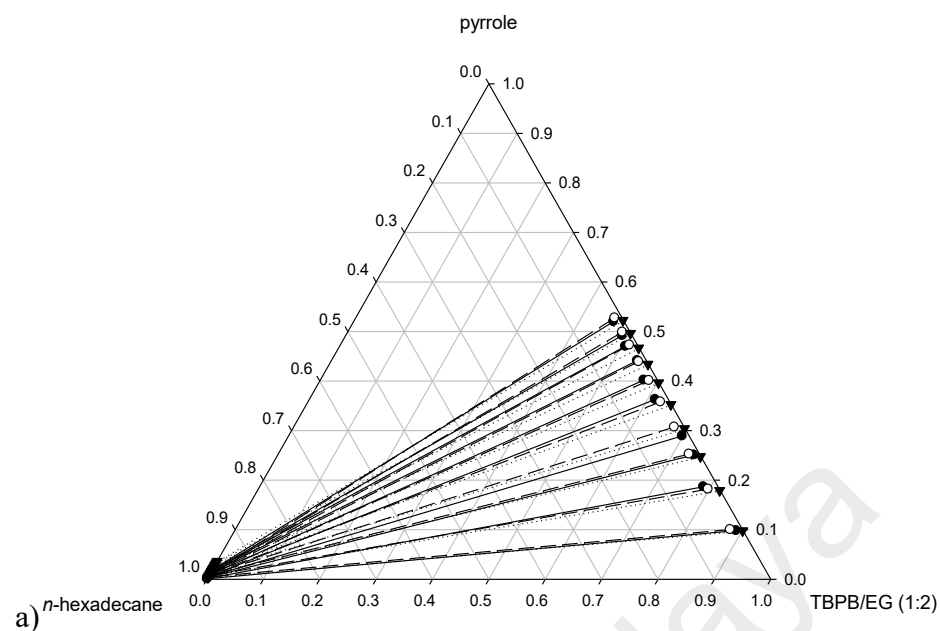


Figure 4.29: Tie-lines for the ternary systems a) TBPB/EG (1:2) (1) + pyrrole (2) + *n*-hexadecane (3), b) TBPB/EG (1:2) (1) + pyridine (2) + *n*-hexadecane (3), c) TBPB/EG (1:2) (1) + indoline (2) + *n*-hexadecane (3), and d) TBPB/EG (1:2) (1) + quinoline (2) + *n*-hexadecane (3) at $T=298.15$ K and P_{atm} . Full circle and solid lines indicate experimental tie-lines, empty circle and dashed lines indicate tie-lines from NRTL calculation, and full triangle and dotted lines indicate calculated tie-lines from COSMO-RS model.

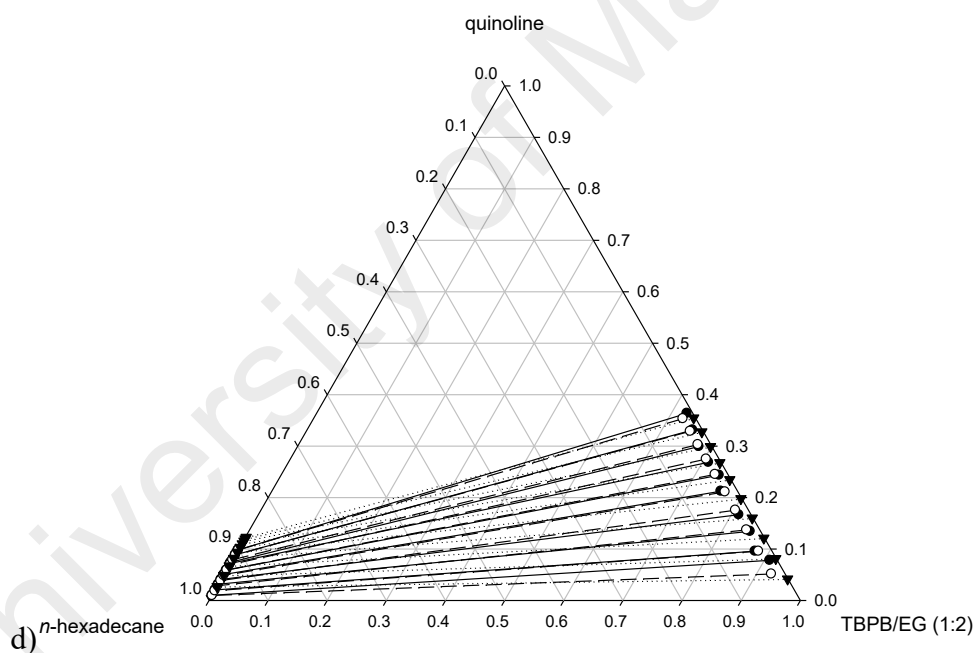
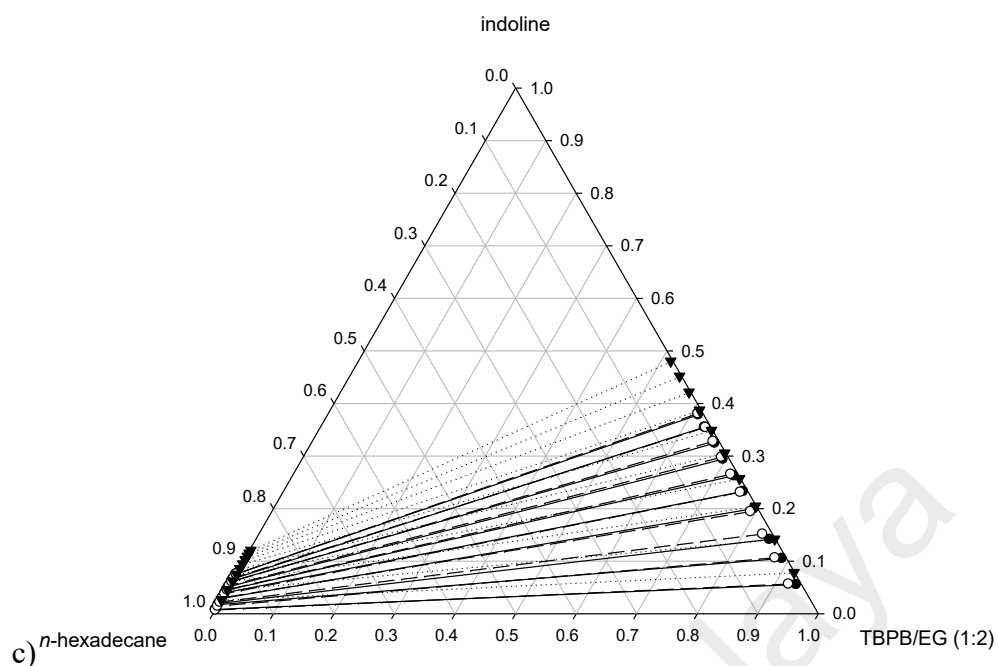


Figure 4.29, continued.

As indicated by the positive slope for all of the ternary systems containing TBPB/EG (1:2), small amount of TBPB/EG (1:2) is sufficient to separate the nitrogen compounds from *n*-hexadecane. As shown by Figures 4.29 a) and c), the systems TBAB/EG (1:2) (1) + pyrrole (2) + *n*-hexadecane (3) and TBAB/EG (1:2) (1) + indoline (2) + *n*-hexadecane (3) contains smaller concentrations of pyrrole and indoline in the

raffinate phase than those of pyridine and quinoline in the systems TBAB/EG (1:2) (1) + pyridine (2) + *n*-hexadecane (3) and TBAB/EG (1:2) (1) + quinoline (2) + *n*-hexadecane (3) as shown in Figures 4.29 b) and d). Thus, higher amount of TBAB/EG (1:2) is required to remove basic compounds from *n*-hexadecane as their concentration in the feed mixture increases. Whereas, increase in concentration of neutral compounds in the feed mixture does not require significantly higher amount of TBPB/EG (1:2) to remove them effectively.

Table 4.38 presents the RMSD values of NRTL correlation and COSMO-RS prediction against the experimental tie-lines whereas Table 4.39 shows the binary interaction parameters of NRTL correlation for systems containing TBPB/EG (1:2).

Table 4.38: RMSD values for NRTL correlation and COSMO-RS prediction of ternary LLE systems containing the DES TBPB/EG (1:2)

System	RMSD	
	NRTL	COSMO-RS
TBPB/EG (1:2) (1) + pyrrole (2) + <i>n</i> -hexadecane (3)	0.67%	1.40%
TBPB/EG (1:2) (1) + pyridine (2) + <i>n</i> -hexadecane (3)	0.62%	1.18%
TBPB/EG (1:2) (1) + indoline (2) + <i>n</i> -hexadecane (3)	0.48%	5.26%
TBPB/EG (1:2) (1) + quinoline (2) + <i>n</i> -hexadecane (3)	0.59%	2.60%

Table 4.39: The values of NRTL binary interaction parameters between TPBP/EG (1:2) and nitrogen compounds and *n*-hexadecane

<i>i - j</i>	τ_{ij}	τ_{ji}
TBPB/EG (1:2) – pyrrole	153.0	449.0
TBPB/EG (1:2) – pyridine	-499.2	1451.3
TBPB/EG (1:2) – indoline	-609.5	1629.7
TBPB/EG (1:2) – quinoline	-477.6	1450.7
TBPB/EG (1:2) – <i>n</i> -hexadecane	625.4	1830.5

Consistent with the other solvents, the NRTL binary interaction parameters between nitrogen compounds and *n*-hexadecane obtained in the regression based on the systems containing [EMIM][EtSO₄] were used. It is observed that the tie-lines obtained using NRTL and COSMO-RS models are in good agreement with experimental data except for COSMO-RS prediction for the system TBPB/EG (1:2) (1) + indoline (2) + *n*-

hexadecane (3), where the COSMO-RS model predicted higher concentrations of indoline in the raffinate phase than what were obtained from experimental methods. Thus, higher value of RMSD for COSMO-RS prediction for the system containing indoline is obtained.

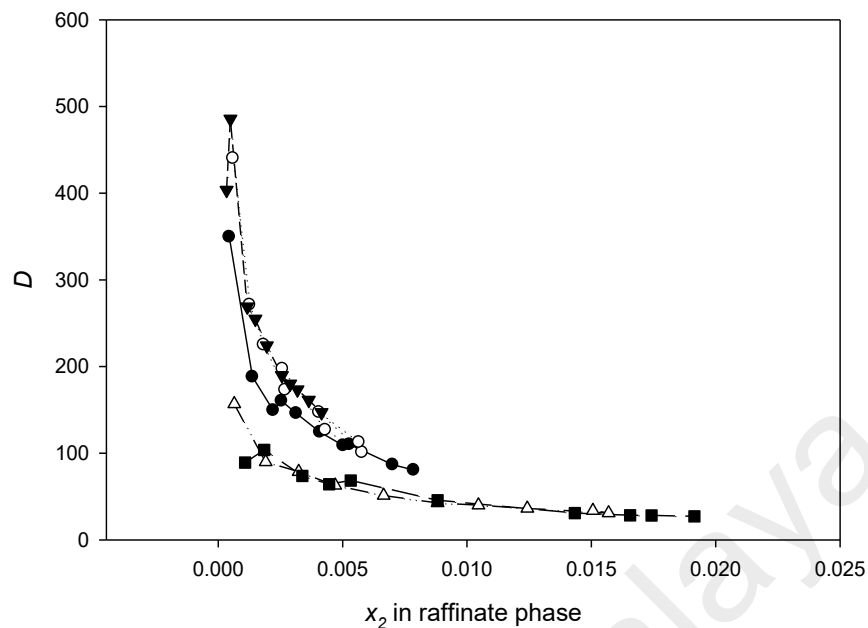
The values of D at the nitrogen compounds concentration in the feed mixture of 5 wt. % for TBPB/EG (1:2) towards aromatic nitrogen compounds follows the order: **pyrrole > indoline > quinoline > pyridine** whereas the values of S at the same feed concentration follows the order: **pyrrole > quinoline > indoline > pyridine**.

4.3.8 Distribution Ratio and Selectivity

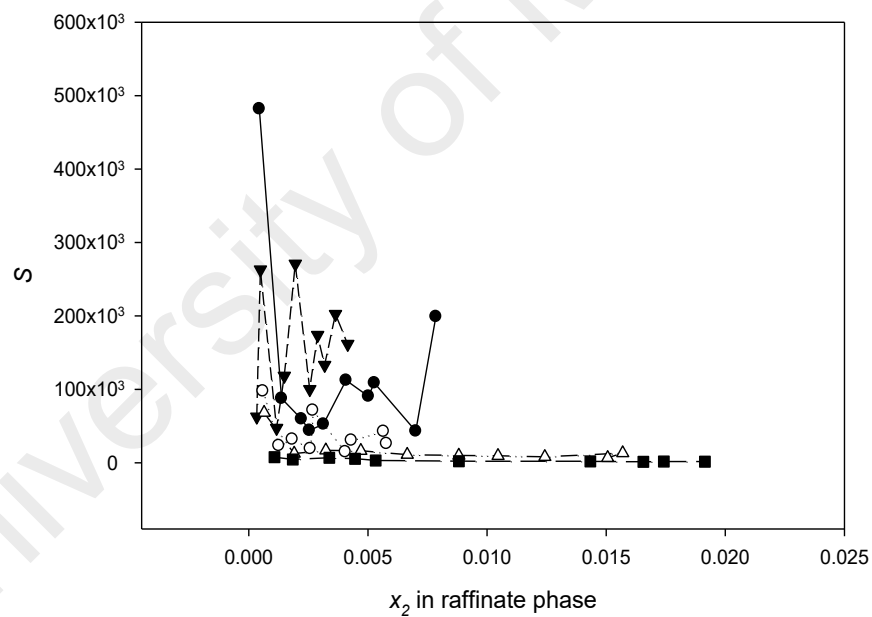
In this section, the effects of different solvents towards the separation efficiency based on the distribution ratio, D , and selectivity, S values are discussed. Indeed, as mentioned previously, the distribution coefficient is used to give a quantitative representation on how the solute is distributed between the two phases, i.e. the extract phase and the raffinate phase. On the other hand, the selectivity of any solvent (IL or DES) measures the affinity of the nitrogen compound in the fuel mixture model toward this solvent.

It was observed that the profiles for distribution coefficient and selectivity vary according to the type of aromatic nitrogen compounds used in the ternary LLE experiment. Although in sections 4.3.2 to 4.3.6 it has been discussed that all ILs and DES used were potential effective solvent for the removal of both neutral and basic nitrogen compound, it is worthwhile to discuss the different profiles of D and S values that these solvents report for different aromatic nitrogen compounds used.

Figure 4.30 a) and b) show the profiles of D and S as a function of pyrrole concentration in the raffinate phase, respectively.



a)



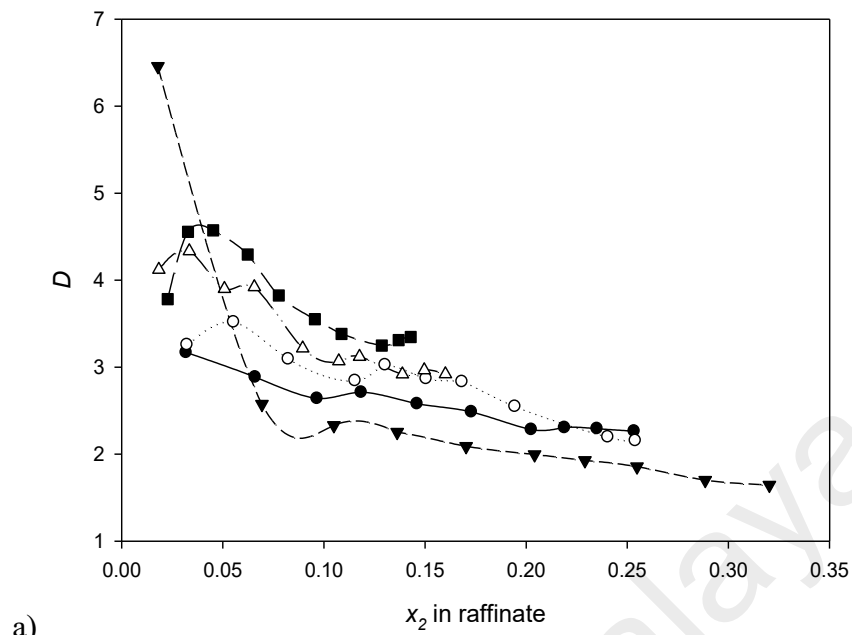
b)

Figure 4.30: Distribution ratio, D (a) and selectivity, S , (b) of pyrrole as a function of pyrrole concentration in the raffinate phase using various solvents in the ternary LLE experiments. Filled circle indicates [EMIM][EtSO₄], empty circle indicate [EMPY][EtSO₄], filled triangle indicate [EMIM][MeSO₃], empty triangle indicate TBAB/EG (1:2) and filled squares indicate TBPB/EG (1:2).

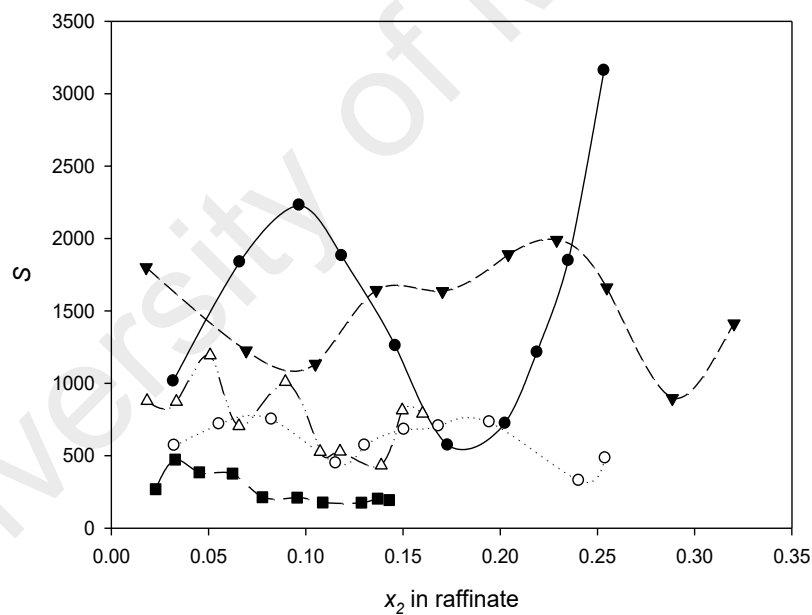
In general, D values decrease with increasing concentration of pyrrole in the raffinate phase. Figure 4.33 a) shows that the values of D for pyrrole are very close to those for the ILs [EMPY][EtSO₄] and [EMIM][MeSO₃] which report the highest D profiles for pyrrole, followed by [EMIM][EtSO₄] IL. However, TBAB/EG (1:2) and TBPB/EG (1:2) DESs report the lowest values of D for pyrrole and their profiles are very close and overlap each other; although TBAB/EG (1:2) reports higher value of D at lower concentrations of pyrrole in the raffinate phase. Thus, the values of D for pyrrole based on the solvent used follows the order: **[EMPY][EtSO₄] > [EMIM][MeSO₃] > [EMIM][EtSO₄] > TBAB/EG (1:2) > TBPB/EG (1:2).**

The selectivity values for pyrrole in Figure 4.30 b) do not show a clear trend with the increase of pyrrole concentration in the raffinate phase. The IL [EMIM][EtSO₄] reports the highest value of S for pyrrole initially, but the S value using [EMIM][EtSO₄] rapidly decreases with increasing pyrrole concentration in the raffinate phase. This is followed by the IL [EMIM][MeSO₃] although this IL showed higher values of S at increasing pyrrole concentration in the raffinate phase compared to [EMIM][EtSO₄] IL. However, both [EMPY][EtSO₄] IL and TBAB/EG (1:2) and TBPB/EG (1:2) DESs have very close profiles of S for pyrrole, but TBAB/EG (1:2) reports lower values of S than [EMPY][EtSO₄], and TBPB/EG (1:2) reports even lower values of S than TBAB/EG (1:2). Hence, the S profile for pyrrole reported by the solvents follows the order: **[EMIM][EtSO₄] > [EMIM][MeSO₃] > [EMPY][EtSO₄] > TBAB/EG (1:2) > TBPB/EG (1:2).**

The D and S profiles for pyridine are shown in Figures 4.31 a) and b).



a)



b)

Figure 4.31: Distribution ratio, D (a) and selectivity, S , (b) of pyridine as a function of pyridine concentration in the raffinate phase using various solvents in the ternary LLE experiments. Filled circle indicates [EMIM][EtSO₄], empty circle indicate [EMPY][EtSO₄], filled triangle indicate [EMIM][MeSO₃], empty triangle indicate TBAB/EG (1:2) and filled squares indicate TBPB/EG (1:2).

The values of D generally decrease with increasing pyridine concentration in the raffinate phase. Initially, [EMIM][MeSO₃] reports the highest values of D for pyridine, but it rapidly decreases with increasing concentration of pyridine and becomes the solvent which reports the lowest D values for pyridine thereafter. Besides, TBAB/EG (1:2) DES reports the second highest value of D initially albeit with gradual decrease in the D values, followed by TBPB/EG (1:2). After the initial concentrations, TBPB/EG (1:2) continues to be the solvent with the highest D profile for pyridine with increasing concentration of pyridine in the raffinate phase. The profile of D values were followed by the ILs [EMPY][EtSO₄] and [EMIM][EtSO₄]. The D profile for pyridine based on the solvents used follows the order: **TBPB/EG (1:2) > TBAB/EG (1:2) > [EMPY][EtSO₄] > [EMIM][EtSO₄] > [EMIM][MeSO₃]**. The selectivity profiles for pyridine as presented in Figure 4.31b) does not show obvious trend for all of the solvents used. The ILs [EMIM][EtSO₄] and [EMIM][MeSO₃] report higher values of S for pyridine followed by TBAB/EG (1:2), [EMPY][EtSO₄] and lastly TBPB/EG (1:2). The trend for S profile for pyridine is **[EMIM]EtSO₄ ≈ [EMIM][MeSO₃] > TBAB/EG (1:2) > [EMPY][EtSO₄] > TBPB/EG (1:2)**.

Similarly for indoline, the values of D generally decrease with increasing concentration of indoline in the raffinate phase as shown in Figure 4.32 a). The highest profile of D values for indoline was reported by the mixed ILs [EMIM][EtSO₄]+[EMPY][EtSO₄], followed by the ILs [EMIM][MeSO₃], [EMPY][EtSO₄], and [EMIM][EtSO₄]. The DESs TBAB/EG (1:2) and TBPB/EG (1:2) report the lowest D profiles for indoline, but they are still considered as highly potential solvents for separating indoline from *n*-hexadecane since the values of D are greater than unity.

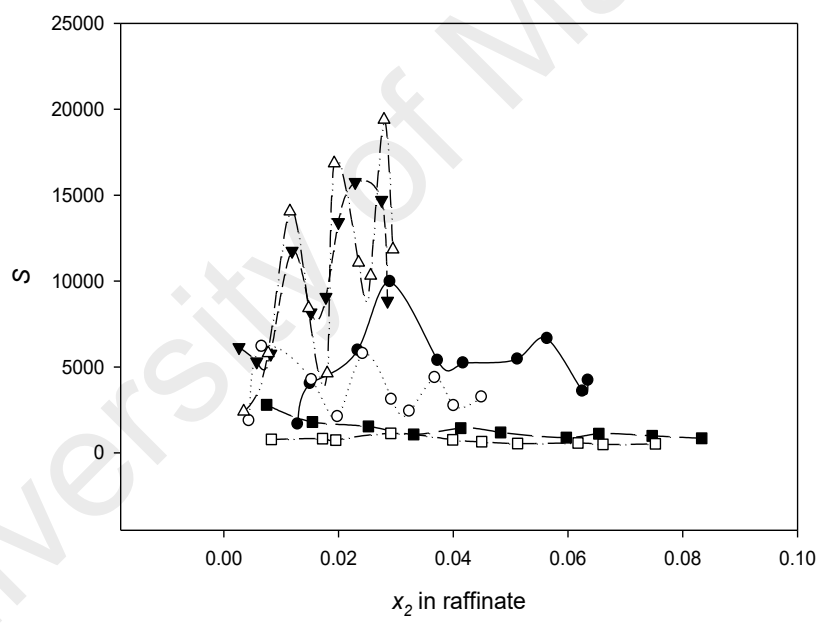
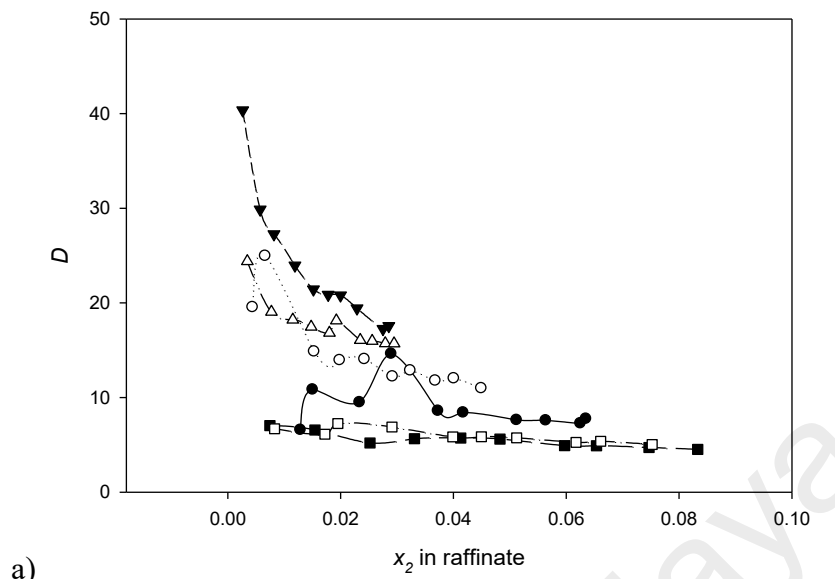
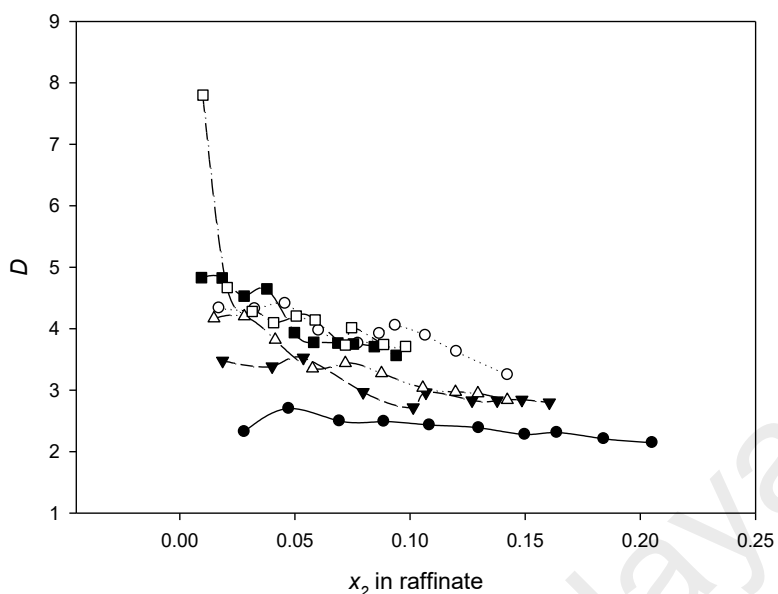


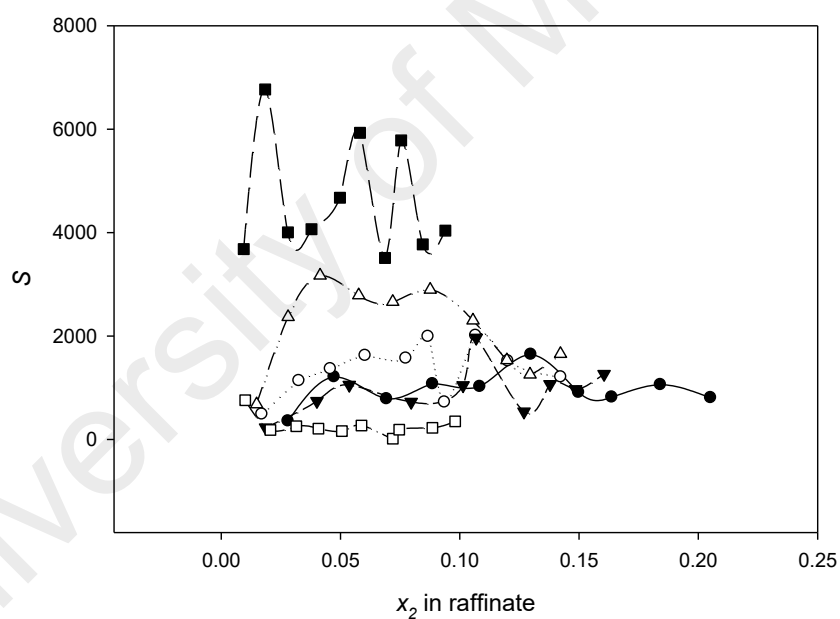
Figure 4.32: Distribution ratio, D (a) and selectivity, S , (b) of indoline as a function of indoline concentration in the raffinate phase using various solvents in the ternary LLE experiments. Filled circle indicates [EMIM][EtSO₄], empty circle indicate [EMPY][EtSO₄], filled triangle indicate [EMIM][EtSO₄] + [EMPY][EtSO₄], empty triangle indicate [EMIM][MeSO₃], filled square indicate TBAB/EG (1:2) and empty square indicate TBPB/EG (1:2).

Figure 4.32 b) presents the *S* profiles for indoline which also shows no obvious trend on the *S* values with increasing indoline concentration in the raffinate phase. [EMIM][MeSO₃] and the mixed ILs [EMIM][EtSO₄]+[EMPY][EtSO₄] report very close values of *S* profiles for indoline, followed by [EMIM][EtSO₄], [EMPY][EtSO₄] and finally TBAB/EG (1:2) and TBPB/EG (1:2) DESs.

The *D* and *S* profiles for quinoline using different solvents are shown in Figure 4.33 a) and b), where similar observation were obtained for the *D* and *S* profiles like the other nitrogen compounds, i.e. decreasing values of *D* with increasing quinoline concentration and no obvious trend regarding the values of *S*. For quinoline, the DES TBPB/EG (1:2) reports the highest *D* profile initially, followed by TBAB/EG (1:2), [EMPY][EtSO₄], [EMIM][MeSO₃], the mixed ILs [EMIM][EtSO₄]+[EMPY][EtSO₄] and finally [EMIM][EtSO₄]. The highest *S* profile for quinoline was reported by the DES TBAB/EG (1:2), followed by the ILs [EMIM][MeSO₃], [EMPY][EtSO₄], and very close profile of *S* values reported using the mixed ILs [EMIM][EtSO₄]+[EMPY][EtSO₄] and individual IL [EMIM][EtSO₄], and lastly TBPB/EG (1:2).



a)



b)

Figure 4.33: Distribution ratio, D (a) and selectivity, S , (b) of quinoline as a function of quinoline concentration in the raffinate phase using various solvents in the ternary LLE experiments. Filled circle indicates [EMIM][EtSO₄], empty circle indicate [EMPY][EtSO₄], filled triangle indicate [EMIM][EtSO₄] + [EMPY][EtSO₄], empty triangle indicate [EMIM][MeSO₃], filled square indicate TBAB/EG (1:2) and empty square indicate TBPB/EG (1:2).

The values of D and S obtained in this work were also compared against the ones reported in Table 2.3 (Chapter 2) where organic solvents i.e. methanol, ethanol, NMF and DMF were used to remove pyrrole, pyridine and quinoline from *n*-hexadecane. When compared against these organic solvents, the selected ILs and DESs reported D and S values which are significantly higher than those reported by the organic solvents for pyrrole. For example, the highest value of D for the removal of pyrrole from *n*-hexadecane using organic solvent is obtained using DMF (45.7) whereas when using ILs and DESs, the values of D are in the order of magnitude of 10^2 . The S values are even higher when using ILs and DESs for removal of pyrrole i.e. in the order of magnitude of at least 10^5 whereas when using organic solvents the highest S value is reported when using methanol (157). However for pyridine and quinoline, the values of D reported using ILs and DESs do not differ much with those reported using organic solvents where they are in the same order of magnitude but the values of S for pyridine and quinoline differ significantly when using ILs and DESs over organic solvents. The values of S obtained using ILs and DESs for pyridine and quinoline reach the order of magnitude in the range of $10^2 - 10^3$ whereas the highest S values obtained using organic solvents are 68 for pyridine (using methanol) and 40 for quinoline (using methanol).

In general, the values of D and S towards neutral nitrogen compounds are higher when using ILs than DESs. On the contrary for basic compounds, the values of D and S are slightly higher when using DESs as solvent than when using ILs. The higher values of D and S towards neutral compounds when using ILs may be attributed to the stronger CH- π interaction between the nitrogen compounds and ILs, whereas the interaction between nitrogen compounds and DESs constituent is only driven by hydrogen bonding. This is consistent with what has been reported in previous sections on the computational elucidation of molecular interaction between selected ILs and heterocyclic nitrogen compounds.

All three ILs report high values of D for all nitrogen compounds with [EMPY][EtSO₄] being the IL which report the highest values of D ; whereas [EMIM][EtSO₄] and [EMIM][MeSO₃] report higher values of S than [EMPY][EtSO₄]. The extraction efficiency is often directly related to the value of D than the value of S . Thus, the experimental results reporting higher values of D obtained when using [EMPY][EtSO₄] is consistent with the previous quantum calculation results, where it was reported that pyridinium-based ILs have better extraction capacity towards heteroaromatic compounds than imidazolium-based ILs containing the same anion. Mixing the ILs [EMIM][EtSO₄] and [EMPY][EtSO₄] has positive impact towards the values of D and S for indoline but little benefit was observed for the extraction of quinoline.

Finally, when comparing the two DESs used in this work, TBPB/EG (1:2) gave higher values of D for all nitrogen compounds compared to TBAB/EG (1:2). This is consistent with what has been predicted by COSMO-RS calculations, where it was reported that tetrabutylphosphonium-based DESs are predicted to have a higher capacity and thus distribution coefficient towards nitrogen compounds than tetrabutylammonium-based DESs. On the other hand, the selectivity profiles indicate that TBAB/EG (1:2) DES reports higher values of selectivity for all the nitrogen compounds than TBPB/EG (1:2) DES. This could be due to the higher concentrations of *n*-hexadecane present in the extract phase for the ternary systems containing TBPB/EG (1:2) than those containing TBAB/EG (1:2). But, although TBPB/EG (1:2) DES has higher distribution coefficient towards all nitrogen compounds, it also has a more favourable interaction with *n*-hexadecane compared to TBAB/EG (1:2) DES. This result is inconsistent with our previous COSMO-RS screening which predicted higher values of selectivity for tetrabutylphosphonium-based DESs towards nitrogen compounds than tetrabutylammonium-based DESs. However, the difference in selectivity values expected

was very small because the sigma profile and sigma potential of tetrabutylphosphonium and tetrabutylammonium cations are very comparable.

University of Malaya

CHAPTER 5: CONCLUSION

Based on the present work, the results are concluded in the following three sections: i) qualitative and quantitative screening of ILs and DESs, ii) quantum chemical calculations, and iii) ternary LLE experimental work.

5.1 Qualitative and Quantitative Screening of ILs and DESs

In total, 18 ILs from the combinations of six cations and three anions were qualitatively screened, using the σ -profile and σ -potential in the COSMO-RS model, for potential use in the extractive denitrogenation of diesel fuel. The σ -profile and σ -potential of each cation, anion, and nitrogen heterocycles confirm the mutual interaction among the three species. Based on σ -profile and σ -potential screening, ILs with aromatic ring cations ([EMIM], [EPY], and [TMPYRA]) have better capacity as HBDs compared with saturated cations, thus enabling better CH- π interaction with heterocyclic nitrogen compounds. Hence, the general recommendation is to select ILs with aromatic cations, combined with [EtSO₄] or [Ac] anions, for increased extraction capability with heterocyclic nitrogen compounds at 298.15 K.

Altogether, 94 DESs based on different combinations of salt cations, anions, HBDs, and salt:HBD molar ratios were screened, using the COSMO-RS approach, for possible use in the extractive denitrogenation of diesel fuel. This was done by predicting the selectivity, capacity, and performance index at infinite dilution (S^∞ , C^∞ , and PI, respectively) using the COSMO-RS-calculated values of the activity coefficient at the infinite dilution, γ^∞ , of the nitrogen compounds in each DES. The studied nitrogen compounds include basic or five-membered compounds (pyrrole, indole, indoline, carbazole, and benzocarbazole) and non-basic or six-membered compounds (pyridine, quinolone, and benzoquinoline). The hydrogen-bonding interaction is the main driving force in the removal of nitrogen compounds from diesel using DESs as the extraction solvent. The heterocyclic structure of nitrogen compounds influences the values of S^∞ and

C^∞ such that neutral compounds have higher values of both S^∞ and C^∞ compared with basic compounds. The values of S^∞ and C^∞ are also lower for compounds with more aromatic rings in their structures. In general, DESs with ammonium-based cations give higher values of S^∞ but lower values of C^∞ , while phosphonium-based DESs give higher values of C^∞ and lower values of S^∞ . For the effect of cation choice on selectivity, the selectivity ranking of the DES cations is as follows: choline-based > tetramethylammonium > phenylammonium > tetramethylphosphonium > phenylphosphonium > tetrabutylphosphonium > tetrabutylammonium. Meanwhile, the capacity ranking of the DES follows the decreasing order of tetrabutylphosphonium \geq tetrabutylammonium > tetramethylphosphonium > tetramethylammonium > phenylphosphonium > phenylammonium > choline-based cations.

A mixed trend is observed for the effect of halide anions on the values of S^∞ and C^∞ . DESs with halide salt show differing values of S^∞ and C^∞ for neutral and basic compounds when combined with different cations. Tetramethyl-based DESs (both ammonium- and phosphonium-based) lead to higher values of S^∞ for all neutral and basic compounds when the anion is combined with the Br^- anion in comparison to when it is combined with the Cl^- anion. However, the same types of DESs lead to higher values of C^∞ when combined with the Br^- anion for all nitrogen compounds. Tetrabutyl-based DESs (both ammonium- and phosphonium-based) lead to higher values of S^∞ for neutral compounds when combined with the Cl^- anion, while higher values of S^∞ are reported for basic compounds when the DESs are combined with the Br^- anion. In terms of C^∞ , tetrabutyl-based DESs lead to higher values of C^∞ for neutral compounds when combined with the Br^- anion, and higher values of C^∞ are reported for basic compounds when they are combined with the Cl^- anion.

HBD choice has a noteworthy effect on the values of S^∞ and C^∞ , which is essentially because the functional group makes up the HBD structure. It was observed

that DESs, when combined with HBDs from alcohol and amide functional groups, give high values of S^∞ but low values of C^∞ . An exception to this trend is urea, an HBD with the amide group, where ChCl combined with urea gives high values of both S^∞ and C^∞ . The DESs with HBDs from the carboxylic acid group give high values of C^∞ but low values of S^∞ . HBDs from sugar alcohol groups (i.e. xylitol, *D*-sorbitol and *D*-isosorbide) are not good candidates to make up DESs for the extractive denitrogenation process. Varying the salt:HBD molar ratio does not have a significant effect on the values of S^∞ and C^∞ , although some increase and decrease in S^∞ and C^∞ was observed when changing the molar ratio.

In conclusion, the choice of cation, anion, HBD, and salt:HBD molar ratio needs to be considered when selecting appropriate DESs for the extractive denitrogenation process. In general, no ideal DES gives high values of both S^∞ and C^∞ . From an economic point of view, the operator may choose a DES based on the operator's ability and willingness to incur capital or operating costs. This is because selectivity has a direct impact on capital cost (i.e., the number of stages in the extraction process), whereas the capacity or distribution ratio has a direct impact on operating cost (i.e., the flow rate of the solvent used for the extraction process). Apart from the criteria of selectivity and capacity, selecting DESs as solvents requires also considering the physical and transport properties of DESs for industrial applications. It should also be noted that the hypothetical DESs included in the screening process in this work may or may not exist at the specified ratio and may or may not be liquid at room temperature. Nevertheless, to select DESs for an application of interest, a systematic approach needs to be taken, such as the predictive quantum chemical model COSMO-RS used here. However, given the limitations of COSMO-RS, these results are appropriate only for preliminary screening rather than for design calculation.

5.2 Quantum Chemical Calculation

A systematic approach to the selection of ILs as solvents for the removal of heterocyclic nitrogen compounds is necessary to produce an ultra-low sulfur fuel via liquid-liquid extraction. One way to execute this is through ab initio calculation via quantum chemical methods. In summary, the optimized geometry of individual cations, anions, heterocyclic nitrogen compounds, complexes of ILs, and complexes of heterocyclic nitrogen compounds with neat ILs have been investigated using ab initio quantum chemical calculations at Hartree-Fock level and 6-31G* basis set. The optimized structure of heterocyclic nitrogen compounds with neat ILs confirms the interaction between ILs and heterocyclic nitrogen compounds through the CH- π and π - π interactions between cation and nitrogen heterocycles and through hydrogen bonding between the anion heteroatom and heterocyclic nitrogen compounds. Based on the optimized geometry, orbital energy values, global scalar properties, interaction energy and partial charge transfer are calculated for each individual species and complex. These parameters are then used to identify ILs suitable for use in the extractive denitrogenation of liquid fuels.

The calculation results suggest that all 18 ILs studied in this work are potential solvents for the denitrogenation of liquid fuels due to favorable interactions as indicated by their orbital energies, global scalar properties, interaction energy, partial charge transfer, and σ -profiles. However, some ILs have better ability to interact with heterocyclic nitrogen compounds based on each parameter investigated. ILs are thus ranked according to each parameter based on the criteria for favorable interaction with nitrogen compounds. Based on LUMO energy values, the HOMO-LUMO gap, global softness, and electrophilicity index, [EPY][EtSO₄] is the most favorable IL for extraction of heterocyclic nitrogen compounds. However, based on interaction energy and partial charge transfer, [TMPYRA][Ac] is the best IL.

5.3 Ternary LLE Experimental Work

In total, 22 ternary LLE experimental results were reported, which comprised 14 systems containing ILs and eight systems containing DESs. The Othmer-Tobias and Hand correlations were utilized to ascertain the reliability and consistency of the experimental data. Based on the values of the regression coefficient R^2 , which are close to unity for all the ternary systems, it can be safely concluded that the ternary LLE experimental results reported in this work are reliable and consistent.

The experimental tie-lines obtained from NMR spectroscopy were reported along with the tie-lines calculated by using NRTL correlations and COSMO-RS predictions. In all ternary systems, the concentration of *n*-hexadecane in the extraction phase is very small. This is favorable because it indicates minimum cross-contamination between the extraction and raffinate phases. The presence of ILs and DES in the raffinate phase for all ternary systems is below the detection limit of NMR spectroscopy and is thus considered to be negligible. The absence of ILs and DES in the raffinate phase is favorable for industrial applications, because fewer steps and thus less energy is then required to recover the solvent for recycling.

The effectiveness of each solvent was evaluated based on the values of the distribution coefficient D and selectivity S . For all ternary systems, the values of D and S are greater than unity, indicating that aromatic nitrogen compounds have better affinity towards the solvent than towards *n*-hexadecane and that all solvents have high potential for use in extractive denitrogenation. The NRTL correlation provides an excellent representation and model of the ternary LLE systems with RMSD values for all systems less than 1%. Thus, the NRTL model and regressed binary interaction parameters may be used in process-simulation software for the conceptual process design of extractive denitrogenation. The COSMO-RS predictions of the ternary LLE tie-lines are also in good agreement with the experimental data, with RMSD values for most systems less than 5%.

An exception is the COSMO-RS prediction for systems containing indoline, where the COSMO-RS model overestimates the concentration of indoline in the raffinate phase.

All ternary phase diagrams show Type 1 behavior, where only one binary system exhibits partial immiscibility and with only one immiscibility region. In all ternary systems, the slope is positive, which means that a small amount of solvent is sufficient to remove the nitrogen compounds from *n*-hexadecane as the model diesel compound.

Based on the values of *D* and *S* discussed in Section 4.3.8, imidazolium- and pyridinium-based ILs are better solvents for use in the removal of neutral nitrogen compounds than the DESs TBAB/EG (1:2) and TBPB/EG (1:2) due to the higher values of *D* and *S* reported for pyrrole and indoline removed by the ILs than by the DESs. By contrast, for basic nitrogen compounds, the DESs reported higher values of *D* and *S* than did the imidazolium- and pyridinium-based ILs. However, all the solvents used may be highly effective solvents for use in the extractive denitrogenation of diesel based on the favorable values of *D* and *S* and based on their ternary phase equilibria behavior. In conclusion, the experimental LLE results validate the computational results conducted in this work. The selected solvents were proven to be effective solvents for the removal of neutral and basic nitrogen compounds from diesel fuel.

5.4 General conclusion

In a nutshell, systematic approach towards the selection and screening of ILs and DESs for any separation process is essential to achieve high separation efficiency. In this work, quantum chemical methods and COSMO-RS model were used to screen and select appropriate ILs and DESs. The calculation results were also used to elucidate the molecular interaction between ILs and DESs and heterocyclic nitrogen compounds. LLE experiments performed proved that the selected ILs and DESs based on the screening method are highly potential solvents for use in extractive denitrogenation.

REFERENCES

- Abbott, A. P., Boothby, D., Capper, G., Davies, D. L., & Rasheed, R. K. (2004). Deep Eutectic Solvents Formed between Choline Chloride and Carboxylic Acids: Versatile Alternatives to Ionic Liquids. *Journal of the American Chemical Society*, 126(29), 9142-9147.
- Abrams, D. S., & Prausnitz, J. M. (1975). Statistical thermodynamics of liquid mixtures: A new expression for the excess Gibbs energy of partly or completely miscible systems. *AIChE Journal*, 21(1), 116-128.
- Al-Barood, A., Qabazard, H., & Stanislaus, A. (2005). A Comparative Study of the HDS Kinetics of Straight Run and Coker Gas Oils Under Deep Desulfurization Conditions. *Petroleum Science and Technology*, 23(7-8), 749-760.
- Almarri, M., Ma, X., & Song, C. (2008). Selective Adsorption for Removal of Nitrogen Compounds from Liquid Hydrocarbon Streams over Carbon- and Alumina-Based Adsorbents. *Industrial & Engineering Chemistry Research*, 48(2), 951-960.
- Alonso, L., Arce, A., Francisco, M. a., & Soto, A. (2010). Extraction Ability of Nitrogen-Containing Compounds Involved in the Desulfurization of Fuels by Using Ionic Liquids. *Journal of Chemical & Engineering Data*, 55(9), 3262-3267.
- Anantharaj, R., & Banerjee, T. (2010a). COSMO-RS-Based Screening of Ionic Liquids as Green Solvents in Denitrification Studies. *Industrial & Engineering Chemistry Research*, 49(18), 8705-8725.
- Anantharaj, R., & Banerjee, T. (2010b). Evaluation and comparison of global scalar properties for the simultaneous interaction of ionic liquids with thiophene and pyridine. *Fluid Phase Equilibria*, 293(1), 22-31.
- Anantharaj, R., & Banerjee, T. (2011a). COSMO-RS based predictions for the desulphurization of diesel oil using ionic liquids: Effect of cation and anion combination. *Fuel Processing Technology*, 92(1), 39-52.
- Anantharaj, R., & Banerjee, T. (2011b). Liquid-liquid equilibria for quaternary systems of imidazolium based ionic liquid+thiophene+pyridine+iso-octane at 298.15K: Experiments and quantum chemical predictions. *Fluid Phase Equilibria*, 312(0), 20-30.
- Anantharaj, R., & Banerjee, T. (2011c). Quantum chemical studies on the simultaneous interaction of thiophene and pyridine with ionic liquid. *AIChE Journal*, 57(3), 749-764.

- Anantharaj, R., & Banerjee, T. (2013). Aromatic sulfur-nitrogen extraction using ionic liquids: Experiments and predictions using an a priori model. *AIChE Journal*, 59(12), 4806-4815.
- Asumana, C., Yu, G., Guan, Y., Yang, S., Zhou, S., & Chen, X. (2011). Extractive denitrogenation of fuel oils with dicyanamide-based ionic liquids. *Green Chemistry*, 13(11), 3300-3305.
- Bacha, J., Freel, J., Gibbs, A., Gibbs, L., Hemighaus, G., Hoekman, K., et al. (2007). Diesel Fuels Technical Review.
- Banerjee, T., & Khanna, A. (2006). Infinite Dilution Activity Coefficients for Trihexyltetradecyl Phosphonium Ionic Liquids: Measurements and COSMO-RS Prediction. *Journal of Chemical & Engineering Data*, 51(6), 2170-2177.
- Banerjee, T., Sahoo, R. K., Rath, S. S., Kumar, R., & Khanna, A. (2007). Multicomponent Liquid-Liquid Equilibria Prediction for Aromatic Extraction Systems Using COSMO-RS. [doi: 10.1021/ie060647d]. *Industrial & Engineering Chemistry Research*, 46(4), 1292-1304.
- Banerjee, T., Verma, K. K., & Khanna, A. (2008). Liquid-liquid equilibrium for ionic liquid systems using COSMO-RS: Effect of cation and anion dissociation. *AIChE Journal*, 54(7), 1874-1885.
- Benedik, M. J., Gibbs, P. R., Riddle, R. R., & Willson, R. C. (1998). Microbial denitrogenation of fossil fuels. *Trends in Biotechnology*, 16(9), 390-395.
- Blanchard, L. A., & Brennecke, J. F. (2000). Recovery of Organic Products from Ionic Liquids Using Supercritical Carbon Dioxide. *Industrial & Engineering Chemistry Research*, 40(1), 287-292.
- Brennecke, J. F., & Maginn, E. J. (2001). Ionic liquids: Innovative fluids for chemical processing. *AIChE Journal*, 47(11), 2384-2389.
- Dai, Y., van Spronsen, J., Witkamp, G.-J., Verpoorte, R., & Choi, Y. H. (2013). Natural deep eutectic solvents as new potential media for green technology. *Analytica Chimica Acta*, 766(0), 61-68.
- Diedenhofen, M., Eckert, F., & Klamt, A. (2003). Prediction of Infinite Dilution Activity Coefficients of Organic Compounds in Ionic Liquids Using COSMO-RS†. *Journal of Chemical & Engineering Data*, 48(3), 475-479.

- Diedenhofen, M., & Klamt, A. (2010). COSMO-RS as a tool for property prediction of IL mixtures—A review. *Fluid Phase Equilibria*, 294 (1–2), 31-38.
- Diedenhofen, M., Klamt, A., Marsh, K., & Schafer, A. (2007). Prediction of the vapor pressure and vaporization enthalpy of 1-n-alkyl-3-methylimidazolium-bis-(trifluoromethanesulfonyl) amide ionic liquids. *Physical Chemistry Chemical Physics*, 9(33), 4653-4656.
- Directive of The European Parliament and of The Council on the quality of petrol and diesel fuels and amending Directive 98/70/EC.* (2001). Brussels.
- Domańska, U., Pobudkowska, A., & Eckert, F. (2006). (Liquid + liquid) phase equilibria of 1-alkyl-3-methylimidazolium methylsulfate with alcohols, or ethers, or ketones. *The Journal of Chemical Thermodynamics*, 38(6), 685-695.
- Domínguez de María, P., & Maugeri, Z. (2011). Ionic liquids in biotransformations: from proof-of-concept to emerging deep-eutectic-solvents. *Current Opinion in Chemical Biology*, 15(2), 220-225.
- Dong, D., Jeong, S., & Massoth, F. E. (1997a). Catalyst Deactivation by Coke Formation Effect of nitrogen compounds on deactivation of hydrotreating catalysts by coke. *Catalysis Today*, 37(3), 267-275.
- Dong, D., Jeong, S., & Massoth, F. E. (1997b). Effect of nitrogen compounds on deactivation of hydrotreating catalysts by coke. *Catalysis Today*, 37(3), 267-275.
- Earle, M. J., Esperanca, J. M. S. S., Gilea, M. A., Canongia Lopes, J. N., Rebelo, L. P. N., Magee, J. W., et al. (2006). The distillation and volatility of ionic liquids. *Nature*, 439(7078), 831-834.
- Earle, M. J., & Seddon, K. R. (2000). Ionic liquids. Green solvents for the future *Pure and Applied Chemistry* (Vol. 72, pp. 1391).
- Eckert, F., & Klamt, A. (2002). Fast solvent screening via quantum chemistry: COSMO-RS approach. *AIChE Journal*, 48(2), 369-385.
- Eijsbouts, S., De Beer, V. H. J., & Prins, R. (1991). Hydrodenitrogenation of quinoline over carbon-supported transition metal sulfides. *Journal of Catalysis*, 127(2), 619-630.

- Fernandes, A. M., Rocha, M. A. A., Freire, M. G., Marrucho, I. M., Coutinho, J. o. A. P., & Santos, L. s. M. N. B. F. (2011). Evaluation of Cation–Anion Interaction Strength in Ionic Liquids. *The Journal of Physical Chemistry B*, 115(14), 4033-4041.
- Ferreira, A. R., Freire, M. G., Ribeiro, J. C., Lopes, F. M., Crespo, J. G., & Coutinho, J. A. P. (2012). Overview of the Liquid–Liquid Equilibria of Ternary Systems Composed of Ionic Liquid and Aromatic and Aliphatic Hydrocarbons, and Their Modeling by COSMO-RS. *Industrial & Engineering Chemistry Research*, 51(8), 3483-3507.
- Ferro, V. R., Ruiz, E., de Riva, J., & Palomar, J. (2012). Introducing process simulation in ionic liquids design/selection for separation processes based on operational and economic criteria through the example of their regeneration. *Separation and Purification Technology*, 97(0), 195-204.
- Francisco, M., Arce, A., & Soto, A. (2010). Ionic liquids on desulfurization of fuel oils. *Fluid Phase Equilibria*, 294(1–2), 39-48.
- Fredenslund, A., Jones, R. L., & Prausnitz, J. M. (1975). Group-contribution estimation of activity coefficients in nonideal liquid mixtures. *AIChE Journal*, 21(6), 1086-1099.
- Freemantle, M. (1998). DESIGNER SOLVENTS. *Chemical & Engineering News Archive*, 76(13), 32-37.
- Freire, M. G., Santos, L. M. N. B. F., Marrucho, I. M., & Coutinho, J. A. P. (2007). Evaluation of COSMO-RS for the prediction of LLE and VLE of alcohols + ionic liquids. *Fluid Phase Equilibria*, 255(2), 167-178.
- Freire, M. G., Ventura, S. P. M., Santos, L. M. N. B. F., Marrucho, I. M., & Coutinho, J. A. P. (2008). Evaluation of COSMO-RS for the prediction of LLE and VLE of water and ionic liquids binary systems. *Fluid Phase Equilibria*, 268(1–2), 74-84.
- Fukui, K. (1982). Role of Frontier Orbitals in Chemical Reactions. *Science*, 218(4574), 747-754.
- Furimsky, E., & Massoth, F. E. (2005). Hydrodenitrogenation of Petroleum. *Catalysis Reviews*, 47(3), 297-489.

- Gao, H., Li, Y., Wu, Y., Luo, M., Li, Q., Xing, J., et al. (2009). Extractive Desulfurization of Fuel Using 3-Methylpyridinium-Based Ionic Liquids. *Energy & Fuels*, 23(5), 2690-2694.
- Gao, H., Luo, M., Xing, J., Wu, Y., Li, Y., Li, W., et al. (2008). Desulfurization of Fuel by Extraction with Pyridinium-Based Ionic Liquids. *Industrial & Engineering Chemistry Research*, 47(21), 8384-8388.
- Garcia-Chavez, L. Y., Hermans, A. J., Schuur, B., & de Haan, A. B. (2012). COSMO-RS assisted solvent screening for liquid-liquid extraction of mono ethylene glycol from aqueous streams. *Separation and Purification Technology*, 97(0), 2-10.
- García, G., Aparicio, S., Ullah, R., & Atilhan, M. (2015). Deep Eutectic Solvents: Physicochemical Properties and Gas Separation Applications. *Energy & Fuels*, 29(4), 2616-2644.
- Garcia, J., Larriba, M., Torrecilla, J. S., & Rodriguez, F. (2011). Comparative evaluation of [Imidazolium][Tf2N] and [Pyridinium][Tf2N] ionic liquids for the liquid-liquid extraction of aromatics. *Chemical Engineering Transactions*, 24, 805-810.
- Gates, B. C., & Topsøe, H. (1997). Reactivities in deep catalytic hydrodesulfurization: challenges, opportunities, and the importance of 4-methyldibenzothiophene and 4,6-dimethyldibenzothiophene. *Polyhedron*, 16(18), 3213-3217.
- Grensemann, H., & Gmehling, J. (2005). Performance of a Conductor-Like Screening Model for Real Solvents Model in Comparison to Classical Group Contribution Methods. *Industrial & Engineering Chemistry Research*, 44(5), 1610-1624.
- Gutiérrez, J. P., Meindersma, G. W., & de Haan, A. B. (2012). COSMO-RS-Based Ionic-Liquid Selection for Extractive Distillation Processes. *Industrial & Engineering Chemistry Research*, 51(35), 11518-11529.
- Hand, D. B. (1929). Dimeric Distribution. *The Journal of Physical Chemistry*, 34(9), 1961-2000.
- Hansmeier, A. R., Meindersma, G. W., & de Haan, A. B. (2011). Desulfurization and denitrogenation of gasoline and diesel fuels by means of ionic liquids. *Green Chemistry*, 13(7), 1907-1913.
- Heard, G. L., & Boyd, R. J. (1997). Density functional theory studies of the quadrupole moments of benzene and naphthalene. *Chemical Physics Letters*, 277(1-3), 252-256.

- Hizaddin, H. F., Sarwono, M., Hashim, M. A., Alnashef, I. M., & Hadj-Kali, M. K. (2015). Coupling the capabilities of different complexing agents into deep eutectic solvents to enhance the separation of aromatics from aliphatics. *The Journal of Chemical Thermodynamics*, 84(0), 67-75.
- Holbrey, J. D., Reichert, W. M., Nieuwenhuyzen, M., Sheppard, O., Hardacre, C., & Rogers, R. D. (2003). Liquid clathrate formation in ionic liquid-aromatic mixtures. *Chemical Communications*, 0(4), 476-477.
- Holbrey, J. D., & Seddon, K. R. (1999). Ionic Liquids. *Clean Products and Processes*, 1(4), 223-236.
- Huddleston, J. G., Willauer, H. D., Swatoski, R. P., Visser, A. E., & Rogers, R. D. (1998). Room temperature ionic liquids as novel media for 'clean' liquid-liquid extraction. *Chemical Communications*(16), 1765-1766.
- Huh, E. S., Zazybin, A., Palgunadi, J., Ahn, S., Hong, J., Kim, H. S., et al. (2009). Zn-Containing Ionic Liquids for the Extractive Denitrogenation of a Model Oil: A Mechanistic Consideration. [doi: 10.1021/ef900073a]. *Energy & Fuels*, 23(6), 3032-3038.
- Hunt, P. A., Gould, I. R., & Kirchner, B. (2007). The Structure of Imidazolium-Based Ionic Liquids: Insights From Ion-Pair Interactions. *Australian Journal of Chemistry*, 60(1), 9-14.
- Hwang, I.-C., Kim, K.-L., Park, S.-J., & Han, K.-J. (2007). Liquid-Liquid Equilibria for Binary System of Ethanol + Hexadecane at Elevated Temperature and the Ternary Systems of Ethanol + Heterocyclic Nitrogen Compounds + Hexadecane at 298.15 K. *Journal of Chemical & Engineering Data*, 52(5), 1919-1924.
- Hwang, I.-C., Park, S.-J., Seo, D.-W., & Han, K.-J. (2008). Binary Liquid-Liquid Equilibrium (LLE) for N-Methylformamide (NMF) + Hexadecane between (288.15 and 318.15) K and Ternary LLE for Systems of NMF + Heterocyclic Nitrogen Compounds + Hexadecane at 298.15 K. *Journal of Chemical & Engineering Data*, 54(1), 78-82.
- Ishihara, A., Wang, D., Dumeignil, F., Amano, H., Qian, E. W., & Kabe, T. (2005). Oxidative desulfurization and denitrogenation of a light gas oil using an oxidation/adsorption continuous flow process. *Applied Catalysis A: General*, 279(1-2), 279-287.
- Jhong, H.-R., Wong, D. S.-H., Wan, C.-C., Wang, Y.-Y., & Wei, T.-C. (2009). A novel deep eutectic solvent-based ionic liquid used as electrolyte for dye-sensitized solar cells. *Electrochemistry Communications*, 11(1), 209-211.

- Jork, C., Kristen, C., Pieraccini, D., Stark, A., Chiappe, C., Beste, Y. A., et al. (2005). Tailor-made ionic liquids. *The Journal of Chemical Thermodynamics*, 37(6), 537-558.
- Kareem, M. A., Mjalli, F. S., Hashim, M. A., & AlNashef, I. M. (2012). Liquid–liquid equilibria for the ternary system (phosphonium based deep eutectic solvent–benzene–hexane) at different temperatures: A new solvent introduced. *Fluid Phase Equilibria*, 314(0), 52-59.
- Kareem, M. A., Mjalli, F. S., Hashim, M. A., Hadj-Kali, M. K. O., Bagh, F. S. G., & Alnashef, I. M. (2012). Phase equilibria of toluene/heptane with tetrabutylphosphonium bromide based deep eutectic solvents for the potential use in the separation of aromatics from naphtha. *Fluid Phase Equilibria*, 333(0), 47-54.
- Kareem, M. A., Mjalli, F. S., Hashim, M. A., Hadj-Kali, M. K. O., Ghareh Bagh, F. S., & Alnashef, I. M. (2013). Phase equilibria of toluene/heptane with deep eutectic solvents based on ethyltriphenylphosphonium iodide for the potential use in the separation of aromatics from naphtha. *The Journal of Chemical Thermodynamics*, 65(0), 138-149.
- Kędra-Królik, K., Fabrice, M., & Jaubert, J.-N. I. (2011). Extraction of Thiophene or Pyridine from n-Heptane Using Ionic Liquids. Gasoline and Diesel Desulfurization. *Industrial & Engineering Chemistry Research*, 50(4), 2296-2306.
- Kędra-Królik, K., Mutelet, F., Moïse, J.-C., & Jaubert, J.-N. I. (2011). Deep Fuels Desulfurization and Denitrogenation Using 1-Butyl-3-methylimidazolium Trifluoromethanesulfonate. *Energy & Fuels*, 25(4), 1559-1565.
- KG, C. G. C. (December 12th 2012). COSMOthermX. A Graphical User Interface to the COSMOtherm Program. User Guide. (Version Version C30_1301). Burscheider Str. 515, D-51381 Leverkusen, Germany.
- Kim, H.-D., Hwang, I.-C., Park, S.-J., & Lee, K. W. (2009). (Liquid + Liquid) Equilibrium for (N,N-Dimethylformamide (DMF) + Hexadecane) at Temperatures between (293.15 and 313.15) K and Ternary Mixtures of (DMF + Hexadecane) with Either Quinoline, or Pyridine, or Pyrrole, or Aniline, or Indole at T = 298.15 K. *Journal of Chemical & Engineering Data*, 55(3), 1266-1270.

- Klamt, A. (1995). Conductor-like Screening Model for Real Solvents: A New Approach to the Quantitative Calculation of Solvation Phenomena. *The Journal of Physical Chemistry*, 99(7), 2224-2235.
- Klamt, A. (2002). Comments on "A Priori Phase Equilibrium Prediction from a Segment Contribution Solvation Model". *Industrial & Engineering Chemistry Research*, 41(9), 2330-2331.
- Klamt, A., & Schüürmann, G. (1993). COSMO: A new approach to dielectric screening in solvents with explicit expressions for the screening energy and its gradient. *Journal of the Chemical Society, Perkin Transactions 2*(5), 799-805.
- Koel, M. (2008). *Ionic Liquids in Chemical Analysis*: CRC Press.
- Koriakin, A., Ponvel, K. M., & Lee, C.-H. (2010). Denitrogenation of raw diesel fuel by lithium-modified mesoporous silica. *Chemical Engineering Journal*, 162(2), 649-655.
- Kumar, A. A. P., & Banerjee, T. (2009). Thiophene separation with ionic liquids for desulphurization: A quantum chemical approach. *Fluid Phase Equilibria*, 278(1-2), 1-8.
- Kwak, C., Lee, J. J., Bae, J. S., & Moon, S. H. (2001). Poisoning effect of nitrogen compounds on the performance of CoMoS/Al₂O₃ catalyst in the hydrodesulfurization of dibenzothiophene, 4-methyldibenzothiophene, and 4,6-dimethyldibenzothiophene. *Applied Catalysis B: Environmental*, 35(1), 59-68.
- Lababidi, H. M. S., Ali, S. H., & Fahim, M. A. (2006). Optimization of Aromatics Extraction of Naphtha Reformate by Propylene Carbonate/Diethylene Glycol Mixed Solvent. *Industrial & Engineering Chemistry Research*, 45(14), 5086-5097.
- Laredo, G. C., Leyva, S., Alvarez, R., Mares, M. T., Castillo, J., & Cano, J. L. (2002). Nitrogen compounds characterization in atmospheric gas oil and light cycle oil from a blend of Mexican crudes. *Fuel*, 81(10), 1341-1350.
- Laredo, G. C., Vega-Merino, P. M., Trejo-Zárraga, F., & Castillo, J. (2013). Denitrogenation of middle distillates using adsorbent materials towards ULSD production: A review. *Fuel Processing Technology*, 106(0), 21-32.
- Laredo S, G. C., De los Reyes H, J. A., Luis Cano D, J., & Jesús Castillo M, J. (2001). Inhibition effects of nitrogen compounds on the hydrodesulfurization of dibenzothiophene. *Applied Catalysis A: General*, 207(1-2), 103-112.

- Lei, Z., Arlt, W., & Wasserscheid, P. (2006). Separation of 1-hexene and n-hexane with ionic liquids. *Fluid Phase Equilibria*, 241(1–2), 290-299.
- Letcher, T. M. (2004). *Chemical Thermodynamics for Industry*: Royal Society of Chemistry.
- Li, C., Li, D., Zou, S., Li, Z., Yin, J., Wang, A., et al. (2013). Extraction desulfurization process of fuels with ammonium-based deep eutectic solvents. *Green Chemistry*, 15(10), 2793-2799.
- Lin, H., Wu, D.-l., Liu, L., & Jia, D.-z. (2008). Theoretical study on molecular structures, intramolecular proton transfer reaction, and solvent effects of 1-phenyl-3-methyl-4-(6-hydro-4-amino-5-sulfo-2,3-pyrazine)-pyrazole-5-one. *Journal of Molecular Structure: THEOCHEM*, 850(1–3), 32-37.
- Lin, S.-T., & Sandler, S. I. (2002). A Priori Phase Equilibrium Prediction from a Segment Contribution Solvation Model. *Industrial & Engineering Chemistry Research*, 41(5), 899-913.
- Lü, R., Lin, J., & Qu, Z. (2013). Theoretical study on interactions between thiophene/dibenzothiophene/cyclohexane/toluene and 1-methyl-3-octylimidazolium tetrafluoroborate. *Structural Chemistry*, 24(2), 507-515.
- Lü, R., Qu, Z., & Lin, J. (2013). Comparative study of interactions between thiophene\pyridine\benzene\heptane and 1-butyl-3-methylimidazolium trifluoromethanesulfonate by density functional theory. *Journal of Molecular Liquids*, 180(0), 207-214.
- Lü, R., Qu, Z., Yu, H., Wang, F., & Wang, S. (2012). Comparative study on interactions between ionic liquids and pyridine/hexane. *Chemical Physics Letters*, 532(0), 13-18.
- Lyu, Z., Zhou, T., Chen, L., Ye, Y., Sundmacher, K., & Qi, Z. (2014). Simulation based ionic liquid screening for benzene–cyclohexane extractive separation. *Chemical Engineering Science*, 113, 45-53.
- Marsh, K., Deev, A., Wu, A.-T., Tran, E., & Klamt, A. (2002). Room temperature ionic liquids as replacements for conventional solvents – A review. *Korean Journal of Chemical Engineering*, 19(3), 357-362.
- Marsh, K. N., Boxall, J. A., & Lichtenthaler, R. (2004). Room temperature ionic liquids and their mixtures—a review. *Fluid Phase Equilibria*, 219(1), 93-98.

- Martínez-Magadán, J.-M., Oviedo-Roa, R., García, P., & Martínez-Palou, R. (2012). DFT study of the interaction between ethanethiol and Fe-containing ionic liquids for desulfuration of natural gasoline. *Fuel Processing Technology*, 97(0), 24-29.
- Mulyono, S., Hizaddin, H. F., Alnashef, I. M., Hashim, M. A., Fakeeha, A. H., & Hadj-Kali, M. K. (2014). Separation of BTEX aromatics from n-octane using a (tetrabutylammonium bromide + sulfolane) deep eutectic solvent - experiments and COSMO-RS prediction. *RSC Advances*, 4(34), 17597-17606.
- Ni, B.-Q., Shan, Y.-Y., Wang, H.-J., & Liu, W.-L. (2008). A DFT Study on the Interactions between Sulfolane and Aromatic Hydrocarbons. *Journal of Solution Chemistry*, 37(10), 1343-1354.
- Nishi, T., Iwahashi, T., Yamane, H., Ouchi, Y., Kanai, K., & Seki, K. (2008). Electronic structures of ionic liquids and studied by ultraviolet photoemission, inverse photoemission, and near-edge X-ray absorption fine structure spectroscopies. *Chemical Physics Letters*, 455(4-6), 213-217.
- Nuzhdin, A. L., Kovalenko, K. A., Dybtsev, D. N., & Bukhtiyarova, G. A. (2010). Removal of nitrogen compounds from liquid hydrocarbon streams by selective sorption on metal-organic framework MIL-101. *Mendeleev Communications*, 20(1), 57-58.
- Oliveira, F. S., Pereiro, A. B., Rebelo, L. P. N., & Marrucho, I. M. (2013). Deep eutectic solvents as extraction media for azeotropic mixtures. *Green Chemistry*, 15(5), 1326-1330.
- Othmer, D. F., & Tobias, P. E. (1942). Liquid-Liquid Extraction Data -Toluene and Acetaldehyde Systems. *Industrial & Engineering Chemistry*, 34(6), 690-692.
- Palomar, J., Ferro, V. R., Torrecilla, J. S., & Rodríguez, F. (2007). Density and Molar Volume Predictions Using COSMO-RS for Ionic Liquids. An Approach to Solvent Design. *Industrial & Engineering Chemistry Research*, 46(18), 6041-6048.
- Palomar, J., Torrecilla, J. S., Ferro, V. R., & Rodríguez, F. (2008). Development of an a Priori Ionic Liquid Design Tool. 1. Integration of a Novel COSMO-RS Molecular Descriptor on Neural Networks. *Industrial & Engineering Chemistry Research*, 47(13), 4523-4532.
- Parr, R. G., Szentpály, L. v., & Liu, S. (1999). Electrophilicity Index. *Journal of the American Chemical Society*, 121(9), 1922-1924.

- Paulechka, Y. U., Zaitsau, D. H., Kabo, G. J., & Strechan, A. A. (2005). Vapor pressure and thermal stability of ionic liquid 1-butyl-3-methylimidazolium Bis(trifluoromethylsulfonyl)amide. *Thermochimica Acta*, 439(1–2), 158-160.
- Pearson, R. G. (1986). Absolute electronegativity and hardness correlated with molecular orbital theory. *Proc. Natl. Acad. Sci. USA*, 83, 8440-8441.
- Potdar, S., Anantharaj, R., & Banerjee, T. (2012). Aromatic Extraction Using Mixed Ionic Liquids: Experiments and COSMO-RS Predictions. *Journal of Chemical & Engineering Data*, 57(4), 1026-1035.
- Qi, J., Yan, Y., Su, Y., Qu, F., & Dai, Y. (1998). Extraction of Nitrogen Compounds from Catalytically Cracked Diesel Oil with a Volatile Carboxylic Acid Based on Reversible Chemical Complexation. *Energy & Fuels*, 12(4), 788-791.
- Ravilla, U. K., & Banerjee, T. (2012). Liquid liquid equilibria of imidazolium based ionic liquid+pyridine+hydrocarbon at 298.15 K: Experiments and correlations. *Fluid Phase Equilibria*, 324(0), 17-27.
- Reddy, P., Aslam Siddiqi, M., Atakan, B., Diedenhofen, M., & Ramjugernath, D. (2013). Activity coefficients at infinite dilution of organic solutes in the ionic liquid PEG-5 cocomonium methylsulfate at T = (313.15, 323.15, 333.15, and 343.15) K: Experimental results and COSMO-RS predictions. *The Journal of Chemical Thermodynamics*, 58, 322-329.
- Renon, H., & Prausnitz, J. M. (1968). Local compositions in thermodynamic excess functions for liquid mixtures. *AIChE Journal*, 14(1), 135-144.
- Rodríguez-Cabo, B., Arce, A., & Soto, A. (2013). Desulfurization of fuels by liquid–liquid extraction with 1-ethyl-3-methylimidazolium ionic liquids. *Fluid Phase Equilibria*, 356(0), 126-135.
- Rodríguez-Cabo, B., Soto, A., & Arce, A. (2013). Desulfurization of fuel-oils with [C2mim][NTf2]: A comparative study. *The Journal of Chemical Thermodynamics*, 57(0), 248-255.
- Rogošić, M., Sander, A., & Pantaler, M. (2014). Application of 1-pentyl-3-methylimidazolium bis(trifluoromethylsulfonyl) imide for desulfurization, denitrification and dearomatization of FCC gasoline. *The Journal of Chemical Thermodynamics*, 76(0), 1-15.

- Ru, & Konig, B. (2012). Low melting mixtures in organic synthesis - an alternative to ionic liquids? *Green Chemistry*, 14(11), 2969-2982.
- Shiraishi, Y., Hirai, T., & Komasaawa, I. (2000). Photochemical Desulfurization and Denitrogenation Process for Vacuum Gas Oil Using an Organic Two-Phase Extraction System. *Industrial & Engineering Chemistry Research*, 40(1), 293-303.
- Shiraishi, Y., Tachibana, K., Hirai, T., & Komasaawa, I. (2002). Desulfurization and Denitrogenation Process for Light Oils Based on Chemical Oxidation followed by Liquid-Liquid Extraction. *Industrial & Engineering Chemistry Research*, 41(17), 4362-4375.
- Simulis®, & thermodynamics. a thermo physical properties calculation server provided by ProSim. <http://www.prosim.net/>
- Smith, E. L., Abbott, A. P., & Ryder, K. S. (2014). Deep Eutectic Solvents (DESs) and Their Applications. *Chemical Reviews*, 114(21), 11060-11082.
- Song, C. (2003). An overview of new approaches to deep desulfurization for ultra-clean gasoline, diesel fuel and jet fuel. *Catalysis Today*, 86(1-4), 211-263.
- Sumbogo Murti, S. D., Sakanishi, K., Okuma, O., Korai, Y., & Mochida, I. (2002). Detailed characterization of heteroatom-containing molecules in light distillates derived from Tanito Harum coal and its hydrotreated oil. *Fuel*, 81(17), 2241-2248.
- Sun, H., Li, Y., Wu, X., & Li, G. (2013). Theoretical study on the structures and properties of mixtures of urea and choline chloride. *Journal of Molecular Modeling*, 19(6), 2433-2441.
- Tassios, D. (1976). Limitations in Correlating Strongly Nonideal Binary Systems with the NRTL and LEMF Equations. *Industrial & Engineering Chemistry Process Design and Development*, 15(4), 574-578.
- Tsuzuki, S., Mikami, M., & Yamada, S. (2007). Origin of Attraction, Magnitude, and Directionality of Interactions in Benzene Complexes with Pyridinium Cations. *Journal of the American Chemical Society*, 129(27), 8656-8662.
- Tsuzuki, S., Tokuda, H., & Mikami, M. (2007). Theoretical analysis of the hydrogen bond of imidazolium C2-H with anions. *Physical Chemistry Chemical Physics*, 9(34), 4780-4784.

Turaga, U. T., Ma, X., & Song, C. (2003). Influence of nitrogen compounds on deep hydrodesulfurization of 4,6-dimethyldibenzothiophene over Al₂O₃- and MCM-41-supported Co-Mo sulfide catalysts. *Catalysis Today*, 86(1–4), 265-275.

TURBOMOLE. (2012). TURBOMOLE Users' Manual (Version 6.4).

US EPA Clean Air Act Tier 2; 1999.

Wagle, D., Kamath, G., & Baker, G. A. (2013). Elucidating Interactions Between Ionic Liquids and Polycyclic Aromatic Hydrocarbons by Quantum Chemical Calculations. *The Journal of Physical Chemistry C*, 117(9), 4521-4532.

Wandas, R., & Chrapek, T. (2004). Hydrotreating of middle distillates from destructive petroleum processing over high-activity catalysts to reduce nitrogen and improve the quality. *Fuel Processing Technology*, 85(11), 1333-1343.

Wang, H., Xie, C., Yu, S., & Liu, F. (2014). Denitrification of simulated oil by extraction with H₂PO₄-based ionic liquids. *Chemical Engineering Journal*, 237(0), 286-290.

Wilkes, J. S., Levisky, J. A., Wilson, R. A., & Hussey, C. L. (1982). Dialkylimidazolium chloroaluminate melts: a new class of room-temperature ionic liquids for electrochemistry, spectroscopy and synthesis. *Inorganic Chemistry*, 21(3), 1263-1264.

Wilson, G. M. (1964). Vapor-Liquid Equilibrium. XI. A New Expression for the Excess Free Energy of Mixing. *Journal of the American Chemical Society*, 86(2), 127-130.

Wiwel, P., Knudsen, K., Zeuthen, P., & Whitehurst, D. (2000). Assessing Compositional Changes of Nitrogen Compounds during Hydrotreating of Typical Diesel Range Gas Oils Using a Novel Preconcentration Technique Coupled with Gas Chromatography and Atomic Emission Detection. *Industrial & Engineering Chemistry Research*, 39(2), 533-540.

Won, D.-B., Park, S.-J., Han, K.-J., & Kim, C.-J. (2002). Liquid–liquid equilibria for methanol + hexadecane + heterocyclic nitrogen-containing compounds at 298.15 K. *Fluid Phase Equilibria*, 193(1–2), 217-227.

- Xie, L.-L., Favre-Reguillon, A., Pellet-Rostaing, S., Wang, X.-X., Fu, X., Estager, J., et al. (2008). Selective Extraction and Identification of Neutral Nitrogen Compounds Contained in Straight-Run Diesel Feed Using Chloride Based Ionic Liquid. *Industrial & Engineering Chemistry Research*, 47(22), 8801-8807.
- Xie, L.-L., Favre-Reguillon, A., Wang, X.-X., Fu, X., & Lemaire, M. (2010). Selective Adsorption of Neutral Nitrogen Compounds from Fuel Using Ion-Exchange Resins. *Journal of Chemical & Engineering Data*, 55(11), 4849-4853.
- Yang, H., Ring, Z., Briker, Y., McLean, N., Friesen, W., & Fairbridge, C. (2002). Neural network prediction of cetane number and density of diesel fuel from its chemical composition determined by LC and GC-MS. *Fuel*, 81(1), 65-74.
- Yang, R. T. (2003). *Adsorbents: Fundamentals and Applications*. New York: Wiley.
- Zaitsau, D. H., Kabo, G. J., Strechan, A. A., Paulechka, Y. U., Tschersich, A., Verevkin, S. P., et al. (2006). Experimental Vapor Pressures of 1-Alkyl-3-methylimidazolium Bis(trifluoromethylsulfonyl)imides and a Correlation Scheme for Estimation of Vaporization Enthalpies of Ionic Liquids. *The Journal of Physical Chemistry A*, 110(22), 7303-7306.
- Zhan, C.-G., Nichols, J. A., & Dixon, D. A. (2003). Ionization Potential, Electron Affinity, Electronegativity, Hardness, and Electron Excitation Energy: Molecular Properties from Density Functional Theory Orbital Energies. *The Journal of Physical Chemistry A*, 107(20), 4184-4195.
- Zhang, H., Li, G., Jia, Y., & Liu, H. (2009). Adsorptive Removal of Nitrogen-Containing Compounds from Fuel. [doi: 10.1021/jc9003004]. *Journal of Chemical & Engineering Data*, 55(1), 173-177.
- Zhang, J., Xu, J., Qian, J., & Liu, L. (2013). Denitrogenation of Straight-run Diesel With Complexing Extraction. *Petroleum Science and Technology*, 31(8), 777-782.
- Zhang, Q., De Oliveira Vigier, K., Royer, S., & Jerome, F. (2012). Deep eutectic solvents: syntheses, properties and applications. *Chemical Society Reviews*, 41(21), 7108-7146.
- Zhang, S., Zhang, Q., & Zhang, Z. C. (2003). Extractive Desulfurization and Denitrogenation of Fuels Using Ionic Liquids. *Industrial & Engineering Chemistry Research*, 43(2), 614-622.

Zhou, J., Mao, J., & Zhang, S. (2008). Ab initio calculations of the interaction between thiophene and ionic liquids. *Fuel Processing Technology*, 89(12), 1456-1460.

Zhou, T., Wang, Z., Ye, Y., Chen, L., Xu, J., & Qi, Z. (2012). Deep Separation of Benzene from Cyclohexane by Liquid Extraction Using Ionic Liquids as the Solvent. *Industrial & Engineering Chemistry Research*, 51(15), 5559-5564.

University of Malaya

LIST OF PUBLICATIONS AND CONFERENCE PROCEEDINGS

Publications

Hizaddin, Hanee F., Hashim, Mohd. Ali, & Ramalingam, Anantharaj. (2013). Evaluation of Molecular Interaction in Binary Mixture of Ionic Liquids + Heterocyclic Nitrogen Compounds: Ab Initio Method and COSMO-RS Model. *Industrial & Engineering Chemistry Research*, 52, 18043–18058

Hizaddin, Hanee F., Hashim, Mohd. Ali, & Ramalingam, Anantharaj. (2014). A quantum chemical study on the molecular interaction between pyrrole and ionic liquids. *Journal of Molecular Liquids*, 194, 20–29

Hizaddin, Hanee F., Ramalingam, Anantharaj, Hashim, Mohd Ali & Hadj-Kali, Mohamed K.O. (2014). Evaluating the Performance of Deep Eutectic Solvents for Use in Extractive Denitrogenation of Liquid Fuels by the Conductor-like Screening Model for Real Solvents. *J. Chem. Eng. Data* 2014, 59, 3470–3487.

Hizaddin, Hanee F., Hadj-Kali, Mohamed Kamel; Ramalingam, Anantharaj; Hashim, Mohd A. (2015) Extraction of nitrogen compounds from diesel fuel using imidazolium- and pyridinium- based ionic liquids: Experiments, COSMO-RS prediction and NRTL correlation. *Fluid Phase Equilibria* 405 (2015) 55–67.

Hizaddin, Hanee F., Hadj-Kali, Mohamed Kamel; Ramalingam, Anantharaj; Hashim, Mohd A. Extractive denitrogenation of diesel fuel using ammonium- and phosphonium-based deep eutectic solvents. *Journal of Chemical Thermodynamics* 95 (2016) 164–173.

Conference Proceedings

Hizaddin, Haneef F., Hashim, Mohd. Ali, Hadj-Kali, Mohamed K.O., Ramalingam, Anantharaj. *Evaluating the Performance of Deep Eutectic Solvents for use in Extractive Denitrogenation of Liquid Fuels by COSMO-RS model*. Presented in the International Conference on Ionic Liquids 2013. 11 – 13 December 2013. Langkawi, Kedah, Malaysia.

Hizaddin, Haneef F., Ramalingam, Anantharaj, Hashim, Mohd. Ali, Hadj-Kali, Mohamed K.O. *Removal of nitrogen compounds for improved efficiency of desulfurization of diesel using ammonium-based Deep Eutectic Solvents*. Presented in the 4th Asia-Pacific Conference on Ionic Liquids and Green Processes / 6th Australasian Symposium on Ionic Liquids, 2014. 28 September – 1 October 2014. Sydney, Australia.

University of Malaya